

**FORMULATION AND EVALUATION OF CAPTOPRIL LOADED  
POLYMETHACRYLATE AND HYDROXYPROPYL METHYLCELLULOSE  
MICROCAPSULES**

A Thesis Submitted to Rhodes University in  
Fulfilment of the Requirements for the Degree of

**DOCTOR OF PHILOSOPHY**

By

Sandile Maswazi Malungelo Khamanga

February 2010

Faculty of Pharmacy

Rhodes University

Grahamstown

South Africa

## ABSTRACT

---

Angiotensin-converting enzyme (ACE) inhibitors are some of the most commonly prescribed medications for hypertension. They are cited in many papers as the treatment most often recommended by guidelines and favoured over other antihypertensive drugs as first-line agents especially when other high-risk conditions are present, such as diabetic nephropathy. The development of captopril (CPT) was amongst the earliest successes of the revolutionary concept of structure-based drug design. Due to its relatively poor pharmacokinetic profile or short half-life of about 1 hour, the formulation of sustained-release microcapsule dosage form is useful to improve patient compliance and to achieve predictable and optimized therapeutic plasma concentrations.

Currently, CPT is mainly administered in tablet form. One of the difficulties of CPT formulation has been reported to be its instability in aqueous solutions. CPT is characterized by a lack of a strong chromophore and, therefore, not able to absorb at the more useful UV–Vis region of the spectrum. For this reason, an accurate, simple, reproducible, and sensitive HPLC-ECD method was developed and validated for the determination of CPT in dosage forms. The method was successfully applied for the determination of CPT in commercial and developed formulations.

Possible drug-excipient and excipient-excipient interactions were investigated prior to formulating CPT microcapsules because successful formulation of a stable and effective solid dosage form depends on careful selection of excipients. Nuclear magnetic resonance spectroscopy, Fourier transform infra-red spectroscopy (FT-IR), differential scanning calorimetry (DSC) and thermogravimetric analysis (TGA) were used for the identification and purity testing of CPT and excipients. The studies revealed no thermal changes during stress testing of binary and whole mixtures which indicate absence of solid state interactions. There were no shifts, appearance and disappearance in the endothermic or exothermic peaks and on the change of other associated enthalpy values on thermal curves obtained with DSC method. Characteristic peaks for common functional groups in the FT-IR were present in all the mixtures indicating the absence of incompatibility. The techniques used in this study can be said to have been efficient in the characterization and evaluation of the drug and excipients.

The technique of microencapsulation by oil-in-oil was used to prepare CPT microcapsules. The effects of polymer molecular weight, homogenizing speed on the particle size, flow properties, morphology, surface properties and release characteristics of the prepared CPT microcapsules were examined. In order to decrease the complexity of the analysis and reduce cost response surface methodology using best polynomial equations was successfully used to quantify the effect of the formulation variables and develop an optimized formulation thereby minimizing the number of experimental trials.

There was a burst effect during the first stage of dissolution. Scanning electron microscopy (SEM) results indicated that the initial burst effect observed in drug release could be attributed to dissolution of CPT crystals present at the surface or embedded in the superficial layer of the matrix. During the preparation of microcapsules, the drug might have been trapped near the surface of the microcapsules and or might have diffused quickly through the porous surface. The release kinetics of CPT from most formulations followed Fickian diffusion mechanism. SEM photographs showed that diffusion took place through pores at the surface of the microcapsules. The Kopcha model diffusion and erosion terms showed predominance of diffusion relative to swelling or erosion throughout the entire test period. Drug release mechanism was also confirmed by Makoid-Banakar and Korsmeyer-Peppas models exponents which further support diffusion release mechanism in most formulations. The models postulate that the total of drug release is a summation of a couple of mechanisms; burst release, relaxation induced controlled-release and diffusional release.

Inspection of the 2D contour and 3D response surfaces allowed the determination of the geometrical nature of the surfaces and further providing results about the interaction of the different variables used in central composite design (CCD). The wide variation indicated that the factor combinations resulted in different drug release rates. Lagrange, canonical and mathematical modelling were used to determine the nature of the stationery point of the models. This represented the optimal variables or stationery points where there is interaction in the experimental space. It is difficult to understand the shape of a fitted response by mere inspection of the algebraic polynomial when there are many independent variables in the model. Canonical and Lagrange analyses facilitated the interpretation of the surface plots after a mathematical transformation of the original variables into new variables. In conclusion, these results suggest the potential application of Eudragit<sup>®</sup> / Methocel<sup>®</sup> microcapsules as suitable sustained-release drug delivery system for CPT.

## ACKNOWLEDGEMENTS

---

This thesis appears in its current form due to the assistance and guidance of several people. It is the result of four years of work during which I have been supported by many people. It is now my great pleasure to take this opportunity to thank them.

- The Dean, Head and my supervisor, Prof R. B. Walker for giving me the opportunity to be part of his Research Group.

I thank him for support, guidance and assistance throughout the course of my studies. His expertise, understanding and patience added considerably to my postgraduate experience. I appreciate his vast knowledge and skill in many areas (method development, formulation studies, etc) and his assistance in writing reports (eg., grant proposals, travel and subsistence applications and this thesis), which have on occasion made me "green" with envy.

It was under Prof Walker's tutelage that I developed a focus and became interested in microencapsulation technology. He drove this project, asking for as much as could be delivered. He kept faith in me throughout. Prof Walker has been instrumental in ensuring my academic and professional well-being ever since. He provided me with direction, technical support and became more of a mentor than a professor. It was through his persistence, understanding and kindness that I completed my PhD degree and was encouraged to apply for a lectureship position in pharmaceuticals. I doubt that I will ever be able to convey my appreciation fully, but I owe him my eternal gratitude.

- Prof Kanfer

Very special thanks go out to Prof Izzy Kanfer without whose motivation and encouragement I would not have considered a postgraduate career in pharmaceutical research.

- Other Faculty members

I mention in particular Dr Sirion Robertson and acknowledge him for proofreading this work. Appreciation also goes out to the technical staff for all of their technical assistance throughout my PhD degree and to the secretarial staff for all the instances in which their assistance helped me along the way. I would like to thank the other staff members in the Faculty of Pharmacy for the assistance they provided at all levels of the research project.

My colleagues in the Biopharmaceutics Research Laboratory and other laboratories in the Faculty of Pharmacy, I thank you so much for the support, philosophical debates, exchange of knowledge and skills which helped enriched my academic experience.

The Dow Chemical Company (Michigan, USA), Colorcon<sup>®</sup> (Kent, UK) and Aspen Pharmacare (Port Elizabeth, South Africa) for their donation of excipients.

I thank Dr Watkins, for allowing me to use the DSC and TGA in the Chemistry Department. The staff at the electron microscopy unit I would like to thank you all. To my undergraduate students in the Faculty of Pharmacy, I want to say ‘thank you’.

To all those who have encouraged me, taught me, prayed for me my and helped make life worth living, funny, though, I never seem to have enough time to let them know how much I appreciate them. Thanks.

To both my late father, Bulente and my sister, Phangisile, I know I gave you my thanks when I said good-bye, this work is dedicated to you.

My mother, KIKI for all that she has meant to me throughout my life, I appreciate the material and spiritual support in all aspects of my life, and to my sister and brothers, I thank you all for your understanding and for supporting me without any complaints. I thank you all for the long lasting support. ‘Make Nkhosi’, you gave me life, you educated me, you are special to me. Without your prayers and efforts I could not have continued with my studies. You are such a special family, God bless you!

My lovely wife, Duduzile, I thank her for the sacrifices she has made to support me while doing my doctoral studies. By providing steadfast support in hard times, she has once again shown the true affection and dedication she has always had towards me. Duduzile, thanks for always bringing me back on the path, and for all those late skype chats that brought many thesis nights to a soothing end. For all that, and for being everything I am not, she has my everlasting love.

My students in Adamson House, I thank you very much for making the atmosphere of our house as friendly as possible.

The list of willing helpers, constructive critics, is much, much longer. By acknowledging the involvement of the above individuals, I do not mean to imply their endorsement of the research work. I am solely responsible for any shortcomings in this work.

In conclusion, I recognize that this research would not have been possible without financial assistance from the Andrew William Mellon Foundation and Rhodes University and I sincerely express my gratitude to those bodies.

I would like to give thanks to Almighty God for giving me strength, protection and for giving me light, vision and the understanding that all is possible in His name; and most importantly, for it is under His grace that we live, learn and flourish.

## STUDY OBJECTIVES

---

Hypertension is recognised as a major contributor to the disease burden globally that is as prevalent in many developing countries, as in the developed world. The capacity for the management of hypertension varies considerably from country to country, but in general the majority of diagnosed hypertensives are inadequately controlled throughout the world (1).

The renin–angiotensin–aldosterone system (RAAS) plays an important role in the pathogenesis of a variety of clinical conditions, including atherosclerosis, hypertension, left ventricular hypertrophy, myocardial infarction and heart failure. Inhibition of the RAAS with angiotensin converting enzyme (ACE) inhibitors has been shown to be effective in lowering blood pressure and reducing cardiovascular mortality and morbidity in many at-risk patient populations. A number of studies have shown that captopril (CPT) is effective in reducing the rate of renal disease progression in patients with diabetic nephropathy. The importance of diabetic nephropathy as a major cardiovascular risk factor has been established by a number of large epidemiologic and interventional studies (2).

CPT is one of the most commonly prescribed ACE inhibitors and is a World Health Organization (WHO) listed drug that is indicated for the treatment of several cardiovascular diseases. It is available in 12.5, 25 and 50 mg tablets. The recommended dose of CPT is 25-150 mg two or three times daily. The maximum permitted daily dose is 450 mg. CPT should be taken on an empty stomach one hour before or two hours after meals since absorption of CPT is reduced when taken with food. CPT has a short biological half-life and is therefore suitable for formulation as a sustained-release product in order to reduce the frequency of administration of doses and to improve patient adherence.

The objectives of this study were therefore:

1. To develop and validate a suitable high performance liquid chromatographic method with electrochemical detection (HPLC-ECD) for the analysis of CPT.
2. To use spectroscopic and thermo-analytical techniques to evaluate the compatibility of CPT with Eudragit<sup>®</sup> RS, Methocel<sup>®</sup> K100M, Methocel<sup>®</sup> K15M, microcrystalline cellulose (MCC) and citric acid.

3. To use response surface methodology (RSM) to investigate pharmaceutical excipients and compositions for the manufacture of CPT microcapsules using a solvent evaporation technique.
4. To use mathematical flow models to study the flow properties of the microcapsules and to evaluate their surface morphology using scanning electron microscopy (SEM).
5. To study the dissolution kinetics and release mechanisms of CPT from microcapsules using mathematical models.
6. To analyze fitted response surface plots of observed responses using Canonical and Lagrange techniques to establish the optimal formulations from formulation studies.



## TABLE OF CONTENTS

---

<b>ABSTRACT</b> .....	<b>ii</b>
<b>ACKNOWLEDGEMENTS</b> .....	<b>iv</b>
<b>STUDY OBJECTIVES</b> .....	<b>vii</b>
<b>TABLE OF CONTENTS</b> .....	<b>ix</b>
<b>LIST OF TABLES</b> .....	<b>xv</b>
<b>LIST OF FIGURES</b> .....	<b>xvii</b>
<b>CHAPTER 1</b> .....	<b>1</b>
<b>CAPTOPRIL, AN ANGIOTENSION CONVERTING ENZYME INHIBITOR</b> .....	<b>1</b>
<b>1.1. INTRODUCTION</b> .....	<b>1</b>
<b>1.2. PHYSICOCHEMICAL PROPERTIES OF CAPTOPRIL</b>	<b>5</b>
1.2.1. Description.....	5
1.2.2. Solubility.....	5
1.2.3. Storage.....	5
1.2.4. pKa.....	6
1.2.5. Melting range.....	6
1.2.6. Optical rotation.....	6
1.2.7. Ultraviolet absorption spectrum	6
1.2.8. Polymorphism	6
<b>1.3. SYNTHETIC PATHWAY</b> .....	<b>6</b>
1.3.1. Synthetic procedure.....	6
1.3.2. Structure activity relationships.....	7
1.3.3. Stereospecificity.....	8
<b>1.4. STABILITY</b> .....	<b>8</b>
1.4.1. Solid state stability.....	8
1.4.2. Solution stability.....	8
<b>1.5. CLINICAL PHARMACOLOGY</b> .....	<b>9</b>
1.5.1. Interactions.....	9
1.5.2. Precautions.....	10
1.5.2.1. Pregnancy.....	10

1.5.2.2.	Paediatric patients.....	12
1.5.2.3.	Geriatric patients.....	12
1.5.2.4.	Smoking.....	13
1.5.2.5.	Lactation.....	13
1.5.2.6.	Food.....	14
1.5.2.7.	Renal impairment.....	14
1.5.2.8.	Adverse effects.....	14
<b>1.6.</b>	<b>CLINICAL PHARMACOKINETICS.....</b>	<b>14</b>
1.6.1.	Absorption.....	14
1.6.2.	Distribution.....	15
1.6.3.	Metabolism.....	15
1.6.4.	Excretion.....	16
<b>1.7.</b>	<b>CONCLUSIONS.....</b>	<b>16</b>
	 <b>CHAPTER 2.....</b>	 <b>18</b>
	<b>CHARACTERIZATION OF CAPTOPRIL USING NMR SPECTROSCOPY.....</b>	<b>18</b>
<b>2.1.</b>	<b>INTRODUCTION.....</b>	<b>18</b>
2.1.1.	The instrument.....	20
2.1.2.	Spectra.....	21
2.1.3.	Chemical Shifts.....	23
2.1.4.	<i>J</i> -coupling.....	25
2.1.5.	NMR.....	26
2.1.5.1.	<sup>1</sup> H and <sup>13</sup> C-MR.....	27
2.1.5.2.	DEPT-135.....	27
2.1.5.3.	COSY, HSQC and HMBC.....	28
<b>2.2.</b>	<b>EXPERIMENTAL.....</b>	<b>29</b>
2.2.1.	Materials and methods.....	29
2.2.2.	Analysis of drugs.....	29
<b>2.3.</b>	<b>RESULTS AND DISCUSSIONS.....</b>	<b>30</b>
<b>2.4.</b>	<b>CONCLUSION.....</b>	<b>37</b>
	 <b>CHAPTER 3.....</b>	 <b>39</b>
	<b>THE USE OF EXPERIMENTAL DESIGN IN THE DEVELOPMENT OF</b>	

	<b>AN HPLC METHOD WITH ELECTROCHEMICAL DETECTION FOR THE ANALYSIS OF CAPTOPRIL.....</b>	<b>39</b>
<b>3.1.</b>	<b>INTRODUCTION.....</b>	<b>39</b>
3.1.1.	Electrochemical cell design.....	41
3.1.2.	Electrochemistry.....	44
3.1.3.	Electrode material.....	47
<b>3.2.</b>	<b>METHOD DEVELOPMENT.....</b>	<b>48</b>
3.2.1.	Experimental design and statistical analysis.....	48
3.2.2.	Inspection of response surface plots.....	52
3.2.3.	Voltammetry.....	55
3.2.3.1.	Hydrodynamic voltammetry.....	56
<b>3.3.</b>	<b>LITERATURE REVIEW.....</b>	<b>57</b>
3.3.1.	Column choice.....	59
3.3.2.	Internal standard.....	61
<b>3.4.</b>	<b>METHODS.....</b>	<b>62</b>
3.4.1.	HPLC Apparatus.....	62
3.4.2.	Chemicals and reagents.....	62
3.4.3.	Preparation of stock solutions.....	63
3.4.4.	Preparation of buffers.....	63
3.4.5.	Preparation of mobile phase.....	64
<b>3.5.</b>	<b>CHROMATOGRAPHIC CONDITIONS.....</b>	<b>64</b>
<b>3.6.</b>	<b>RESULTS AND DISCUSSION.....</b>	<b>64</b>
<b>3.7.</b>	<b>CONCLUSIONS.....</b>	<b>79</b>
	<b>CHAPTER 4.....</b>	<b>81</b>
	<b>THE VALIDATION OF A HIGH PERFORMANCE LIQUID CHROMATOGRAPHIC METHOD WITH ELECTROCHEMICAL DETECTION FOR THE QUANTITATION OF CAPTOPRIL.....</b>	<b>81</b>
<b>4.1.</b>	<b>INTRODUCTION.....</b>	<b>81</b>
<b>4.2.</b>	<b>VALIDATION.....</b>	<b>82</b>
4.2.1.	Calibration, Linearity and Range.....	82
4.2.2.	Precision.....	83
4.2.2.1.	Repeatability or intra-day precision.....	83

4.2.2.2.	Intermediate Precision.....	83
4.2.2.3.	Reproducibility.....	84
4.2.3.	Accuracy and bias.....	87
4.2.3.1.	Assay.....	88
4.2.4.	Limits of quantitation and detection.....	90
4.2.5.	Specificity.....	91
4.2.6.	Robustness.....	91
<b>4.3.</b>	<b>CONCLUSIONS.....</b>	<b>92</b>
	 <b>CHAPTER 5.....</b>	 <b>93</b>
	<b>COMPATIBILITY STUDIES WITH CAPTOPRIL USING SPECTROSCOPIC AND THERMOANALYTICAL TECHNIQUES.....</b>	<b>93</b>
<b>5.1.</b>	<b>INTRODUCTION.....</b>	<b>93</b>
<b>5.2.</b>	<b>METHODS.....</b>	<b>98</b>
5.2.1.	Differential scanning calorimetry.....	98
5.2.2.	Thermogravimetric analysis.....	99
5.2.3.	Infrared spectroscopy.....	99
<b>5.3.</b>	<b>EXCIPIENTS.....</b>	<b>99</b>
5.3.1	Hydroxypropyl methylcellulose (HPMC).....	100
5.3.2.	Microcrystalline cellulose (MCC).....	100
5.3.3.	Citric acid.....	100
5.3.4.	Methacrylic acid copolymers.....	101
<b>5.4.</b>	<b>RESULTS AND DISCUSSION.....</b>	<b>101</b>
<b>5.5.</b>	<b>CONCLUSION.....</b>	<b>121</b>
	 <b>CHAPTER 6.....</b>	 <b>123</b>
	<b>THE EVALUATION OF CAPTOPRIL MICROCAPSULES MANUFACTURED USING AN OIL IN OIL SOLVENT EVAPORATION TECHNIQUE.....</b>	<b>123</b>
<b>6.1.</b>	<b>INTRODUCTION.....</b>	<b>123</b>
6.1.1.	Solvent evaporation.....	125
6.1.2.	Aim.....	129

<b>6.2.</b>	<b>EXPERIMENTAL</b> .....	<b>129</b>
6.2.1.	Materials.....	129
6.2.2.	Method.....	129
6.2.2.1.	Experimental design for response surface methodology.....	129
6.2.2.2.	Manufacture of microcapsules.....	131
6.2.2.3.	Determination of the mean particle size.....	134
6.2.2.4.	Flowability.....	134
6.2.2.4.1.	Angle of repose.....	134
6.2.2.4.2.	Bulk and tapped bulk density.....	135
6.2.2.4.3.	Hausner ratio.....	135
6.2.2.4.4.	Kawakita analysis.....	136
6.2.2.5.	Encapsulation efficiency (EE).....	137
6.2.2.6.	Scanning electron microscopy (SEM).....	137
6.2.2.7.	Drug release studies.....	137
<b>6.3.</b>	<b>RESULTS AND DISCUSSION</b> .....	<b>140</b>
6.3.1.	Particle size distribution.....	153
6.3.2.	Microencapsulation.....	154
6.3.3.	Encapsulation efficiency.....	154
6.3.4.	Flowability.....	155
6.3.5.	Scanning Electron Microscopy.....	160
6.3.6.	<i>In vitro</i> drug release.....	163
<b>6.4.</b>	<b>CONCLUSION</b> .....	<b>171</b>
	 <b>CHAPTER 7</b> .....	 <b>173</b>
	<b>MATHEMATICAL MODELING OF CAPTOPRIL RELEASE FROM MICROCAPSULES</b> .....	<b>173</b>
<b>7.1.</b>	<b>INTRODUCTION</b> .....	<b>173</b>
7.1.1.	Canonical analysis.....	175
7.1.2.	Lagrange’s criteria.....	176
7.1.2.1.	Lagrange’s criterion for four variable functions.....	176
7.1.3.	Mathematical Modeling.....	177
<b>7.2.</b>	<b>METHOD</b> .....	<b>177</b>
7.2.1.	Model Fitting.....	177
7.2.1.1.	Canonical analysis.....	177
7.2.1.2.	Lagrange’s Criterion.....	178

7.2.1.3.	Mathematical Modeling.....	179
<b>7.3.</b>	<b>RESULTS AND DISCUSSION.....</b>	<b>181</b>
7.3.1.	Canonical analysis.....	181
7.3.2.	Lagrange’s Criterion.....	185
7.3.3.	Mathematical Modeling.....	186
<b>7.4.</b>	<b>CONCLUSIONS.....</b>	<b>191</b>
	<b>CHAPTER 8.....</b>	<b>192</b>
	<b>CONCLUSIONS .....</b>	<b>192</b>
	<b>REFERENCES.....</b>	<b>196</b>
	<b>APPENDIX ONE.....</b>	<b>249</b>
	<b>APPENDIX TWO.....</b>	<b>280</b>

## LIST OF TABLES

---

<b>Table 3.1.</b>	Applications of electrochemical detection for the period 1980-2008.....	43
<b>Table 3.2.</b>	Presentation of 20 experiments (Exp 1 – 20) with coded values for factor Levels for the CCD.....	51
<b>Table 3.3.</b>	Experimental factors and levels used in the CDC.....	55
<b>Table 3.4.</b>	Summary of the published analytical methods for the determination of CPT.....	59
<b>Table 3.5.</b>	ANOVA Table for Response Surface Quadratic Model for retention time.....	72
<b>Table 3.6.</b>	ANOVA Table for Response Surface Model for retention time (model reduction).....	74
<b>Table 3.7.</b>	ANOVA Table for Response Surface Quadratic Model for peak area/height ratio.....	75
<b>Table 4.1.</b>	Linearity data.....	83
<b>Table 4.2.</b>	Intra-assay precision and accuracy data for CPT analysis (n = 6).....	85
<b>Table 4.3.</b>	Inter-day precision and accuracy data for CPT analysis.....	85
<b>Table 4.4.</b>	Inter-day precision and accuracy data for CPT analysis.....	86
<b>Table 4.5.</b>	Accuracy test results of blinded samples.....	86
<b>Table 4.6.</b>	Results of analysis of commercially available CPT products (n =5).....	89
<b>Table 5.1.</b>	Excipients used in the compatibility studies.....	102
<b>Table 5.2.</b>	IR assignments for CPT.....	115
<b>Table 6.1.</b>	Reasons for microencapsulation of API.....	124
<b>Table 6.2.</b>	Main methods of microencapsulation.....	125
<b>Table 6.3.</b>	Steps used in the microencapsulation process.....	126
<b>Table 6.4.</b>	Alternate methods to encapsulate hydrophilic drugs.....	126
<b>Table 6.5.</b>	Criteria used to select solvents for microencapsulation.....	128
<b>Table 6.6.</b>	Coded levels for independent variables used in experimental design.....	131
<b>Table 6.7.</b>	Formulations used to manufacture microcapsules.....	132
<b>Table 6.8.</b>	Summary of general dissolution conditions for basket and reciprocating cylinder dissolution test methods.....	139
<b>Table 6.9.</b>	ANOVA Table for Response Surface Quadratic Model for percent drug release.....	141
<b>Table 6.10.</b>	Response data generated for each experiment.....	157
<b>Table 6.11.</b>	Packability and flowability parameters for CPT microcapsules.....	158

<b>Table 7.1.</b>	Mathematical representation of the models used to fit CPT release from microcapsules...	180
<b>Table 7.2.</b>	Results of model fitting of release profiles.....	187



## LIST OF FIGURES

---

<b>Figure 1.1.</b>	Schematic representation of the structure of the ACE zinc ion and the bound CPT are shown in green and red, respectively.....	2
<b>Figure 1.2.</b>	Site of action of ACE inhibitors (A) and receptor blockers (B).....	3
<b>Figure 1.3.</b>	Classification of ACE inhibitors.....	4
<b>Figure 1.4.</b>	Chemical structure of CPT [C <sub>9</sub> H <sub>15</sub> NO <sub>3</sub> S] (MW = 217.3).....	5
<b>Figure 1.5.</b>	Synthesis of CPT.....	7
<b>Figure 2.1.</b>	400 MHz <sup>1</sup> H NMR spectrum of CPT in CDCl <sub>3</sub> .....	31
<b>Figure 2.2.</b>	400 MHz <sup>13</sup> C NMR spectrum of CPT in CDCl <sub>3</sub> .....	33
<b>Figure 2.3.</b>	DEPT 135 NMR spectrum of CPT in CDCl <sub>3</sub> .....	34
<b>Figure 2.4.</b>	400 MHz COSY NMR spectrum of CPT in CDCl <sub>3</sub> .....	35
<b>Figure 2.5.</b>	400 MHz HSQC NMR spectrum of CPT in CDCl <sub>3</sub> .....	36
<b>Figure 2.6.</b>	400 MHz HMBC NMR spectrum of CPT in CDCl <sub>3</sub> .....	36
<b>Figure 3.1.</b>	Schematic diagram of a Coulochem Model 5010 detector cell, showing the relative positions of the working electrode and the counter and reference electrodes.....	41
<b>Figure 3.2.</b>	Schematic diagram of a Coulochem <sup>®</sup> Model 5020 Cell showing the relative position of the electrode, counter and reference electrode.....	42
<b>Figure 3.3.</b>	Disciplines that have used ECD for the period 1980-2008.....	43
<b>Figure 3.4.</b>	Schematic diagram of processes occurring at an electrode when an analyte flows over a static electrode held at an appropriate voltage.....	46
<b>Figure 3.5.</b>	Concentration profile for an analyte near an electrode surface with laminar dynamic flow.....	47
<b>Figure 3.6.</b>	Typical hydrodynamic voltammograms used to study electrode kinetics.....	56
<b>Figure 3.7.</b>	HDV for the oxidation of CPT and CYC recorded in the potential range 0.0-1.2 V.....	65
<b>Figure 3.8.</b>	Typical HPLC chromatogram of CPT (50 µg/ml) in the presence of the I.S. CYC (20 µg/ml).....	66
<b>Figure 3.9.</b>	Contour plots for the retention time as a function of buffer pH (X-axis) and ACN concentration (Y-axis) of the mobile phase.....	67
<b>Figure 3.10.</b>	Contour plots for the retention time as a function of molarity (X-axis) and buffer pH (Y-axis) of the mobile phase.....	68

<b>Figure 3.11.</b>	Contour plots for the retention time as a function of molarity (X-axis) and ACN concentration (Y-axis) of the mobile phase.....	68
<b>Figure 3.12.</b>	Response surface plots for the retention time as a function of buffer pH (X-axis) and ACN concentration (Y-axis) of the mobile phase.....	69
<b>Figure 3.13.</b>	Response surface plots for the retention time as a function of buffer molarity (X-axis) buffer pH (Y-axis) of the mobile phase.....	69
<b>Figure 3.14.</b>	Response surface plots for the retention time as a function of buffer molarity (X-axis) and ACN concentration (Y-axis) of the mobile phase.....	70
<b>Figure 3.15.</b>	Normal probability plot of residual for retention time.....	77
<b>Figure 3.16.</b>	Plot of residual vs. predicted response for retention time.....	77
<b>Figure 3.17.</b>	Normal probability plot of residual for ratio of peak areas.....	78
<b>Figure 3.18.</b>	Plot of residual vs. predicted response for peak area ratios.....	78
<b>Figure 5.1.</b>	Differential Scanning Calorimetry.....	96
<b>Figure 5.2.</b>	A typical DSC plot for CPT determined at a heating rate of 10° C/min.....	103
<b>Figure 5.3.</b>	A typical DSC plot for CPT: HPMC K15M generated at a heating rate of 10° C/min.....	104
<b>Figure 5.4.</b>	A typical DSC plot for CPT: HPMC K100M generated at a heating rate of 10° C/min....	105
<b>Figure 5.5.</b>	A typical DSC plot for CPT: MCC generated at a heating rate of 10° C/min.....	106
<b>Figure 5.6.</b>	A typical DSC plot for CPT: Eudragit RS generated at a heating rate of 10° C/min.....	107
<b>Figure 5.7.</b>	A typical DSC plot for CPT: citric acid generated at a heating rate of 10° C/min.....	108
<b>Figure 5.8.</b>	A typical DSC plot for mixture (all excipients) generated at a heating rate of 10° C/min.....	109
<b>Figure 5.9.</b>	A typical TGA plot generated for CPT at a heating rate of 10° C/min.....	111
<b>Figure 5.10.</b>	A typical TGA plot for CPT: HPMC K15 M generated at a heating rate of 10° C/min....	111
<b>Figure 5.11.</b>	A typical TGA plot for CPT: HPMC K100 M generated at a heating rate of 10° C/min.....	112
<b>Figure 5.12.</b>	A typical TGA plot for CPT: MCC generated at a heating rate of 10° C/min.....	112
<b>Figure 5.13.</b>	A typical TGA plot for CPT: Eudragit RS generated at a heating rate of 10° C/min.....	113
<b>Figure 5.14.</b>	A typical TGA plot for CPT: citric acid generated at a heating rate of 10° C/min.....	113
<b>Figure 5.15.</b>	A typical TGA plot for mixture (all excipients used) generated at a heating rate of 10° C/min.....	114
<b>Figure 5.16.</b>	Infrared spectrum for CPT powder.....	117
<b>Figure 5.17.</b>	Infrared spectrum of a CPT: HPMC K 15M binary mixture.....	117
<b>Figure 5.18.</b>	Infrared spectrum of a binary mixture of CPT and HPMC K 100 M (1:4).....	118
<b>Figure 5.19.</b>	Infrared spectrum of a binary mixture of CPT: MCC (1:4).....	118
<b>Figure 5.20.</b>	Infrared spectrum of a binary mixture of CPT: Eudragit® RS (1:4).....	119
<b>Figure 5.21.</b>	Infrared spectrum of a binary mixture of a CPT: citric acid (1:4).....	119
<b>Figure 5.22.</b>	Infrared spectrum of physical mixture (all excipients used).....	120

<b>Figure 6.1.</b>	Schematic diagram of two types of microcapsules.....	124
<b>Figure 6.2.</b>	Schematic representation of the factors influencing the properties of Microcapsules.....	127
<b>Figure 6.3.</b>	Basic steps of microencapsulation using a solvent evaporation process.....	133
<b>Figure 6.4.</b>	Contour plots showing the effect of Eudragit® RS and Methocel® K15M on drug Release.....	145
<b>Figure 6.5.</b>	Contour plots showing the effects of Eudragit® RS and Methocel® K100M on drug Release.....	147
<b>Figure 6.6.</b>	Contour plots showing the effects of Eudragit® RS and homogenizing speed on drug release.....	147
<b>Figure 6.7.</b>	Contour plots showing the effects of Methocel® K15M and Methocel® K100M on drug release.....	148
<b>Figure 6.8.</b>	Contour plots showing the effects of Methocel® K15M and homogenizing speed on drug release.....	149
<b>Figure 6.9.</b>	Contour plots showing the effects of Methocel® K100M and homogenizing speed on drug release.....	149
<b>Figure 6.10.</b>	Response surface graph showing the effect of Eudragit® RS and Methocel® K15M on drug release.....	150
<b>Figure 6.11.</b>	Response surface graph showing the effect of Eudragit® RS and Methocel® K100M on drug release.....	150
<b>Figure 6.12.</b>	Response surface graph showing the effect of Eudragit® RS and homogenizing speed on drug release.....	151
<b>Figure 6.13.</b>	Response surface graph showing the effect of Methocel® K15M and Methocel® K100M on drug release.....	151
<b>Figure 6.14.</b>	Response surface graph showing the effect of Methocel® K15M and homogenizing speed on drug release.....	152
<b>Figure 6.15.</b>	Response surface graph representing the interaction between Methocel® K100M and Homogenizing speed.....	152
<b>Figure 6.16.</b>	Schematic representation of a solvent diffusion and evaporation.....	159
<b>Figure 6.17.</b>	SEM of a microcapsule from batch CPT-002.....	161
<b>Figure 6.18.</b>	SEM of a microcapsule from batch CPT-006.....	161
<b>Figure 6.19.</b>	SEM of a microcapsule from batch CPT-009.....	161
<b>Figure 6.20.</b>	SEM of a microcapsule from batch CPT-015.....	161
<b>Figure 6.21.</b>	SEM of a microcapsule from batch CPT-020.....	162
<b>Figure 6.22.</b>	SEM of a microcapsule from batch CPT-025.....	162
<b>Figure 6.23.</b>	SEM of a microcapsule from batch CPT-030.....	162
<b>Figure 6.24.</b>	SEM of a microcapsule from batch CPT-029.....	162
<b>Figure 6.25.</b>	SEM of a microcapsule from batch CPT-022.....	163
<b>Figure 6.26.</b>	Cumulative % drug released for CPT-002 (mean $\pm$ SD, n = 3).....	166

<b>Figure 6.27.</b>	Cumulative % drug released for CPT-006 (mean $\pm$ SD, n = 3).....	166
<b>Figure 6.28.</b>	Cumulative % drug released for CPT-009 (mean $\pm$ SD, n = 3).....	167
<b>Figure 6.29.</b>	Cumulative % drug released for CPT-015 (mean $\pm$ SD, n = 3).....	167
<b>Figure 6.30.</b>	Cumulative % drug released for CPT-020 (mean $\pm$ SD, n = 3).....	168
<b>Figure 6.31.</b>	Cumulative % drug released for CPT-025 (mean $\pm$ SD, n = 3).....	168
<b>Figure 6.32.</b>	Cumulative % drug released for CPT-029 (mean $\pm$ SD, n = 3).....	169
<b>Figure 6.33.</b>	Cumulative % drug released for CPT-030 (mean $\pm$ SD, n = 3).....	169
<b>Figure 6.34.</b>	Cumulative % drug released for CPT-008 (mean $\pm$ SD, n = 3).....	170

## CHAPTER 1

---

### CAPTOPRIL, AN ANGIOTENSION CONVERTING ENZYME INHIBITOR

#### 1.1. INTRODUCTION

Hypertension is a risk factor in the development of cardiovascular disease and is responsible for more deaths worldwide than any other cardiovascular disease (1, 2). The angiotensin I (AI) converting enzyme is a causal factor for hypertension and facilitates the production of angiotensin II (AII) that causes vasoconstriction and degradation of the vasodilating compound, bradykinin. Therefore, inhibition of angiotensin converting enzyme (ACE) is considered an important therapeutic approach in the control of hypertension. With the development of a model structure of ACE, specific inhibitors that bind to the active site of the enzyme active have been developed (3). Despite the fact that synthetic inhibitors of the ACE are remarkably effective as antihypertensive drugs, they often cause adverse and unwanted side effects (1).

In the 1960s, Vane was actively investigating the cause(s) of hypertension and Ferreira, a member of the research team, had an extract of the bradykinin potentiating factor (BPF) isolated from the venom of the Brazilian viper *Bothrops jararaca*. Ferreira had already established that BPF potentiated the activity of bradykinin through inhibition of the enzyme that deactivated it. The BPF was tested on ACESQ 881 and found to be a potent inhibitor thereof, precipitating a strong interest in the use of the ACE inhibitor for the management of hypertension (4).

In order to elucidate the properties of other ACE molecules, other peptide analogs were used (5-7). There are two forms of ACE in humans, the ubiquitous somatic ACE and the sperm-specific germinal ACE, both encoded by the same gene through transcription from alternative promoters (8).

The crystal structures of the ACE were determined using a multiple isomorphous replacement technique at a resolution of 2.4 Å. ACE is 615 amino acids long and is structurally comprised of 21  $\alpha$ -helices and three antiparallel  $\beta$ -strands (Figure 1.1).

Captopril (CPT) is a competitive inhibitor of the ACE, and binds to human ACE with an enzyme affinity ( $K_i$ s) of 1.4 which mimics the two carboxy-terminal residues of the enzyme substrate (9, 10). The sulfhydryl functional group of CPT replaces the zinc-binding water molecule and directly interacts with the zinc ion in a distorted tetrahedral geometry as shown in Figure 1.1 b. The carboxy-end of the proline moiety is held in place by three highly conserved residues *viz.*, Gln-265, Lys-495 and Tyr-504, through ionic and hydrogen bonding. The residues prevent sliding of the substrate from the catalytic site in the large internal channel of the enzyme. Locking mechanisms of this type may slip when the negative charge of the carboxy terminus is masked by amidation. For most substrates the ACE cleaves the carboxy-terminal dipeptide and can hydrolyze three amino acids from substance P and luteinizing releasing hormone where the carboxy-termini are also modified by amidation (11). The sulfhydryl functional group and the terminal proline moieties of CPT are connected by a peptide bond. The position of the carbonyl oxygen of the peptide bond is locked by three hydrogen bonds of significant strength with residues His-337, His-497 and Tyr-507 (11).

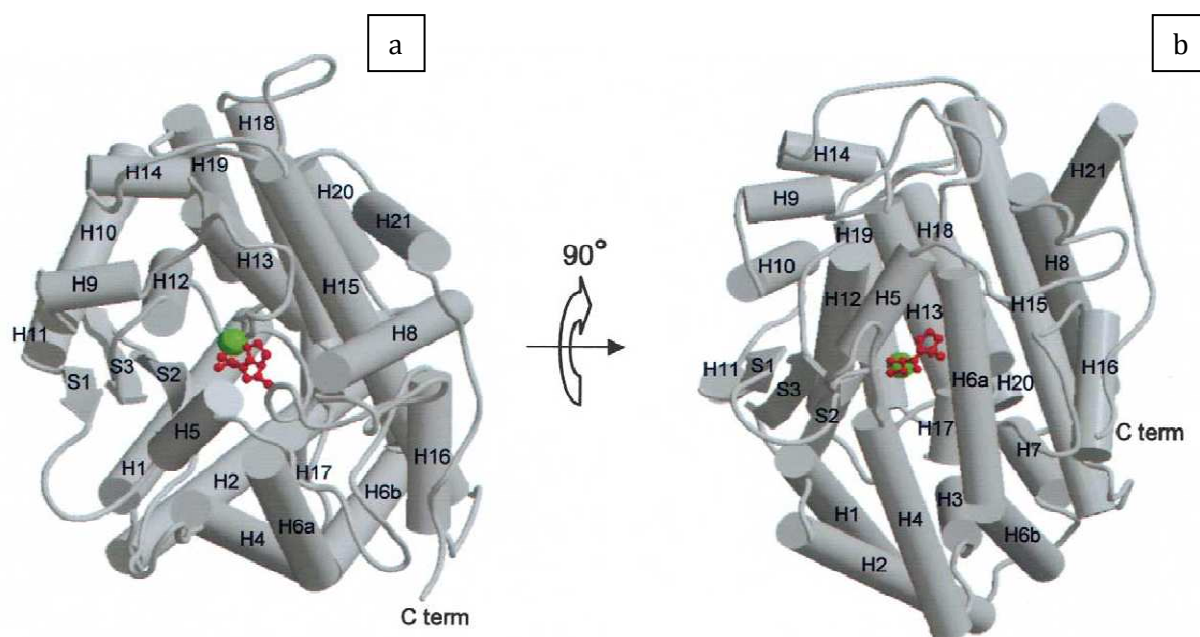


**Figure 1.1 (a, b).** Schematic representation of the structure of the ACE zinc ion and the bound CPT are shown in green and red, respectively (11).

The ACE has a large internal channel encompassing throughout the protein molecule and this highly unusual substrate-binding channel is comprised of two chambers, similar to a peanut shell. The zinc ion which is critical for catalysis is located in a narrow bottleneck that connects the two chambers.

The ACE plays a critical role in cardiovascular functioning and cleaves the carboxy terminal His-Leu dipeptide from AI to produce a potent vasopressor octapeptide, AII (Figure 1.2). ACE inhibitors are a first line of therapy for the treatment of hypertension, heart failure, myocardial infarction and diabetic nephropathy (11). Interestingly, the ACE inhibitors were developed without any knowledge of the molecular structure of human ACE, and rather on the basis of an assumed mechanistic homology of the enzyme with carboxypeptidase A (11-13).

CPT is routinely used in the management of hypertension and is commercially available as immediate release tablets ranging in dose from 12.5-50 mg (14). The acceptance of CPT inspired the development of a new generation of ACE inhibiting molecules as the ACE was a well-validated therapeutic target.

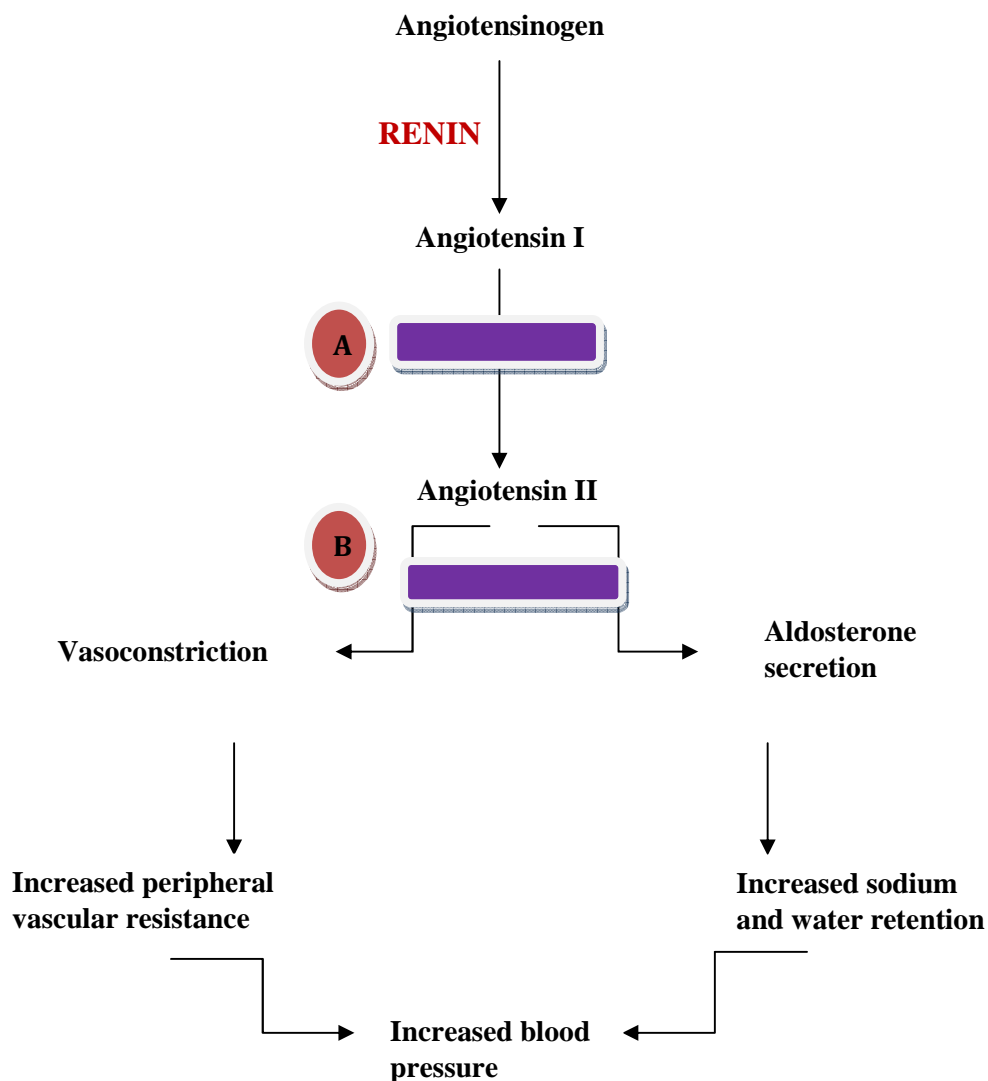


**Figure 1.2.** Site of action of ACE inhibitors (A) and receptor blockers (B) (adapted from 16).

CPT has been widely used for the treatment of hypertension and congestive heart failure and has a short elimination half-life following oral administration. Consequently, CPT may be a suitable candidate for inclusion in sustained release dosage forms. The development of a once daily CPT formulation for oral administration would be a significant advantage in the promotion of patient adherence. Furthermore, the added advantage of a minimization of side effects and reduced fluctuations in blood levels on long term therapy may well result in better therapeutic outcomes (7). Attempts have been made to design long acting technologies for the delivery of CPT and have taken the form of sustained or controlled release dosage forms (15).

Current hypertension guidelines differ in their recommendations for first line antihypertension therapy. In a study done in Canada, it was observed that prescribing ACE inhibitors as first line therapy in patients without cardiovascular morbidity could not be recommended (17). In South Africa, ACE inhibitors have proved to be effective blood lowering agents with an excellent tolerability profile. ACE inhibitors available in South Africa have been classified by means of the system Objectified Judgement Analysis (SOJA) method (18). In general, there are three classes of ACE inhibitors (Figure 1.3) based on their chemical composition, namely, sulfhydryl-containing inhibitors exemplified by CPT, dicarboxylate-containing inhibitors exemplified by enalapril and phosphonate-containing inhibitors exemplified by fosinopril.

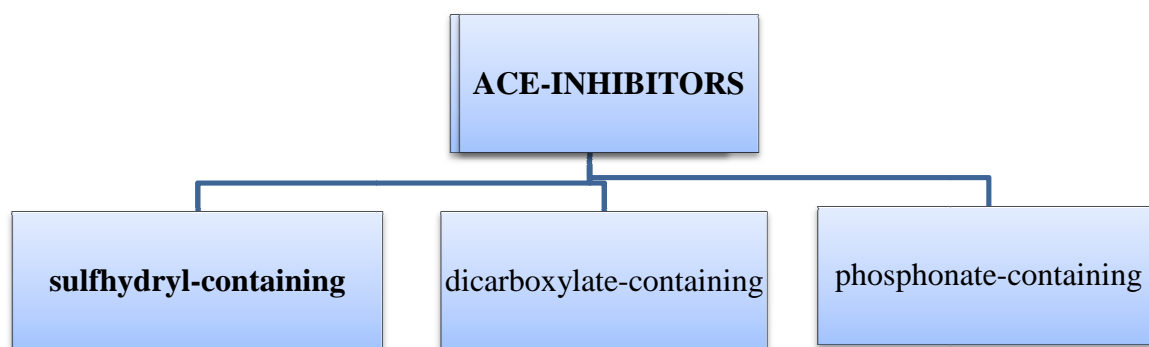


**Figure 1.3.** Classification of ACE inhibitors

CPT and fosinopril are the lone representatives of their respective chemical sub-classifications whereas the majority of the inhibitors contain the dicarboxylate functionality. All of these compounds effectively block the conversion of AI to AII and have similar therapeutic and physiological effects to each other. The compounds differ primarily in their potency and pharmacokinetic profiles.



## 1.2. PHYSICOCHEMICAL PROPERTIES OF CAPTOPRIL

### 1.2.1. Description

Captopril is known as 1-[3-mercapto-2-(*S*)-methyl-1-oxopropyl]-*S* (L) proline (19, 20) and is a crystalline powder that occurs as white crystals. The crystalline powder has a slight sulfurous odour. It contains not less than 98.0% and not more than 102.0% of CPT calculated on an anhydrous basis (20).

The chemical structure of CPT (21) is depicted in Figure 1.4.

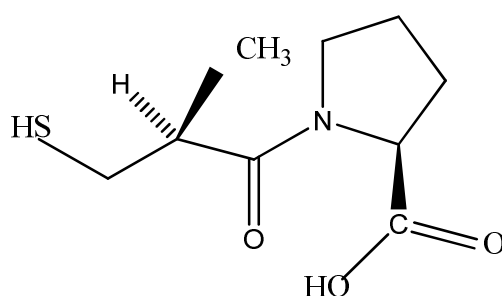


**Figure 1.4.** Chemical structure of CPT [C<sub>9</sub>H<sub>15</sub>NO<sub>3</sub>S] (MW = 217.3)

Despite the fact that CPT has two stereogenic centres, the molecule was developed and is marketed as a single enantiomer, as only one of the four possible isomers can bind with the active site of ACE (20).

### 1.2.2. Solubility

CPT has an aqueous solubility of 160 mg/ml at 25 °C (22) and solubility versus temperature is linear up to 40 °C, above which CPT shows extraordinarily high water solubility. CPT is freely soluble at >100 mg/ml in methanol, ethanol, isopropanol, chloroform, or methylene chloride but its solubility in oils is less than 1 mg/ml at 25 °C (22).

### 1.2.3. Storage

CPT should be stored at room temperature in tightly closed containers and protected from light, moisture and heat (23).

#### **1.2.4. pKa**

CPT is a weakly acidic compound, whereas all other ACE inhibitors are amphoteric in nature. The carboxylic acid functional group attached to the pyrrolle ring is a common structural feature of ACE inhibitors. CPT has a pKa in the range of 2.5-3.5 and is ionized at physiological pH. The pKa and ionization of the secondary amine present in the dicarboxylate chain depends on the adjacent functional group and whether it is in the product or active form (24).

#### **1.2.5. Melting range**

CPT melts over a 1-3 °C temperature range at between 106-109 °C (25).

#### **1.2.6. Optical rotation**

The optical rotation of CPT in ethanol was  $\alpha_D^{25} = -127.8^\circ$ . The R, S isomer rotates approximately  $+5^\circ$  (22).

#### **1.2.7. Ultraviolet absorption spectrum**

A solution of CPT in methanol, water, 0.1 M sodium hydroxide and 0.1 M hydrochloric acid yield two wavelengths of maximum absorption, which occur at around 200 nm (due to the thiol functional group) and 225 nm (due to weak sulfhydryl absorption) (22).

#### **1.2.8. Polymorphism**

An unstable, low (86° C) melting and stable, high (106° C) melting form of CPT have been observed) (22).

### **1.3. SYNTHETIC PATHWAY**

#### **1.3.1. Synthetic Procedure**

Chirumamilla *et al* (26) have used chiral intermediates in the synthesis of CPT. These intermediates were obtained by resolution of racemic compounds or by chemical, biocatalytic methods and or by asymmetric synthesis by biochemical process (26). The synthesis of CPT with 3-acetylthio-2-methylpropanoic acid as the starting material was first reported by Cushman *et al* (27) and the resultant overall yield was approximately 12%. More recently, a simple synthetic procedure for CPT has been reported (28). The resultant yield from this synthesis was approximately 26%, however, the conversion of methacrylic acid to the optically active starting material, R-3-hydroxy-2-methylpropanoic acid, using a microbial

oxidative transformation, was poor (29, 30). A more convenient synthetic procedure for CPT using methacrylic acid as a starting material is shown in Figure 1.5 (31).

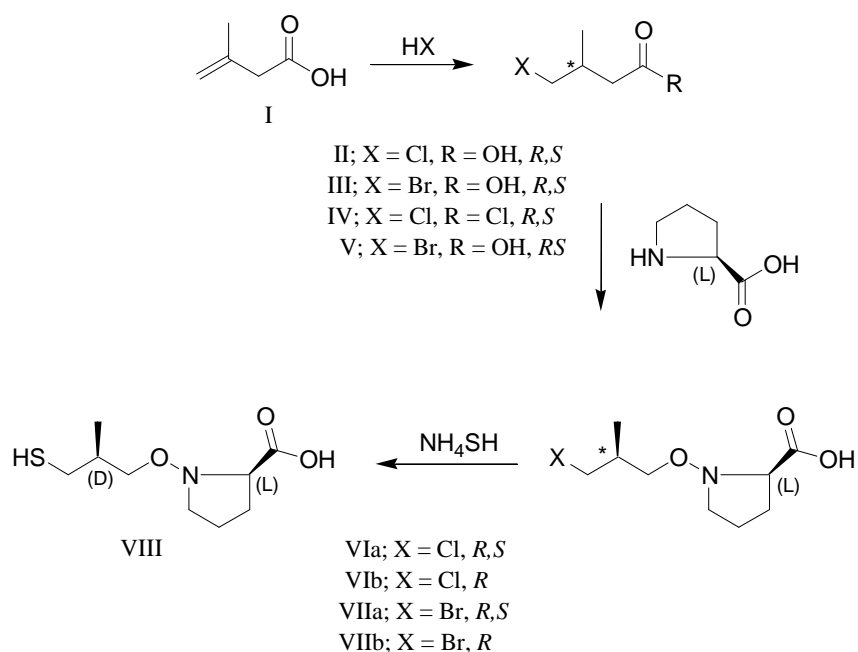


**Figure 1.5.** Synthesis of CPT (31)

In order to develop a more reliable synthetic procedure for CPT with, methacrylic acid as the starting material, Groszkowski *et al* added a hydrogen halide (32). The carboxylic acids **II** and **III** were converted to their corresponding acyl halides **IV** and **V** in nearly 95% yields, using *N,N*-dimethylformamide as the catalyst (33). To avoid protection of the carboxylic acid function of L-proline with **IV** or **V**, a procedure defined by Hongo *et al* was used with a resultant 90% yield (34). *N*-(*R,S*-3-Halogeno-2-methylpropanoyl)-L-proline (**VIa** or **VIIa**) was then separated into optically pure diastereoisomers using dicyclohexylamine. The treatment of the halides of **VIb** or **VIIb** with methanolic ammonium hydrosulfide produced a 28% overall yield of CPT. This synthetic procedure is an improvement over that reported by Cushman *et al* (27) and is more convenient than the method reported by Shimazaki *et al* (28) which also involves a fermentation step.

### 1.3.2. Structure Activity Relationships

ACE is a stereoselective drug target and the currently approved ACE inhibitors act as either di- or tripeptide substrate analogs. Consequently, their stereochemistry must be consistent with the L-amino acids present in their natural substrates. This criterion was established early in the development of ACE inhibitors when compounds with carboxyl-terminal D-amino

acids were discovered to be very poor inhibitors of the enzyme (35, 36) and this was subsequently confirmed by Patchett *et al* (37) and a 100- to 1000-fold loss in inhibitor activity whenever the configuration of the carboxylate was altered (35).

CPT was introduced as a useful and popular orally active antihypertensive agent, and the proof of principle demonstrating that a peptidomimetic inhibitor of the rennin-angiotensin-aldosterone system would be an excellent way to control hypertension, is a remarkable milestone in drug discovery. In order to enhance therapy, ACE inhibitors can be combined with diuretics to produce a synergistic control of blood pressure (38).

### **1.3.3. Stereospecificity**

CPT has two chiral centres, one associated with the proline moiety and the other associated with the 3-mercapto-2-methylpropionic acid side chain. Accordingly, there are three other possible stereoisomers of which *S*-captopril is biologically active and *R*-captopril, 1-[3-mercapto-2(*S*)-methyl-1-oxopropyl]-*R* (*D*)-proline possesses no inhibiting activity for the ACE (39).

Some commonly used drugs used in human medicine are chiral in nature and are sold as racemic mixtures (40). CPT is manufactured and commercially available as an *S, S* stereoisomer (40).

## **1.4. STABILITY**

### **1.4.1. Solid state stability**

No significant decomposition of CPT was observed in bulk samples when stored at 5 °C, 33 °C and 50 °C for up to 6 months or when exposed to 900 foot-candles in a light box for 30 days, when compared to samples stored at -20°C samples and which were used as the control (22).

### **1.4.2. Solution stability**

CPT undergoes a first order free radical oxidation in aqueous solution to yield captopril disulfide (41). CPT is stable at pH 1.2 and as the pH increases the stability decreases (42, 43). CPT oxidation may be reduced by addition of chelating agents and antioxidants to solution or by use of nitrogen or low oxygen headspace in containers (44).

## **1.5. CLINICAL PHARMACOLOGY**

CPT reduces blood pressure in human patients with low, normal, and high renin levels that present with essential hypertension and in patients with renovascular hypertension and hypertension associated with chronic renal failure. In hypertensive patients with high plasma renin activity, CPT exerts most of its pharmacological effects through inhibition of ACE. The exact mechanism by which CPT reduces high blood pressure associated with low or normal plasma renin-angiotensin (PRA) is not known, but it is clear that CPT does not act on an overactive PRA system in these cases. The antihypertensive effect of CPT is enhanced when it is given in combination with a diuretic or following salt depletion (45).

The sulfhydryl functional group in the CPT is essential for the excellent inhibitory activity of ACE, but is however also the reason for the two most common side effects; skin rashes and taste disturbances such as a metallic aftertaste or loss of taste. These side effects usually subside after a reduction in the dose or discontinuation of CPT use. The side effects are similar to those observed for penicillamine that is used to treat Wilson's disease and rheumatoid arthritis and where a sulfhydryl functional group is present (46, 47).

### **1.5.1. Interactions**

It had been established that the simultaneous administration of CPT with commonly used non-steroidal anti-inflammatory drugs (NSAID) such as diclofenac sodium, flurbiprofen, mefenamic acid, meloxicam and tiaprofenic may alter the antihypertensive effect of CPT. In order to establish the kinetic and thermodynamic behavior of CPT in the presence of NSAID's, studies were performed in buffers of pH 4.0, 7.4 and 9.0 at 37 °C and at higher temperatures. The studies revealed that most of the NSAID bind to CPT, forming charge-transfer complexes that are likely to decrease the availability of CPT and therefore concurrent administration of NSAID with CPT should be avoided (48).

The effects of CPT on serum digoxin concentrations were studied in patients with severe congestive heart failure. Serum digoxin concentrations were measured prior to and following administration of CPT for 1 week in patients on chronic digoxin therapy. Each patient that was taking 0.25 mg of digoxin four times a day orally was administered 12.5 mg of CPT three times a day for 7 days, also orally. The peak serum concentration of digoxin ( $C_{max}$ ) prior to and following CPT administration were 1.7 ng/ml and 2.7 ng/ml, the time to peak ( $t_{max}$ ) was 2.4 h and 1.3 h, and the area under the 24 h digoxin concentration-time curve

(AUC<sub>0-24h</sub>) was 30.0 ng. h/ml and 41.7 ng. h/ml on days 0 and 7 respectively. It is clear that CPT causes an increase in the peak serum concentration and the area under the digoxin concentration-time curve and the time to peak is reduced. However, no patients developed or showed evidence of digoxin toxicity. The concomitant administration of CPT and digoxin increases serum digoxin concentrations in patients with severe congestive heart failure (49). In this study, there was evidence of a direct pharmacokinetic captopril-digoxin interaction.

H<sub>2</sub>-receptor antagonists block gastric acid secretions and some cardiovascular effects of histamine presence. In view of this fact, the simultaneous administration of CPT and H<sub>2</sub>-receptor antagonists may alter the antihypertensive effect of CPT, and combination therapy should be avoided. However, in healthy subjects, cimetidine administration did not affect the pharmacokinetic parameters of unchanged CPT or the inhibition of plasma ACE activity (50).

In other studies, *in vitro* availability studies of CPT in the presence of commonly used H<sub>2</sub>-receptor antagonists such as cimetidine, ranitidine and famotidine was performed in buffers of pH 4.0, 7.4 and 9.0 at 37 °C. These studies clearly indicate that most of the H<sub>2</sub>-receptor antagonists bound to CPT, forming charge-transfer complexes. As a result, the availability of CPT was affected by the concurrent administration of H<sub>2</sub>-receptor antagonists and co-administration of the drugs should be avoided (51).

The administration of an aluminium/magnesium containing antacid reduced the bioavailability of unchanged CPT by approximately 45 % in healthy individuals; therefore co-administration should be avoided (52).

## **1.5.2. Precautions**

### **1.5.2.1. Pregnancy**

The widespread availability and use of ACE inhibitors has resulted in numerous reports on their effect during pregnancy (53-57). The administration of CPT during pregnancy in experimental animals is associated with an increase in the number of stillbirths and a high incidence of intrauterine death (53, 54). CPT use during pregnancy is therefore opposed, as adverse toxic effects on the foetus have been reported (55). Intrauterine growth retardation, respiratory and circulatory abnormalities and patent ductus arteriosus have been reported in children whose mothers were treated with CPT whilst they were pregnant (56, 57). The

mechanism underlying the toxic effects of CPT on the foetus has not yet been elucidated; however, a decreased maternal and foetal placental blood flow appears to be an important consideration (58, 59). CPT-induced foetal toxicity may be explained by a decrease in AII levels leading to a reduction in uterine blood flow (60) and consequently foetal oxygen deprivation (58). Similarly, the toxic effect of CPT may also be a consequence of the decreased formation of AII on the foetal side of the placental circulation. It has been concluded that the toxic effects of CPT may be due to a reduction of foetal placental blood flow via a potentiation of the vasoconstrictor effect of endogenous bradykinin, an effect likely to be mediated via the release of prostanoids (61).

Although the deleterious effects of ACE inhibitors on foetal development may be dependent on the stage of pregnancy in which CPT is used, the foetal effects of their use during the first trimester of pregnancy remains controversial. In a survey of Michigan Medicaid recipients, there was no association between the use of ACE inhibitors during the first trimester of pregnancy and congenital foetal defects (62). The absence of firm evidence for a teratogenic effect of ACE inhibitors has prompted some investigators to state that it would not be appropriate to terminate pregnancy due to CPT exposure early in pregnancy (63). The adverse foetal effects may be a consequence of the pharmacologic effect of ACE inhibitors and not a result of any dysmorphogenic or genetic effect. However, there are several reports of malformed fetuses in mothers who have used ACE inhibitors during the first trimester of pregnancy. The foetal effects noted include phocomelia, death, omphalocele, congenital heart defects, hypertrichosis, growth retardation, respiratory failure, renal failure, and intraventricular hemorrhage (64-66). The interpretation of these observations and the role of early first trimester ACE inhibitor administration is confounded by the fact that use of such drugs often occurs throughout pregnancy and was not limited to use in the first trimester. Furthermore, virtually all mothers were taking other medications in addition to the ACE inhibitors during their pregnancy.

The use of ACE inhibitors during the second or third trimesters of pregnancy is believed to have adverse effects on the foetus (67). The most commonly reported adverse effects of ACE inhibitors taken during these stages of pregnancy include intrauterine growth retardation, neonatal hypotension, renal failure, oligohydramnios and patent ductus arteriosus (64-67).

### **1.5.2.2. Paediatric patients**

Preterm infants with renovascular hypertension and treated with CPT, developed significant trilineage bone marrow suppression (68). CPT-associated pancytopenia is a rare complication that was thought to be dose-related and caused by accumulation of the drug through defective renal tubular excretion. However, it appears that the combination of renal artery stenosis and renal tubular dysfunction of premature infants may have caused pancytopenia. CPT should be used with caution in premature and newborn infants that have underlying renal or renovascular disease, even if overt renal dysfunction is not evident. The monitoring of creatinine clearance or free serum CPT levels may help establish the degree of accumulation of CPT before the manifestation of pancytopenia (68).

The safety and efficacy of CPT therapy in children with severe and refractory hypertension has been evaluated in a collaborative international study which enrolled a group of 73 patients, 15 years of age or younger. Most patients had hypertension associated with renal disease or vascular abnormalities. CPT was administered for periods of less than 3 months to more than 1 year. A significant decrease in both systolic and diastolic blood pressures was produced by the administration of CPT, usually in conjunction with other antihypertensive agents (most commonly diuretics and/or beta-blockers). CPT was demonstrated to be an effective and safe drug for the treatment of children with severe hypertension (68).

### **1.5.2.3. Geriatric patients**

The safety and efficacy of CPT in geriatric patients with mild to moderate hypertension was examined in an eight-week multicenter study that included 99 patients. Following a placebo period, patients were treated with 25 mg of CPT twice daily. Patients who were uncontrolled after two weeks of active therapy were randomly selected to receive either 25 mg CPT and 15 mg hydrochlorothiazide or 50 mg of CPT twice daily. The average decrease in blood pressure on completion of study completion was 16.9/11.9 mmHg for the diastolic and systolic pressures respectively. At the conclusion of the trial, 75.8% of patients had responded positively to CPT. Furthermore, the CPT was well tolerated and believed to be a good therapeutic alternative for treating hypertension in the elderly population (69).



#### **1.5.2.4. Smoking**

A study was conducted to assess whether an interaction exists between the renin-angiotensin system and the sympathetic nervous system at the level of the adrenal medulla in human subjects that smoked. Thirteen habitual smoking volunteers were studied in a randomized, single-dose, double-blind, cross-over fashion using 50 mg CPT versus placebo followed by smoking of two high nicotine content cigarettes within 15 min of the dose. Blood samples were withdrawn before, during and after smoking. It was found that the increase in the concentration of plasma adrenaline during cigarette smoking was modest. There was no difference in the adrenaline levels in all subjects. Thus, the adrenaline response to cigarette smoking was not reduced by acute blockade of the production of AII. A significant increase in heart rate and blood pressure was found in the subjects. The plasma renin concentration increased significantly during CPT treatment, whereas it decreased throughout the study period in the placebo phase. Plasma AII concentrations decreased in both the CPT and placebo groups throughout the study period, but this effect was more pronounced during CPT treatment. In conclusion, cigarette smoking-induced activation of the sympathetic nervous system was not affected by acute ACE-inhibition with CPT. This is an indication that AII does not facilitate smoking-induced activation of sympathoadrenal activity in humans (70).

#### **1.5.2.5. Lactation**

In a study of 12 normotensive lactating women who were given 100 mg of CPT three times daily, for 7 doses, the mean  $C_{max}$  for CPT in breast milk was  $4.7 \pm 0.7$   $\mu\text{g/ml}$ . The mean area under the curve ( $AUC_{0-8hr}$ ) for CPT in blood was 1067.2  $\text{ng}\cdot\text{hr}/\text{ml}$ , while that for milk was 22.9  $\text{ng}\cdot\text{hr}/\text{ml}$  (71). Therefore, the concentration of CPT in milk was 1% of that found in the blood, and the peak milk concentration occurred much later than the time-to-peak blood concentration of CPT. The area under the milk concentration versus time curve was about 3% of that under the blood curve. Based on these findings, the American Academy of Paediatrics suggests that CPT is suitable for use in patients who wish to breast feed (71).

In another study (72), thorough investigation of CPT in human plasma and breast milk demonstrated a delayed excretion of CPT in the milk, with levels in the range of 0.6% of the maternal plasma levels. This study suggested selective restriction of the passage of CPT from blood into milk and "safe" levels for breast-feeding despite a relatively high daily dose of 300 mg per day.

#### **1.5.2.6. Food**

The presence of food in the GI tract has been reported to reduce the absorption of CPT by approximately 30 to 40%. Although more recent investigations suggest that food is unlikely to significantly alter the effects of CPT, it is advisable to administer the drug one hour before or two hours after meals. Food does not appear to alter the absorption of most of the other angiotensin converting enzyme inhibitors (73).

#### **1.5.2.7. Renal impairment**

The major route of elimination of CPT is via urinary excretion and it would be expected that the diminished renal function that is often associated with severe hypertension and congestive heart failure would prolong the elimination half-life of CPT (74-76). The inhibition of ACE activity by CPT has been shown to be prolonged in patients with renal dysfunction as compared to that observed in healthy subjects (77). Therefore there is a need to reduce the dose of CPT when treating patients with renal failure (78).

#### **1.5.2.8. Adverse effects**

CPT generally is well tolerated, and side effects are usually mild and transient. A dry, persistent cough has been reported commonly with the use of CPT. Coughing resolves after discontinuing the drug. Other side effects include abdominal pain, constipation, diarrhea, rash, dizziness, fatigue, headache, loss of taste, loss of appetite and numbness or tingling in the hands or feet. CPT may cause kidney failure and increased levels of potassium in the blood. Serious but fortunately very rare side effects are liver failure and angioedema (1-3).

### **1.6. CLINICAL PHARMACOKINETICS**

#### **1.6.1. Absorption**

CPT is rapidly absorbed and blood levels of the drug are detected 15 minutes after oral dosing (22). These findings are similar to those in reports that suggest that the onset of antihypertensive activity occurs as soon as 15 minutes after a single dose of CPT to hypertensive patients. CPT has a relatively short half-life in plasma with estimates in humans ranging from 1.6 to 1.9 h (22). Approximately 70% of an ingested oral dose is absorbed in healthy fasting human subjects, and an absolute bioavailability of 60% has been reported when compared to an IV dose (16).

Kripalani *et al* (79) reported the possibility that CPT may exhibit complex nonlinear pharmacokinetics, yet this phenomenon has not been reported by other authors (14, 20, 21). A single-dose pharmacokinetic study of CPT given in either a 25 or 50 mg dose to a group of 12 volunteers was undertaken. CPT has been shown to be rapidly absorbed and a  $C_{max}$  was observed 0.5-1.0 h following oral administration. Doubling the dose from 25 to 50 mg resulted in a  $C_{max50}/C_{max25}$  of 1.914 suggesting that CPT does not exhibit dose dependent or non-linear kinetics. After reaching peak concentration, blood levels of CPT declined rapidly and were generally undetectable at 6-8 h post-dose (80).

### **1.6.2. Distribution**

CPT readily binds to serum albumin and other plasma proteins (81). The drug also forms mixed disulphides with endogenous thiol-containing compounds such as cysteine and glutathione in addition to forming a disulphide dimer of the parent compound. These components in blood and urine are measured collectively as total CPT. Since the formation of these inactive disulphides is reversible, the total amount of CPT may serve as a reservoir of the pharmacologically active moiety and thus contribute to a duration of action that is longer than that predicted by the blood concentration of unchanged CPT. To measure free or unchanged concentrations of CPT, a chemical stabiliser must be added to biological samples to prevent the formation of disulphides of CPT, *ex vivo*. Following IV administration of CPT intravenously to healthy subjects, the total body clearance of CPT and steady-state volume of distribution was about 0.7 L/h/kg and 0.8 L/kg respectively. In healthy subjects, peak blood concentrations are reached about 45 to 60 minutes after oral administration. The bioavailability of CPT is altered neither in patients of different ages nor those who are taking concomitant medications including diuretics, procainamide, allopurinol, cimetidine or digoxin (81, 82).

### **1.6.3. Metabolism**

CPT is mainly eliminated by metabolism and its bioavailability is 65 %. Methylation is one of the major metabolic routes of CPT and the variability may contribute to the modulation of the intracellular concentration of CPT (83-85). The liver is the primary site of captopril methylation, whereas the intestine plays only a minor role. The kidney may also contribute to the excretion of CPT (84, 86). The methyltransferase enzyme in human red blood cells (RBC) has been implicated in the *S*-methylation of CPT (83). The rate of methylation of CPT ranged over one order of magnitude in the liver and kidney. In the human liver, the mean rate of CPT

methylation was greater in women than in men, whereas in the kidney no differences in metabolism based on the sex of the volunteers was observed, and the mean rate of methylation for all cases was  $47 \pm 23$  pmol/min/mg (83).

#### **1.6.4. Excretion**

The concentration of CPT in blood and urine of healthy subjects and patients with chronic renal failure following oral administration of 50 mg were determined by high-performance liquid chromatography. The maximum blood concentration of free CPT in healthy subjects was observed within 1 hour of administration and was not detectable 6 hours after dosing and 41% of administered CPT was excreted in the urine as free CPT and metabolic products within 2 hours of dosing and 58% was excreted within 6 hours. In patients with chronic renal failure, an average serum creatinine of 5.1 mg/dl was observed and the absorption rate constant ( $k_a$ ),  $C_{max}$  and AUC were not significantly different from those observed in normal subjects. However, the elimination rate constant ( $k_e$ ) and biological half-life ( $t_{1/2}$ ) revealed that the elimination of CPT from the plasma would be delayed. The cumulative amount of drug excreted in the urine as CPT and metabolic products were decreased at 2, 4, and 6 hours in patients with chronic renal failure. Consequently, impaired renal function is an important factor in the retention of CPT in the blood (87).

The elimination half-life of unchanged CPT was approximately 2 hours. The primary route of elimination of CPT is via the kidney. The renal clearance of unchanged CPT exceeds the glomerular filtration rate, due to active tubular secretion of the drug (81, 82).

### **1.7. CONCLUSIONS**

CPT is an orally effective AI converting enzyme inhibitor and is used for the treatment of hypertension and congestive heart failure. CPT has a relatively short elimination half-life in plasma. It is considered a drug of choice in antihypertensive therapy due to its effectiveness and low toxicity. It is usually prescribed to patients who are chronically ill and require long-term therapy. The development of a once or twice daily oral formulation of CPT would be a significant advantage for the promotion of patient adherence, and in addition, the side effects of the drug would be minimized as a result of reduction of concentration fluctuations in the blood on long term therapy (7, 19). More particularly, some of the challenges would be to formulate a dosage form that may improve the taste, odour of CPT and enhance its release. An approach to use CPT loaded microcapsules which will maintain a constant therapeutic

concentration and reduce the number of times the drug must be taken will be prepared using a range of polymers.

### CHARACTERIZATION OF CAPTOPRIL USING NMR SPECTROSCOPY

#### 2.1. INTRODUCTION

Half a century ago, nuclear magnetic resonance (NMR) spectroscopy was first introduced as an analytical tool for structure elucidation of small organic molecules (88). Since then, NMR spectroscopy has evolved at a tremendous pace and the technique has subsequently been applied in the fields of inorganic chemistry, structural biology and medicine (88). Recent improvements in sensitivity (88) have ensured that NMR spectroscopy has become an important technique in structural-based drug design and drug discovery, and it has shown its potential for playing a greater role in the pharmaceutical industry (88, 89). Whilst the reproducibility of NMR spectroscopic methods is undoubtedly very high, the European Pharmacopoeia limits the use of NMR to the identification of drugs and reagents (88).

NMR is being increasingly applied to study the properties and quality control of drugs (90). To date, no data have been published on the analysis of CPT Active Pharmaceutical Ingredient (API) by physical methods such as NMR. NMR offers high speed analysis and is sufficiently informative to judge both the structural and quality attributes of the substance undergoing analysis (91). During the last years, NMR spectroscopy and NMR imaging (magnetic resonance imaging, MRI) have been used to monitor drug delivery system performance *in vitro* and *in vivo*. However, the high installation and running costs of superconducting magnet technology limits the application range and prevents the further spread of this technology (92).

Advanced NMR spectrometers with proton resonance frequencies of 300 MHz and higher have been used in analytical practice to study low density lipoproteins (LDL) (93), carbohydrates (94-96), enalapril (97), lisinopril (98), ramipril (99), quinapril (100), perindopril (101) and benazepril (102-105). This has also been used in analytical procedures to study angiotensin II receptor antagonists such as valsartan (106), losartan (107), irebesartan (108), telmisartan (109), candesartan (110) and eprosartan (111).

The first and most obvious advantage of NMR at higher magnetic fields is the greater potential for intrinsic separation of resulting resonances. The chemical shift that occurs

following application of the magnetic field is unaffected by changes in spectrometer magnetic field-strength ( $B_0$ ) and the resonant frequencies of nuclei; hence, their observed differences in hertz change linearly with changes of  $B_0$ . Moreover, homonuclear scalar couplings remain constant with  $B_0$  and therefore complex multiplets overlap less with neighbouring resonances at higher field-strengths. This allows fine-structures to be interpreted relatively easily (96).

One of the most important criteria in the assessment of drug quality and quality assurance is the determination of API content in bulk drug substances and in pharmaceutical dosage forms. Conventional methods of analysis such as gravimetric and volumetric techniques are the more common analytical tools recommended by different Pharmacopoeia's and Drug Standard suppliers. In spite of the simplicity, specificity and accuracy of the modern advanced instrumental analysis, techniques such as spectrophotometric (IR, UV, and NMR), chromatographic methods (TLC, GC and HPLC) and others are used for analysis of drugs (112). In fact, apart from UV analysis, there are only a few examples of use of other instrumental techniques reported in monographs in the different Pharmacopoeias. It seems that official compendia are reluctant to adopt more of these techniques (112), which may well be a consequence of the lack of such instrumental facilities in some parts of the world (112). It must be noted that NMR is more specific (113) than other techniques such as UV spectrophotometry. For example, several different compounds may have the same or similar  $\lambda_{\text{max}}$  value as CPT, which could result in an incorrect decision when using UV method described in most pharmacopoeias. When compounds have similar  $^1\text{H}$  spectra due to their related structures, it is usually impossible to distinguish them, and as such 2D NMR should be used, because it permits better separation of peaks.

Since the development of high resolution NMR spectrophotometers in the 1950s, NMR spectra have been a major means of studying both newly synthesized molecules and natural products. Since drugs in clinical use are synthetic or natural products, NMR spectroscopy has been mainly applied to the elucidation and confirmation of their chemical structures. NMR methods have also been applied to quantitative analysis of compounds in order to determine the impurity profile of these materials (114-115), to characterize the composition of drug products and to investigate metabolites of drugs in biological fluids (116-118). The application of solid state measurements can provide information about polymorphism of drug powders (119-120) and the conformation of drugs in tablets.

### 2.1.1. The instrument

NMR is a spectroscopic technique that relies on the evaluation of the magnetic properties of an atomic nucleus. When placed in a strong magnetic field, certain nuclei resonate at characteristic frequencies in the radio frequency range of the electromagnetic spectrum (121).

NMR is essentially an absorption phenomenon, similar to that observed in UV and IR techniques. However, the energy of NMR is from radio frequency radiation by nuclei exposed to the mass field. A magnet is the core of an NMR instrument and should create a static, stable and homogeneous magnetic field when in use. The magnet consists of a closed loop ('solenoid') of conducting Nb/Ti alloy wire immersed in a bath of liquid helium (b.p. 4K). A large current flows around the loop, creating a strong continuous field with no external power supply. The helium container is insulated with a vacuum jacket and is cooled further by the use of liquid nitrogen (b.p. 77K). The probe is a coil of wire positioned around the sample that alternately transmits and receives radio frequency signals. A computer directs the transmitter to send a high power, short duration pulse of radio frequency to the probe coil. Immediately after, the generation of the pulse weak signals called free induction decay (FID) received by the probe coil are amplified, converted to an audio frequency and sampled at regular intervals of time by the analog digital converter (ADC) to produce a digital FID signal. The computer determines the timing and intensity of the output pulse by the transmitter and receiver and processes the digital information supplied by the ADC. The computer performs Fourier transformation of the signals to produce and plot NMR (121, 122).

Organic compounds are basically composed of the elements hydrogen and carbon, and in some cases phosphorus, nitrogen and oxygen. Additionally halogens such as fluorine, chlorine, bromine and iodine or metal atoms may be present. Each of the aforementioned elements has an isotopic nucleus which can be detected by NMR in appropriately designed experiments. The low natural abundance of  $^{15}\text{N}$  and  $^{17}\text{O}$  in nature prevents NMR being routinely applied to these elements without the use of labelled reference substances, but  $^1\text{H}$ -,  $^{13}\text{C}$ -,  $^{19}\text{F}$ - and  $^{31}\text{P}$  NMR spectroscopy have become routine techniques for daily analytical work (123). Modern NMR spectrometers are available with field strengths up to 18.8 Tesla or a proton resonance frequency of 800 MHz (124), and at times 900 MHz (125-126). Routine analysis is made at proton frequencies of between 300 and 500 MHz (127).



### 2.1.2. Spectra

Fundamentally, NMR spectra can be generated using either continuous wave or Fourier transform acquisition (126-128). Continuous wave NMR spectra are generated along similar principles to those recorded using optical spectrometers. A sample is placed into a strong magnetic field and the frequency of the sample is slowly scanned. In Fourier Transform NMR (FT-NMR), the magnitude of the energy changes is small. This means that the sensitivity is a major limitation. These instruments are not usually available (129). The frequency at which an NMR signal appears depends mainly on the magnetic field strength. The chemical environment in which an active nucleus is located can lead to a small shift in the resonance frequency and is referred to as the 'Chemical Shift'. The presence of different functional groups finds their expression in this 'Chemical Shift'. The result is that an intensity-/frequency-diagram or NMR spectrum is generated. In  $^1\text{H}$  NMR spectroscopy the presence of each H-atom leads to the generation of at least one signal and since most molecules of analytical interest contain more than one H-atom, the resultant spectra are generally more complex than conventional chromatograms. What is crucial to interpreting the information contained in NMR spectra is the spectral dispersion which is a linear function of the applied magnetic field strength. The homonuclear spin coupling of protons leads to a low dispersion in  $^1\text{H}$  NMR spectroscopy. In  $^1\text{H}$  NMR spectra of complex mixtures, it is often not possible to detect single components, but the sum of functional groups in the mixture can be determined. In  $^{13}\text{C}$  NMR spectra, the dispersion is much higher.

Even though NMR spectroscopy is mainly a technique used for structural analysis, it has many applications as a quantitative analytical tool (126-130). The most attractive feature of NMR spectroscopy is that in a given solution and under appropriate conditions, the molar response factor is exactly the same for all resonating. This allows an analyst to perform quantitative analyses without the need for analytical standard of the analyte through the use of simple and well characterized primary standards, as used for volumetric analysis. Quantitative analysis using NMR is normally achieved by evaluation of the ratio of the integral of a signal generated by a test compound and the integral of a signal produced by a primary standard of that same compound. Furthermore, under quantitative conditions, matching integrals of signals with the structural formula of a compound are indicative of the purity of that material (130).

The European Pharmacopoeia promoted the use of NMR spectroscopy for the identification of drugs and reagents, and in some cases NMR spectra replace the use of IR spectroscopy. Thus, the  $^1\text{H}$  NMR spectra are used in the same manner as IR spectra, which can be described as a sort of pattern recognition. An increasing number of reagents, adenine, butoxycaine and aesculin have been identified by  $^1\text{H}$  and  $^{13}\text{C}$ -NMR spectra in the USP Pharmacopoeia (123). NMR spectroscopy, being a primary ratio method of measurement, is highly suitable to evaluate the quality of drugs. NMR spectroscopy can be used for the identification of a drug substance, the identification and quantification of impurities arising from the synthesis pathway and degradation or residual solvents, as well as the determination of the content in the assay (131).

Following the discovery of an active pharmaceutical ingredient (API) with potential for therapeutic use, it is vital to completely characterize the solid-state form of the bulk API and of any formulated product containing that API. The solid-state form of an API - in particular the crystalline, amorphous or solvate nature - can have a dramatic effect on the dissolution rate, solubility, bioavailability, physical stability and potential for interaction with excipients of that compound. Formulation and processing of an API has been shown to impact some of these physical properties (132).

There are many analytical techniques that can be used to identify the solid-state form of an API. Traditional techniques used for solid-state analysis include differential scanning calorimetry (DSC) (132), Fourier Transform Infrared Spectroscopy (FT-IR) (133), Raman Spectroscopy (134), and Powder X-ray Diffraction (PXRD) (135). While there are many advantages to using these methods, one most notable disadvantage is that many of the techniques cannot be easily used to characterize the individual components contained in a formulated product. NMR can provide information about both the API and a formulated product. Although NMR is currently not widely used due to its expense and lack of availability, its use to characterize pharmaceutical products is becoming more prevalent since information can be obtained from NMR spectra about an API and/or the drug product in which the API is formulated.

The motivation for using NMR spectroscopy to characterize pharmaceuticals can be readily ascertained by highlighting areas in which NMR can provide unique information about a particular system. Such areas include the following:

- a. NMR is a non-destructive and non-invasive technique that can be applied to the analysis of an API or drug product (136),
- b. Quantization of solid-state forms of API and delivery systems is possible (137),
- c. Low levels of API in a drug product can be investigated using isotopic labelling (138),
- d. The conformation and arrangement of molecules can be established (139), and
- e. The molecular dynamics of a system can be determined (140).

The use of NMR is not currently widespread within the pharmaceutical industry due firstly to its expense (140-141). Secondly, lengthy analysis time and low throughput are barriers in the use of NMR, but the development of a multiple sample probe, as well as other advancements, are likely to increase the potential for use of this technique in the near future (140).

NMR is particularly rich in the number and type of spectroscopic observables it can offer. Chemical shifts, *J*-couplings and dipolar couplings are but a few of the parameters that can be measured via NMR (135). However, for these NMR parameters to have some utility, they must be able to be applied to the structural elucidation of compounds. In this study, focus is mainly on the chemical shift and *J*-coupling.

### **2.1.3. Chemical shifts**

Chemical shifts in NMR spectra are the cornerstone of the technique. These shifts provide positional information about individual NMR peaks, which in turn can be ascribed or assigned to individual atoms within the chemical structure of the compound under investigation. Unlike most other forms of spectroscopy, major spectroscopic values (chemical shifts) in NMR are reported using a relative rather than an absolute measure as chemical shifts are field dependent and are fundamentally an electronic phenomenon. As a result, all chemical shifts are measured in parts per million (ppm) as opposed to absolute frequencies in Hertz (Hz). These shifts arise primarily due to the geometry or distribution of electrons surrounding the nuclei that are monitored using NMR (142).

The theoretical treatment of chemical shifts for simple systems comprised of a free atom with no orbital or spin angular momentum can be determined using Lamb's formula (143) in Equation 2.1:

$$\delta = \frac{4\pi e^2 B_0}{3mc^2} \int r \rho(r) \delta$$

**Equation 2.1**

- $\rho(r)$  = electron density from the nucleus,
- $r$  = distance of the electron density from the nucleus,
- $B_0$  = strength of the magnetic field of the NMR,
- $c$  = speed of light,
- $m$  = mass of light,
- $m$  = mass of an electron,
- $e$  = charge (cgs).

In essence, the chemical shift is proportional to the electrostatic potential energy of interaction between the nucleus and electrons (144).

If the nucleus is in a molecule where the electrons are not free to move in circles around the direction of the applied magnetic field, a theoretical expression for the chemical shift, defined by Ramsey, is normally used (136, 145, 146).

It is evident that there is an inverse relationship between the distance of an electron from a nucleus and the resultant chemical shift observed for that electron. When electrons are pushed away from the nucleus the chemical shift is small and the nucleus is said to be deshielded. In NMR, these changes are generally plotted in reverse so that shielded nuclei have low or upfield chemical shifts (around 1 ppm for H), and deshielded nuclei have high or downfield chemical shifts (around 8 ppm for H). Chemical shifts vary according to the characteristic electronic and nuclear structure of each element of a molecule. Chemical shifts provide detailed information about the covalent structure of atoms and molecules in a structure (142).

Once a compound of interest is ready for NMR analysis, and suitable solution conditions have been determined, a series of 2 or 3D experiments are conducted. The outcome of such experiments is the collection of sufficiently detailed spectral data to assign every observed peak or resonance to all detectable atoms in a compound - a process called sequential assignment. Two types of 2D experiments are normally undertaken. Initially a Correlation spectroscopy (COSY) experiment is performed in order to allow individual carbons to be identified as a consequence of distinct chemical shifts. Following the COSY, Heteronuclear Multiple Quantum Coherence (HMQC) and Heteronuclear Multiple Bond Coherence (HMBC) experiments are performed to develop spectra that are almost identical to the COSY spectrum. All of these spectra are displayed using a software package called MestRe-C Version 4.3.6.0 or MestRe Nova (Mestrelab Research, Santiago de Compostela, Spain, 2006).

Once the sequential assignment is completed, it is possible to begin the structure elucidation process (147).

#### **2.1.4. *J*-coupling**

Nuclei that are subject to the same chemical environment are equivalent, and those exposed to different environments or having different chemical shifts are non-equivalent. Nuclei that are close to one another also exert an influence on the magnetic field of each other and which are depicted in NMR spectra if the nuclei are non-equivalent. If the distance between non-equivalent nuclei is less than or equal to three bond lengths, this effect is clearly visible in NMR spectra and is referred to as spin-spin coupling or *J*-coupling.

One of the primary goals of an analytical laboratory is to identify and characterize any impurities that may be present in bulk drug or formulated products. The nature of impurities that may be present is important to ensure that stable formulations and interactions with excipients can be respectively produced and identified. Furthermore, regulatory agencies require that impurities present at levels > 0.1% must be identified. Complex mixtures, especially those with low amounts of individual components, are a challenge to analytical chemists working in pharmaceutical research and development (148).

CPT contains two asymmetric centres, one associated with the (S)-proline functionality and the other with the 3-mercapto-2-methylpropionic acid side chain. The compound is normally administered as enantiomerically pure, with both centres of dissymmetry being completely resolved. The physicochemical and analytical characteristics of CPT have been described by Kadin (149) and by Caplar *et al* (150). Many of the details in these published profiles are similar; however the ultraviolet absorption curves are substantially different. Kadin showed (149) UV spectrum with a single maximum around 200 nm and no other absorption bands at any other wavelength. This observation is in contrast to that reported by Caplar *et al* (150), in which the spectrum of CPT consisted of two maxima at wavelengths of 207 and 327 nm respectively. In addition, circular dichroism (CD) with band maxima at 225 and 242 nm was also reported (151).

A distinguishing characteristic of CPT (Figure 1.3) is that it is a relatively simple chemical compound that is comprised of condensed, simple amino acids. A hydrogen bond can be presumed to exist between the hydrogen atom of the carboxylic acid and the carbonyl group,

and another hydrogen bond is presumed to exist between the hydrogen from a sulfhydryl group and a carbonyl group.

The reactions of thiol compounds with molecular oxygen are well documented (152), and it is a challenge to resolve this difficulty as ambient oxygen pressure is always present. The reactions of oxygen with thiol compounds in aqueous solutions are most often described by Equations 2.2 and 2.3:



The products of such reactions are disulfides and hydrogen peroxide or water (114). However, it is known that the oxidation of thiol compounds can produce products containing a sulfur atom in different oxidation states depending on the reaction conditions. Under mild conditions (pH 7-9), thiol compounds are oxidised to produce disulfides (153), whereas at pH 12, these compounds are transformed predominantly into sulfinic ( $\text{RSO}_2\text{H}$ ) and sulfonic ( $\text{RSO}_3\text{H}$ ) acids (123).

Published data (154-155), reveal that the rate of self oxidation of CPT is linearly dependent on the concentration of oxygen. However, the reaction can follow the zero- or first-order kinetics with respect to the concentration of thiol compounds and their source (156). Despite the prevalence of substantial information, the data on oxidation of thiol compounds are contradictory and it is difficult to estimate the reliability of many proposed reactions (156).

This study aims to show that 2D NMR can be used to perform precise and accurate qualitative analysis of bulk material since the conditions of storage of raw material are critically important for CPT powder, in particular when oxidative degradation may prevail.

#### 2.1.5. NMR

Total assignments of  $^1\text{H}$  NMR,  $^{13}\text{C}$  NMR spectrum for the structures are made with the help of distortionless enhancement by polarization transfer (DEPT),  $^1\text{H}$ - $^1\text{H}$  correlation spectroscopy ( $^1\text{H}$ - $^1\text{H}$  COSY), as well as heteronuclear multiple quantum coherence (HMQC) and heteronuclear multiple-bond correlation (HMBC) techniques.  $^{13}\text{C}$  NMR data are well known for better dispersion and significantly less sensitivity to environmental effects, such as that due to pH, solvent used, temperature, etc., than those of protons. Yet  $^1\text{H}$  has remained a

favourable tool for identification and/or high-throughput analysis of small and medium sized molecules and for the characterization of complex mixtures, such as those of metabolites due in part to sensitivity concerns.

#### **2.1.5.1. $^1\text{H}$ and $^{13}\text{C}$ -NMR**

Both  $^1\text{H}$  and  $^{13}\text{C}$ -NMR give information about the number of non-chemically equivalent nuclei or non-equivalent hydrogen and carbon atoms as well as information about the environment of the nuclei or hybridization state and attached atoms. It is convenient to use FT-NMR techniques for  $^1\text{H}$  NMR and it is standard practice for  $^{13}\text{C}$ -NMR as the signal for a C atom is in the order of  $10^{-4}$  weaker than the signal generated for a hydrogen atom. A signal for a  $^{13}\text{C}$  nucleus is only about 1% as intense as that for  $^1\text{H}$  because of the magnetic properties of the nucleus.  $^{13}\text{C}$  are spread over a much wider range than  $^1\text{H}$  signals making it easier to identify and count individual responses. Separate distinct peaks appear for each of the carbons in the molecule of interest.  $^{13}\text{C}$  shifts are most affected by the hybridization state and electro-negativity of the carbon and attached functional groups.

CPT has three functional groups of importance *viz.*, thiol, amide and carboxylic acid. The best estimate for the S-C-C- bond in CPT is  $109.5^\circ$ . As can be seen from the structure of CPT, there are 9 lone pairs, 0 open octets, 10  $\text{sp}^3$  hybridized atoms, 4  $\text{sp}^2$  hybridized atoms, 0  $\text{sp}$  hybridized atoms and 15 atoms that are unhybridized. The hydroxyl (OH) group is the most polar bond in CPT. The  $\text{sp}^3$  hybridized C atom is shielded more than that of the  $\text{sp}^2$  and an electronegative atom deshields the carbon to which it is attached.

#### **2.1.5.2. DEPT-135**

DEPT-135 is a distortionless enhancement of polarization transfer that uses a 135 degree decoupler pulse. It is a technique that is used to distinguish different types of carbons in a spectrum. A DEPT spectrum is made up of 3 components, *viz.*, (i) regular spectrum (ii) DEPT-90 spectrum and (iii) DEPT-135 spectrum. To analyze CPT, only the DEPT-135 spectrum that shows positive peaks for carbon atoms in  $\text{CH}_3$  and CH groups, and DEPT-135 that shows negative peaks of carbon atoms from  $\text{CH}_2$  groups were evaluated. DEPT-135 is used to count the H attached to C. In DEPT-135, a second transformer irradiates H, which affects the appearance of C spectrum. Some C signals stay the same, some disappear and

some are inverted. The experiment (distortionless enhancement by polarization transfer, DEPT) were obtained using variable pulse  $q = 135^\circ$ .

### 2.1.5.3. COSY, HSQC and HMBC

The term COSY is an acronym for correlation spectroscopy. In COSY experiments, chemical shifts between nuclei that are  $J$ -coupled or separated by two or three covalent bonds are generated, resulting in every peak having two chemical shift values (*viz.*, an x- and y- value). Those that have identical x- and y- values are called diagonal peaks. Those that have different x- and y- values are called off-diagonal or cross peaks. Identifying COSY cross peaks and the two atoms that gave rise to the x- and y-shifts respectively, allows any two coupled spins to be identified by simple inspection. This is very useful in determining the covalent connectivity of all atoms within a molecule (157).

COSY spectra are therefore useful to identify coupled protons. Cross-peaks indicate pairs of protons that are coupled. The 2D  $^1\text{H}$ - $^1\text{H}$  correlation spectroscopy (COSY) and heteronuclear simple quantum correlation (HSQC) spectra were obtained with a digital resolution of 5.425 Hz after zero filling. Zero filling (one) were performed in the F1 dimension of a 512'512 matrix, the data were 2D transformed and the magnitude spectra multiplied by a sine window in each dimension and symmetrised along the diagonal (158).

HSQC is an acronym for heteronuclear simple quantum correlation, meaning that two different types of nuclei (usually  $^1\text{H}$  and  $^{13}\text{C}$ ) are correlated in a 2D experiment by the evolution and transfer of single-quantum (SQ) coherence, the simple magnetization that can be represented by vectors in the x-y plane. HMBC is heteronuclear multiple bond correlation, which is identical to HMQC except that the  $J$ - value selected for the coherence transfer is much smaller (10 Hz for HMBC versus 100 Hz for HMQC), so that the two and three bond relationships are detected ( $^{2,3}J_{\text{CH}} \sim 10\text{Hz}$ ) and the one bond relationship is rejected ( $^1J_{\text{CH}} \sim 100\text{Hz}$ ) (158).

To date, only a small number of manuscripts describing the use of NMR to study ACE inhibitors have been published (97, 98, 101-105), none of which have focused on the use of 2-D NMR evaluation of the drug. The purpose of this work is to describe an NMR method for the determination of the purity of CPT.



## 2.2. EXPERIMENTAL

### 2.2.1. Materials and methods

NMR spectra were generated in deuterated chloroform ( $\text{CDCl}_3$ ) using a Bruker 400 MHz NMR spectrometer (Rheinstetten, Germany) in the  $^2\text{H}$  lock mode. Chemical shifts were reported in parts per million (ppm) relative to tetramethylsilane (TMS) which was used as standard in  $^1\text{H}$  and  $^{13}\text{C}$  measurements. Each sample was transferred to 178 mm glass ultra precision ASTM Type 1 Class A borosilicate thin-walled NMR tubes (Norell, Inc. Mays Landing, NJ). These tubes are specifically designed to be used for high resolution NMR and are recommended for chemical structure determination, low and high temperature applications, and low temperature sample storage. The  $^1\text{H}$  (400 MHz),  $^{13}\text{C}$  (100 MHz), DEPT-135, HMQC, HMBC, COSY-90 NMR spectra were all recorded using standard pulse sequences. Experimental data was obtained using the following conditions: All NMR spectra were recorded at 298 K, at a frequency of 400.13MHz with a 5mm probe and  $p_w (90^\circ) = 12.6$  s. All chemical shifts were recorded and analyzed using MestRe-C and MestRe Nova software.

### 2.2.2. Analysis of drugs

CPT was donated by Protea (Midrand, South Africa), and Deuteriochloroform ( $\text{CDCl}_3$ ) and tetramethylsilane (TMS,  $\text{Si}(\text{CH}_3)_4$ ) were obtained from Sigma Aldrich Chemical Co. (Milwaukee, WI, USA). Because all twelve hydrogen atoms in a tetramethylsilane molecule are equivalent, the chemical shift of this singlet is assigned as  $\delta 0.0$ , and all other chemical shifts are determined relative to it. The majority of compounds studied by  $^1\text{H}$  NMR spectroscopy absorb downfield of the TMS signal, and thus there is usually no interference between a standard and sample being tested. Samples of CPT were dissolved in  $\text{CDCl}_3$  and  $^1\text{H}$  NMR spectra recorded on a 400 MHz instrument. Deuterated solvents are used as they enhance spectral resolution and solvents containing hydrogen yield signals that may swamp those of the sample of interest. Approximately 20 mg of CPT powder was dissolved in 1 ml of solvent to yield a sample depth of at least 4.5 cm in the NMR tube. Despite these advances, NMR measurements are usually made on single samples, and therefore throughput is limited by this serial approach.

Following analysis, samples were transferred from NMR tubes into screw-cap glass vials and labelled appropriately. Prior to commencing analysis, cleanliness of the tubes was ensured so as to avoid the development of poor quality spectra. Additionally, caution was made so that

they had no cracks or chips. Labels were therefore put on the tube caps. It is better to have a slightly lower concentration and a sample of reasonable height than a shorter sample with a higher concentration. The natural ‘magnets’ in the atoms of the sample align with the NMR magnet just as iron filings would on a toy magnet. The sample was then exposed to a series of split-second radio-wave pulses that disrupt the magnetic equilibrium in the nuclei of selected atoms.

Prior to dissolving CPT, the deuterated chloroform was spiked with 1% TMS, as an internal standard.

### 2.3. RESULTS AND DISCUSSION

To prove the purity of CPT, NMR studies were conducted. Proton NMR spectroscopy has been used to study flurazepam dihydrochloride (159). Kuwayama *et al* (160) examined the solvated species of flurazepam dihydrochloride using  $^1\text{H}$ -NMR but found the spectra to be so complex that assignment of signal was not possible and therefore  $^{13}\text{C}$ -NMR spectroscopy was selected as the method of choice. It is for this reason that both  $^1\text{H}$ - and  $^{13}\text{C}$ -NMR studies were conducted in this work and results of these studies are shown in Figures 2.1 and 2.2.

Kuwayama and Yashiro (161) studied the  $^{13}\text{C}$ -NMR spectra of diazepam and fludiazepam. The use of NMR for the detection and quantitation of various benzodiazepines was summarized by Dawson (162) as one of several categories of abused drugs easily assessed using this technique.

The usefulness of  $^1\text{H}$  and  $^{13}\text{C}$  Fourier transform (FT) NMR spectroscopy ( $^1\text{H}$ - and  $^{13}\text{C}$ -NMR) as quantitative methods, stems from the potential direct relationship between the area under an NMR peak and the number of a particular type of nucleus that give rise to that signal. Experimental limitations that have to be overcome in order to obtain quantitative  $^{13}\text{C}$ -NMR spectra are associated with the relaxation time, the nuclear Overhauser effect (NOE), and the NMR instrument itself (filter characteristics, power level of the exciting pulse, dynamic range and digital resolution). Practical problems aside,  $^{13}\text{C}$ -NMR has a greater potential than  $^1\text{H}$ -NMR for the study of organic systems. The sensitivity of  $^{13}\text{C}$  chemical shifts to small differences in the molecular environment, and coupled with a large chemical shift range, gives a “chromatographic” separation of resonances of interest and has made  $^{13}\text{C}$ -NMR attractive as a potentially useful technique for quality assurance of pharmaceuticals (163).

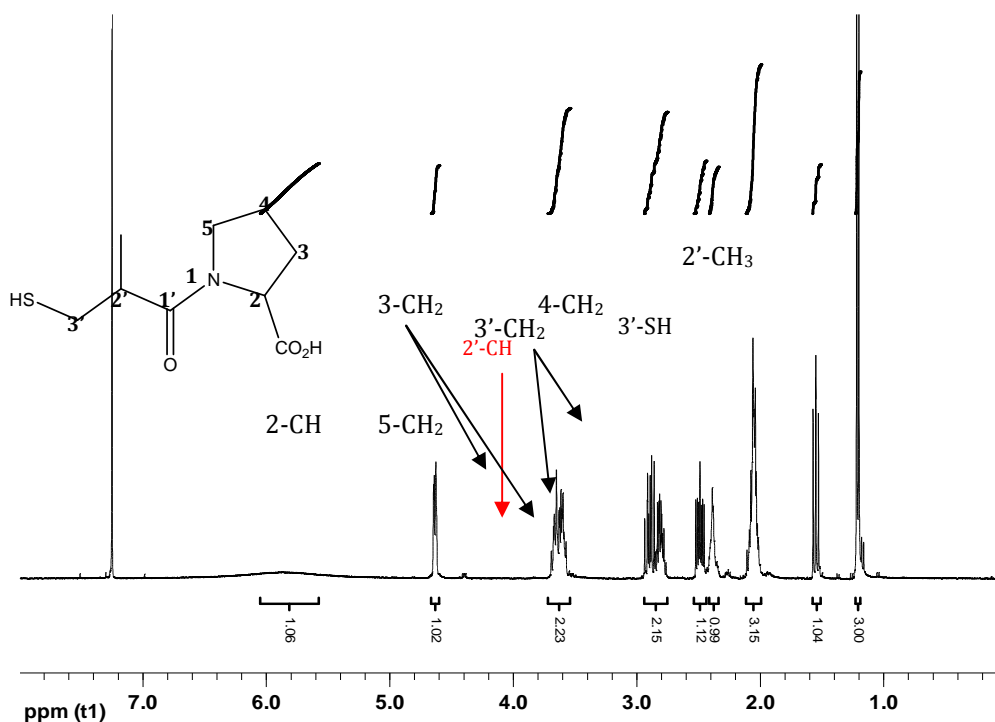


**Figure 2.1.** 400 MHz  $^1\text{H}$  NMR spectrum of CPT in  $\text{CDCl}_3$

The structure of CPT is shown in § 1.2.1 and in Figure 2.1 together with the tentative peak assignments. The  $^1\text{H}$  NMR spectrum (Figure 2.1) of CPT reveals: a doublet at 1.21 ppm corresponding to 2'-methyl protons; a triplet at 1.55 ppm corresponding to the thiol proton; a multiplet at 2.05 ppm corresponding to the diastereotopic 4-methylene protons; two multiplets at 2.10 and 2.38 ppm corresponding to the diastereotopic 3'-methylene protons; a multiplet at 2.81 ppm corresponding to the 2'-methine protons; two multiplets at 2.49 and 2.89 ppm corresponding to the diastereotopic 3-methylene protons; a multiplet at 3.63 ppm corresponding to the 5-methylene protons; a multiplet at 4.63 ppm corresponding to the 2-methine proton; and a broad peak at *ca.* 5.85 ppm corresponding to the carboxylic OH.

Solid-state  $^{13}\text{C}$  NMR spectroscopy has also been successfully applied in the determination of polymorphism in certain groups of molecules and both solid-state  $^{13}\text{C}$  NMR spectroscopy and powder X-ray diffraction have been used to analyze mixtures of solid forms of neotame (164).

One- and two-dimensional ( $^1\text{H}$ , APT, gCOSY, gHSQC and gHMBC) NMR spectra have been used in combination with LC-MS for structure elucidation of unknown impurities in compounds (165).

Three impurities in the API anastrozole were detected by simple isocratic reversed-phase high performance liquid chromatography (HPLC). The impurities were isolated and characterized by LC-MS/MS, GCMS and  $^1\text{H}$ ,  $^{13}\text{C}$  and DEPT NMR experiments (166). A rapid, selective and accurate quantitative 2D NMR (HMBC) method was developed for the simultaneous analysis of obidoxime chloride and atropine sulphate (167). The conformational properties of the AT1 antagonist, valsartan, have been analyzed in solution and at receptor binding sites. Low energy conformations of valsartan in solution were explored and elucidated using a combination of NMR spectroscopy ( $^1\text{H}$ ,  $^{13}\text{C}$ , HSQC, HMBC, ROESY and NOESY) and molecular modeling techniques. The NMR results revealed the existence of two distinct and almost isoenergetic conformations for valsartan (with a *cis:trans* ratio around the amide bond of 40:60) (168).

It is abundantly clear that the physical characterization of API is crucial to the successful development of a successful product (169-171). It has long been known that pharmaceutical solids can exist in more than one solid form (crystal, amorphous) (169, 172-174) and that different solid forms of a drug may display significantly different physical and chemical properties, including colouration, morphology, stability, dissolution and bioavailability (169, 172). Typically, the most thermodynamic and stable form of a compound is chosen for development into a product, however metastable forms have been used due to enhanced dissolution or bioavailability profiles. In either case, a full characterization of the API is necessary in order to understand the chemical and physical properties of the material. Extending this concept, qualitative analysis must encompass the API at two levels: the bulk drug substance as well as the final drug product (169, 171), and quantitative analysis at both levels may also be necessary.

The  $^{13}\text{C}$  NMR spectrum (Figure 2.2) reveals 9 carbon signals. The C-2' methyl nucleus resonates at 17.2 ppm; the C-4, C-3 and C-3' methylene nucleus at 24.8, 27.5 and 27.6 ppm; the C-2' methine nucleus at 42.6 ppm; the C-5 methylene nucleus at 47.8 ppm; the C-2 methine nucleus at 65.9 ppm; and the two carbonyl carbons at 172.8 and 176.5 ppm. The molecular formula of CPT is  $\text{C}_9\text{H}_{15}\text{NO}_3\text{S}$ .  $^{13}\text{C}$  NMR spectrum (Figure 2.2) shows 9 peaks of different C atoms, which is consistent with the basis of molecular symmetry.

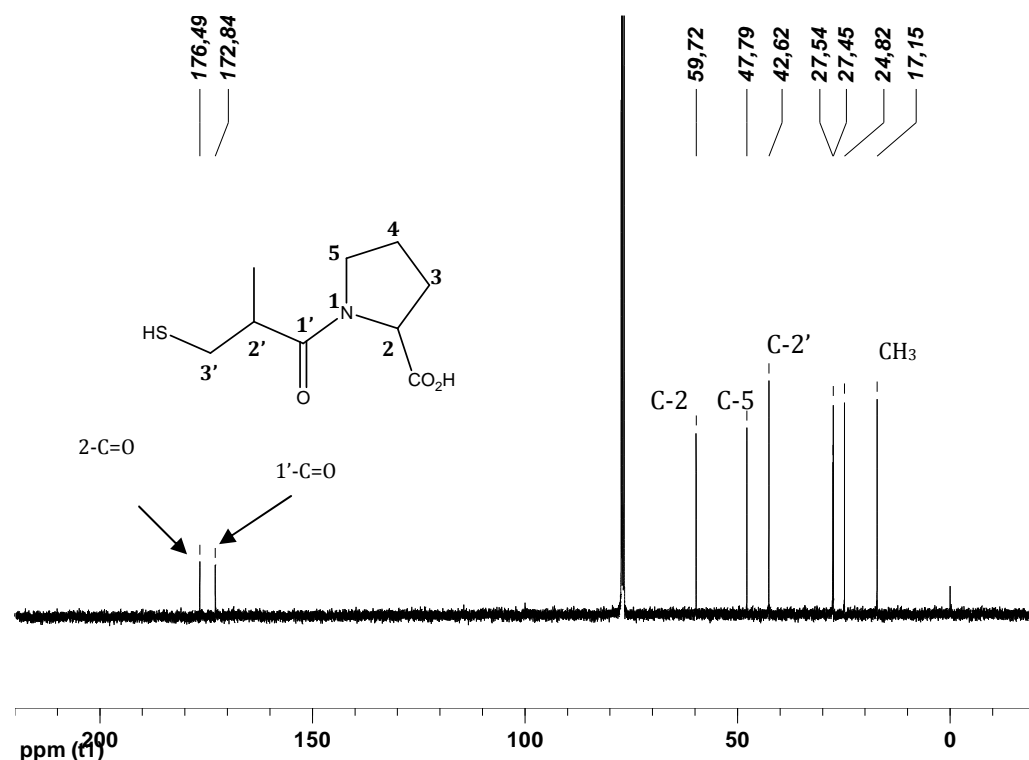


**Figure 2.2.** 400 MHz  $^{13}\text{C}$  NMR spectrum of CPT in  $\text{CDCl}_3$

The DEPT 135 spectrum (Figure 2.3) confirms the presence of four methylene carbons, C-4, C-3, C-3' and C-5, which resonate at 24.8, 27.5, 27.6 and 47.8 ppm respectively; and two methane carbons, C-2' and C-2, which resonate 42.6 and 59.7 ppm respectively. The DEPT spectrum gives the CH, CH<sub>2</sub> and CH<sub>3</sub> signals in which CH and CH<sub>3</sub> carbons appear as positive peaks and CH<sub>2</sub> appear as negative peaks in DEPT 135 spectrum. The C recorded in  $^{13}\text{C}$  NMR are not shown in DEPT are C without any attached H.

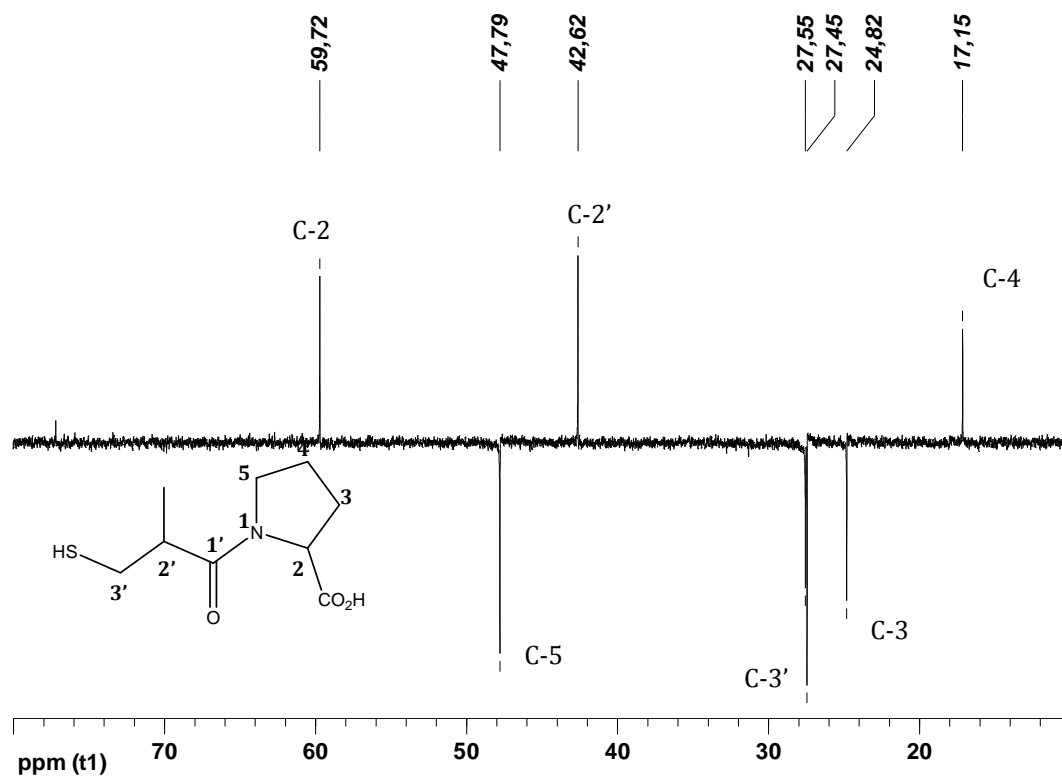


**Figure 2.3.** DEPT 135 NMR spectrum of CPT in  $\text{CDCl}_3$ .

The COSY spectrum (Figure 2.4) reveals a vicinal coupling (at cross peak A) between the 2'-methine proton and 2'-methyl protons; a long range coupling (at cross peak B) between 2-methine proton and 4-methylene protons; vicinal coupling (at cross peak C) between 4-methylene protons and 3-methylene protons; and a geminal coupling (at cross peak D) between 3-methylene protons.

The HSQC (Figure 2.5) reveals that in cross peak A the 2'-methyl protons are bonded to the carbon that resonates at 17.2 ppm; cross peak B reveals that 4-methylene protons are bonded to the carbon that resonates at 24.8 ppm; cross peak C reveals that diastereotopic 3'-methylene protons are bonded to the carbon that resonates at 27.5 ppm; cross peak D reveals that diastereotopic 3-methylene protons are bonded to the carbon that resonates at 27.6 ppm; cross peak E reveals that 2'-methine proton is bonded to the carbon that resonates at 42.6 ppm; cross peak F reveals that 5-methylene protons are bonded to the carbon that resonates at 47.8 ppm; and cross peak G reveals that 2-methine proton is bonded to the carbon that resonates at 59.7 ppm.

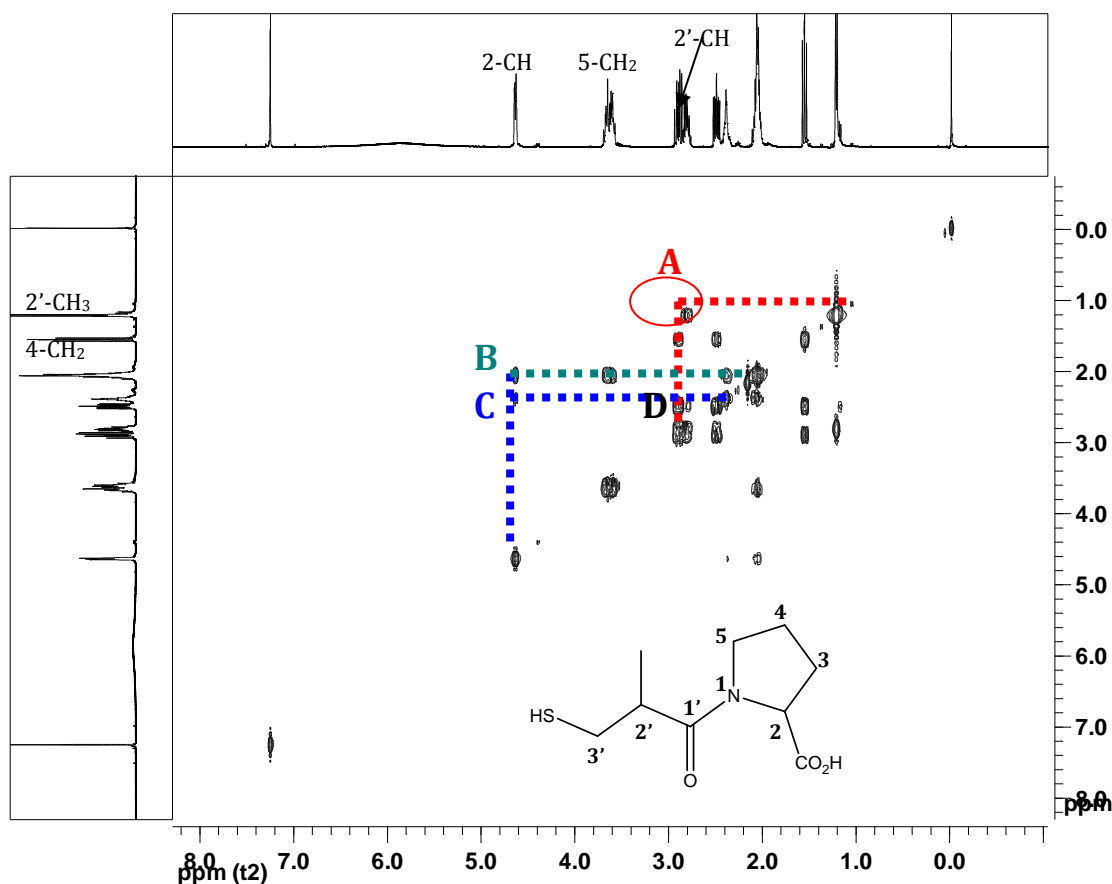


**Figure 2.4.** 400 MHz COSY NMR spectrum of CPT in  $\text{CDCl}_3$ .

The HMBC spectrum (Figure 2.6) was used to support the structural assignment which reveals that 2'-methyl protons connects to C-3' ( $^3J_{\text{C,H}}$ ), C-2' ( $^2J_{\text{C,H}}$ ) and 1'-C=O ( $^3J_{\text{C,H}}$ ); 5-methylene protons connects to C-4 ( $^2J_{\text{C,H}}$ ); and 2-methine proton connect to C-4 ( $^3J_{\text{C,H}}$ ) and 1'-C=O ( $^3J_{\text{C,H}}$ ).

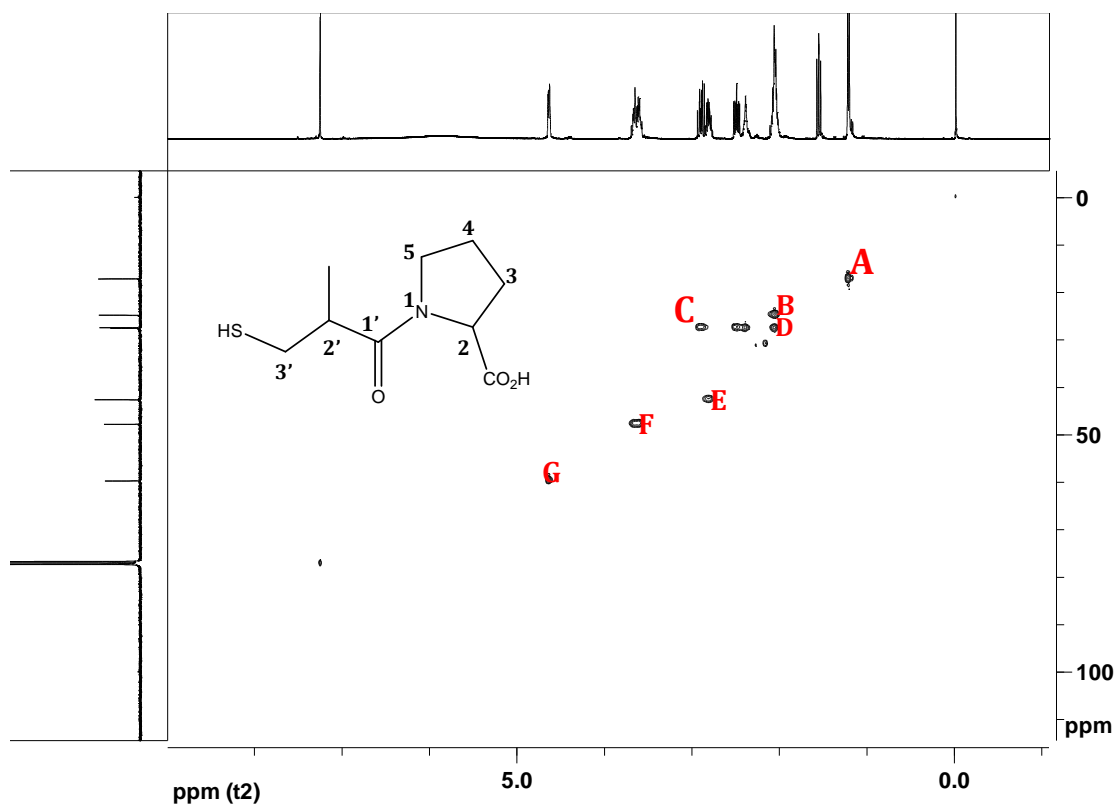


Figure 2.5. 400 MHz HSQC NMR spectrum of CPT in  $\text{CDCl}_3$ .

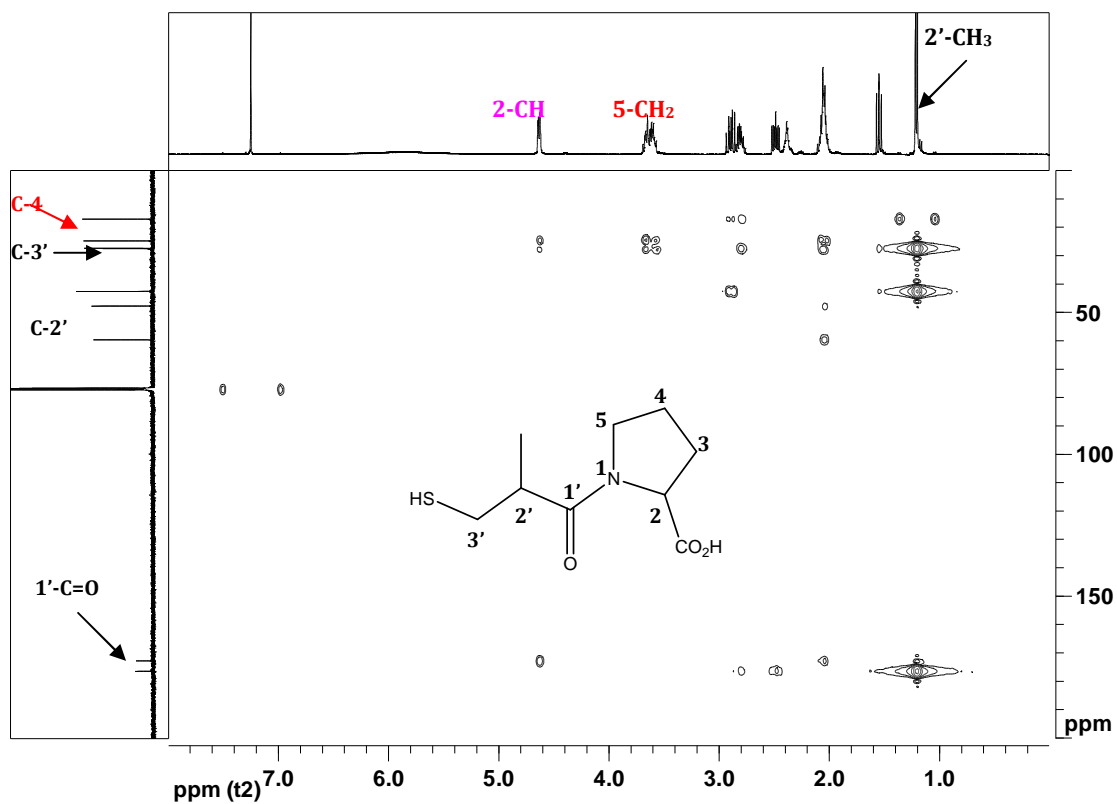


Figure 2.6. 400 MHz HMBC NMR spectrum of CPT in  $\text{CDCl}_3$ .



The structural elucidation of CPT was accomplished by use of a combination of 2D COSY techniques,  $^1\text{H}$ - $^1\text{H}$  and HSQC with  $^1\text{H}$  and  $^{13}\text{C}$  NMR spectra. In this study, all functional groups were well characterized. The elucidation of the structure was very important in the analysis of the bulk material. The  $^1\text{H}$  chemical shift values were reported on the  $\delta$  scale in ppm, relative to TMS ( $\delta = 0.00$  ppm)

## 2.4. CONCLUSION

The characterization of CPT using 2D heteronuclear correlated spectra is arguably the first of its kind using these techniques. By use of  $^1\text{H}$  NMR,  $^{13}\text{C}$  NMR, DEPT 135, COSY, HMBC and HSQC, complete information of the structure of CPT was obtained. Confirming the structure of a bulk material using NMR is the first in a process that can ultimately help confirm whether there have been changes in a drug in a bulk material during shipment, storage and exposure to humidity and air. NMR is a powerful and useful tool in pharmaceutical analysis and identification of small molecules. This study has demonstrated the usefulness of NMR, and it is quite clear that NMR will play a leading role in drug discovery, development and analysis. The technique can be used with other analytical tests for the elucidation of chemical and structural information pertaining to molecules under investigation. The spectra obtained in deuterated chloroform showed well-separated signals which did not suffer interference for the residual proton of chloroform, which sometimes may pose a problem in  $^1\text{H}$  during analysis. Aside from the costs involved and expertise needed, it is proposed that this method can be an effective tool to monitor degradants and to facilitate chiral discrimination and may result in the development of products in which chiral compounds are delivered as single enantiomers, thereby addressing the requirements being imposed by many regulatory authorities. In particular, this can also help and generate a fresh enthusiasm in the interest of improving enantioselective synthesis and increase demand for accurate, reliable and convenient methods of measuring enantiomeric compositions.

Additionally, NMR technology has been proposed in other studies (175) as a valuable tool for fast identification of illegally produced sildenafil citrate tablets. It can be used in stereochemical differentiation or conformational polymorphism. This tool can also help equip researchers with advanced understanding in accelerated pace within pharmaceutical research and development. While these advances create high optimism for the analysis of pharmaceuticals, they also challenge the analytical methods that are integral components in

the drug development and formulation. Thus far, it seems that this technique is underutilized in modern pharmaceutical research as a consequence of resource barrier.

A detailed NMR spectroscopic study of CPT was carried out and can be applied for the analysis / and or certification of CPT bulk material.

## CHAPTER 3

---

### THE USE OF EXPERIMENTAL DESIGN IN THE DEVELOPMENT OF AN HPLC METHOD WITH ELECTROCHEMICAL DETECTION FOR THE ANALYSIS OF CAPTOPRIL

#### 3.1. INTRODUCTION

Over the past few decades there have been extensive developments in the automation of chemical and pharmaceutical methods of analysis. The use of automation has been stimulated by the need for rapid analyses of increased numbers of samples in the clinical, pharmaceutical and environmental chemistry disciplines in addition to the demand for continuous monitoring of different analytes during industrial processes (176). A significant part of these modern approaches of automated analysis has been based on liquid flow analytical techniques operated under hydro-dynamically controlled conditions (177).

Several methods of detection have been used in flow analytical techniques (177). Electrochemical detection is the one most commonly used in the chemical industry (178-183).

Electrochemical detectors (ECD) are highly selective detectors that have a limited range of application, as compared with the commonly used spectrophotometric detectors. However, the appropriate application of ECD allows for analytical methods that can be superior to those using other detection systems. ECD are simple in design and relatively easy to use. However, their use requires knowledge and experience in the use of electrochemistry, in contrast to the use of UV-Vis spectrophotometric detectors (183).

A response using ECD depends on the transport of an analyte towards an electrode. The selectivity of electrochemical detectors is their prominent advantage and their selectivity can be modified or controlled through physical and chemical modification of the electrode surface in use (184-187).

ECD are of two types: Bulk and Solute property detectors. Bulk property detectors measure changes in an electrochemical property of bulk fluid flowing through the detector cell. The most popular detectors of this class are conductivity detectors in which a potential is applied across a cell, thereby allowing ions in solution an opportunity to move towards an electrode

(depending on the charge) with a consequent change in the conductivity of the electrode (188).

Two major disadvantages of conductivity detectors are that the use of buffer salts in the mobile phase should generally be avoided, and the system is temperature sensitive (189). Nevertheless, these detectors have found some application in the quantitation of both organic and inorganic ions in a variety of matrices (190-192).

In contrast, solute property detectors monitor the change in potential or current at the electrode as a solute passes through the detector cell. The more popular of these detectors are coulometric and amperometric detectors, of which the latter are more widely used. If a solute passes over an electrode which is held at a constant potential sufficiently high to allow electron transfer and oxidation or reduction to occur, a current will be produced which is proportional to the solute concentration (189). The difference between amperometric and coulometric detectors is that for the former, the concentration of solute entering and leaving the detector is nominally the same (in practice up to 5% may be converted to product) whereas in coulometric detectors about 95% of the solute is almost completely converted (193).

A limitation of electrochemical detection in general is that the mobile phase composition cannot use high concentrations of non-polar organic solvents since these do not support conductivity. To ensure conductivity of the mobile phase, buffers in the 0.01-0.1 M concentration range are used to provide conductivity whilst maintaining a low background current. It must be emphasized that the constituents of a mobile phase must be of the highest purity to minimize excessive background current (189). The most popular detector cells for electrochemical detection are thin layer in nature, and may be used with either amperometric or coulometric detectors (188).

The classes of compounds that have been analyzed using electrochemical detection include aromatic amines (194, 195), thiols (196), phenothiazines (197) and tricyclic antidepressant drugs (198). A number of hints / guidelines (188) specific to the successful use of electrochemical detection include:

- i) Ensuring that the electrode materials are compatible with the components of the mobile phase and that the electrode surfaces are in good condition,
- ii) Operation of the detector at the minimum potentials required to oxidize or reduce the solute of interest,
- iii) Minimization of temperature fluctuations around the detector cell,
- iv) Ensuring that no air bubbles are present in the flow cell,
- v) Ensuring that all constituents of the mobile phase are of the highest quality and are pure.

### 3.1.1. Electrochemical cell design

At present the ESA Coulochem<sup>®</sup> coulometric detector is the only commercially available detector of its type. Several types of cell are now available, most of which contain two analytical electrodes in series and the standard cell (Model 5010, Figure 3.1) contains porous graphite electrodes (PGE) of equal size.

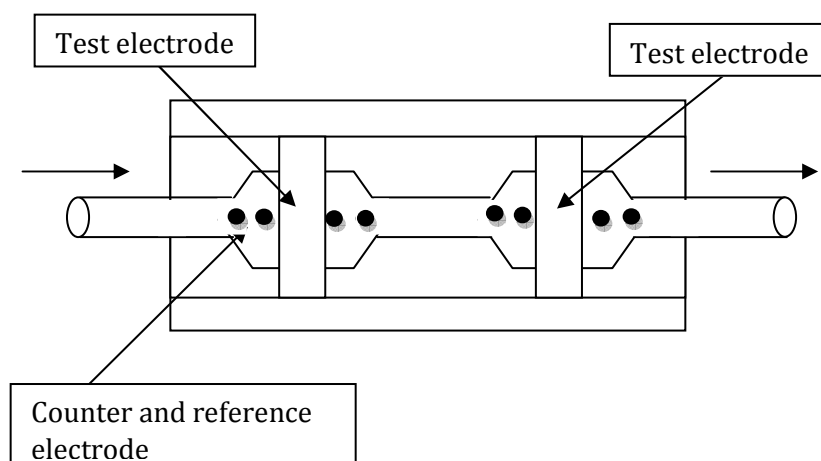


**Figure 3.1.** Schematic diagram of a Coulochem<sup>®</sup> Model 5010 detector cell, showing the relative positions of the working electrode and the counter and reference electrodes.

Coulochem<sup>®</sup> cells are unique in their design and use a patented Environmental Sciences Associates (ESA) flow-through porous graphite electrode. The low-volume analytical cells contain two working electrodes with a large surface area resulting in a complete reaction of the electroactive compound. The first or screening electrode can be used to eliminate compounds that have the potential to interfere with the analysis of the compound(s) of interest at the second or analytical electrode. The cell contains two thin, porous graphite electrodes with solid state hydrogen reference electrodes (199-200). The detector cells with

dual PGE can be operated in one of three modes that are often referred to as ‘screen’, ‘difference’ and ‘redox’ modes. In the screen mode the potential of the first electrode ( $E_1$ ) in the analytical cell is typically set at a potential of 0.2-0.3 V below that of the second electrode ( $E_2$ ). The aim of this strategy is to reduce the concentration of any unwanted readily oxidizable components that may interfere with the analyte reaching the second electrode (201).

Electrochemical selectivity is achieved by oxidizing or reducing many undesirable electroactive compounds that may interfere with the analysis at the first electrode. Any compound with a reaction potential less than that of the compound of interest reacts at the first electrode and is therefore excluded from reacting at the analytical electrode. In addition, many compounds can be readily oxidized and reduced in sequence which may ensure greater selectivity of this technique than with other detection systems (202).

The Model 5010A Standard Analytical Cell provides excellent long-term stability and day-to-day reproducibility for analysis and the large surface area of the coulometric electrodes permits long periods of operation without reduction in sensitivity and signal response.

The Model 5020 Guard Cell (Figure 3.2) is designed to withstand high pressure and has a single large porous graphite electrode that removes electroactive impurities from the mobile phase prior to the mobile phase passing through the injection port, column and analytical cell. This approach results in a decrease in background current and therefore a reduction in baseline noise (202-203).

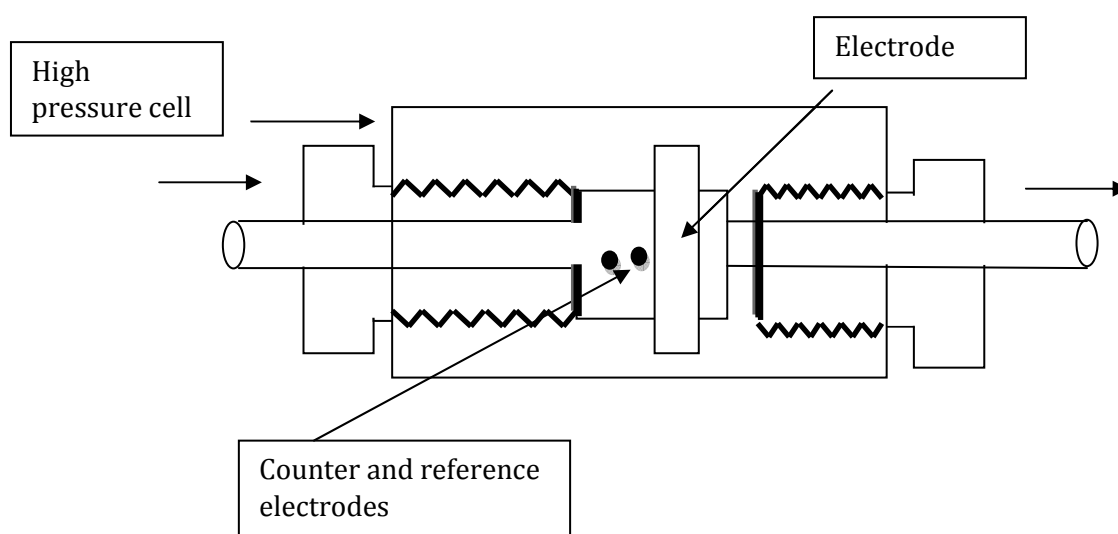


**Figure 3.2.** Schematic diagram of a Coulochem<sup>®</sup> Model 5020 Cell showing the relative position of the electrode, counter and reference electrode.

ECD has been used for immunoassay of heterogeneous enzymes (203) in clinical chemistry. The analysis of serotonin (204) and DNA entrapped in polypyrrole-polyvinyl sulfonate (30) has also used ECD. Furthermore non-electroactive and electroactive analytes in microchip electrophoresis (206) and environmental pollutants (207) have also been monitored using ECD. Trace carbofuran (208), low level of antioxidants in food (209) and trace metals in petroleum (210) have also been monitored using ECD. Wilhelm *et al* (211) used reductive electrochemical detection to analyze benzodiazepines in forensic samples. The number of publications and disciplines that have used ECD in analysis are summarized in Table 3.1 and Figure 3.3.

**Table 3.1.** Applications of electrochemical detection for the period 1980-2008

Applications	Number of Publications
Pharmaceuticals	3222
Clinical Chemistry	1890
Neuroscience	1478
Biochemistry	1405
Chemical	2881
Environmental	1136
Industrial	829
Forensic	201

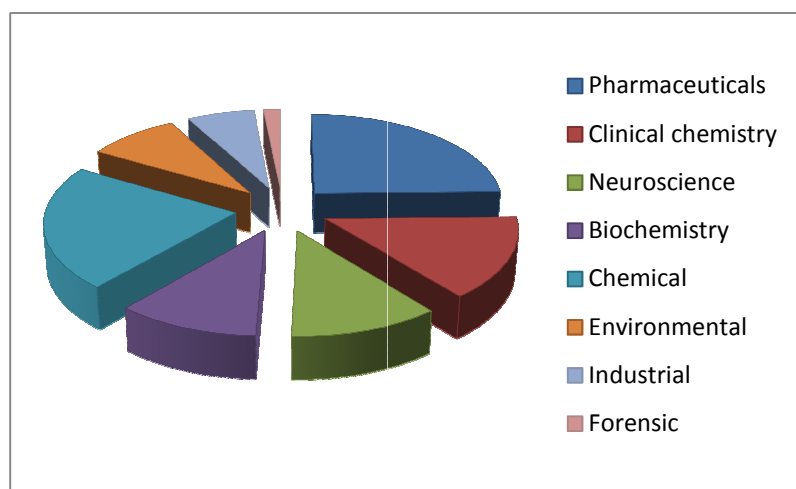


**Figure 3.3.** Disciplines that have used ECD for the period 1980-2008

When using ECD, the eluant flows over the surface of an ‘inert’ electrode maintained at an appropriate positive or negative potential relative to a reference electrode. At the electrode surface analytes possessing functional groups that are electroactive undergo oxidation or reduction depending on their characteristics (212).

ECD is at least 100 times more sensitive towards responsive compounds than standard UV detectors, with the added benefit that they are more selective. Unfortunately over time reaction products of oxidation tend to accumulate at the electrode surface leading to a loss of activity and hence loss of detector response, which is a major reason for the use of EC detection remaining specialized field (201).

ECD requires more care and thought in routine analysis than does the use of spectrophotometric detectors, principally because of the problems of electrode deactivation when operating at higher potentials (213).

### 3.1.2. Electrochemistry

In the solid state atoms in a metal are closely packed and the well-defined electron energy levels that are found in single atoms are not present. There is a continuum of levels and the available electrons fill the states from the lowest energy state upwards towards the highest level known as the Fermi level. Hence electrons in metals are relatively mobile and metals are generally good conductors of electricity. When a metal electrode is dipped into a solution of corresponding ions it will equilibrate according to Equation 3.1:



and the potential at the electrode will be a function of the equilibrium position for a reaction (201). The potential of an electrode is therefore the difference in the potential established between an electrode and a solution when the electrode is immersed in that solution.

The empirical laws of electrolysis developed by Faraday relate the current of an electrochemical reaction and state that ‘the amount of substance deposited at each electrode of an electrolytic cell is directly proportional to the quantity of electricity that passes through the cell (214). When all the analyte in a solution is electrolysed at an electrode, the measurable response is directly related to the molar amount of analyte as shown by Equation 3.2:



$$Q = nFN \quad \text{Equation 3.2}$$

where  $Q$  = the total amount of charge transferred,  
 $n$  = the number of electrons transferred or equivalents per mole,  
 $F$  = Faraday's constant,  
 $N$  = the number of chemical equivalents of analyte present.

Thus, Faraday's constant is the product of the charge on an electron multiplied by Avogadro's number. By definition, an electrical current ( $i$ ), measured in amperes (A), is determined as coulombs per second as shown in Equation 3.3:

$$i = \frac{dQ}{dt} = nF \frac{dN}{dt} \quad \text{Equation 3.3}$$

The equation shows that the rate at which electrons are moved across an electrode-solution interface, or the current, is directly related to the rate of the reaction occurring at the surface of the interface (201).

There are some other sources of current in addition to Faradic current. This current is due to the reaction of the analyte. Such currents are collectively referred to as background current. This current is due to the electrolysis of impurities, the electrolyte, the electrode material and capacitive or charging current. The first three contributions are Faradic currents of the system, whereas the last is a property of the interface between the electrode and the solution. This interface behaves in a similar fashion to an electrical capacitor in that it can store charge and at a first approximation it obeys Equation 3.4:

$$Q = CV \quad \text{Equation 3.4}$$

where  $Q$  = the charge stored  
 $C$  = the capacitance in Farads  
 $V$  = the potential difference across the interface

An equation for the capacitance current ( $i_c$ ), can be obtained by differentiating Equation 3.4 to generate Equation 3.5:

$$i_c = \frac{dQ}{dt} = C \left( \frac{dV}{dt} \right) \quad \text{Equation 3.5}$$

The total current ( $i_c$ ) is the summation of all currents, including the Faradic currents for the analyte, the electrolyte and the electrode material in addition to the capacitive current. Currents other than those derived from the analyte are generally undesirable and their

magnitude should be minimized. The capacitive current can be eliminated by operating the electrode at a fixed potential and that is indicated by Equation 3.6:

$$\left(\frac{dV}{dt} = 0\right) \quad \text{Equation 3.6}$$

An electrochemical reaction at a solid surface electrode over which a liquid stream is flowing as shown in Figure 3.4 is characterized by the following three separate and distinct stages;

- i) Diffusion of the electroactive analyte to the electrode surface,
- ii) Electron transfer as dictated by the electrochemical reaction, and
- iii) Diffusion of the reaction product(s) away from the electrode surface.

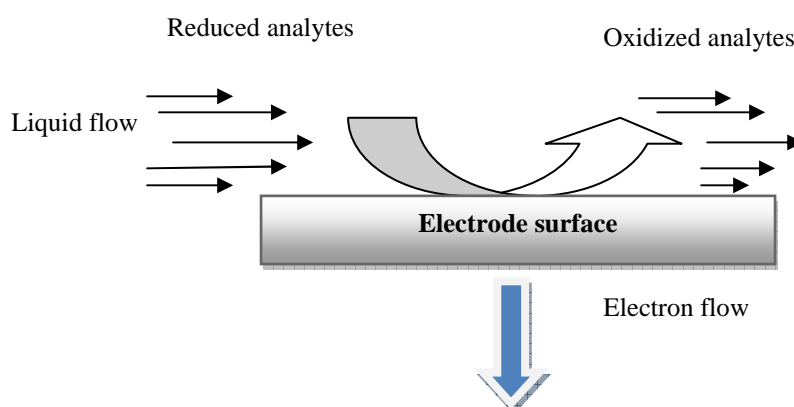


**Figure 3.4.** Schematic diagram of processes occurring at an electrode when an analyte flows over a static electrode held at an appropriate voltage.

The rate-limiting component in this reaction scheme is the slowest of the necessary steps and in ECD it is usually a mass transfer step (i.e. i or iii). Due to flow induced mixing, the analyte is always present at a constant concentration throughout the eluant flow except for a narrow layer of thickness  $\delta$  that is located immediately above the electrode surface. Consumption of the analyte, either by oxidation or reduction, creates a concentration gradient as shown in Figure 3.5. The thickness of the diffusion layer above the electrode surface is therefore critical to the electrochemistry that occurs in the system (201).

The diffusion equation or Fick's second law describes the rate of change of the analyte concentration above any planar surface. This analyte flux is proportional to the diffusion coefficient of the analyte ( $D$ ) and the flux therefore governs the limiting current ( $i_{lim}$ ) and is

directly proportional to the surface area of the electrode and concentration of the analyte, ( $C$ ) and is inversely proportional to the thickness ( $\delta$ ) of the diffusion layer (Equation 3.7):

$$i_{\text{lim}} = \frac{nFADC}{\delta} \quad \text{Equation 3.7}$$

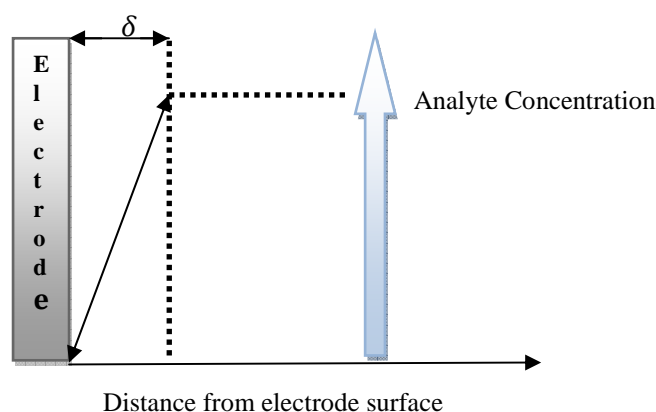


**Figure 3.5.** Concentration profile for an analyte near an electrode surface with laminar dynamic flow

Under hydrodynamic conditions the solution beyond the electrode surface consists of the Nernst diffusion layer ( $\delta$ ) just adjacent to the electrode surface, the laminar flow region and the turbulent flow region. Hydrodynamic voltammetry is the application of voltammetry under forced convection. The concentration gradient remains constant and current does not decay over time. The Nernst diffusion layer remains stagnant owing to the friction between the solution and the surface of the electrode. Immediately beyond the Nernst diffusion layer is a laminar flow region where the flow of a solution is parallel to the surface of the electrode. Any solution beyond the laminar flow region in a turbulent flow region as there is no specific direction to the flow at this point. The diffusion layer remains narrow and fixed under hydrodynamic conditions (215).

### 3.1.3. Electrode material

In order for an electrode to function in an HPLC application the working electrode material must:

- i) Be able to conduct electrical currents,
- ii) Operate at a low potential for the required EC measurement,

- iii) Be mechanically robust and malleable to form suitable shapes,
- iv) Be able to be polished to a very smooth surface,
- v) Withstand a constant flow or jet of eluant (201).

In addition the material must be inert with respect to the mobile phase composition, impurities in the eluant, other sample components and any reactive species that might be formed by electrolysis of the analyte. The most popular material used for solid electrodes is carbon, since it is a robust and not readily deactivated during routine use. Carbon is therefore particularly useful for oxidative electrochemistry applications (196-198).

Carbon paste electrodes exhibit low background current at positive potentials and have excellent mechanical stability. However, carbon paste electrodes are incompatible with mobile phases containing more than 20 % v/v organic solvent and therefore glassy carbon electrodes have become more common than carbon paste electrodes in HPLC applications. Glassy carbon electrodes are compatible with organic solvents and are easier to use. In addition, glassy carbon typically exhibits lower background current than do carbon paste electrodes at negative potentials (189).

More recently, diamond electrodes have been investigated due to their chemical stability, high electrical conductivity and to the large amplitude of their electroactive window in aqueous media (216). Mercury electrodes have also been used with ECD (217). However, due to poor mechanical stability of mercury alone it is often amalgamated with gold to form the electrode (218-221).

Progressive loss of sensitivity due to contamination of the electrode surface with the products of an electrochemical reaction of both a solute and components of the mobile phase is unavoidable since ECD are based on an electrochemical reaction at the operating electrode(s) (222-223).

## **3.2. METHOD DEVELOPMENT**

### **3.2.1. Experimental design and statistical analysis**

Successful HPLC method development depends on the selection of suitable operating variables in order to optimize a separation. Therefore, it is important to determine the operating variables or parameters at which the required response reaches an optimum level. The optimum level may be either a maximum or a minimum of a function of the design

parameters. One of the methods for determining optimum results for a specific set of experiments is response surface methodology (RSM).

RSM is a collection of statistical and mathematical methods that have been used in modeling and analyzing engineering problems. The main objective is to optimize the response surface that is influenced by different process parameters. RSM also quantifies the relationships between controllable input parameters and the resultant response surfaces that have been generated (224). It has been reported that RSM helps provide information about surface contours, and this can help visualize potential interactions between the parameters under investigation. In engineering applications RSM has been used to identify critical steps or parameters that optimize method development responses (225). RSM approach was used to study factors that are important in HPLC method development in these studies.

Therefore a RSM study begins with the definition of a problem concerning which response is to be measured and how it is to be measured. The experiment plan is then designed. The initial step was to construct a model using experimental data relating design parameters to measured responses. The next step involved identifying the most appropriate design parameters based on this model. The model itself provides only an approximation of the true relationship between the design parameters and resultant responses.

If the model developed is appropriate, three-dimensional and contour graphs are plotted and interpreted. In brief, in an appropriate model the goodness of fit must be significant and the lack-of-fit insignificant. The coefficient of determination or  $R^2$  values should be as close to 1 as possible and diagnostic plots should exhibit trends that are associated with an appropriate model with an excellent fit (226). The literature is replete with reports advocating the use of optimization techniques to improve analytical method development in the pharmaceutical sciences (227-229).

In the context of this study a RSM approach was used sequentially to identify the optimal solution to an HPLC method development problem for CPT using ECD. The iterative procedure used in these studies included performing experiments in the region of the best known solution, fitting a response model to the experimental data and then optimizing the estimated response model.

The use of central composite design (CCD) methodologies has been successful in designing an experimental program to model the effects of different variables (230). Box-Behnken designs have been used for the optimization and modeling of many methods (231). Screening experiments such as fractional and Plackett-Burman designs have also been used to identify important factors that affect analytical method performance (232).

CCD is an effective alternative to a factorial design approach. It was originally developed by Box and Wilson (233) and improved upon the method reported by Box and Hunter (234). CCD gives almost as much information as a three-level factorial design approach but requires fewer tests to be conducted than a full factorial design technique and has been shown to be sufficient to describe the majority of steady-state process responses (235 - 237).

The number of tests required for a CCD approach includes the standard  $2^k$  factorial with its origin at the centre,  $2k$  points fixed axially at a distance, say  $\beta$ , from the centre to generate quadratic terms in addition to replicate tests at the centre, where  $k$  is the number of variables. The axial points are chosen such that they allow rotatability (234), which ensures that the variance of model prediction is constant at all points equidistant from the centre of the experimental design. Replicate conduction of experiments at the centre of the design is most important, as they provide an independent estimate of the experimental error. For three variables, the recommended number of tests to be conducted at the centre is six (234). Hence the total number of tests required for three independently chosen variables (buffer pH, buffer molarity and organic solvent concentration) is  $2^3 + (2 \times 3) + 6 = 20$  (234, 238).

Once the desired range of values of the variables was defined, they were coded to lie at  $\pm 1$  for the factorial points (Fact), 0 for the centre points (Centre) and  $\pm \beta$  for the axial points (Axial) (239). The codes are calculated as functions of the range of interest of each factor as shown in Table 3.2. When the response data are generated, regression analysis is performed to determine the coefficients of the response model ( $\beta_1, \beta_2, \dots, \beta_n$ ), standard errors of the estimation of the coefficients and the significance of the coefficient. In addition to the constant ( $\beta_0$ ) and error ( $\epsilon$ ) terms, the response model incorporates the linear, interaction and quadratic terms (238, 240).

**Table 3.2.** Presentation of 20 experiments (Exp 1 – 20) with coded values for factor levels for the CCD

Experiment (run)	Standard	Type	Mobile phase pH	Mobile phase molarity	Organic solvent concentration
	Run number		X <sub>1</sub>	X <sub>2</sub>	X <sub>3</sub>
1	8	Fact	-1	-1	-1
2	9	Fact	+1	-1	-1
3	10	Fact	-1	+1	-1
4	4	Fact	+1	+1	-1
5	6	Fact	-1	-1	+1
6	1	Fact	+1	-1	+1
7	3	Fact	-1	+1	+1
8	11	Fact	+1	+1	+1
9	12	Centre	0	0	0
10	5	Centre	0	0	0
11	2	Centre	0	0	0
12	7	Centre	0	0	0
13	16	Axial	-1.682	0	0
14	15	Axial	1.682	0	0
15	13	Axial	0	-1.682	0
16	19	Axial	0	1.682	0
17	14	Axial	0	0	-1.682
18	20	Axial	0	0	1.682
19	17	Centre	0	0	0
20	18	Centre	0	0	0

The 20 experiments can be divided into three groups as follows;

- i.  $NF = 20$  factorial experiments carried out at the corners of the cube,
- ii.  $Na = 2 \times 3$  axial experiments carried out on the axes at a distance of  $\pm \alpha$  from the centre of the design,
- iii. The distance  $a$  is calculated so as to obtain the rotatability and a three variable CCD is rotatable if

$$\alpha = \pm (NF)^{1/4} = \pm 1.6818$$

- iv.  $N_0$  experiments are performed at the centre of the experimental domain.

In this case, the  $N_0$  value is fixed at 6 so as to obtain rotatability. The coefficients, i.e. the main effect ( $b_i$ ) and two-factor interactions ( $b_{ij}$ ) can be estimated from the experimental results using Design Expert (Version 7.0.1, Stat-Ease Inc., Minneapolis, USA).

The response model for the three variables under consideration is shown in Equation 3.8:

$$Y = (\beta_0 + \varepsilon) + \sum_{i=1}^3 \beta_i x_i + \sum_{i=1}^3 \beta_{ii} x_i^2 + \sum_{i=1}^3 \sum_{j=i+1}^3 \beta_{ij} x_i x_j \quad \text{Equation 3.8}$$

$Y$  is the experimental response to be optimized,  $\beta_0$  is a constant term,  $\beta_1$ ,  $\beta_2$  and  $\beta_3$  are coefficients of the linear terms,  $\beta_{11}$ ,  $\beta_{22}$  and  $\beta_{33}$  are co-efficients of the quadratic terms and  $\beta_{12}$ ,  $\beta_{13}$  and  $\beta_{23}$  are co-efficients of the interaction between the factors under investigation .

### 3.2.2. Inspection of response surface plots

In an analytical process where several independent variables ( $X_1$ ,  $X_2$  and  $X_3$ ) influence an experimental response, the observed response ( $Y$ ) is a function of the levels of the variables,  $Y = f(X_1, X_2, \dots, X_n)$ . The surface that is represented by this function is called the response surface, which is an  $n$ -dimensional surface in the  $(n + 1)$  dimensional space. In order to plot a useful graph, a 2D representation of a 3D or a contour graph can be drawn. When a response surface can be generated, inspection of the 2D surface or corresponding contour diagram allows for the assessment of the geometrical nature of the surface, eg. a stationary ridge, a rising ridge, a simple maximum, a simple minimum or a saddle point (minimax) (241, 242). A saddle point is defined as the stationary point of a surface response which presents the



maximum response for the levels of some variables and simultaneously the minimum response for the levels of other variables of the analytical system under investigation (243).

The response surface can be inspected using Canonical analysis and / or Lagrange's criteria (241). In this study Lagrange's criterion was used to determine the nature of the response surfaces generated. Lagrange's criterion is based on the calculation of the Hessian determinant of  $Y$  (241).

If the quadratic function shows only one stationary point  $(X_1, X_2, X_3)$ , four situations are possible:

- i). There is no information:  $\Delta_2=0$ ,
- ii). A relative maximum exists:  $\Delta_1<0; \Delta_2>0; \Delta_3<0$ ,
- iii). A relative minimum exists:  $\Delta_1>0; \Delta_2>0; \Delta_3>0$ ,
- iv). The presence of a saddle point exists: none of the above situations applies.

where,  $\Delta_3$  is the Hessian determinant of the function  $H(X_{10}, X_{20}, X_{30})$ ,  $\Delta_2$  and  $\Delta_1$  are calculated using Equation 3.9:

$$A = \begin{pmatrix} a_{11} & a_{12} & a_{13} \\ a_{21} & a_{22} & a_{23} \\ a_{31} & a_{32} & a_{33} \end{pmatrix}$$

$$\Delta_1 = a_{11},$$

$$\Delta_2 = \begin{pmatrix} a_{11} & a_{12} \\ a_{21} & a_{22} \end{pmatrix}$$

$$\text{where } a_{11} = \frac{\partial^2 Y}{\partial X^2}$$

$$\Delta_3 = \begin{pmatrix} a_{11} & a_{12} & a_{13} \\ a_{21} & a_{22} & a_{23} \\ a_{31} & a_{32} & a_{33} \end{pmatrix}$$

$$\text{Det (A)} = |A| = \begin{vmatrix} a_{11} & a_{12} & a_{13} \\ a_{21} & a_{22} & a_{23} \\ a_{31} & a_{32} & a_{33} \end{vmatrix} = a_{11} \begin{vmatrix} a_{22} & a_{23} \\ a_{32} & a_{33} \end{vmatrix} - a_{12} \begin{vmatrix} a_{21} & a_{23} \\ a_{31} & a_{33} \end{vmatrix} + a_{13} \begin{vmatrix} a_{21} & a_{22} \\ a_{31} & a_{32} \end{vmatrix} \quad \text{Equation}$$

### 3.9

A critical point of the function of several variables is a point at which the gradient of the function is either the zero vector 0 or is undefined. A first partial derivative will always vanish at the critical point if a function is made equal to 0.

The traditional approach of changing one factor at a time in method development is not an efficient or economic strategy since it does not provide any information about the position of the optimum and can, at best, lead only to a local optimum of the system. The one-at-a-time optimization approach also ignores interactions between factors and results in the need to conduct numerous analytical experiments. With the rapid increase in costs of experiments, it is vitally important that the development and optimization of any analytical method is achieved with as few experiments and as low a cost as possible (244-245).

In HPLC with ECD the composition, molarity and pH of the mobile phase are three critical factors that must be carefully selected in the early stages of method development.

Bearing these considerations in mind, an experimental design was performed to establish the characteristics of the mobile phase that produced the best analytical signal, since these parameters are known to influence the shape and retention of the analytical response of both the experimental blank and samples of CPT. The factors studied were the percent composition of acetonitrile, the pH and the molarity of the buffer used in the mobile phase. When applying experimental design methodologies, it is advisable to keep the number of variables to a minimum in order to avoid the development of highly complex response models and large degrees of variability (246).

A CCD approach was used to locate the optimum pH and molarity of buffer and organic solvent concentration conditions for the HPLC analysis of CPT by mapping the chromatographic response surface. This design is considered an efficient option in response surface methodology and an ideal alternative to the use of Box–Behnken designs (247-249). Furthermore CCD is a rotatable design and therefore, the factor levels are evenly spaced and readily coded for low, medium and high settings, as  $-1$ ,  $0$  and  $+1$ .

The CCD approach combines a fractional factorial with incomplete block designs to avoid extreme vertices and to present an approximately rotatable design with three levels per factor. The three chromatographic factors and levels selected for evaluation and in which experimental optimization, in terms of overall response ( $Y$ ), could be performed are shown in Table 3.3.

**Table 3.3** Experimental factors and levels used in the CDC

<b>Factor</b>	<b>Level (-)</b>	<b>Level (0)</b>	<b>Level (+1)</b>
Buffer pH	2.7	3.0	3.3
Buffer molarity (mM)	25	50	75
Organic solvent concentration (v/v)	25	30	35

The factors and ranges selected for consideration were based on previous univariate studies and chromatographic intuition. The composition of the mobile phase was defined as the volume of ACN with respect to total volume of solution.

The data generated were analyzed using Design Expert (Version 7.0.1, Stat-Ease Inc., Minneapolis, USA) statistical software. The significance of the Factors was calculated by Fisher's statistical test for Analysis of Variance (ANOVA) models that were estimated and run to their first order interaction terms. ANOVA for linear regression partitions the total variation of a sample into components. These components were then used to compute an  $F$ -ratio that evaluates the effectiveness of the model. If the probability associated with the  $F$ -ratio is low, the model is considered a better statistical fit for the data. In these calculations the higher-order interaction terms were assumed not to contribute to the behaviour of the statistical model to any great extent.

### **3.2.3. Voltammetry**

The technique for studying the relationship between applied potential and current generated is known as voltammetry. Voltammetry can be performed in a number of ways including Cyclic (250), Square-wave (251), Staircase (252), Linear-sweep (253), Fast cyclic (254), Stripping (255) and Hydrodynamic voltammetry (256).

Most of the voltammetric procedures have been applied to research applications for HPLC with ECD, however they have rarely been used for the routine analysis of pharmaceuticals.

Therefore only the hydrodynamic voltammetric approach relevant to the current study is discussed.

### 3.2.3.1. Hydrodynamic voltammetry

Hydrodynamic voltammetry (HDV) is a steady state technique in which the electrode potential is altered prior to the injection of an analyte and the resultant current is plotted as a function of potential. An ideal HDV for a mobile phase and an oxidizable species are shown in Figure 3.6. The HDV of a compound commences at a potential where the compound is not electroactive and therefore no Faradic current is evident and proceeds through a region in which the current increases to a plateau, where the compound reaching the electrode surface is completely oxidized. The HDV is characterized by the half-wave potential,  $E_{1/2}$ , which is defined as the potential at which the current is one-half its limiting value. The HDV is used to select the operating potential for liquid chromatography-electrochemical detection (LCEC) experiments. Two considerations are of major importance. Firstly quantitative determinations are based on the extent to which the redox current from the analyte can be distinguished from the background current, therefore, operating at the lowest applied potential means that the background current will increase with an increase in the applied potential. Secondly, operating on the limiting current plateau means that the redox current from the analyte is independent of an applied potential.

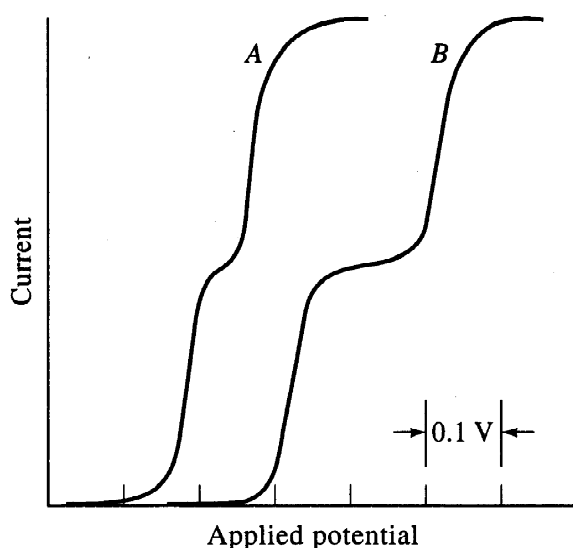


**Figure 3.6.** Typical hydrodynamic voltammograms used to study electrode kinetics

As can be seen in Figure 3.6 a voltammogram is a plot of current/ height or area response vs applied voltage ( $E_{\text{appl}}$ ). From this arrangement the current / response generated will measure the rate at which a species can be brought to the surface of an electrode.

Most analysts rely on HDV to determine operating potentials as cyclic voltammetry is not available to everyone. It is possible to construct a peak height –voltage curve through repeat injections of solutions of the analyte at different detector voltages.

CPT has a thiol functional group that may act as a scavenger of free radicals in living systems (257, 258). Several methods have been reported for the determination of CPT, including HPLC (259-263), Capillary Zone Electrophoresis (CZE) (264), GC (265-266) and GC-MS (267). The thiol functional group of CPT can undergo electrochemical oxidation at the surface of various electrodes (268-270) and therefore coulometric detection was selected for use in these studies to develop a method for the determination of CPT in pharmaceutical dosage forms.

CPT is a relatively unstable compound lacking appreciable UV absorbance. This makes assay of dosage forms very difficult (271), and the development of a simple ECD method may therefore play a major role in the analysis of CPT in dosage forms.

None of the analytical methods makes use of coulometric detection. Electrochemical detectors are able to detect weak currents of <1 nA generated in oxidative or reductive reactions of interest (272).

### **3.3. LITERATURE REVIEW**

Several methods for the analysis of CPT have been published using a variety of analytical techniques (259-267) and include the assay of CPT in dosage forms (268-275).

A summary of the information pertaining to the analysis of CPT is listed in Table 3.4. It is clear that derivatization is commonly used to facilitate the detection of CPT (259, 260, 262, 265) and that the most commonly used organic modifiers include ACN and MEOH (259, 263). ACN is preferred due to its low viscosity and polarity (273). Therefore, prior to commencing method development for the analysis of CPT it was decided that none of the conditions of published methods was suitable as derivatization formed part of most of the methods. Consequently it was decided to develop a HPLC-ECD method for the determination

of CPT. The parameters considered important were choice of column, internal standard, mobile phase composition and buffer due to the fact that CPT is a highly unstable drug in solution.

**Table 3.4.** Summary of the published analytical methods for the determination of CPT.

Compound	Sample	Technique	Mobile Phase /column conditions	Internal Standard	$\lambda$ (nm)	Reference
CPT	Plasma Tablets	HPLC	0.2% trifluoroacetic acid (pH 1.8)] and (acetonitrile): 87:13 (A:B)- pBPB as the derivatization reagent	sulphadimidine	263	<b>259</b>
CPT	Plasma	HPLC	n-hexane-2-propanol-methanol-acetic acid (68:15:15:2)- 2-bromo-2'-acetonaphthone	3,5 dinitro benzoic acid	246	<b>260</b>
CPT	Plasma	HPLC	acetonitrile-acetic acid 100%, pH 2.30 (42:58, v/v), N-(1-Pyrenyl)maleimide (NPM),	N-Acetyl-L-cysteine	340 (ex) 389(em)	<b>261</b>
CPT	Plasma	HPLC	acetonitrile-water acetic acid, (225:270:5, v/v/v)- pBPB as the derivatization reagent	Thiosalicylic acid	263	<b>262</b>
CPT	Plasma	HPLC	72.5:27.5 mixture of 0.1% phosphoric acid and methanol	Ascorbic acid	220	<b>263</b>
CPT	Tablets Plasma	CZE	100 Mm Borate at pH 9.0			<b>264</b>
CPT	Plasma	GC	n-hexane-2-propanol-methanol-acetic acid (68:15:15:2)- 2-bromo-2'-acetonaphthone as a derivatization reagent	3,5 dinitro benzoic acid	246	<b>265</b>
CPT	Plasma Urine	GC	The flow-rate of carrier gas (helium) was 30 ml/min.  The temperature of the column was 195" and those of the injection port and ion source were 27W. The acceleratig voltage, ionization voltage and trap current were 3.5 kV, 70 eV and 60 PA, respectively-Flame ionization detector	captopril-N-hexylmaleimide adduct		<b>266</b>
CPT	PlasmaUrine	GC-MS	The flow-rate of carrier gas (helium) was 30 ml/min.  The temperature of the column was 230 o C, and the injection port and ion source were kept at 270°C. The accelerating voltage, ionization voltage and trap current were 3.5 kV, 70 eV and 60 P-IA, respectively-derivatized with N-ethylmaleimide (NEM)	S-benzylcaptopril		<b>267</b>

### 3.3.1. Column choice

In all cases columns were allowed equilibrate for 30 minutes with the mobile phase delivered at a flow rate of 1.0ml/min prior to sample injection. Chromatographic system efficiency was established quantitatively by calculating the number of theoretical plates of the column using either Equation 3.12 or Equation 3.13:

$$N = 5.54 \frac{t_R}{W_{1/2}} \quad \text{Equation 3.12}$$

$$N = 16 \left( \frac{t_R}{W} \right)^{1/2} \quad \text{Equation 3.13}$$

where

- $N$  = the number of theoretical plates,
- $t_R$  = the retention time of a test peak,
- $W_{1/2}$  = the peak width at half peak height, and
- $W$  = the peak width at the baseline.

Band shape (101) was characterized by determining the asymmetric factor or tailing factor and the peak asymmetry factor,  $A_s$ , was calculated using Equation 3.14:

$$A_s = \frac{B}{A} \quad \text{Equation 3.14}$$

where

- $A_s$  = the peak asymmetry factor,
- $A$  = the width of the peak to the leading edge of the peak at 10% of the peak height, and
- $B$  = the width of the peak to the tailing edge of the peak at 10% of the peak height.

Symmetrical peaks will have a value of  $A_s = 1.0$  and usable columns produce peaks with  $A_s$  values of 0.90 to 1.3. Peak asymmetry was measured at 10% of the full peak height (276) and the calculation of column efficiency or number of theoretical plates,  $N$ , for these columns using equations 2.1 or 2.3 was based on the assumption that the peaks were Gaussian in nature (276, 277).



During the development of the analytical method an Inertsil<sup>®</sup> ODS 5  $\mu\text{m}$ , 15 cm x 4.6 mm column (Metachem Technologies Inc. Torrance, CA, USA), Supelcosil<sup>®</sup> ODS 5  $\mu\text{m}$ , 15 cm x 4.6 mm column (Alltech, Deerfield, IL, USA) and Phenomenex<sup>®</sup> C<sub>18</sub> Luna column, 150 mm x 2 mm, i.d. 5  $\mu\text{m}$  (Phenomenex<sup>®</sup>, Torrance, CA, USA) were tested. The Phenomenex<sup>®</sup> column was determined to have a plate count number of approximately 6000 and both the Inertsil<sup>®</sup> and Supelcosil<sup>®</sup> columns had  $N$  values of  $< 4500$ . Peak resolution and retention times were different for all columns. The peak tailing factor (PTF) calculated at 5% of full peak height for CPT ( $n = 3$ ) was 1.17 and the % RSD was 1.91. The asymmetric factor measured at 10% of full peak height was 1.33 with a % RSD of 1.73. Therefore the peaks generated when using the Phenomenex<sup>®</sup> column were better in terms of peak shape than those obtained using the other two columns. The Phenomenex<sup>®</sup> column was selected as a column of choice for use in the analysis of CPT

The effects of organic modifier, buffer molarity and mobile phase pH on the retention characteristics of CPT were also investigated.

### **3.3.2. Internal standard**

Many analysts prefer the use of an internal standard for quantitative analyses (278-280). The purpose of including an internal standard is to minimise system and procedure variability thereby eliminating variations in precision as a function of sample volume (281). The use of an IS minimises error that may be introduced as a result of sample preparation, apparatus and analytical technique (282, 283). Lindholm *et al* (283) and Hammerstrand (284) reported that the use of an internal standard is one method used to improve the accuracy of an analytical method and it compensates for varying injection volumes and day to day instrumental changes, thereby promoting method accuracy.

A known compound of fixed concentration is added to a sample of unknown concentration to produce a separate peak on the chromatogram. A plot of ratio of peak area/height to internal standard peak area/height versus concentration may be used to generate a calibration curve from which data from analysis of samples of unknown concentration can be determined by interpolation. The choice of an internal standard is most important and the peak must be completely resolved from all other peaks that may be present and the IS should elute near the peaks of interest. Other important considerations are that it must not react with other

components in the sample matrix and it must not be present in the original sample matrix (282).

Enalapril maleate, flouxetine, diazepam, acyclovir, fluconazole, imipramine and CYC were considered possible choices for use as internal standards due to their structural similarity to CPT.

CYC was selected as the internal standard of choice for this assay, based on chromatographic resolution, peak shape, run time and a hydrodynamic voltammogram or current-voltage (CV) curve at the working electrode similar to that generated for CPT.

### **3.4. METHOD**

#### **3.4.1. HPLC apparatus**

A modular HPLC system consisted of Waters Model M 6000A dual piston constant flow pump (Waters Associates, Milford, MA, USA), an automated Waters Intelligent Sample Processor Model 710B (Waters Associates, Milford, MA, USA.), a Model 5100A Coulochem dual electrode electrochemical detector with a Model 5010 analytical cell (Environmental Sciences Associates, Bedford, MA, USA) preceded by a carbon filter and a Spectra-Physics Integrator Model SP4290 (San Jose, California, USA) with attenuation set at 128. The mobile phase was constantly degassed using an in-line degasser Model ERC- 3000 (Erma Optical Works, Tokyo, Japan). The system included a Model 5020 guard cell (Environmental Sciences Associates) preceded by a carbon filter. The analytical column was 15 cm × 4.1 mm i.d. stainless-steel, packed with Phenomenex® Luna 5 $\mu$ m (C<sub>18</sub>) material (Phenomenex®, Torrance, CA, USA). This column was preceded by an Uptight Precolumn Kit (Upchurch Scientific, Oak Harbor, WA, USA) packed with glass beads. Both the guard and analytical columns were maintained at 22° C with a Model LC-22 temperature controller (Bioanalytical Systems, West Lafayette, IN, USA).

#### **3.4.2. Chemicals and Reagents**

All reagents were HPLC grade. CPT was a kind donation from Protea Chemicals (Midrand, South Africa) and the internal standard (IS), cyclizine (CYC) were donated by Aspen Pharmacare (Port Elizabeth, South Africa). As there are no solvents designed specifically for ECD, HPLC far UV grade acetonitrile (ACN) was purchased from Microsep (Port Elizabeth, South Africa). A Milli-Q Academic A10 water purification system (Millipore, Bedford, MA,

USA) that consisted of an Ion-ion<sup>®</sup>-exchange cartridge and a Quantum EX-ultrapore organex cartridge, which was fitted with a 0.22 µm Millipak<sup>®</sup> 40 sterile filters (Millipore<sup>®</sup>) prior to use was used in-house to further purify water that was used for the preparation of buffers. Potassium hydrogen phosphate, *o*-phosphoric acid (85%) and Sodium hydroxide pellets (analytical grade) were purchased from Merck Laboratories (Merck, Wadeville, South Africa).

### 3.4.3. Preparation of stock solutions

Standard stock solutions of CPT (100 µg/ml) and 500 µg/ml IS were prepared by accurately weighing approximately 10 mg and 50 mg of CPT and CYC, respectively on a top-loading analytical balance (Mettler Model AE163, Zurich, Switzerland) and then dissolving in 100 ml mobile phase. The stock solutions were sonicated for 5 minutes using a Branson B12 sonicator (Shelton, CN, USA). The stock was diluted serially with mobile phase to produce solutions of CPT of 2, 3, 5, 10, 20, 30, 50 and 70 µg/ml concentrations. All working standards were prepared with the internal standard, CYC at a concentration of 20 µg/ml. The solutions were stable for one day when stored at room temperature. Stock and standard solutions were protected from light using aluminium foil and placed at a cool temperature. Samples were not refrigerated as ECD is sensitive to dissolved gases and cold solutions contain more gas. The solutions were prepared on a daily basis, stored in the dark at about 10 °C, and used on the day they were prepared.

### 3.4.4. Preparation of buffers

Phosphate buffer (50mM) was prepared by accurately pipetting 3.4 ml of *o*-phosphoric acid (85%) into a 1L volumetric flask and making up to volume with HPLC grade water. The pH of the buffer was adjusted with 0.1M NaOH to a pH of 3. 0.1M NaOH was prepared by dissolving exactly 4.0 g of sodium hydroxide pellets in a 1L volumetric flask containing HPLC grade water. The pH was measured with a Crison GLP 21 pH-meter (Crison Instruments, Johannesburg, South Africa) at ambient temperature prior to the addition of acetonitrile. This approach leads to some uncertainty as to the actual pH of the final mobile phase, as the addition of organic solvents may change the pH of the mobile phase. However, this is much less important than poor reproducibility of the mobile-phase pH (*ie.* when the pH is measured after addition of the organic solvent) (273).

### 3.4.5. Preparation of mobile phase

The initial mobile phase was comprised of 50mM phosphate buffer: acetonitrile (70:30, v/v) adjusted to pH 3.0. The mobile phase was prepared daily, degassed by sonication and filtered using 0.45  $\mu\text{m}$  Durapore<sup>®</sup> membrane HVLP filters (Millipore Corporation, Ireland) before use. The mobile phase was recycled during long term analysis.

### 3.5. CHROMATOGRAPHIC CONDITIONS

The mobile phase was 50 Mm phosphate buffer (pH 3)-acetonitrile (70:30, v/v) which had been degassed and filtered through a 0.22 $\mu\text{m}$  Millipore membrane filter (Durapore type HVLP, Millipore). The flow rate was 1.0 ml min<sup>-1</sup> with a column back pressure of 120 atm. A full scan multi channel ESA Coulometric 5100A model detector was operated in the “oxidative-screen” mode with the upstream electrode ( $E_1$ ) set at +600 mV and the downstream or analytical electrode ( $E_2$ ) set at +950 mV, while the potential of the guard cell was set at +1050 mV. The detector gain was set at 300.  $E_1$  was set at a lower voltage than  $E_2$  and was used as an oxidative screen to eliminate compounds that oxidize at lower potentials than the compounds of interest, thereby minimizing the potential for interference. In order to ensure selectivity the potential for  $E_2$  was set at or above the oxidation potential that had been established for the compounds of interest. The potential applied to the electrodes of the analytical and guard cells were optimized to ensure oxidative efficiency and to reduce background noise. The voltage applied to the guard cell allowed mobile phase oxidation without modification of the response generated by the electrodes of the analytical cell. The potentials used generated a peak area response with minimum background noise and were therefore used as the basis for quantitation. Under these conditions CPT and CYC eluted at approximately 3.5 min and 7.5 min, respectively.

### 3.6. RESULTS AND DISCUSSION

CPT undergoes oxidation to form a dimer, captopril disulfide (285, 286). Amide hydrolysis has also been reported in aqueous solution (286). Timmins (286) showed that oxidation of CPT predominates in the pH range 2 to 5.6 and becomes an increasingly important consideration as the pH increases. A buffer pH of 3.0 was selected as the starting pH for these studies.

In addition, the wavelength of maximum absorption for CPT is situated in the far ultraviolet range (200 nm) (287-288), in which a lot of interferences may occur, therefore ECD was selected as a potential method for detection of CPT.

The HDV for the oxidation of CPT and CYC is shown in Figure 3.7. The limiting current plateau is reached at potentials  $> +1.1$  V for CPT and at potentials  $> +1.0$  V for CYC. Therefore a potential of  $+ 0.9$  V was selected for the detection of CPT. As can be seen, the response for CPT was sigmoid, and can be mathematically explained as a logistic function voltammogram. The porous graphite electrodes exhibited low residual current and noise. The background current was found to be  $< 14$  nA for the electrode settings selected for use.

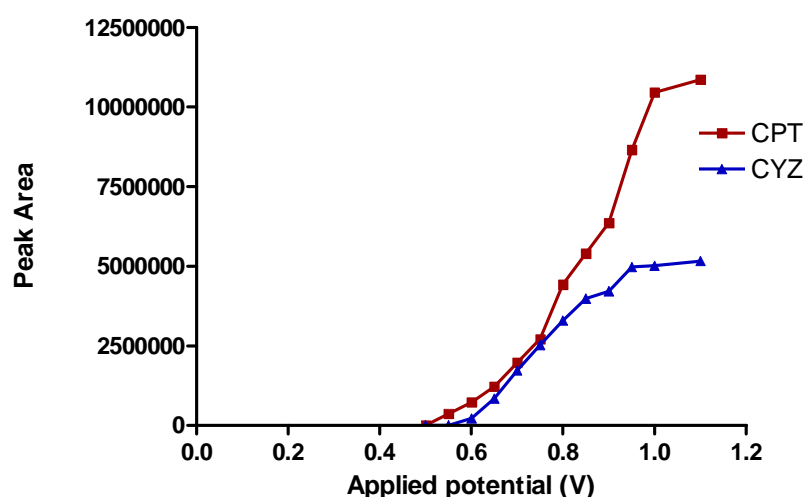


**Figure 3.7.** HDV for the oxidation of CPT and CYC recorded in the potential range 0.0–1.2 V.

The chosen chromatographic conditions revealed a good separation for CPT (50  $\mu$ g/ml) and the internal standard, CYC (20  $\mu$ g/ml) and no decomposition of CPT was observed during analysis. A typical chromatogram of the separation is shown in Figure 3.8.

The capacity factor calculated for this separation was within accepted values of  $> 2$  for the first peak and  $< 1$  for the second peak. The tailing factor was within the limits established by the FDA (289) guidelines. Lastly the resolution between the two peaks of interest was more than adequate for the method. Therefore, this method can be applied to its intended purpose.



**Figure 3.8.** Typical HPLC chromatogram of CPT (50  $\mu\text{g/ml}$ ) in the presence of the I.S. CYC (20  $\mu\text{g/ml}$ )

Two-dimensional contour plots and three-dimensional response plots are presented in Figures 3.9-3.14, which are very useful for studying the interaction effects of the factors on the responses. The retention time for CPT decreases as the ACN v/v % increases (Figure 3.9), when the molarity and pH of the buffer are constant. An increase in buffer molarity at constant pH and constant ACN v/v % results in decrease in the retention time of CPT (Figure 3.10), most likely due to the increasing competition of buffer cations for silanol sites which are preferentially attached to the column. This effect is prominent when the buffer molarity is greater than 50 mM.

Silica-based analytical columns show optimum stability and performance at pH values above 2.0. The effect of mobile phase pH on the retention time of CPT was therefore investigated in a pH range of 2.8-3.2. As can be seen from the contour plots, an increase in buffer pH (Figure 3.9, constant % v/v ACN) did not produce any change in retention time of CPT. However, the effect of buffer molarity and buffer pH on retention time showed a non-linear relationship (Figure 3.10). Figure 3.11 exhibits a nearly-linear relationship of buffer molarity and ACN concentration. Once more, the effect of % ACN is significant. An increase in buffer molarity slightly decreased the retention time of CPT as a consequence of increasing competition of

buffer cations for active silanol sites on the stationary phase. Since an increase of buffer molarity resulted in shorter retention times, a buffer of 50mM was chosen. The contour and response surface plots for the peak height ratios were not shown. Retention time was considered more critical in terms of sampling times during analysis. Buffer molarity and ACN concentration were significant for the regression model assumed.

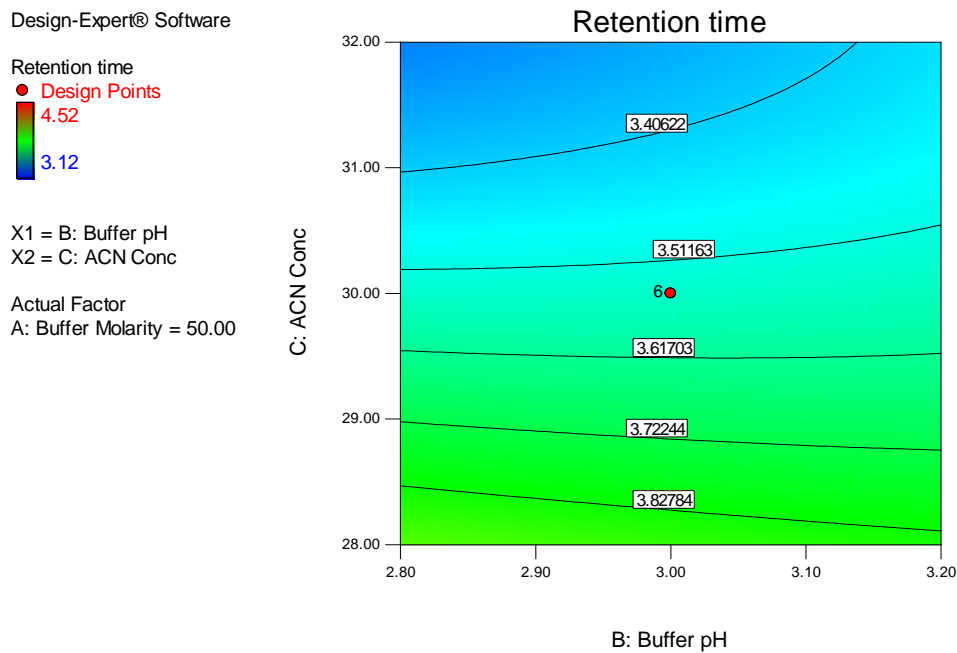


**Figure 3.9.** Contour plots for the retention time as a function of buffer pH (X-axis) and ACN concentration (Y-axis) of the mobile phase

Design-Expert® Software

Retention time  
● Design Points  
4.52  
3.12

X1 = A: Buffer Molarity  
X2 = B: Buffer pH

Actual Factor  
C: ACN Conc = 30.00

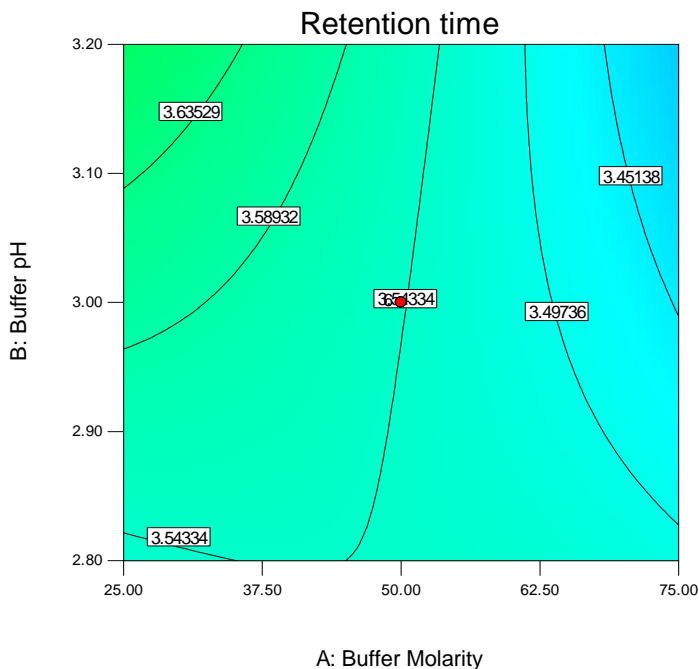


**Figure 3.10.** Contour plots for the retention time as a function of molarity (X-axis) and buffer pH (Y-axis) of the mobile phase

Design-Expert® Software

Retention time  
● Design Points  
4.52  
3.12

X1 = A: Buffer Molarity  
X2 = C: ACN Conc

Actual Factor  
B: Buffer pH = 3.00

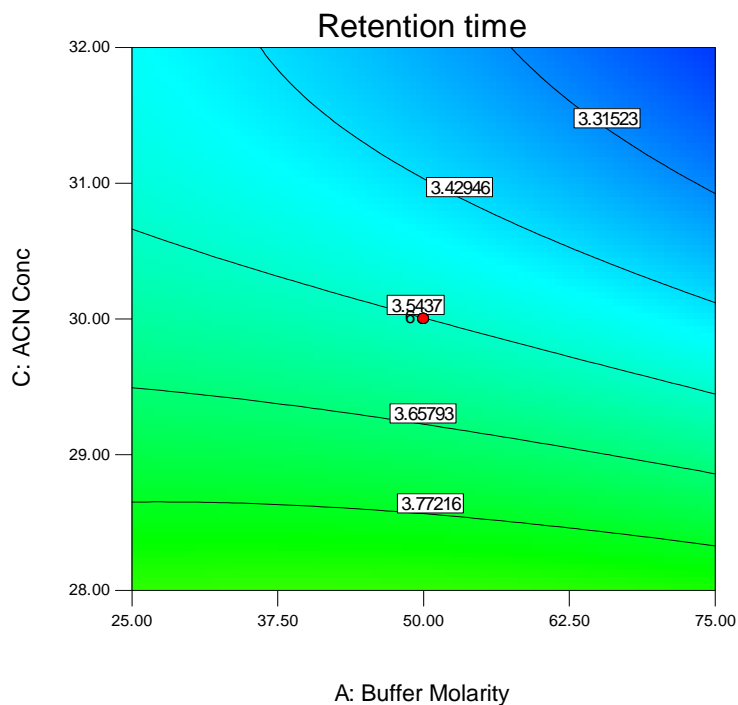


**Figure 3.11.** Contour plots for the retention time as a function of molarity (X-axis) and ACN concentration (Y-axis) of the mobile phase.



Response surface plots (Figure 3.12-3.14) show the relationship between these factors even clearer.

Design-Expert® Software

Retention time

○ Design points below predicted value



X1 = B: Buffer pH  
X2 = C: ACN Conc

Actual Factor  
A: Buffer Molarity = 50.00

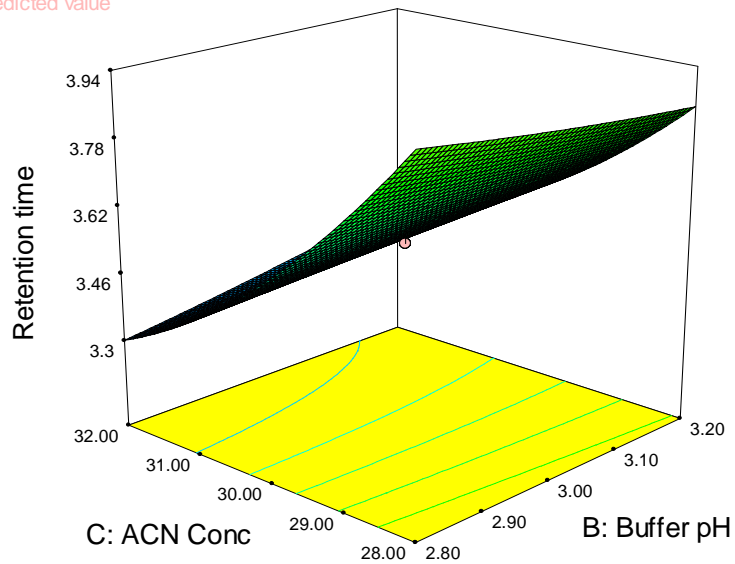


**Figure 3.12.** Response surface plots for the retention time as a function of buffer pH (X-axis) and ACN concentration (Y-axis) of the mobile phase

Design-Expert® Software

Retention time

○ Design points below predicted value



X1 = A: Buffer Molarity  
X2 = B: Buffer pH

Actual Factor  
C: ACN Conc = 30.00

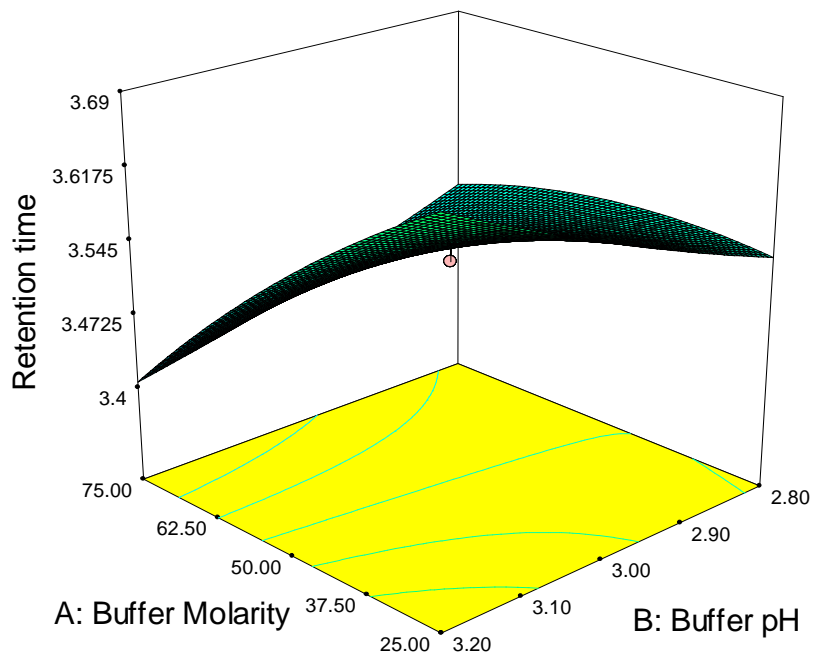


**Figure 3.13.** Response surface plots for the retention time as a function of buffer molarity (X-axis) buffer pH (Y-axis) of the mobile phase

Retention time

○ Design points below predicted value



X1 = A: Buffer Molarity

X2 = C: ACN Conc

Actual Factor

B: Buffer pH = 3.00

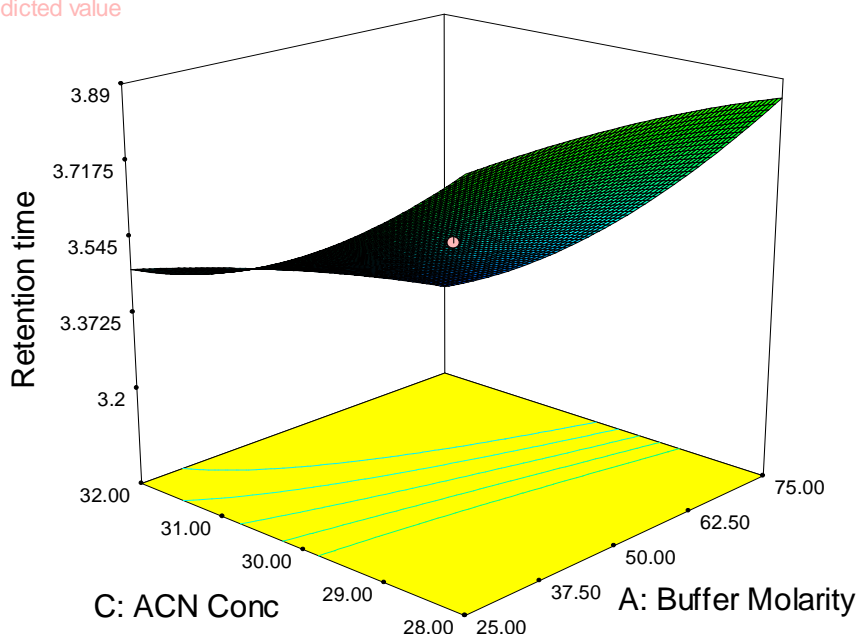


**Figure 3.14.** Response surface plots for the retention time as a function of buffer molarity (X-axis) and ACN concentration (Y-axis) of the mobile phase

The chosen model had seven main effects and nine first-order interactions. All experiments were performed in a randomized fashion in order to minimize the effects of uncontrolled factors that may introduce bias on the response. A classical second-degree model with a cubic experimental domain was postulated. The coefficients for the second-order polynomial model were estimated by least squares regression. The equation for the  $Y_1$  (retention time) factor is shown in Equation 3.15:

$$Y_1 = 3.54 - 0.077X_1 + 0.011X_2 - 0.26X_3 - 0.061X_1X_2 - 0.061X_1X_3 + 0.054X_2X_3 - 0.019X_1^2 + 0.00704X_2^2 + 0.076X_3^2$$

**Equation 3.15**

$$\text{Retention time} = 3.54 - 0.077\text{Molarity} + 0.011\text{Buffer pH} - 0.26\text{ACN concentration} - 0.061 \text{Molarity Buffer pH} - 0.061\text{Molarity: ACN concentration} + 0.054 \text{Buffer pH: CAN concentration} - 0.019 \text{Molarity}^2 + 0.00704 \text{Buffer pH}^2 + 0.076 \text{ACN Concentration}^2$$

The equation for  $Y_2$  (peak height ratio) is shown in Equation 3.16:

$$Y_2 = 0.53 + 0.11X_1 - 0.10X_2 + 0.52X_3 + 0.67X_1X_2 - 0.35X_1X_3 - 0.49X_2X_3 + 0.20X_1^2 + 0.24X_2^2 + 0.62X_3^2$$

**Equation 3.16**

The solution of the quadratic models was obtained by matrix calculation with Cramer's rule and Eigenvalue method (290) using determinants and Eigenfunctions, respectively to determine the optimized conditions of chromatography. The solutions that were obtained for  $Y_1$  (retention time) were:

1.  $X_1$  (buffer molarity) = 51 mM,
2.  $X_2$  (buffer pH) = 2.97
3.  $X_3$  (% ACN) = 31.01 % v/v

The optimized chromatographic conditions were then used for all future analytical studies. The typical chromatogram shown (Figure 3.8) in § 3.6 was obtained by using the set conditions.

The model was validated by analysis of variance (ANOVA) using Design Expert software that had been used to develop the experimental plan for RSM. The test was performed and the Fisher  $F$ -ratio was calculated. This ratio was used to measure the significance of the model under investigation with respect to the variance of all the terms included in the error term at  $p = 0.05$ . In ANOVA analysis, a model that is significant is desired. The  $p$ -values listed in Table 3.5 reveal that for all responses, the cross product contribution of the model was not significant.

The Model  $F$ -value of 2.81 (Table 3.5) implies there is a 7.00% chance that a "*Model F-Value*" this large may occur due to noise. The values of "Prob > F" less than 0.0500 indicate that the terms in a model are significant, however in this case Prob > F is greater than 0.05 which indicates that the model is not significant. This means that the terms in the model do not have a significant effect on the response. Conversely, the effect of ACN concentration is significant. The lack of fit is said to be not significant and this is desirable as a model that fits the data is essential in optimisation studies. Since there are a number of model terms that were not significant it was necessary to perform a model reduction step in order to improve the model.

**Table 3.5.** ANOVA Table for Response Surface Quadratic Model for retention time

Source	Sum of Squares	df	Mean Square	F-value	p-value Prob > F	
<b>Block</b>	0.035	1	0.035			
<b>Model</b>	1.20	9	0.13	2.81	0.0700	<b>not significant</b>
A-Buffer Molarity	0.080	1	0.080	1.69	0.2257	
B-Buffer pH	1.618E-003	1	1.618E-003	0.034	0.8576	
C-ACN Conc	<b>0.94</b>	<b>1</b>	<b>0.94</b>	<b>19.82</b>	<b>0.0016</b>	<b>significant</b>
AB	0.030	1	0.030	0.63	0.4470	
AC	0.030	1	0.030	0.63	0.4470	
BC	0.023	1	0.023	0.49	0.5029	
A <sup>2</sup>	5.459E-003	1	5.459E-003	0.12	0.7423	
B <sup>2</sup>	7.148E-004	1	7.148E-004	0.015	0.9050	
C <sup>2</sup>	0.083	1	0.083	1.75	0.2183	
<b>Residual</b>	0.43	9	0.047			
<b>Lack of Fit</b>	0.43	5	0.085			
<b>Pure Error</b>	0.000	4	0.000			
<b>Cor Total</b>	1.66	19				

<b>Std. Dev.</b>	0.22	<b>R<sup>2</sup></b>	0.7374
<b>Mean</b>	3.58	<b>Adj R<sup>2</sup></b>	0.4748
<b>C.V. %</b>	6.09	<b>Pred R<sup>2</sup></b>	-1.7108
<b>PRESS</b>	4.41	<b>Adeq Precision</b>	6.680

A background elimination procedure was selected as the method of choice to reduce the number of insignificant terms and the resulting ANOVA table for the reduced quadratic model is shown in Table 3.6. The results clearly indicate that the model is significant. To reduce a model in the presence of collinearity, backward selection is considered more robust than forward or stepwise selection. The significant model term is the concentration of ACN and this is the only variable that significantly influences the retention time of CPT ( $p = 0.0016$ ). The lack of fit is also not significant. The  $R^2$  value obtained is 0.5783. The predicted  $R^2$  value is in agreement with the adjusted  $R^2$  value. The adjusted  $R^2$  value is particularly useful when comparing models with different numbers of terms. This comparison is however performed in the background when model reduction is undertaken. Precision was used to compare the ranges of predicted values generated at the points of the experimental design to the average prediction error. Values for the ratio  $> 4$  indicate adequate model discrimination. In this particular case the value was well above 4.

A negative "Pred R-Squared" implies that the overall mean is a better predictor of response than the current model. The term "Adeq Precision" was used to measure the signal to noise ratio. The ratio of 6.680 indicates an adequate signal and hence this model can be used to navigate the resultant design space.

The "Model F-value" of 2.00 (Table 3.7) for peak area ratio implies that the model is not significant relative to the noise. There is a 15.79 % chance that a "Model F-value" this large would occur due to noise. Values of "Prob  $> F$ " less than 0.0500 indicate that the model terms are significant.

In this case  $B^2$  and  $C^2$ , the square of the buffer pH and ACN concentration, respectively, are significant model terms. Values greater than 0.1000 indicate that the model terms are not significant. If there were many insignificant model terms excluding those required to support hierarchy, model reduction was to be performed to improve the model.

**Table 3.6.** ANOVA Table for Response Surface Model for retention time (model reduction)

Source	Sum of Squares	df	Mean Square	F-value	p-value Prob> F	
Block	0.035	1	0.035	23.31	0.0002	
Model	0.94	1	0.94	23.31	0.0002	<b>significant</b>
C-ACN Conc	0.94	1	0.94			
Residual	0.69	17	0.040			
Lack of Fit	0.69	13	0.053			
Pure Error	0.000	4	0.000			
Cor Total	1.66	19				

<b>Std. Dev.</b>	<b>0.20</b>	<b>R<sup>2</sup></b>	<b>0.5783</b>
<b>Mean</b>	3.58	<b>Adj R<sup>2</sup></b>	0.5535
<b>C.V. %</b>	5.61	<b>Pred R<sup>2</sup></b>	0.3195
<b>PRESS</b>	1.11	<b>Adeq Precision</b>	11.346

**Table 3.7.** ANOVA Table for Response Surface Quadratic Model for peak area/height ratio

Source	Sum of Squares	df	Mean Square	F-value	p-value Prob > F	
Block	424.64	1	424.64			
Model	4496.35	9	499.59	2.00	0.1579	<b>not significant</b>
A-Buffer Molarity	17.48	1	17.48	0.070	0.7972	
B-Buffer pH	840.02	1	840.02	3.37	0.0997	
C-ACN Conc	4.14	1	4.14	0.017	0.9004	
AB	361.75	1	361.75	1.45	0.2593	
AC	98.50	1	98.50	0.39	0.5454	
BC	192.55	1	192.55	0.77	0.4026	
A <sup>2</sup>	100.88	1	100.88	0.40	0.5407	
B <sup>2</sup>	<b>1578.55</b>	<b>1</b>	<b>1578.55</b>	<b>6.33</b>	<b>0.0330</b>	<b>significant</b>
C <sup>2</sup>	<b>1375.91</b>	<b>1</b>	<b>1375.91</b>	<b>5.51</b>	<b>0.0434</b>	<b>significant</b>
Residual	2245.89	9	249.54			
<b>Lack of Fit</b>	2242.63	5	448.53	551.47	< 0.0001	
<b>Pure Error</b>	3.25	4	0.81			
Cor Total	7166.87	19				

<b>Std. Dev.</b>	15.80	<b>R<sup>2</sup></b>	0.6669
<b>Mean</b>	19.08	<b>Adj R<sup>2</sup></b>	0.3338
<b>C.V. %</b>	82.79	<b>Pred R<sup>2</sup></b>	-2.3726
<b>PRESS</b>	22738.61	<b>Adeq Precision</b>	4.455

As noted earlier, the negative "Pred R-Squared" implies that the overall mean is a better predictor of response than the current model. A ratio of 4.455 indicates an adequate signal and that this model can be used to navigate the design space.

The model that has been developed can be used to predict the retention time of CPT and peak ratio within the limits of the experiments. The normal probability plot of the residuals and the plot of the residuals versus the predicted response for both the retention time and peak areas are shown in Figures 3.15-3.18.

Close inspection of Figures 3.15 and 3.17 reveals that the residuals generally fall on a straight line which indicates that the errors are normally distributed, thus supporting the fact that the model fits the data adequately. These plots are very important and are required to check the normality assumption in a fitted model. This will ensure that the model provides an adequate approximation to the optimization process. It is clear that there is no obvious pattern followed in the residual versus predicted response as shown in Figures 3.16 and 3.18. The plots reveal an almost equal scatter above and below the x-axis, implying that the proposed models are adequate and there is no reason to suspect any violation of the independence or constant variance assumption.



Design-Expert® Software  
Retention time

Color points by value of  
Retention time:

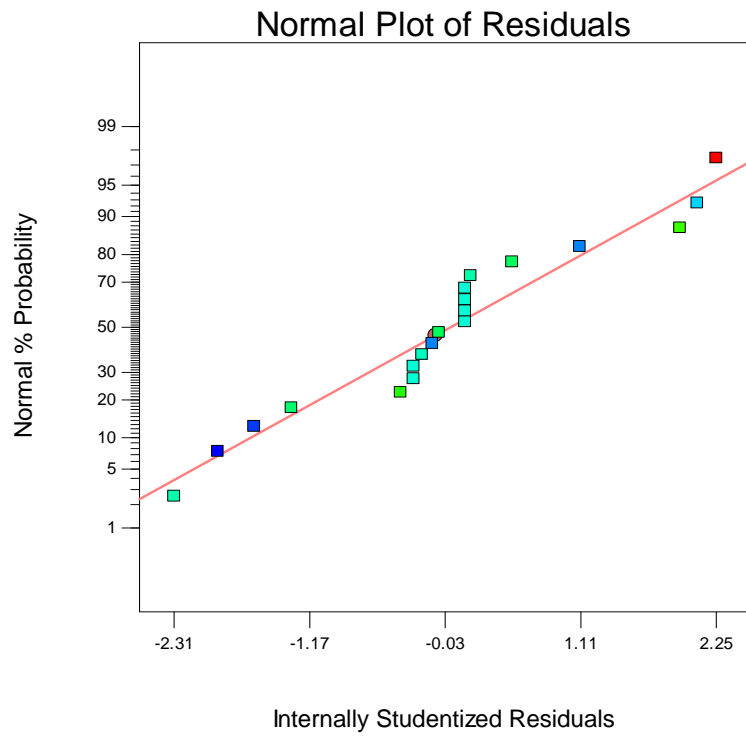


Figure 3.15. Normal probability plot of residual for retention time.

Design-Expert® Software  
Retention time

Color points by value of  
Retention time:

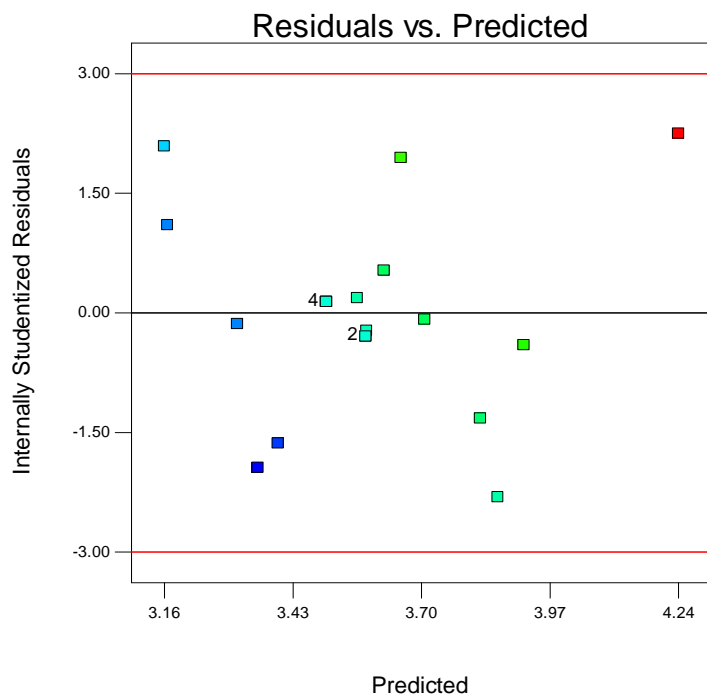


Figure 3.16. Plot of residual vs. predicted response for retention time.

Design-Expert® Software  
Peak Ratio

Color points by value of  
Peak Ratio:

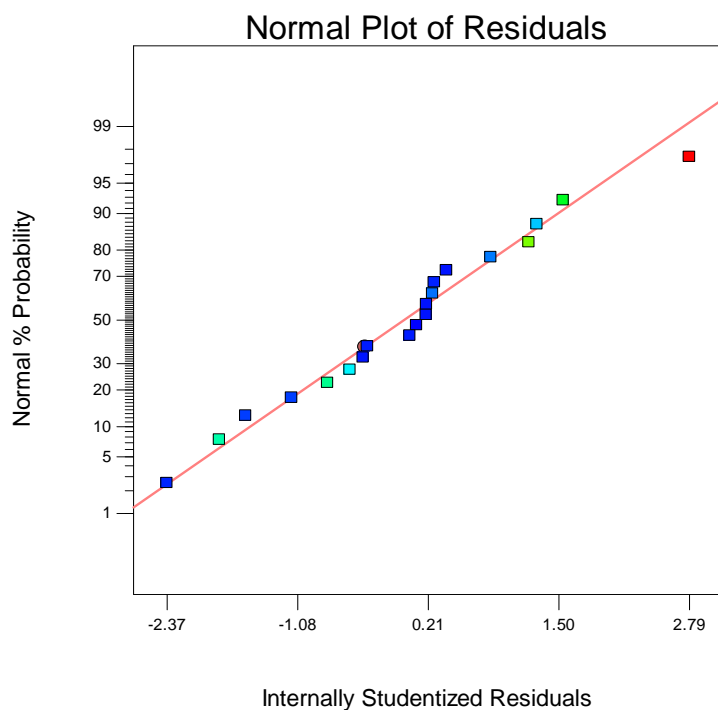


Figure 3.17. Normal probability plot of residual for ratio of peak areas.

Design-Expert® Software  
Peak Ratio

Color points by value of  
Peak Ratio:

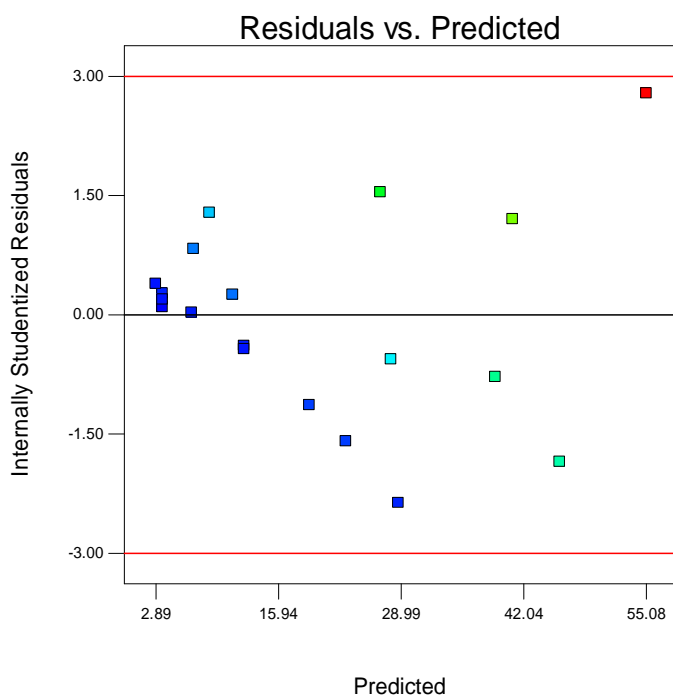


Figure 3.18. Plot of residual vs. predicted response for peak area ratios.

### 3.7. CONCLUSIONS

Although there are HPLC methods available for measuring CPT in dosage forms (99, 100) there is no reported method in which coulometric ECD has been used. In particular the major advantage of this HPLC-ECD method over UV detection is that time-consuming pre-column derivatization procedures are eliminated. The advantages of this method over the use of derivatisation used for detection with UV lies in the improvement of the detectability, that is to say lower detection limits and or more sensitive response. Furthermore, the derivatives can be difficult to prepare and reaction products often need to be removed before analysis. Most of the derivatising agents are odorous and hazardous and the reaction conditions are frequently severe which could result in short life time of the guard and analytical columns used. On the other hand, the disadvantages of derivatisation include possible interference by excess reagent and the formation of artifacts.

HPLC-ECD is highly selective, sensitive and is simpler than the derivatization procedure which has the potential of some steps in the reaction not going to completion. Furthermore, sample components may be absorbed by the column resulting in low detector response.

The ESA coulometric ECD offers several advantages in that close to 100 % of the analyte is oxidized in the flow-through porous graphite electrodes. In the coulometric mode, measurement is based on oxidation of the sulfhydryl functional group of CPT and there is minimal electrode oxidation, a longer electrode half-life and excellent baseline stability.

The application of RSM in conjunction with CCD to modelling and optimizing the performance of an HPLC method has been discussed. CCD was used to design an experimental program for modeling the effects of mobile phase pH and molarity and concentration of ACN on the peak area ratio and retention time of CPT. Twenty experiments including centre points were conducted. Equations for the mathematical model were derived for both peak height ratio and retention time for CPT by using the experimental data and the statistical software package Design Expert 7.1.

The predicted values from the model equations were found to be in good agreement with observed values, and to gain a better understanding of the three variables evaluated to achieve an optimal retention time, the models were presented as 3D response surface plots. The models allow for the confident prediction of performance by interpolation of data over the

range of information used to construct the response surface plots. The results reveal that the concentration of ACN has a significant effect on retention, whereas buffer molarity has a smaller effect. This study demonstrates that RSM and CCD can be applied to modeling and optimizing retention time and that it is an economical method that can be used to generate a maximum amount of information in a short period of time with a small number of experiments.

The observed responses were close to the predicted values for the optimized method. It can be concluded that the characterization and optimization of the analysis was performed in a very short time and with a small number of experimental runs. It is clear that experimental design methodology is an economic approach for extracting the maximum amount of information and saves significant amounts of time in addition to the minimization of use of materials and personnel costs.

The proposed method will be validated to determine whether it is suitable for routine analysis and content uniformity testing of CPT in tablets. This study has also presented significant progress in the identification of optimal HPLC operating conditions for the analysis of CPT. The experimental design was deemed suitable for the exploration of quadratic response surfaces and for the construction of second-order polynomial models, thus facilitating the optimization process with a limited number of experiments. For the three-level three-factorial CCD, 20 experiments were required. The resultant model contained quadratic terms explaining the non-linear nature of the responses observed, and which were adequately predicted. The experimental design approach resolved a two-factor interaction effect for the individual terms and allows a mid-level setting (0) for the combination of factors.

The mobile phase and chromatographic conditions selected for the validation process from the model are ACN (30 %), pH = 3 and Buffer molarity (50 mM) and the analytical method validation process can now be conducted.

### THE VALIDATION OF A HIGH PERFORMANCE LIQUID CHROMATOGRAPHIC METHOD WITH ELECTROCHEMICAL DETECTION FOR THE QUANTITATION OF CAPTOPRIL

#### 4.1. INTRODUCTION

The validation of bioanalytical methods has been frequently discussed over the last decade at meetings in London and Arlington (291-292). The main issues discussed at these meetings related to the type and nature of certain aspects of analytical methods that must be investigated and reported in a validation protocol for bioanalytical methods in order to support an application for market authorisation with bioavailability, bioequivalence and pharmacokinetic studies in man and animals. As a consequence of these discussions, the US Food and Drug Administration (FDA) issued detailed recommendations for validation of bioanalytical methods (291, 293). The International Conference on Harmonisation (ICH) has also provided definitions relating to validation issues included in “analytical procedures” for the fields of bioanalytical methodology, pharmaceutical and biotechnological processes (291, 294-296).

Several protocols or guidelines validation of analytical methods have been produced and are recommended by bodies such as the ICH, the International Union of Pure and Applied Chemistry (IUPAC) and FDA (297-298). Prior to use in routine analysis an analytical method must first be validated in order to demonstrate its suitability for the intended purpose (299). Validation parameters such as selectivity, linearity, accuracy, precision and recovery must be evaluated in every analytical application. The limits of quantitation (LOQ) and detection (LOD), stability, and ruggedness/robustness should also be investigated, however these have been evaluated to a lesser extent in the past (299). The LOQ should be included in the construction of the calibration curve, whereas the LOD should not, as the former is a more stable parameter of an analytical method. Ruggedness and/or robustness tests have rarely been performed in many of methods reported in the literature (299, 300).

The validation process is often viewed as a test of the acceptability of a specific method. However, the real goal of a validation process is to challenge the method and establish the limits of variability for the conditions needed to run the method, such that a desired outcome will be achieved (301). It is best to prioritize the components of any validation procedure and

typically, specificity, linearity, accuracy, and precision studies are needed initially, after which stability and ruggedness studies are conducted (301).

The HPLC method with ECD detection for the analysis of CPT was validated in accordance with some validation procedures used for validation of pharmaceutical methods (302-307).

## **4.2. VALIDATION**

### **4.2.1. Calibration, linearity and range**

The linearity within a given range of an analytical procedure is an indication of the ability to obtain a measured response that is directly proportional to the concentration of analyte in the sample. The linearity of the analytical method was established by fitting calibration curve data to a least squares linear regression model using GraphPad Prism (Version 5.01 for windows, GraphPad Software, San Diego, CA, USA) software.

The linearity of an analytical method is used to show that test results are either directly, or by a well-defined mathematical transformation, proportional to the concentration of an analyte in samples within a given range (308).

The linear correlation co-efficient is normally used as a measure of the linearity of a method and a value of  $\geq 0.99$  is usually required to consider a method to be linear in that range (299, 308). However a high value for the correlation co-efficient does not necessarily indicate a method has a linear standard curve (309).

The range of an analytical method is the interval between upper and lower levels, inclusive of the limits of analyte that have been determined with a suitable level of precision, accuracy and linearity using the method as described (310).

The CPT/CYC peak area of response was plotted against concentration of CPT to generate the calibration curve. The response of six standard solutions of 2.0, 5.0, 10.0, 30.0, 50.0 and 70.0  $\mu\text{g/ml}$  concentration were subject to regression analysis to establish the calibration equation and a correlation coefficient. The detector responses were found to be linear over the concentration range studied and the results are summarised in Table 4.1.

**Table 4.1.** Linearity data

<b>Parameter</b>	
Concentration range ( $\mu\text{g/ml}$ )	2- 70
Regression equation	$y = 0.0131x + 0.0275$
Correlation coefficient ( $R^2$ )	0.978
Standard error on estimation ( $S_e$ )	0.058

Prior to analysis of samples the analytical column was equilibrated for at least 30 min with the mobile phase. Each sample was analysed in replicates of five to verify the reproducibility of detector response at each concentration level.

The calibration curve had a slope of 0.0131 and a y-intercept of 0.0275 with a correlation coefficient of 0.978.

#### **4.2.2. Precision**

The precision of an analytical method is the degree of agreement among individual test results when the procedure is applied repeatedly to multiple aliquots of a homogeneous sample (311-313). Reproducibility of results using different instruments, analysts, sample preparations, laboratories, data obtained on a single day or over multiple days may all constitute an assessment of the precision of an analytical method. In addition different levels of precision are often assessed as part of the method development process (311-313).

The precision of a method is usually reported as the percent relative standard deviation (% RSD) of a set of responses. The precision can be subdivided into three categories, *viz.* repeatability (intra-day precision), intermediate precision (inter-day precision) and reproducibility (between laboratories precision) (314-317).

Precision at two levels was established for this method, *viz.* repeatability and intermediate precision and the tolerance for RSD and relative error (RE) were set at  $\pm 5\%$  for these studies.

##### **4.2.2.1. Repeatability or intra-day precision**

The repeatability of a method is established when analysis is performed in one laboratory by a single analyst using the same equipment on the same day. Repeatability can be tested by analysis of a minimum of five determinations at three different concentrations, *viz.*, low,

medium and high within the range of concentrations expected. However the ICH guidelines recommend that repeatability be assessed by analysis of three different concentrations in triplicate or by analysing samples at 100% of the test concentration six times (317, 318).

The intra-day precision obtained following analysis of three different standard solutions of CPT with the internal standard, CYC, and the resultant data are summarized in Table 4.2.

The results reveal that all RSD and RE values were less than 5% and are within the limits set in our laboratory, confirming that the method is repeatable.

#### **4.2.2.2. Intermediate precision**

Intermediate precision or inter-day variability is the agreement of complete measurements including standards when the same method is applied to samples many times within the same laboratory (313). Such determinations may include complete analysis of samples on different days with the same or different instruments by the same or different analysts, but would involve the preparation of multiple samples and standards. The inter-day variability of this method was assessed over three days at three low, medium and high concentrations of CPT standard in replicates of six. Sample preparation was conducted as detailed in § 3.3.3 and the results are given in Tables 4.3 and 4.4.

The inter-day precision was found to be < 5%, confirming that the method is precise.

#### **4.2.2.3. Reproducibility**

The reproducibility of a method establishes the precision between laboratories and is often determined in collaborative studies or method transfer experiments (301). As all analysis were performed by the same analyst in one laboratory using the same equipment it was not necessary to establish the reproducibility of this method.



**Table 4.2.** Intra-assay precision and accuracy data for CPT analysis (n = 6)

Concentration (µg/ml)	Calculated Concentration Mean ± SD;	% RSD	% RE
5.00	4.92 ± 0.15	3.05	+ 1.60
10.00	9.89 ± 0.08	0.81	+1.10
30.11	28.97 ± 1.12	3.87	+3.79

**Table 4.3.** Inter-day precision and accuracy data for CPT analysis

Quality Control	CPT								
	Day 1 (n = 6)				Day 2 (n = 6)			Day 3 (n = 6)	
<b>Theoretical concentration (µg/ml)</b>	5.00	10.14	30.01	5.07	10.05	30.04	5.02	10.11	30.24
<b>Calculated concentration (µg/ml)</b>	5.03	10.04	30.34	5.10	9.80	29.67	5.01	9.73	30.04
<b>% RSD %</b>	0.91	0.65	1.94	0.03	0.06	0.02	0.02	0.06	0.59
<b>% RE</b>	-0.60	0.99	-1.10	-0.59	2.49	1.23	0.20	3.76	0.66

% Relative error = [(added- found)/added] x 100

**Table 4.4.** Inter-day precision and accuracy data for CPT analysis

<b>Drug</b>	<b>Average Theoretical Value (µg/ml)</b>			<b>% RSD</b>			<b>% RE</b>		
CPT	5.05	9.86	30.02	0.99	1.62	0.40	-0.40	2.38	0.27

**Table 4.5.** Accuracy test results of blinded samples

<b>Theoretical concentration (µg/ml)</b>	<b>Mean concentration determined (µg/ml) ± SD</b>	<b>% RSD</b>	<b>% Bias</b>
5.02	5.07 ± 0.115	2.27	+ 0.99
9.98	10.06 ± 0.042	0.42	+0.80
30.01	30.11 ± 0.156	0.52	+0.33

### **4.2.3. Accuracy and bias**

The accuracy of an analytical method is defined as the closeness of a measured value to the true value of an analyte in a sample (301, 313, 315, 316). A tolerance of 2% was set for % RSD for this parameter as this complies with the limits set by a number of pharmaceutical industries (317). The bias is an indication of the influence of an analyst on the performance of a method. Accuracy and bias were assessed by repeat measurement of three samples of different concentration. The FDA recommends that accuracy studies for drug products be performed at 80, 100 and 120% of the target concentration (318). The results of accuracy studies are listed in Table 4.5, and reveal that the greatest bias was 0.99%, indicating that no value for bias deviated by approximately more than 2.00% of the stated value. The RSD values for all but the 5.0 µg/ml sample were less than 5% and the Bias values (Table 4.5) were all less than 1% suggesting that the method was accurate.

Accuracy was evaluated by injecting samples of three different concentrations equivalent to 80, 100 and 120% of the intended content of active ingredient, following addition of a known amount of CPT to the sample and calculating the % recovery and RSD for each concentration.

The % recovery achieved ranged between 95.65 and 99.88% (Table 4.6) and the corresponding % RSD values were well below 5 % indicating the method is accurate.

#### 4.2.3.1. Assay

In order to establish the applicability of the method for the analysis of CPT in dosage forms, five commercially available pharmaceutical products were purchased and subjected to analysis. The products were:

- i. CaptoHexal® 50
- ii. MERCK-CAPTOPRIL
- iii. ZAPTO-50
- iv. Sandoz Captopril 50
- v. ADCO-CAPTOMAX 50

The average drug content was found to be 95.65 and 99.88% of the labelled claim for all products tested. No interfering peaks were observed in the resultant chromatograms indicating that there was no interference from excipients used in the manufacture of the tablets. The results are shown in Table 4.6.

Accuracy of the developed HPLC analytical method was evaluated by the recoveries of known amounts of CPT which were added to the drug product.

**Table 4.6.** Results of analysis of commercially available CPT products (n =5)

<b>Analyte</b>	<b>Amount Added</b>	<b>Found (mg / tablet) ± SD</b>	<b>Recovery (%)</b>	<b>% RSD</b>
<b>Label claim (50mg)</b>	<b>(mg)</b>			
CaptoHEXAL® 50	50.0	49.56 ± 0.57	99.76	1.15
MERCK-CAPTOPRIL	50.0	49.57 ± 1.03	99.78	2.08
ZAPTO-50	50.0	49.41 ± 0.47	99.46	0.95
Sandoz Captopril 50	50.0	49.44 ± 1.02	99.51	2.06
ADCO-CAPTOMAX 50	50.0	49.03 ± 1.62	98.69	3.30

#### 4.2.4. Limits of quantitation and detection

Recent articles have included much discussion regarding the determination of the limits of quantitation (LOQ) and detection (LOD) values for an HPLC method (311, 320-321). Paino and Moore (322) described four techniques to establish the LOQ and LOD of analytical methods systems. The determination of the parameters may be achieved by establishing

- i) The lowest concentration for which the  $RSD \leq 5\%$ ,
- ii) A plot of standard deviation versus concentration,
- iii) A confidence interval for the best-fit line,
- iv) The signal-to-noise ratio.

The LOQ is the lowest concentration of analyte that can be determined with an acceptable level of certainty. It should be established using an appropriate measurement standard or sample and it is usually the lowest calibration standard used to construct a calibration curve (excluding the blank).

The LOD for an analyte is often determined by repeated analysis of a blank test sample and is the analyte concentration for which the response is equivalent to the mean response of blank plus three standard deviations. The value of the LOD is likely to be different for samples of different type and matrix (323).

The LOQ is also defined as the lowest amount of analyte in a sample that can be quantitatively determined with precision and accuracy under the stated experimental conditions (313, 316) and the LOD is the lowest amount of an analyte in a sample that can be detected but not quantitated as an exact value (313, 316). For chromatographic analysis the LOD may be defined as that concentration that produces a peak height response three times greater than that of the baseline noise. Although various methods for estimating the LOD have been described, an experimental assessment provides the best measure of the operating limits of an analytical method and the associated instrumentation.

The LOQ is generally determined by the analysis of samples of known concentration and the establishment of the minimum level at which the analyte can be quantitated with acceptable accuracy and precision.

The LOQ and LOD of the method developed for the analysis of CPT were established using a precision of  $\leq 5.0\%$ . By convention, the LOD was taken as  $0.3 \times \text{LOQ}$  (322). The LOQ was found to be  $2.0\mu\text{g/ml}$  ( $\% \text{RSD} = 2.27$ ), and LOD based on this approach was  $0.6 \mu\text{g/ml}$ .

#### **4.2.5. Specificity**

The specificity of an analytical method is a measure of the ability of that analytical method to produce a definite response to only the analyte of interest and no other compounds that may be present in a sample such as tablet excipients and related substances or impurities (323-324). The specificity of the method was assessed by comparing chromatograms developed from the analysis of a standard solution of CPT only with that from a sample produced by dissolving commercially available tablets of CPT in mobile phase buffer. The peaks observed in the chromatograms (§ 3.6) were well resolved from the solvent front and there were no apparent peaks that interfered with that for CPT. Therefore, the method was considered specific.

#### **4.2.6. Robustness**

As defined by the ICH, the robustness of an analytical procedure is reflected by the ability of the procedure to remain unaffected by small but deliberate changes in the method (302-303). A design of experiment (DOE) approach was used to test robustness of the method, and three factors were considered as described in §3.2.1. The experimental domain for the variables selected is described in §3.3.3. The experiments were performed in a randomized fashion so as to minimize the effects of uncontrolled factors that may introduce bias on the ultimate response of the method. The interpretation of results commences with the analysis of entire model equation rather than analysis of individual coefficients contained in that model. An examination of the ANOVA data (§ 3.6) and analysis of the response surface revealed that  $Y_4$  is not robust for factor  $X_1$ . Thus, precautionary measures need to be taken into account for this analytical procedure as small changes in ACN volume may result in a change in retention time and most likely the peak shape as well may be affected.

### 4.3. CONCLUSIONS

A reversed phase HPLC method for the *in vitro* quantitation of CPT has been validated and subsequently applied to the assessment of commercially available dosage forms. The linearity of the CPT/CYC peak area ratio versus CPT concentration was demonstrated and statistical analysis proved that the method is repeatable for the analysis of CPT as raw material drug and in pharmaceutical formulations, and that it is free from interference with the excipients. The method was also linear and precise and the chromatographic run time of 7.5 minutes permits the analysis of a large number of samples in a short period of time. This method can be recommended for the quality control of drug content in CPT tablets.

The chromatographic conditions yield sharp, symmetrical peaks with a high degree of resolution. CPT and CYC were well separated and resolved and the retention times were approximately 3.0 and 7.5 minutes, respectively.

The HPLC method that has been developed is an improvement on the method presented in the USP monograph for CPT, where the use of UV is recommended; even though CPT lacks a strong chromophore. The validated HPLC-ECD method is simple, selective, accurate, precise, rapid, sensitive and linear. It is appropriate for the analysis of *in vitro* release and analysis of CPT in pharmaceutical dosage forms.



### COMPATIBILITY STUDIES WITH CAPTOPRIL USING SPECTROSCOPIC AND THERMOANALYTICAL TECHNIQUES

#### 5.1. INTRODUCTION

Recently published research has highlighted the application of differential scanning calorimetry (DSC), differential thermal analysis (DTA), thermogravimetric analysis (TGA) and infrared spectroscopy (IR) for the rapid evaluation of compatibility of active pharmaceutical ingredients (API) with pharmaceutical adjuncts or excipients (325-333). In general judgments relating to incompatibilities are expressed on the basis of the modifications observed in DSC thermograms of an API in the absence and presence of potential formulation excipients. Although some authors acknowledge that the presence of a physical or chemical interaction does not necessarily indicate an incompatibility, there is agreement that a change observed in a DSC thermogram is definite proof of an interaction between an API and an excipient (325). Therefore as part of this study an investigation will be taken into whether a change in a DSC thermogram is sufficient to prove that an interaction will occur between CPT and several potential excipients.

The solid-state properties of APIs are critical factors that must be considered in pharmaceutical formulation development. The most relevant properties can, and often do, affect the therapeutic efficacy, toxicity, bioavailability, pharmaceutical processing and stability (334, 335) of an API. Most API molecules can adopt a variety of conformations and therefore this may give rise to solid structures differing from each other in their lattice space type or molecular conformation, or simultaneously in both features when associated with specific interactions between polar groups that are often found in those molecules (334, 336). The interrelationship between the presence of an amorphous form and drug degradation has posed continuous challenges for the development of pharmaceutical formulations (334, 337). Thermal analytical techniques have been used for drug quality control whenever possible (334). The use of a combination of DSC and thermogravimetry/derivative thermogravimetry (TG/ DTG), scanning electron microscopy (SEM) and X-ray powder diffraction provides state-of-the-art techniques for assessing incompatibilities. These techniques offer a rapid means of properly interpreting potential instabilities. Furthermore their use offers the possibility of analytical quantification of such instabilities and incompatibilities (334, 338-

340). The use of DSC in particular permits the acquisition of quantitative information relating to the purity of compounds, thereby making it possible not only to establish the melting temperature interval for any API, but also to study the phenomenon of polymorphism and associated characteristics of drug compounds. Thermogravimetric analysis is an analytical, quantitative, and comparative method that affords a formulation scientist the opportunity of producing rapid reproducible results. TGA can be used in drug quality control to improve a product through the determination of stability by isothermal and non-isothermal kinetic methods (334).

Drug-excipient compatibility studies are essential in the development of different formulations and the results facilitate the selection of appropriate excipients and increase the probability of producing a stable solid oral dosage form. The use of thermoanalytical methods in drug excipient compatibility studies offers many advantages over the classical methods of incompatibility detection between an API and potential formulation excipients (341). Conventional methods of incompatibility detection involve adding an API to excipients and then subjecting the mixture to elevated levels of temperature and humidity for considerable periods of time. Following exposure to different climatic conditions the mixtures are analyzed using a variety of techniques such as HPLC and thin-layer chromatography (TLC) amongst others. This approach often takes several weeks or months to generate sufficient data to support or exclude any evidence of an incompatibility. In contrast one of the major advantages of using thermoanalytical techniques is that they permit rapid assessment of samples and include the possibility of detecting physical interactions such as the formation of eutectic mixtures or the adsorption of API to excipients or *vice versa* (341-343).

Of all the available thermoanalytical techniques, DSC is the most important one used for drug-excipient compatibility studies. However, data generated using DSC are more readily interpreted when supported by thermogravimetry (TG). Therefore the application of DSC and TG in early formulation studies is common (341-347).

The most frequently used DSC calibration standards are metals with melting temperatures and enthalpies measured using adiabatic calorimetry under near-equilibrium conditions. Indium is most often chosen as the standard material. However there are indications that it may be desirable to calibrate equipment using substances that have similar thermal properties to the compound under investigation (348-349).

In DSC heat effects associated with phase transitions and chemical reactions are monitored as a function of temperature. Consequently the difference in heat flow to a sample and a reference, exposed at the same temperature, is recorded as a function of temperature. The reference is usually an inert material such as aluminium, tin, zinc or indium, or as in many cases, an empty aluminium pan. The temperature of both the sample and reference are increased at a constant rate and the resultant heat flow difference can be either positive or negative (350). In this instance the rate of change of heat flow, or  $\frac{dH}{dt}$  is measured in  $\text{mcal sec}^{-1}$ . If an endothermic process prevails, as is the case for most phase transitions, heat is absorbed and therefore the resultant heat flow to a sample is higher than that to the reference. Thus  $\Delta \frac{dH}{dt}$  is positive.

The DSC consists of a sample holder and a reference holder as shown in Figure 5.1. Both holders are constructed of platinum to permit high temperature operation. Located under each holder is a resistance heater and temperature sensor. Current is applied to both heaters to increase the temperature of each holder at a specific rate. The difference in current applied to the holders, necessary to maintain the holders at the same temperature, is used to calculate  $\Delta \frac{dH}{dt}$ . An inert gas is purged over the samples to ensure that a reproducible and dry atmosphere is maintained for the duration of analysis. Maintenance of an atmosphere of  $\text{N}_2$  prevents oxidation of samples at high temperatures, and the oxidation tendency is further reduced as the sample is sealed into small aluminium pans (350). The reference pan is usually an empty pan and cover. The pans hold up to about 10 mg of material.

Mura et al (351) and Adeyeye and Brittain (352) have reported data from a number of investigations in which DSC was used as the primary tool for establishing the compatibility of various excipients for ketoprofen (352, 353) and picotamide (352, 354). In another study (355), the DSC investigations were combined with scanning electron and hot stage microscopy to generate the necessary data to better interpret the DSC thermograms. Misinterpretation of DSC results may lead to incorrect conclusions regarding incompatibilities. Supporting microscopic methods provide a means of inferring genuine incompatibilities (352).

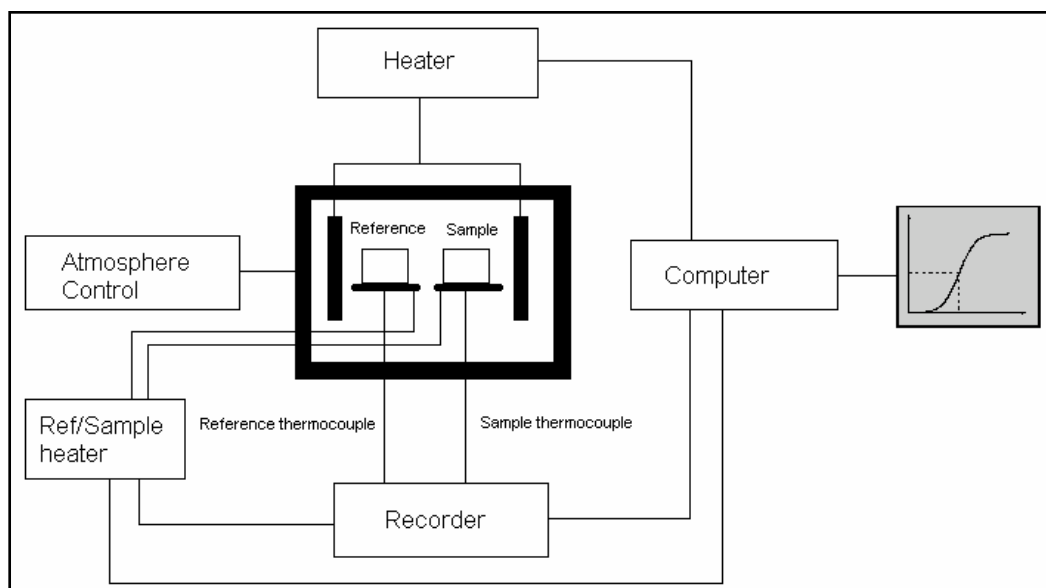


**Figure 5.1.** Differential Scanning Calorimeter

The danger of false positive drug-excipient interactions is always present when only DSC analysis is used to detect such incompatibilities. Incorrect conclusions are more likely when investigators use 1:1 binary mixtures to determine whether interactions do occur. DSC screening of mixtures and formulations remains a viable method for the detection of reactions between API and excipients, but any conclusion reached upon completion of those studies should be tested using a reference method such as infra-red spectroscopy (352).

It has been suggested (356, 357) that the use of thermal analysis in the development of solid dosage forms is invaluable. To determine the potential problem of mixing excipients with CPT, the decomposition process of CPT alone was initially investigated.

The area under a DSC peak is directly proportional to the heat absorbed or produced by a thermal event, and the integration of the peak area yields the heat of reaction in units of joules/second. gram. An exothermic reaction is plotted as a positive thermal event whereas an endothermic reaction is usually displayed as a negative event. The calibration of DSC instruments is normally accomplished through the use of compounds having accurately known transition temperatures and heats of fusion. An extensive list of references is available for this purpose. Once a DSC system is properly calibrated, it is relatively simple to determine the melting point and enthalpy of fusion data of any compound on integration of its empirically determined endotherm profile and application of calibration parameters (358).

Despite the importance of drug-excipient compatibility testing, there is no universally accepted protocol available for this purpose. The term thermal analysis refers to a group of analytical techniques in which the physical properties of a substance and/or reaction products are measured as a function of temperature whilst the substance is subjected to a controlled exposure to temperature program. The use of DSC involves the application of a heating or cooling signal to a sample and to a reference (359, 360). This method has been extensively used for compatibility testing of excipients with a number of APIs (359, 361-366). However, caution needs to be exercised in the interpretation of DSC results since high temperatures are required (359).

Another method commonly used to evaluate drug-excipient compatibility is isothermal stress testing (IST). IST involves storing the drug-excipient blends with or without moisture at high temperatures and determining the drug content (359, 363, 367, 368). DSC can be used in combination with IST to evaluate the compatibility of an API with excipients (359).

Drug development is a complex, costly and time consuming process which makes concurrent use of many advanced technologies to ensure success. It is not all the compounds that are analyzed that will ultimately end up in a commercial formulation (369).

A systematic study is presented in which, CPT alone and in 20: 80 w/w mixtures with five common excipients was investigated and the physicochemical characterization of the excipients tested was primarily inferred from published information.

Due to the sensitivity of molecular vibrations to changes in chemical or physical environments, and the ease with which such properties can be studied, techniques such as vibrational spectroscopy can be extremely important in the study of API-excipient interactions. The energies characterising the fundamental vibrational modes of drug substances lie within the range of 400-4000  $\text{cm}^{-1}$ . This spectral region corresponds to what is referred to as the mid-IR electromagnetic radiation spectrum (370). Transitions in vibrational energy levels can therefore be observed directly through their absorbance in the IR region of a spectrum or indirectly through an elastic scattering of incident energy via the Raman Effect. IR absorption spectroscopy, especially when measured by means of Fourier Transform IR (FT-IR), has been shown to be a powerful technique for the physical characterization of

pharmaceutical solids. FT-IR spectra are often used to generate information relating to the chemical and physical reactions associated with API-excipient interactions (370).

As part of an ongoing project on the development of extended release formulations of CPT, thermal analysis techniques were used to study CPT-excipient compatibility. The possible interaction between CPT and Eudragit<sup>®</sup> RS, Hydroxymethyl cellulose (Methocel K4M and Methocel K100M), Microcrystalline cellulose and citric acid were studied. Each of the identified substances was subjected to spectroscopic and thermoanalytical characterization and mixtures, after appropriate conditioning, were analysed by DSC, TGA and IR in an attempt to correlate changes in DSC analyses with chemical modification of an API in a blend.

## **5.2. METHOD**

Homogeneous, binary mixtures of CPT with different excipients were prepared by mechanical shaking and stored in 25 ml glass-stoppered erlenmeyer flasks at 25 °C. Physical mixtures of CPT-excipient were weighed in appropriate amounts and were then stored in 4 ml flat-bottomed amber glass vials. The physical mixtures were prepared using a CPT: excipient (mass ratio) of 20:80. This composition was selected to study the influence of the relative amount of an excipient, in a rather wide range, using reasonable quantities of the API of interest. The binary mixtures were stored in the dark because CPT is light sensitive. TGA and DSC studies were performed in a dry nitrogen atmosphere in aluminium and/ or platinum crucibles with an empty platinum crucible as a reference. CPT was used without any further treatment.

### **5.2.1. Differential scanning calorimetry**

DSC curves were generated using a Model DSC-7 Perkin Elmer Differential Scanning Calorimeter (Perkin Elmer AG, USA). Pyris Software for Windows was used to analyse the data that were generated. The DSC was connected to a computer via a TAC 7/ DX Thermal Analysis Instrument Controller. Approximately 2 mg of CPT powder was hermetically sealed into an aluminium pan. The sample was placed directly onto a micro hot stage DSC. Individual samples (CPT and excipients) as well as physical mixtures of API and selected excipients (all passed through 60-mesh sieve) were weighed directly into aluminium DSC pans. The temperature of the DSC microscopy cell was monitored using a central processor.

The heating rate of the DSC assembly was controlled at 10 °C/min over a temperature range of 25-500 °C. Each spectrum generated during the heating process was performed using 10 scans with a resolution of 4 per cm. An inert atmosphere was maintained during testing by passing nitrogen gas through the system at a rate of 25 ml/min. The DSC cell was calibrated with Indium (mp 156.6 C;  $\Delta H_{\text{fus}} = 28.54 \text{ J/g}$ ) (371) prior to commencing studies with CPT. Measurements were performed in replicates of three. The heating rate of 10 °C/min is a useful compromise, in DSC, between speed of analysis and detecting any heating-rate dependent phenomena. In our laboratory we have an interest in developing methods for estimating thermal properties of compounds and much of our effort is now directed towards developing models for estimating enthalpies of compounds.

### **5.2.2. Thermogravimetric analysis**

TG experiments were conducted using a Model TGA 7 Perkin Elmer Thermogravimetric Analyzer (Norwalk, CT, USA) fitted with a platinum sample holder. Pyris Software was used for data analysis. Approximately 4 mg of dry CPT and/or the binary mixtures to be tested were placed in platinum crucibles. Measurements were performed in N<sub>2</sub> atmosphere at a flow rate of 25 ml/min, a heating rate of 10 °C /min, and a temperature range of 25 °C to 600 °C. All sample measurements were repeated on at least three separate occasions.

### **5.2.3. Infrared spectroscopy**

Infrared spectra were recorded using a Bruker Model Verter 70 (Beaconsfield, Bucks, England) apparatus and the KBr disc method in a wavelength range of 4000-400 cm<sup>-1</sup>. The powder samples were compressed with KBr using a stainless steel die and a Karver press. The microscopic spectrophotometer was equipped with a TENSOR 27 RT-Dlatgs detector. The velocity of the scanner was set at 10 kHz. Sample combinations showing promise in terms of compatibility were collected successively from the actual analysis area by a mapping process. An automated X-Y stage for mapping was used to obtain complete IR spectra from all samples at 18 mm intervals. The samples for analysis were prepared by grinding 2 mg of dry powder and CPT together with 200 mg of KBr to produce a fine powder of particle size < 5 µm. The mixture was then compressed to form a clear disk.

## **5.3. EXCIPIENTS**

All materials used in these studies are generally recognised as safe (GRAS) and appear in the FDA Indicative Ingredients Guide for general inclusion in oral formulations (372).

### **5.3.1. Hydroxypropyl methylcellulose (HPMC)**

Use of HPMC in sustained-release dosage forms has been widely reported (373-380). HPMC is a non-ionic, non-toxic polymer that has been used in the manufacture of topical formulations and for tablet production. It has been used as a binder and as a sustained release matrix-forming excipient (372). HPMC is available in a variety of different grades depending on the degree of substitution and average molecular weight of the polymer components (372).

HPMC polymer controlled release dosage forms have been classified as swelling controlled release systems (373-380). Generally in swelling controlled matrix technologies two major factors control the rate of release of API from the matrix: the rate of aqueous medium infiltration into the matrix and the subsequent relaxation of polymer resulting in either hydration or gelation and swelling of the polymer, respectively. As a consequence of these simultaneous processes, two fronts are evident in a matrix: the swelling front (glassy polymer/gel interface) and an eroding front (gel/medium interface). The distance between the two fronts depends on the relative rates at which the swelling and eroding fronts move in relation to each other, and is termed the diffusion layer (376).

### **5.3.2. Microcrystalline cellulose (MCC)**

MCC is purified, partially depolymerized cellulose occurring as a white, odourless, tasteless, crystalline powder composed of particles of different sizes and in grades that have different properties and applications (372). MCC is widely used as a diluent in oral tablet and capsule formulations prepared by either wet-granulation or direct-compression processes (372). Emcocel<sup>®</sup> 90M has a mean particle size of 91  $\mu\text{m}$  and a moisture content of < 5%. The angle of repose of MCC is 34.4° and the material has bulk and tapped densities of 0.29g/cm<sup>3</sup> and 0.35g/cm<sup>3</sup> respectively (372).

### **5.3.3. Citric acid**

Citric acid occurs as colourless translucent crystals, or as a white crystalline powder powder. It is odourless and has a strong acidic taste. The crystal structure of citric acid is monoclinic holohedral. It is widely used in pharmaceutical formulations and food products to adjust the pH of solutions. It has also been used experimentally to adjust the pH of tablet matrices in enteric coated formulations for colon specific delivery (381-382).



#### **5.3.4. Methacrylic acid copolymers**

Methacrylic acid copolymer is a fully polymerized copolymer of methacrylic acid and an acrylic or methacrylic ester. Three types of polymers, type A (Eudragit<sup>®</sup> L, Eudragit<sup>®</sup> RL), type B (Eudragit<sup>®</sup> S, Eudragit<sup>®</sup> RS) and type C (Eudragit<sup>®</sup> L 30 D-55) have been defined. They vary in methacrylic acid ester content and solution viscosity (372). Typically, the molecular mass of these polymers is in excess of 100 000 mass units. Solid polymers may be used in direct compression tableting in proportions of 10-50% (372).

Acrylic copolymers have been used as enteric and sustained release coatings in the pharmaceutical field due to their biological safety (383-387). Eudragit<sup>®</sup> RS is composed of poly (ethylacrylate-methylmethacrylate-trimethylammonioethyl methacrylate chloride) copolymers with ratios of 1:2:0.1. Eudragit<sup>®</sup> RS is a water-insoluble polymer and the drug delivery systems prepared from this material show pH-independent sustained-release due to the presence of quaternary ammonium functional groups (384, 388-389). Some studies on drug release from monolithic Eudragit<sup>®</sup> RS films have been performed considering the glass transition temperatures ( $T_g$ ) of the material.

Eudragit<sup>®</sup> RS is comprised of approximately 5% of quaternary ammonium functional groups. The ammonium groups are present as salts that impart pH-independent permeability to the polymers (372). The acrylate-methacrylate polymers have been used in the preparation of matrix tablets for oral sustained release in tablet coating and in microencapsulation applications for API (390).

#### **5.4. RESULTS AND DISCUSSION**

Excipients have been classified according to the function they perform in a formulation, although many excipients fulfil multiple roles in a dosage form. The excipients selected for use have been described in § 5.3. The commercial names, functions and suppliers of the excipients are summarized in Table 5.1. The excipients were selected for their potential suitability to develop sustained-release microcapsules of CPT. The polymers were selected for use due to their matrix forming capacity, hydrophilicity and swelling characteristics.

**Table 5.1.** Excipients used in the compatibility studies

<b>Excipient</b>	<b>Commercial name</b>	<b>Function</b>	<b>Supplier</b>
Captopril		Active	Aspen Pharmacare
Hydroxypropylmethylcellulose	Methocel <sup>®</sup>	Binder	Colorcon
Microcrystalline cellulose 101	Avicel <sup>®</sup>	Diluent	FMC
Acrylic copolymer	Eudragit <sup>®</sup> RS	Binder	Rohm Pharma
Citric Acid		pH adjuster	BDH Chemicals

Representative DSC scans of CPT and CPT-excipient mixtures are shown in Figures 5.2-5.8. The figures reveal typical heat flow curves vs temperature for DSC studies. The melting point endotherm for CPT occurred between 104 and 106 °C for all mixtures studied except where citric acid was evaluated.

The DSC trace of pure CPT (Figure 5.2) showed a sharp endotherm peak,  $T_{peak}$ , at 105.8 °C and  $T_{onset} = 103$  °C. The characteristic peak pattern generated indicates the presence of the alpha form of CPT, which undergoes thermal transition at 106 °C, this being the melting endotherm of alpha form. Furthermore the  $\Delta H_{fus}$  for the alpha form (25J/g) was in agreement with a previously reportedly value (391). In the majority of cases, the melting endotherm of CPT was unaffected in all mixtures tested, with only slight changes observed in terms of peak broadening or shifting towards lower or higher temperatures. It has been reported that the quantity of material used, especially in API-excipient mixtures, can affect peak shape and enthalpy in such studies (392-393). The minor changes in the melting endotherm of CPT may be due to the mixing of CPT and the excipient which lowers the purity of each component in the mixture and therefore does not necessarily indicate that a potential incompatibility (394) exists. To determine whether an incompatibility exists, additional techniques were used.

Interactions in a sample are observed in DSC thermograms as changes in thermal events, such as the appearance of new peaks or a change in melting point of a material. However, broadening of peaks leading to changes in area, peak onset and changes in peak temperature occurred with CPT and citric acid. This may indicate an incompatibility for this binary mixture.

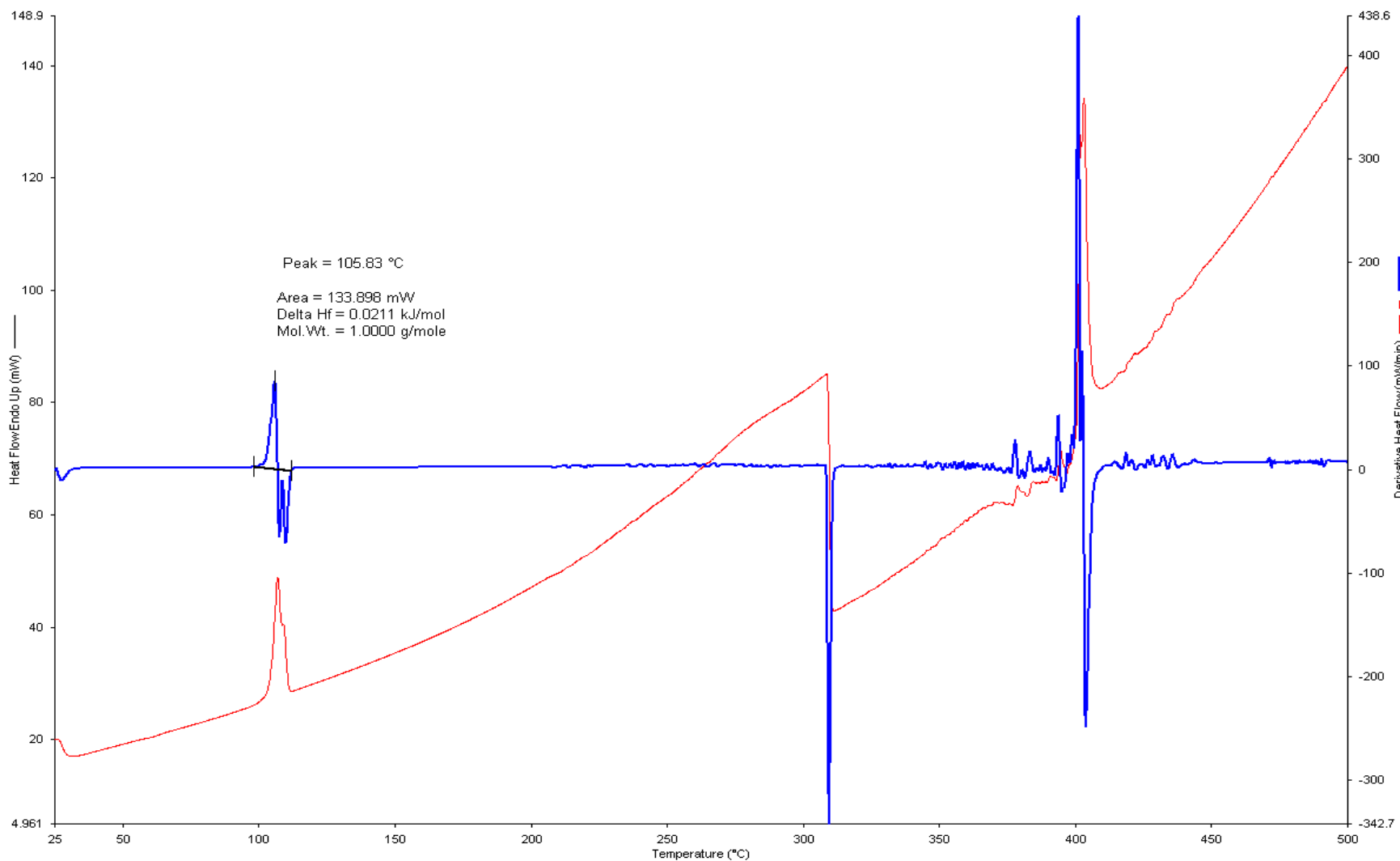


**Figure 5.2.** A typical DSC plot for CPT determined at a heating rate of 10° C/min.

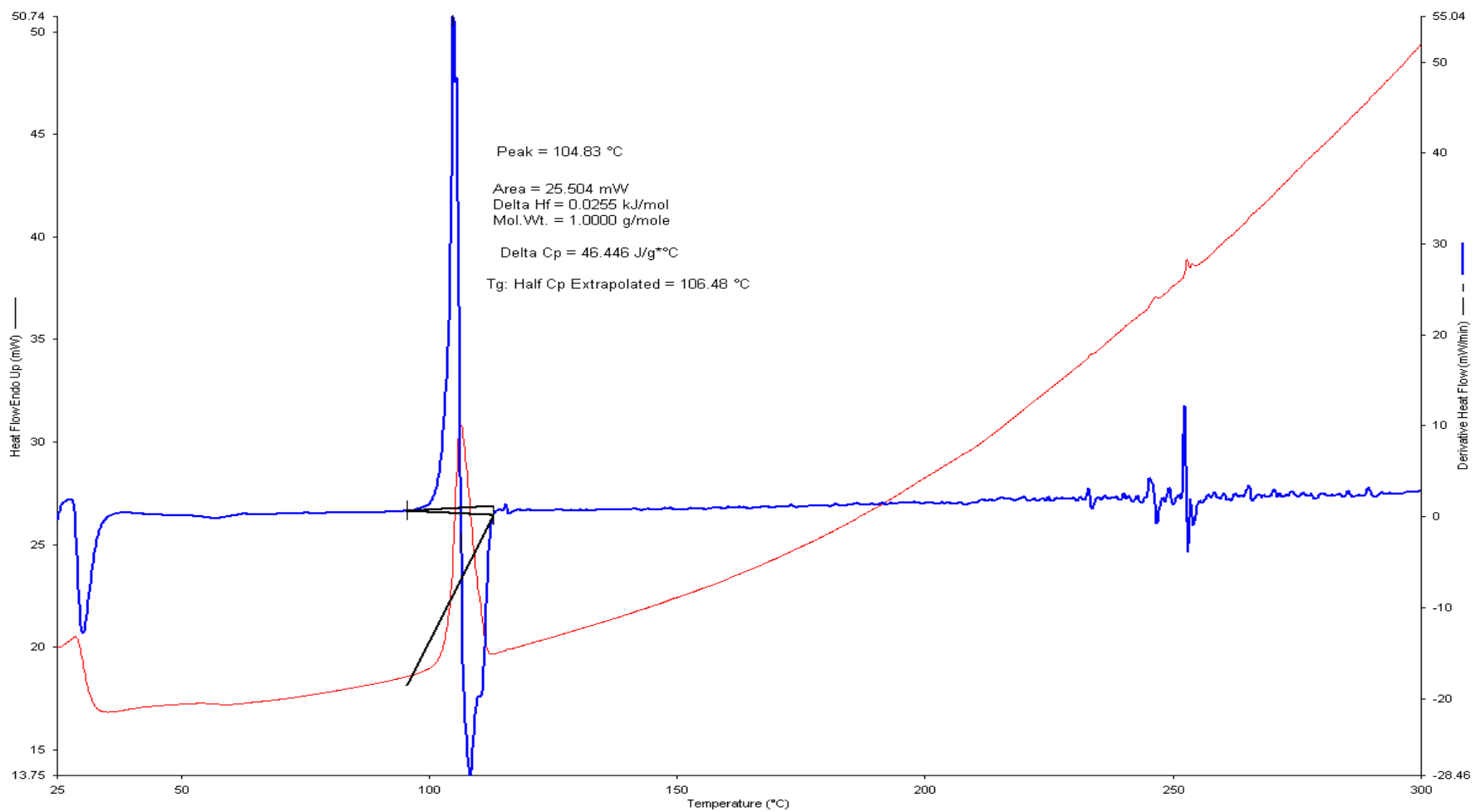


**Figure 5.3.** A typical DSC plot for CPT: HPMC K15M generated at a heating rate of 10° C/min.

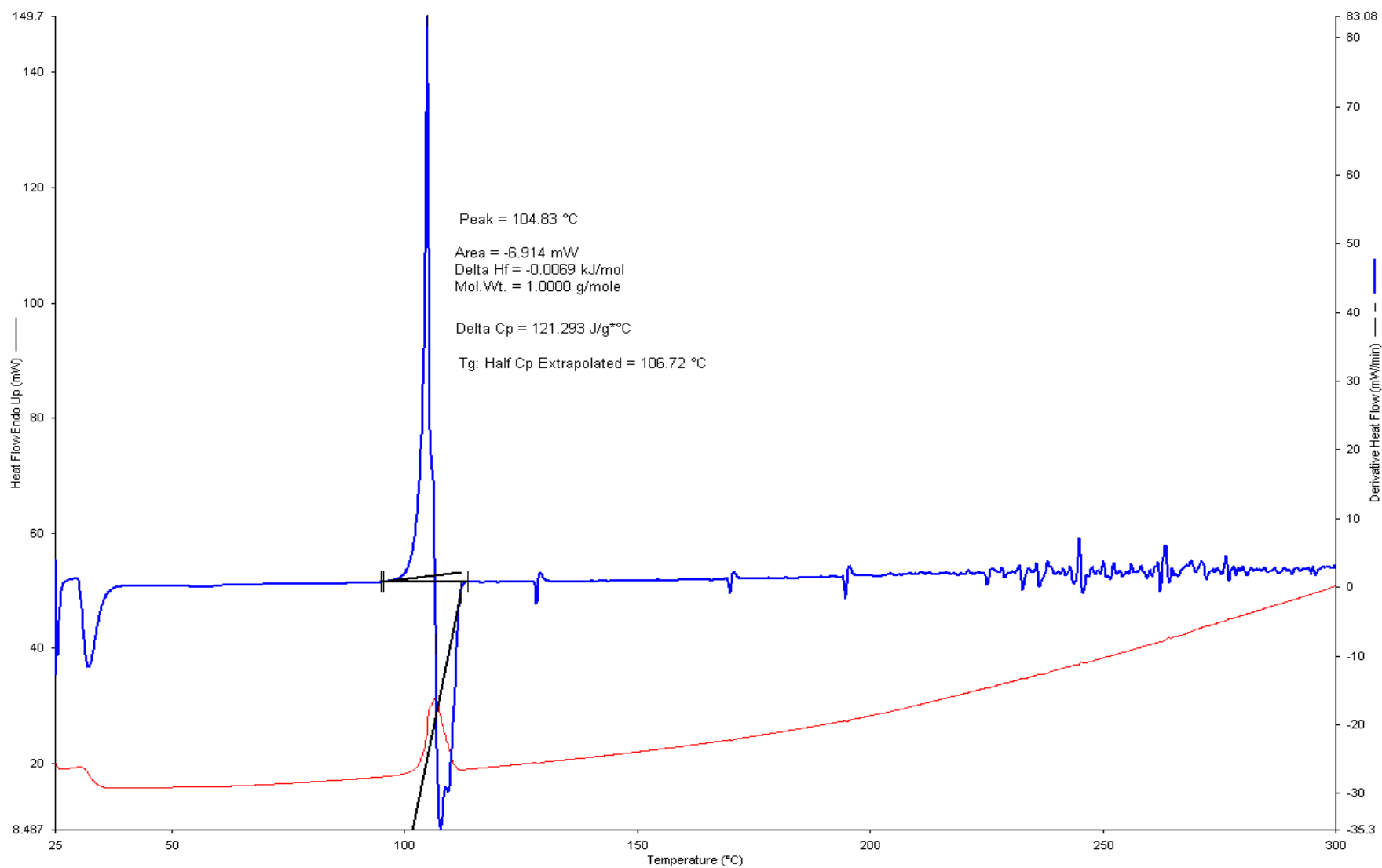


**Figure 5.4.** A typical DSC plot for CPT: HPMC K100M generated at a heating rate of 10° C/min.

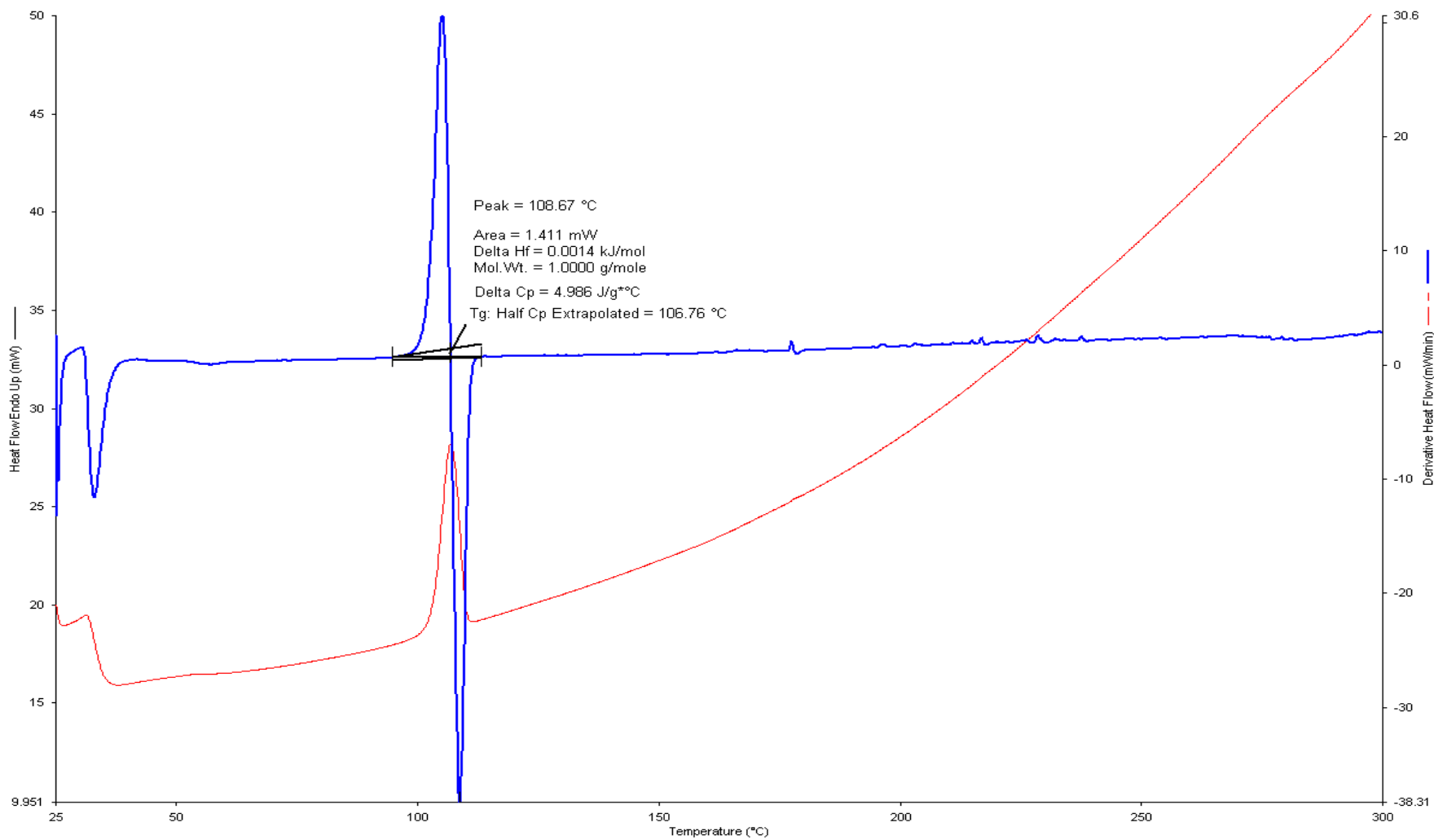


**Figure 5.5.** A typical DSC plot for CPT: MCC generated at a heating rate of 10° C/min.

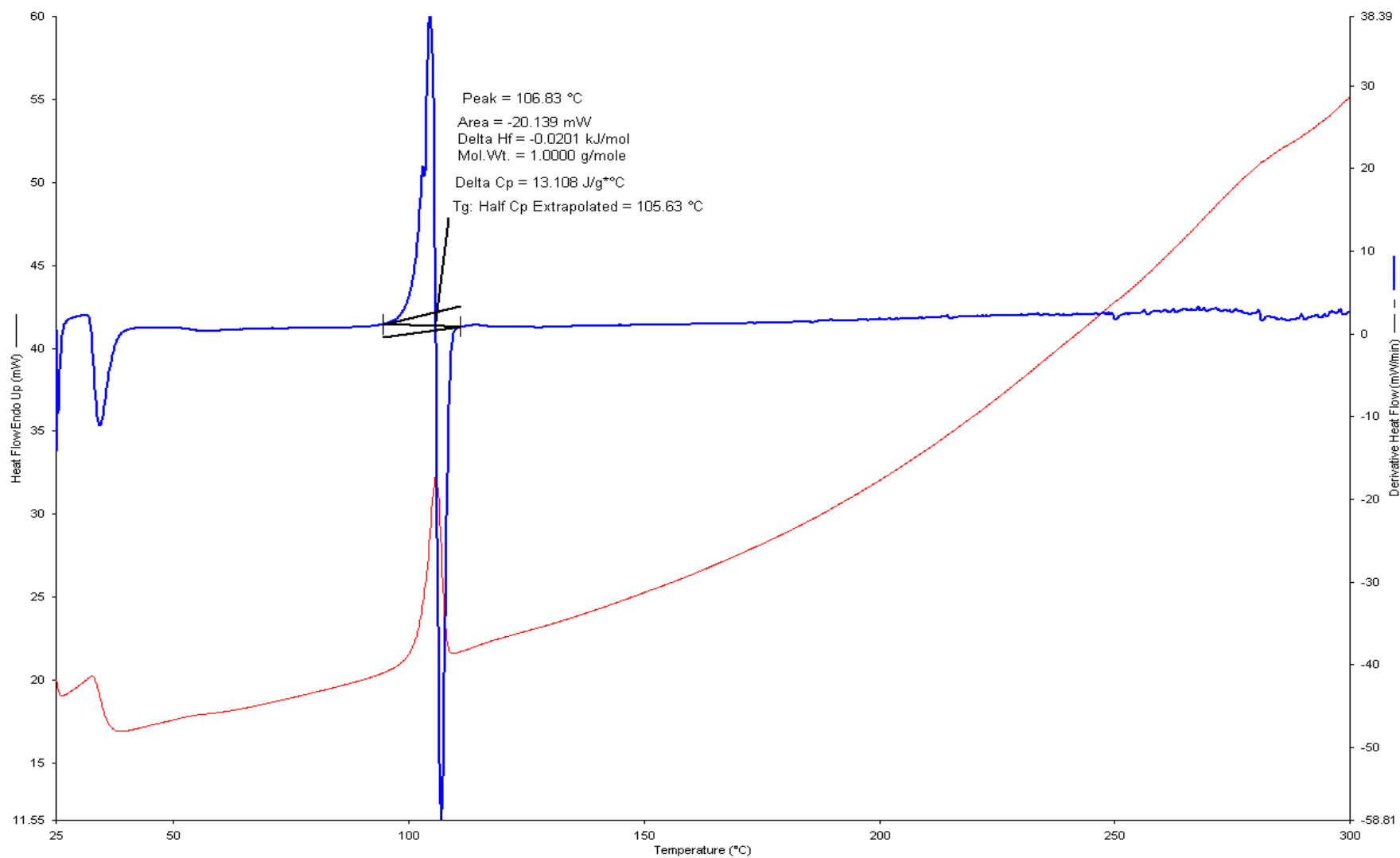


**Figure 5.6.** A typical DSC plot for CPT: Eudragit RS generated at a heating rate of 10° C/min.

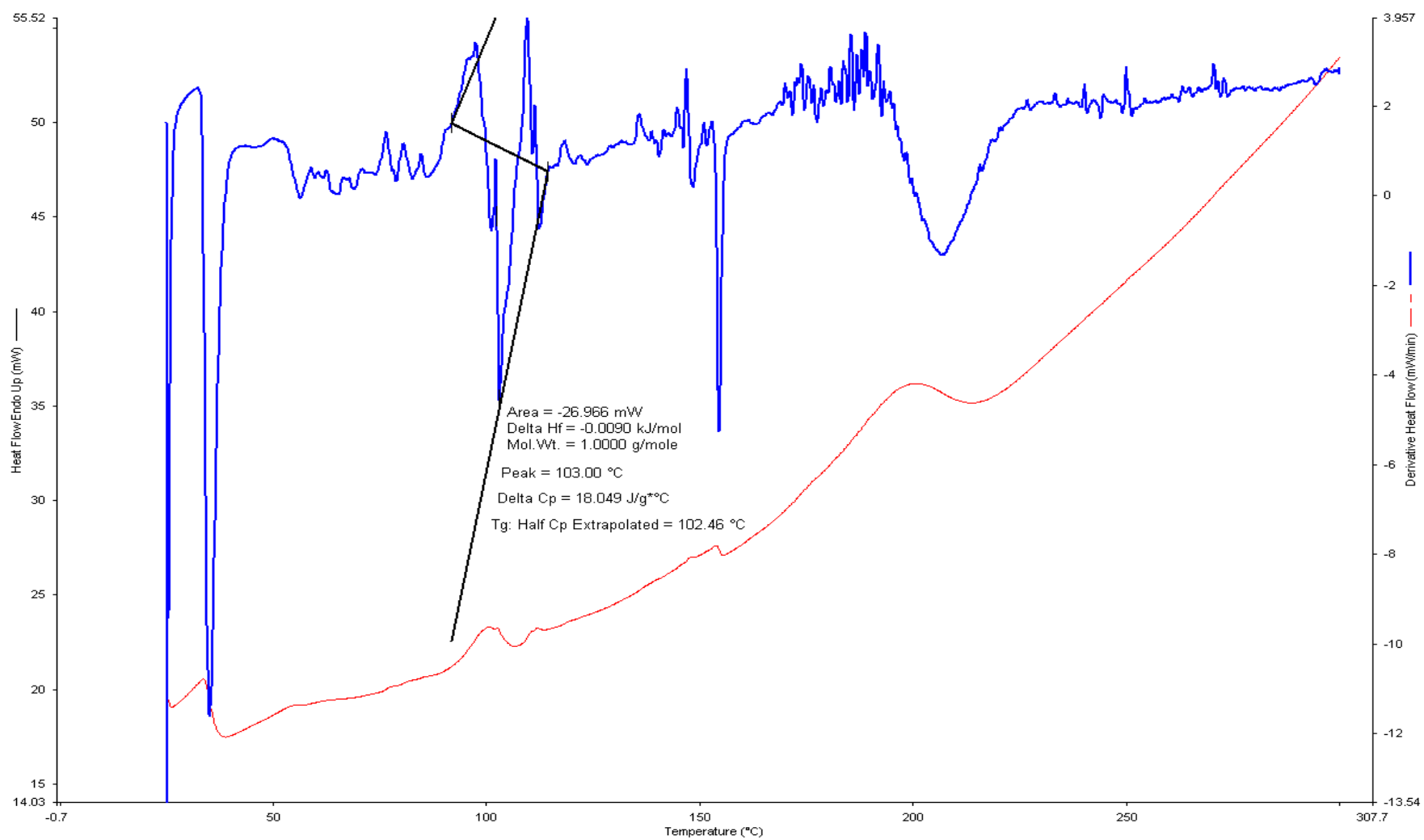


**Figure 5.7.** A typical DSC plot for CPT: citric acid generated at a heating rate of 10° C/min.



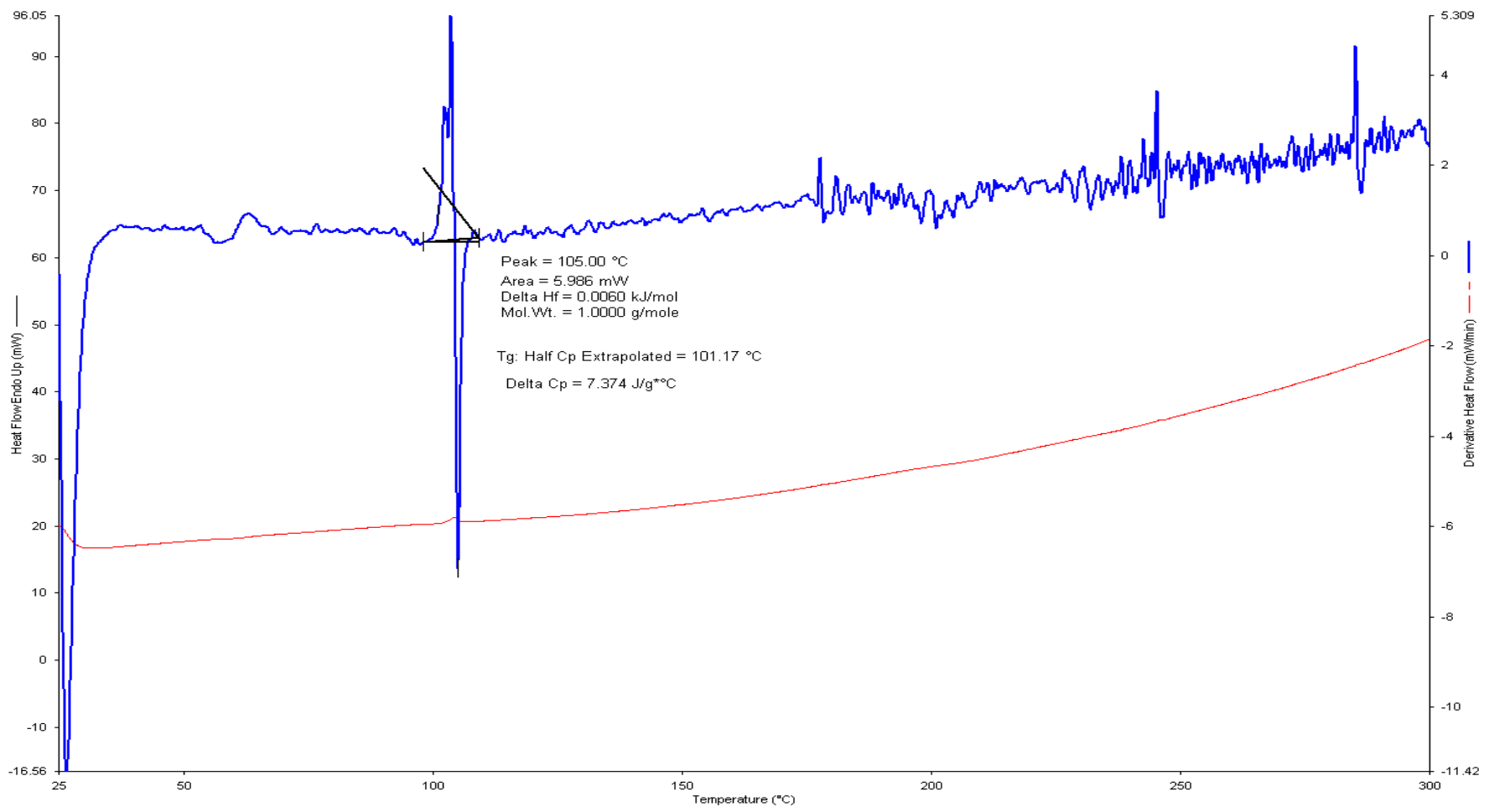


**Figure 5.8.** A typical DSC plot for mixture (all excipients) generated at a heating rate of 10° C/min.

TG generated (Figure 5.9) in a nitrogen atmosphere reveals that CPT is stable up to a temperature of approximately 175 °C and then it decomposes in three distinct steps, the first of which corresponds to approximately 61% loss in mass and which is indicative of the elimination or degradation of the cyano (C-N) bond present in CPT. The second decomposition process commences at about 230°C and is complete by 360 °C with a maximum rate of decomposition occurring at 340°C. The last residue is completely degraded at about 450 and 520 °C.

The shapes of all TGA curves for CPT were similar or nearly identical to that observed in Figure 5.9. The TG and DTG data reveal a DTG curve roughly symmetrical around the peak temperature of about 245 °C. CPT decomposes over the temperature range of 150-550 °C when tested alone.

The first noticeable blip on the DTG curve occurs at the peak temperature for melting of CPT. The main decomposition of CPT occurs in the region of the first peak and no residue was observed at the end of the TG experiment.

The shape of the other TGA curves revealed a 3-step degradation process for all samples examined, indicating a high degree of stability. MCC is thermally stable up to 300 °C and HPMC up to 200 °C (Figures 5.9-5.15)

The compatibility of CPT and excipients was further investigated using IR spectroscopy.

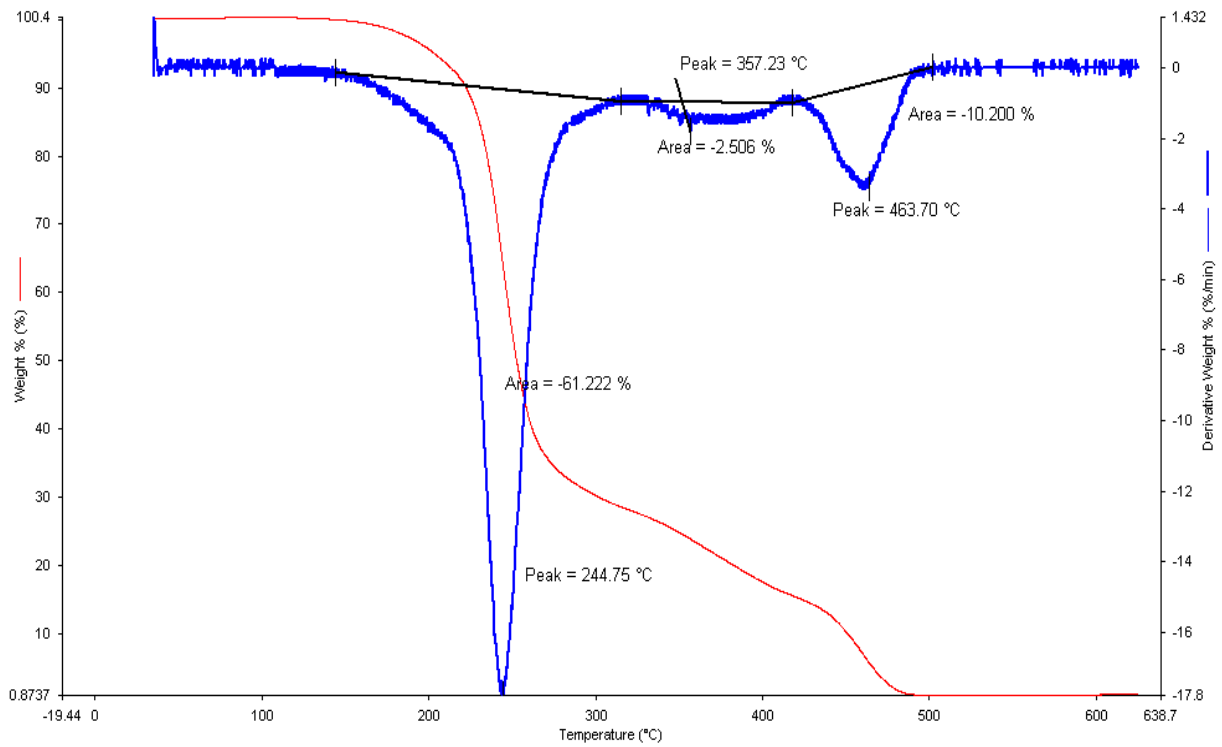


**Figure 5.9.** A typical TGA plot generated for CPT at a heating rate of 10° C/min.

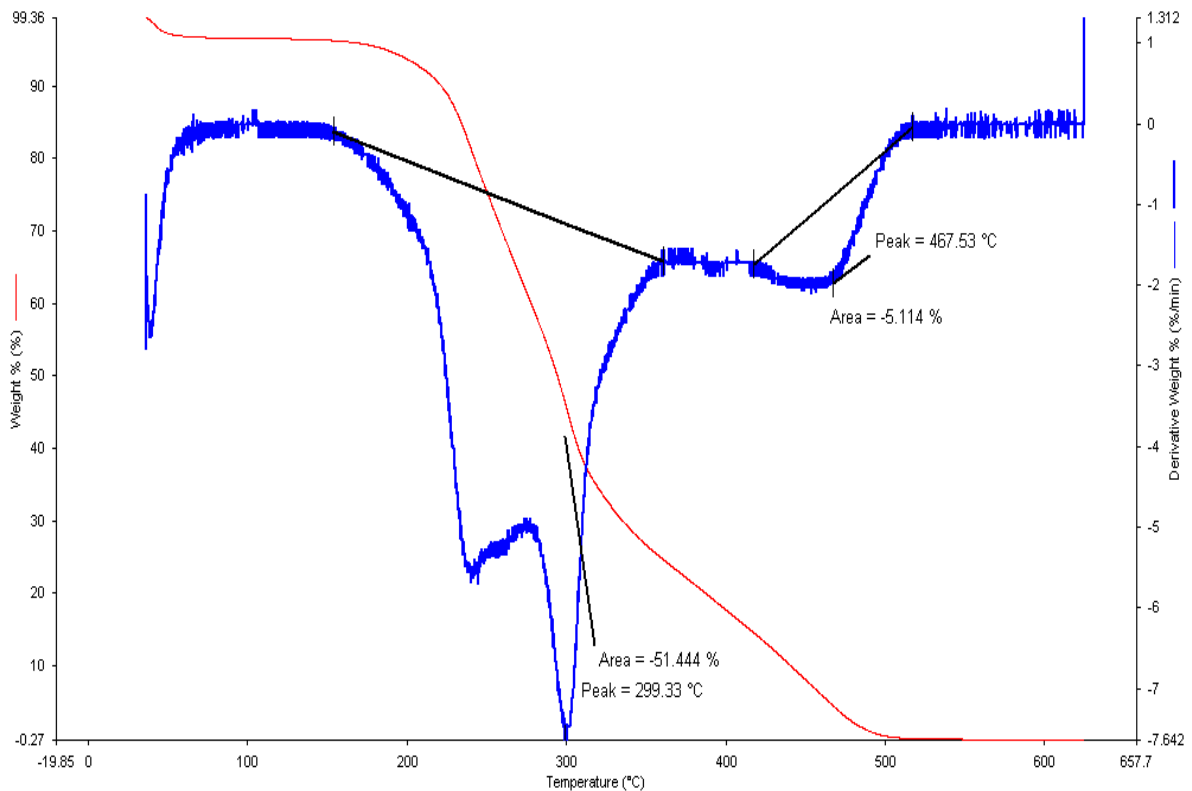


**Figure 5.10.** A typical TGA plot for CPT: HPMC K15 M generated at a heating rate of 10° C/min.

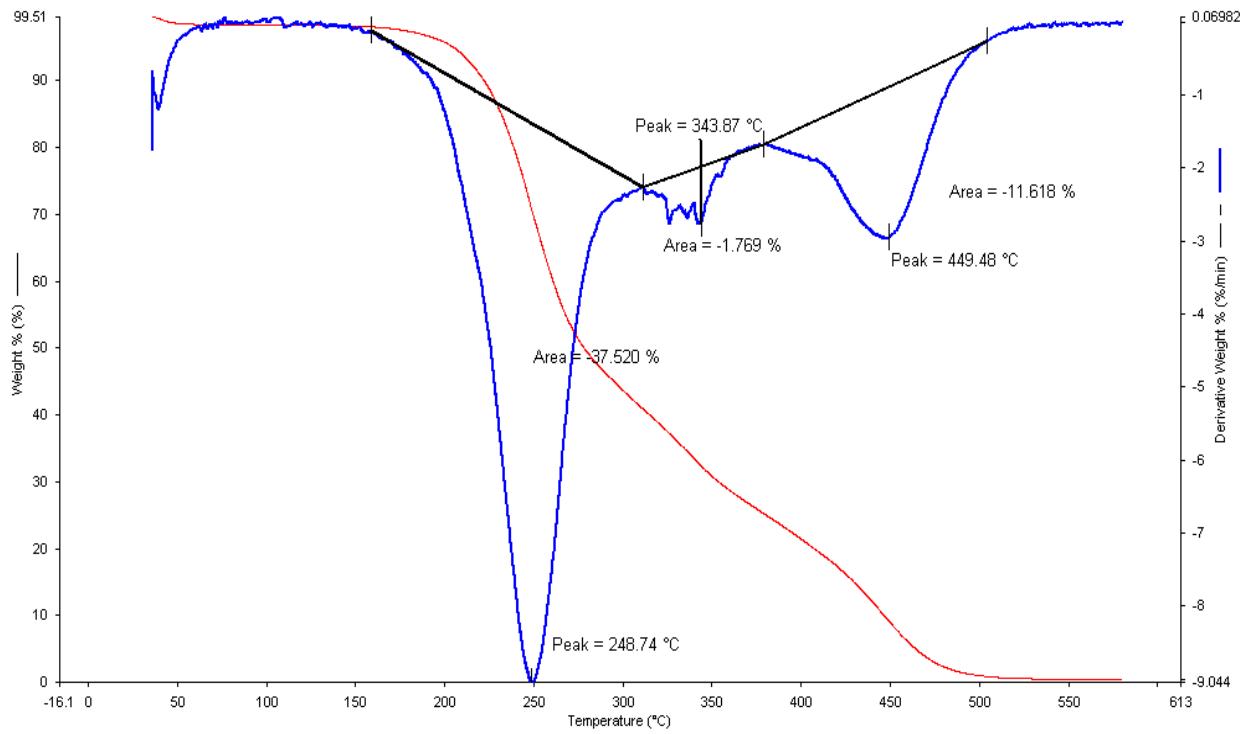


**Figure 5.11.** A typical TGA plot for CPT: HPMC K100 M generated at a heating rate of 10° C/min.

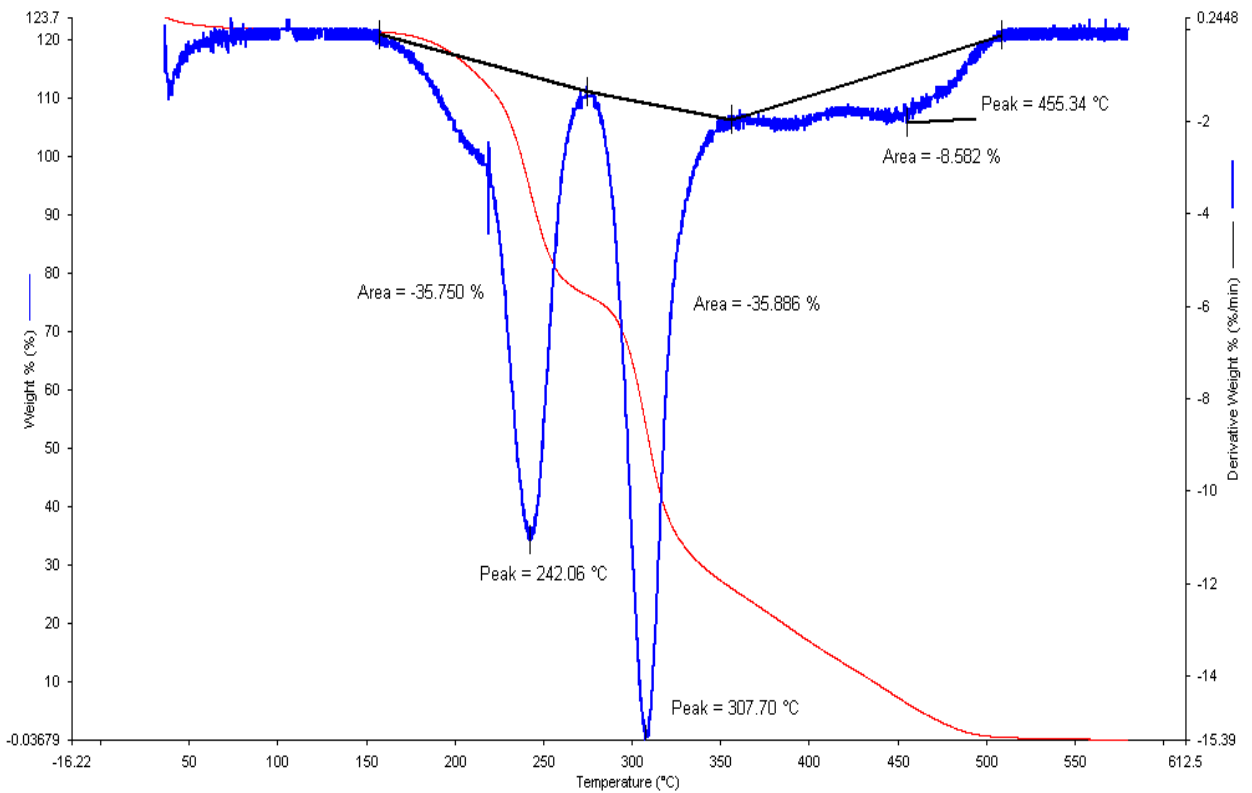


**Figure 5.12.** A typical TGA plot for CPT: MCC generated at a heating rate of 10° C/min.

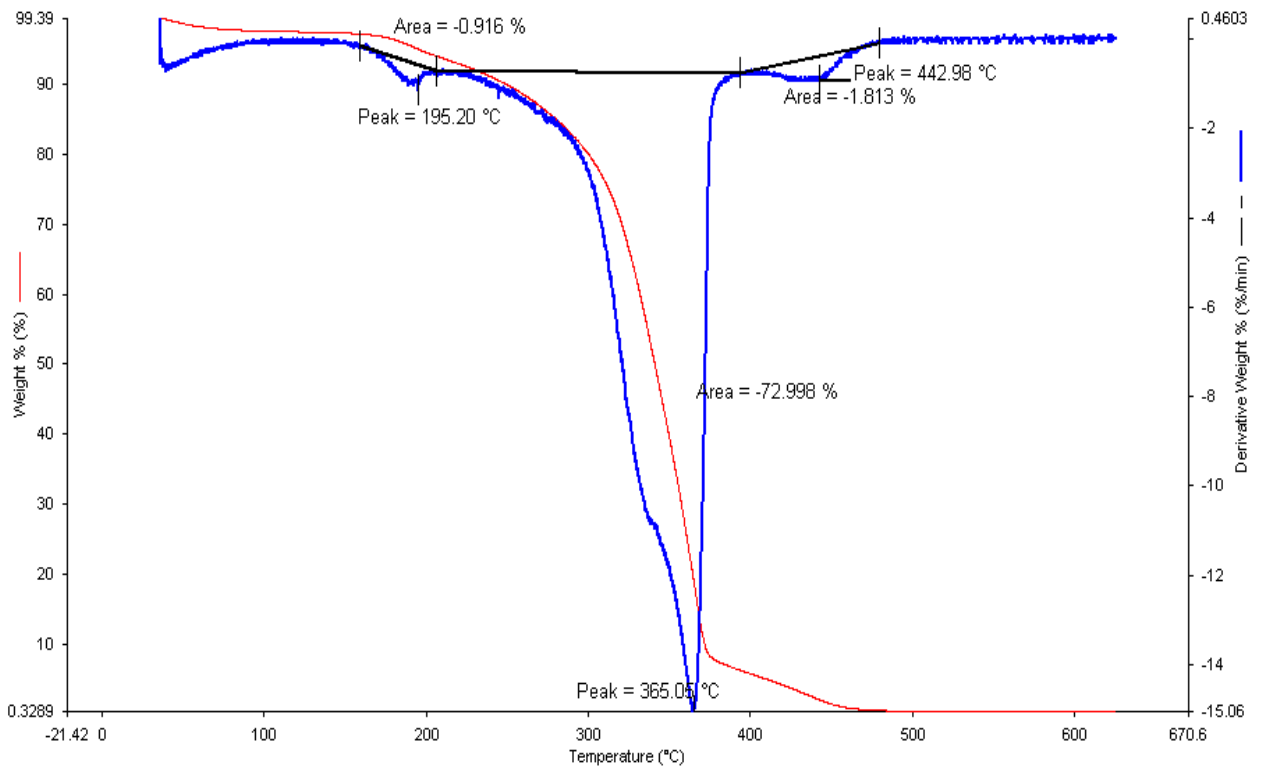


**Figure 5.13.** A typical TGA plot for CPT: Eudragit RS generated at a heating rate of 10° C/min.

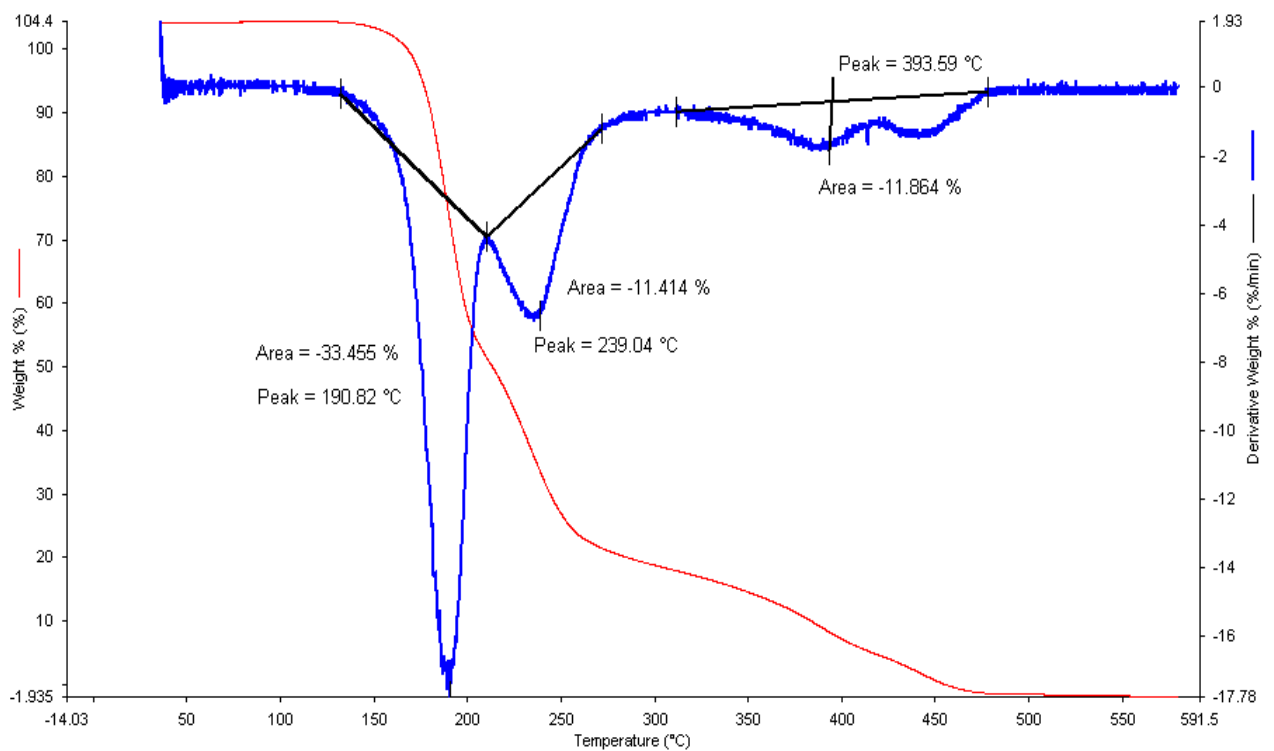


**Figure 5.14.** A typical TGA plot for CPT: citric acid generated at a heating rate of 10° C/min.

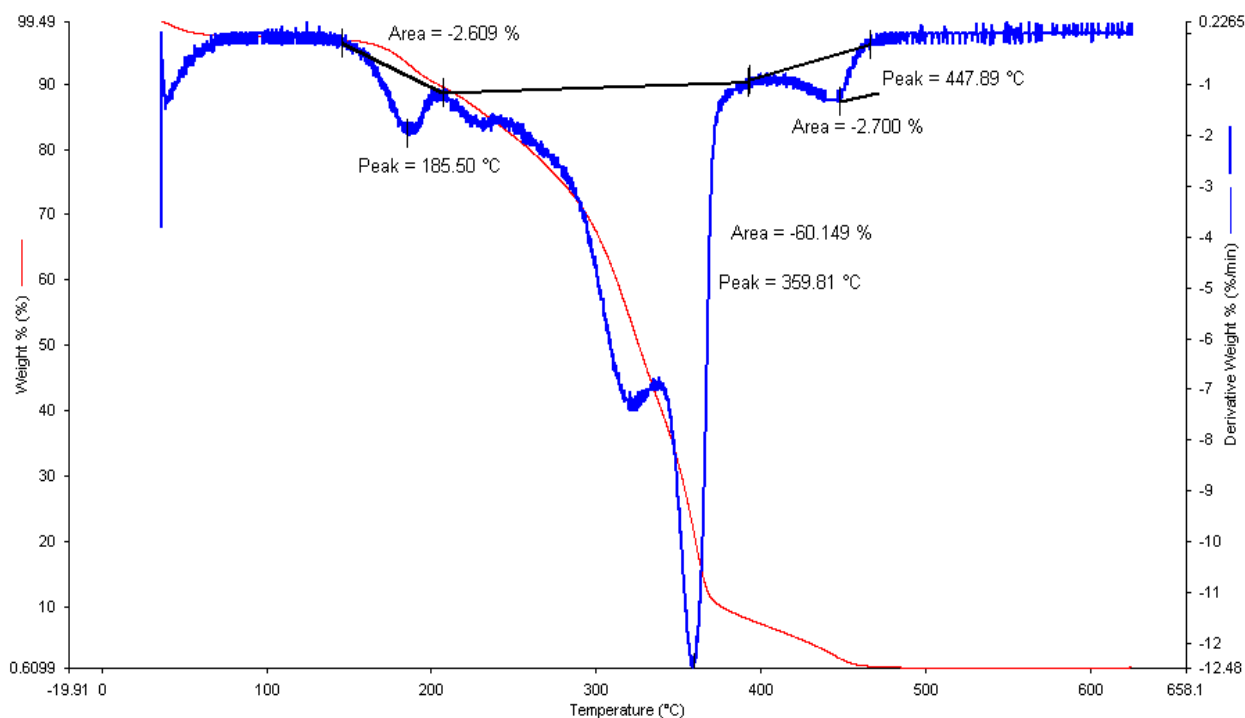


**Figure 5.15.** A typical TGA plot for mixture (all excipients used) generated at a heating rate of 10° C/min.

Infrared studies revealed that all characteristic bands for CPT were present in all spectra generated. These are shown in Figures 5.16-5.20 and 5.22. No new bands or shifts in the characteristic peaks were evident in mixtures except in the case of CPT and citric acid (Figure 5.21).

The IR spectrum of CPT shows an OH-stretching mode of water at 3600  $\text{cm}^{-1}$ , together with a broad band assigned to the aromatic CH at 3110-3000  $\text{cm}^{-1}$ . The IR bands for CPT are shown in Table 5.2.

In DSC, samples are subjected to a higher temperature range. Therefore the identification of potential interactions under ambient conditions may not be a simple exercise. The results of this study provide factual support for the suggestion that degradation reactions, transformations or interactions occurring at these elevated temperatures may not necessarily take place at room temperature. Therefore DSC alone should not be used for studying CPT/excipient interactions. The data generated in DSC studies should be supported by FT-IR studies.

**Table 5.2.** IR assignments for CPT

Assignment (cm <sup>-1</sup> )	Functional group
800	C-C stretching vibration
1300	C-H/CH <sub>3</sub> bending /symmetric vibration
1450	C-H stretching / asymmetric vibration
1500	Amide band
1580	C=C stretching
1750	-COOH (C=O stretching)
2600	-SH stretching vibration
2800	CH <sub>3</sub> stretching vibration (symmetric)
3000	CH <sub>3</sub> and CH <sub>2</sub> stretching (asymmetric)
3400	-OH functional group

The FT-IR spectra of pure CPT shown in Figure 5.16 depicts triple characteristic bands for CPT occurring at 1300 cm<sup>-1</sup>, 1450 cm<sup>-1</sup> and 1580 cm<sup>-1</sup>, due to C-H bending/ symmetric CH<sub>3</sub> bending vibrations, C-H stretching and C=C stretching, respectively. Another sharp band is observed at 800 cm<sup>-1</sup>, due to C-C stretching vibrations. The carbonyl vibration band –COOH (C=O stretching) and amide band were demonstrated in the 1750 cm<sup>-1</sup> and 1500 cm<sup>-1</sup> regions respectively. The FT-IR spectra of CPT loaded polymer combinations and diluent (Eudragit<sup>®</sup>, HPMC and MCC) are shown in Figure 5.22. They indicate that the characteristic bands of CPT, and also of the polymers, are evident in all figures except where citric acid was tested. It can therefore be concluded that there is a possibility of interaction between CPT and citric acid. A slight shift in the bands was observed in the combination formulation, which may be due to the reduction in purity of the substances being tested. The spectrum of CPT, and a physical mixture with Eudragit<sup>®</sup>, HPMC and MCC (Figure 5.22) is of lower intensity than that observed for pure CPT.

The plots of the FT-IR spectra of CPT within the ranges 4000-400 cm<sup>-1</sup> are shown in Figure 5.16. The peaks at 3000 and 2900 cm<sup>-1</sup> were assigned to the asymmetric CH<sub>3</sub> and CH<sub>2</sub> stretching vibration and the peak at 2800 cm<sup>-1</sup> was due to the symmetric CH<sub>3</sub> stretching mode. The peak at 2600 cm<sup>-1</sup> corresponded to the -SH stretching vibration (393-394).

The spectra shown in Figure 5.21 also confirmed the results observed in DSC studies undertaken with CPT and citric acid. In particular the lack of a peak in the IR spectrum is indicative of a potential incompatibility / interaction for this combination. The IR spectrum shown in Figure 5.21 reveals the presence of a small peak at 1700 cm<sup>-1</sup>, which was of

decreased intensity, and there were no other peaks present. Since the carboxylic acid group of CPT is an H-donor, and the carboxylate anion of citric acid is likely to be a stronger H-bond receptor, the carboxylic acid and  $\text{CO}^-$  function of acid may form and might change the bond distance of C-O in the  $\text{COO}^-$  functional group of the citric acid, resulting in a shift in the peaks observed. The presence of water may also cause a shift at  $3400\text{ cm}^{-1}$ . Although the IR spectral region from  $3100\text{-}3700\text{ cm}^{-1}$  corresponds to -OH functional group of many molecules, the -OH functional group of water molecules also makes an important contribution to this area and it may not be possible to differentiate the two sources of the shift. The moisture-related IR spectra were compared to TGA events. Mixing is most likely to cause or enhance adsorption of water from the atmosphere and the water content may induce an interaction of CPT with citric acid through H-bonds, leading to the formation of unique interactions that can be observed using IR.

Similarly the endotherm peak observed in the DSC thermogram shifted to  $103\text{ }^\circ\text{C}$  for the CPT/citric acid mixture. The enthalpy of the endothermic peak was very different from that observed when CPT was evaluated alone. This shift might have been caused by a change in the crystallinity of CPT. Citric acid is a tri-carboxylic acid and acts as an Arrhenius acid since it is a source of  $\text{H}_3\text{O}^+$  ions when dissolved in water and can act as a Bronsted acid by donating a proton to  $\text{H}_2\text{O}$ . Therefore the peaks for the OH- and C=O stretch vibration of CPT were shifted to  $3430\text{ cm}^{-1}$ . This suggests that there may be an H-bonding interaction between the OH<sup>-</sup> and COOH functional groups of CPT.



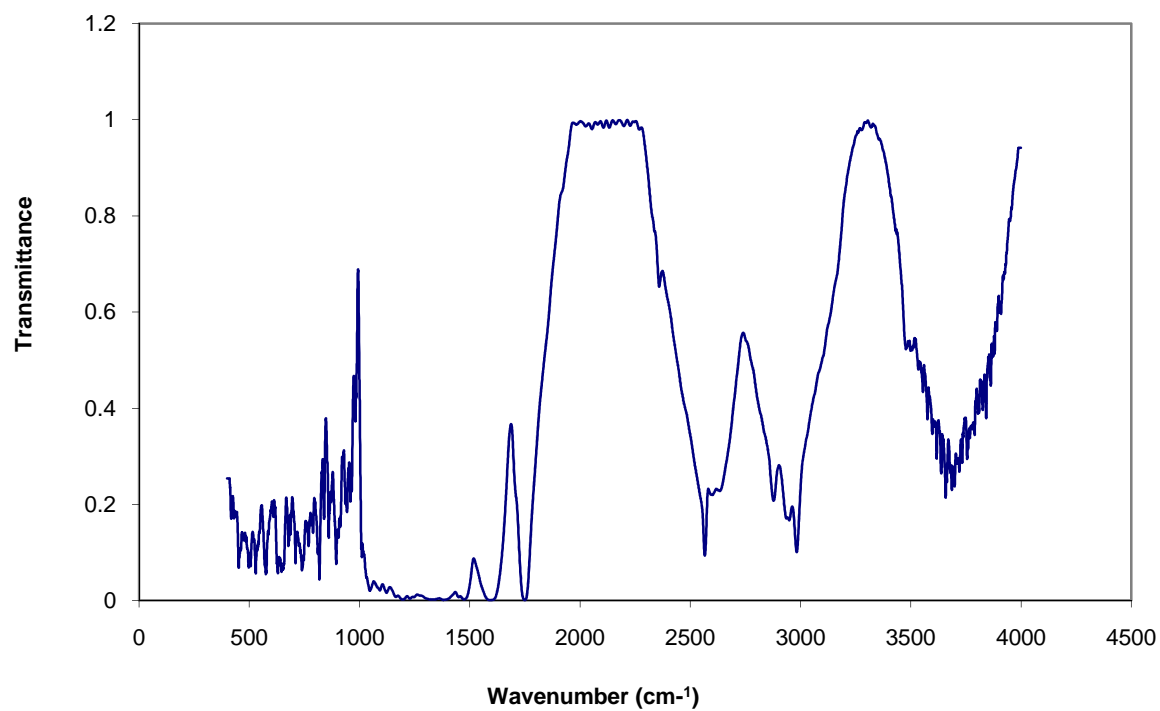


**Figure 5.16.** Infrared spectrum for CPT powder

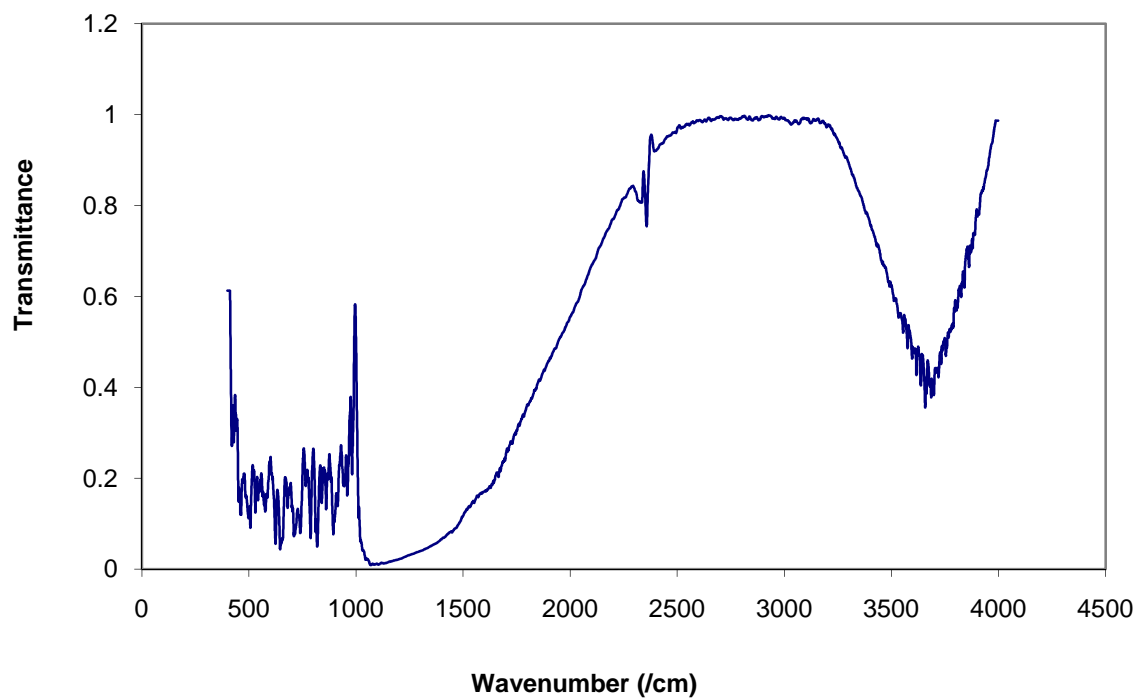


**Figure 5.17.** Infrared spectrum of a CPT: HPMC K 15M binary mixture

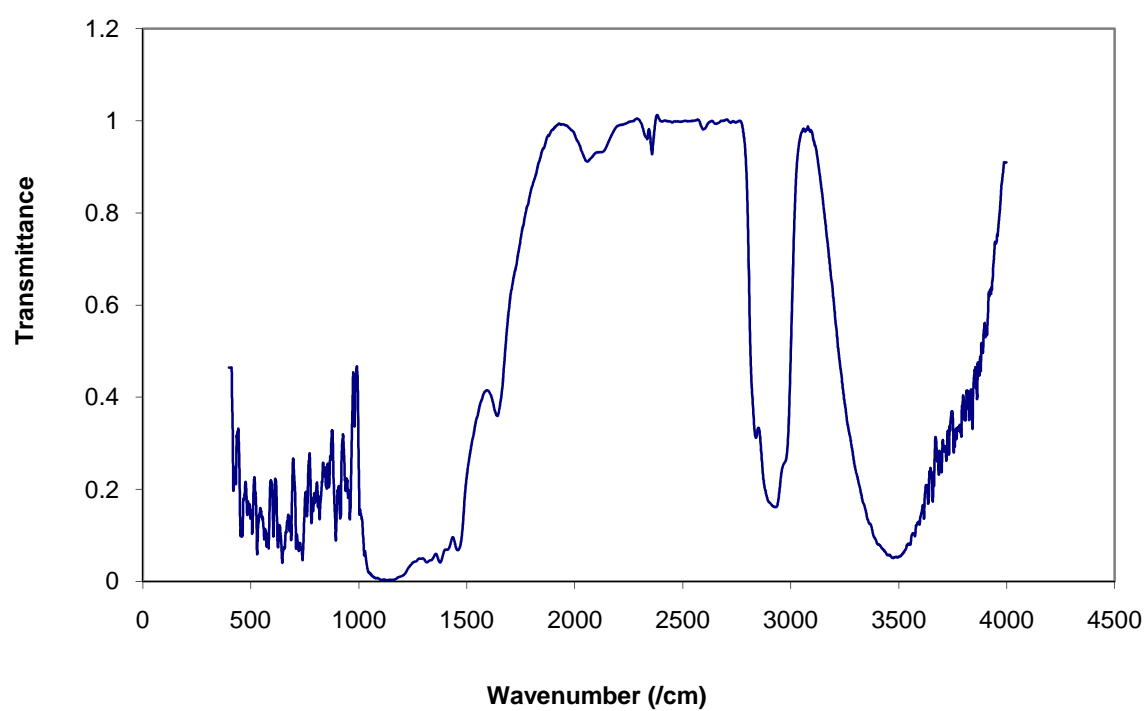


**Figure 5.18.** Infrared spectrum of a binary mixture of CPT and HPMC K 100 M (1:4)

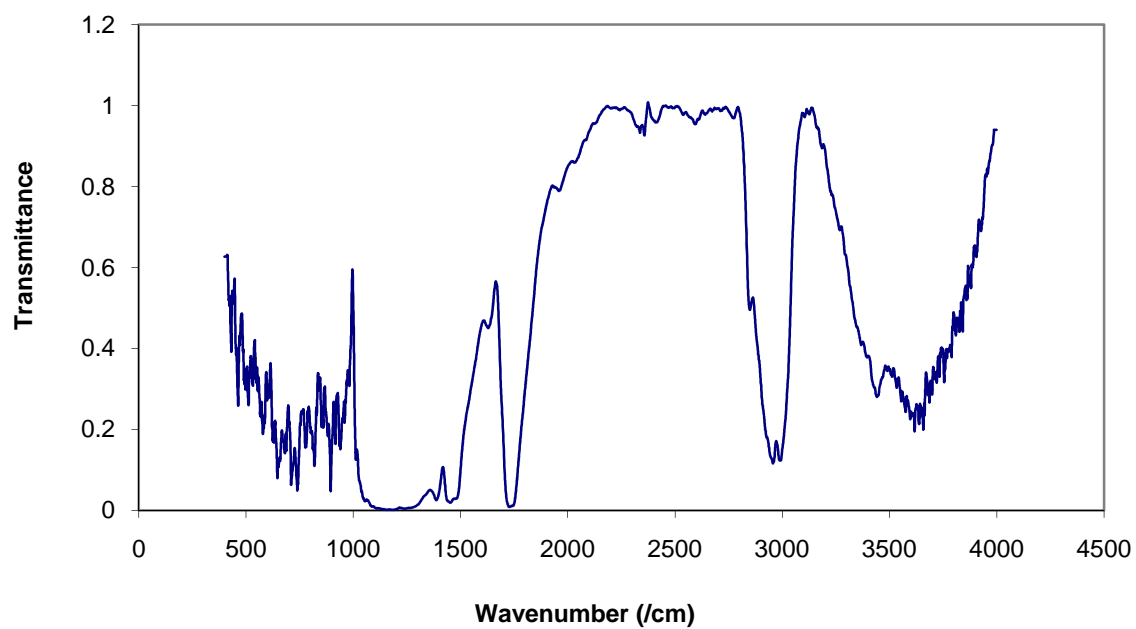


**Figure 5.19.** Infrared spectrum of a binary mixture of CPT: MCC (1:4)

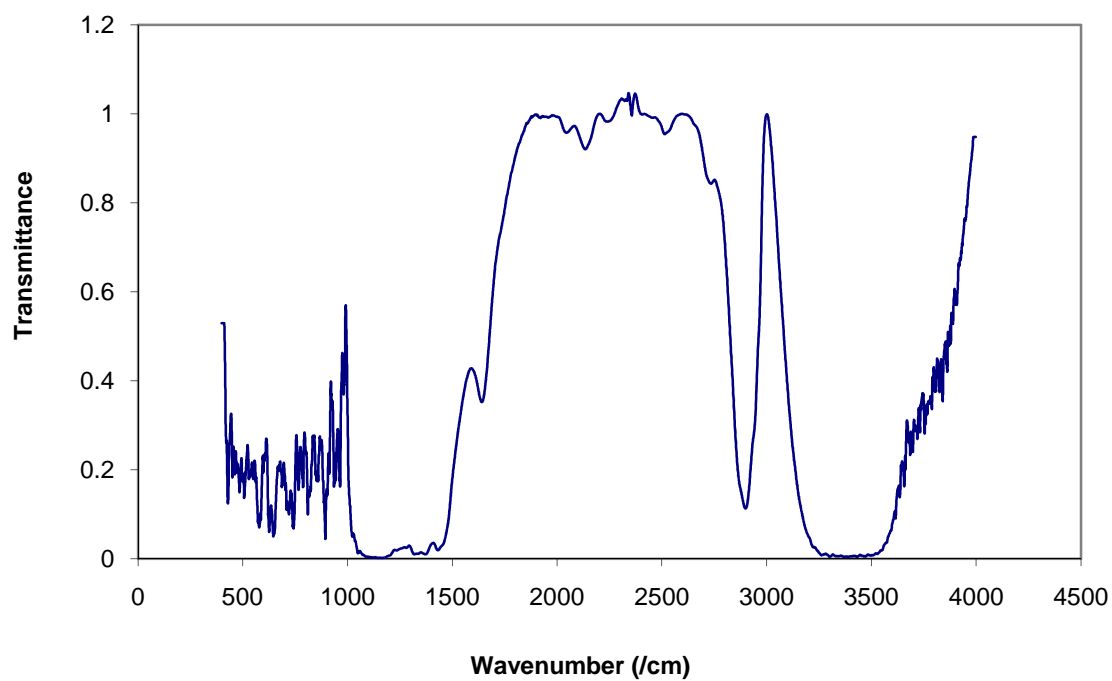


**Figure 5.20.** Infrared spectrum of a binary mixture of CPT: Eudragit<sup>®</sup> RS (1:4)

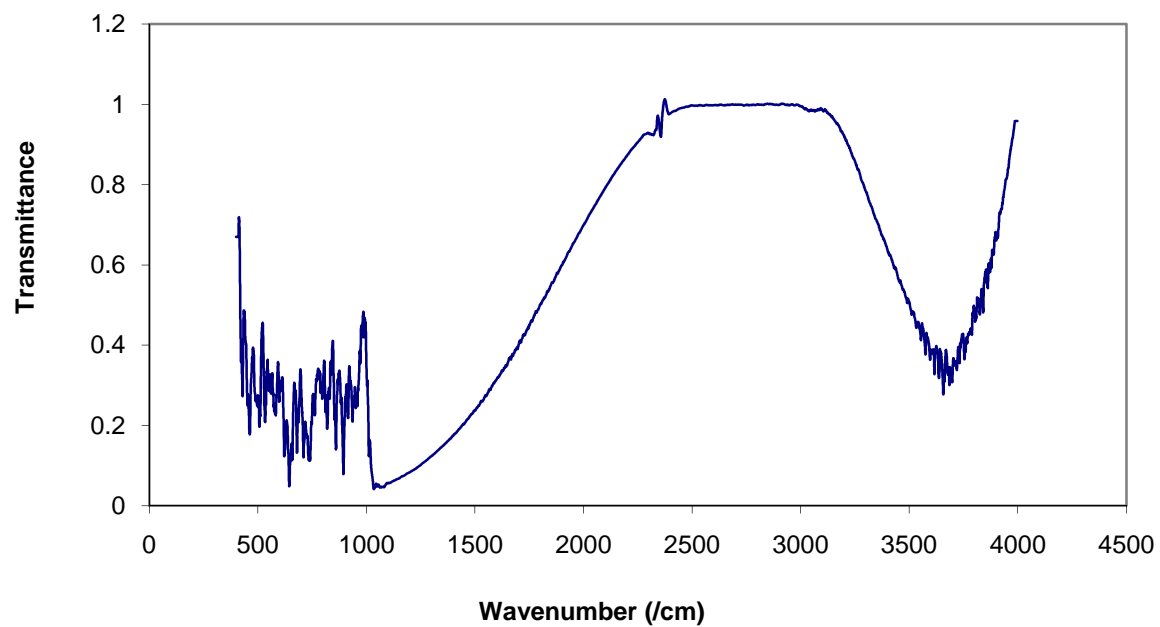


**Figure 5.21.** Infrared spectrum of a binary mixture of a CPT: citric acid (1:4)

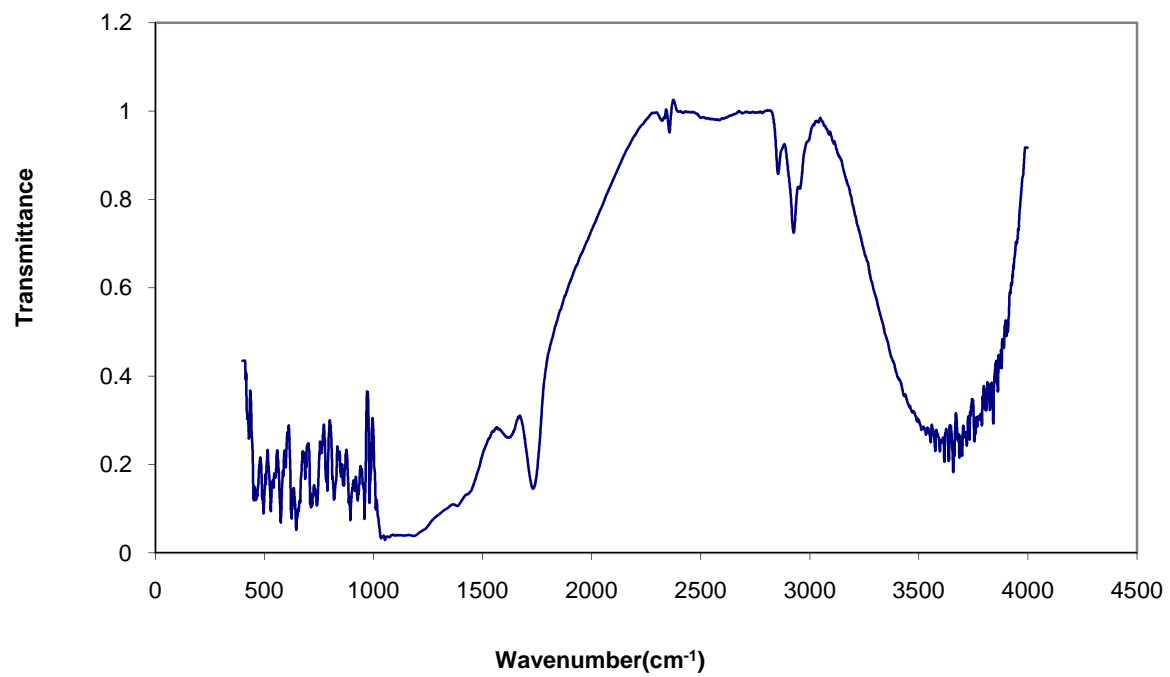


**Figure 5.22.** Infrared spectrum of physical mixture (all excipients used)

## 5.5. CONCLUSION

To certify the quality of a pharmaceutical formulation, parameters such as the interaction between a selected API and excipients to be used in formulation development studies must be analysed. The data generated in these studies clearly indicate the excipients that are compatible with CPT. The presence of moisture associated with potential excipients to be used appears to be an important factor to consider during formulation development.

Based on the results from preliminary screening, all excipients except citric acid can be selected for formulation development. Infrared spectroscopic studies confirmed the possibility of an interaction between CPT and citric acid. Consequently the model blends tested showed compatibility with CPT for the excipients evaluated. From the well-constructed compatibility studies, Eudragit<sup>®</sup> RS, Methocel K4M, Methocel K100M and Microcrystalline cellulose were finally selected for formulation development.

The DSC data generated for the different binary mixtures evaluated indicate that the characteristic endothermic peak of about 105.6 °C for CPT was present in all thermograms. This study demonstrates that DSC and FT-IR techniques are sensitive techniques that can reveal potential interactions, whereas TG is not as sensitive to the presence of interactions. TG analysis revealed that the thermal degradation of CPT takes place in two major and one minor step, and that these occur in different temperature ranges. Each thermal degradation stage produced an endothermic peak on the DSC thermogram and where the melting transition was also observed immediately prior to the commencement of decomposition. It is clear that quality control is vital due to the potential for changes in the final product arising from variations in the production process.

The quantitative effects on a DSC response for an API may only be revealed in excipient-rich mixtures. The effects appear to be related to moisture-driven mechanisms of the interaction. Consequently these findings may be valuable in defining the composition of the ultimate commercial formulation and the necessary precautions for storing the product. While DSC is a well known technique for the characterization of pharmaceutical and polymeric materials, it has certain limitations in practical use. It is unable to provide insight into the changes to thermal events or reactions at a molecular level. Therefore it is essential to combine DSC with other techniques to permit greater understanding of any changes in the materials to be

used. The understanding of polymorphic changes in pharmaceuticals is of great concern and DSC allows one to correlate structural changes with thermal events.

The theoretical basis of DSC/TGA and IR experiments has been examined. The overall goal to provide practical guidelines for compatibility studies of CPT with several excipients has been achieved. Thermal analysis has been applied to both a research objective and to practical problem solving in formulation development.

## CHAPTER SIX

---

### THE EVALUATION OF CAPTOPRIL MICROCAPSULES MANUFACTURED USING AN OIL IN OIL SOLVENT EVAPORATION TECHNIQUE

#### 6.1. INTRODUCTION

Microencapsulation is a technique used to manufacture tiny packaged materials that are referred to as microcapsules. Microcapsules are minute heterogeneous containers that are normally spherical if enclosing a fluid or are roughly the shape of a particle if manufactured to contain a solid (395). This technique has been used in a diverse range of fields and there has been widespread interest in microencapsulation technologies. The first industrial product manufactured using microencapsulation was introduced by Green and Schleicher in the 1950s (395-396) to produce dye containing pressure-sensitive microcapsules for the manufacture of carbonless copying paper (395, 397). The microcapsules were manufactured by complex coacervation of gelatin and gum Arabic (395, 396). Carbonless copy paper is still produced commercially and is one of the most significant products developed that utilizes microencapsulation technology. The technologies developed for carbonless copy paper have led to the development of a variety of microcapsule products. Since the 1950s, many products of this type have appeared on the market, for pharmaceutical, cosmetic, agricultural chemical, food additive, coating, printing ink, adhesive, catalyst and dye applications (395, 398-400) and various others are under development (395, 401-403). The main reasons for the use of microencapsulation technologies are shown in Table 6.1.

The term “capsule” is used when an encapsulated substance, referred to as the core, active agent, fill material, internal phase, nucleus or payload, is surrounded by a membrane referred to as an encapsulant, carrier, coating, membrane, shell or wall. The term “sphere” or just “particle” is used when the core material is dispersed or dissolved in a carrier substance.

**Table 6.1.** Reasons for microencapsulation of API (404)

- 
1. Controlled release of drugs,
  2. Protection of encapsulated materials against oxidation or deactivation due to reaction in the environment,
  3. Masking of odour and/or taste,
  4. Isolation of materials from undesirable phenomena,
  5. Easy handling of powder-like materials
- 

Particles or capsules between 1 and 5000  $\mu\text{m}$  are called microparticles or microcapsules. Those below 1  $\mu\text{m}$  are usually referred to as nanocapsules or nanoparticles, whereas those above 5000  $\mu\text{m}$  in size are called macrocapsules or coated particles. Microcapsules are usually spherical, but they may also be irregular in shape and the differences between microparticles and some typical geometries are illustrated in Figure 6.1(405).

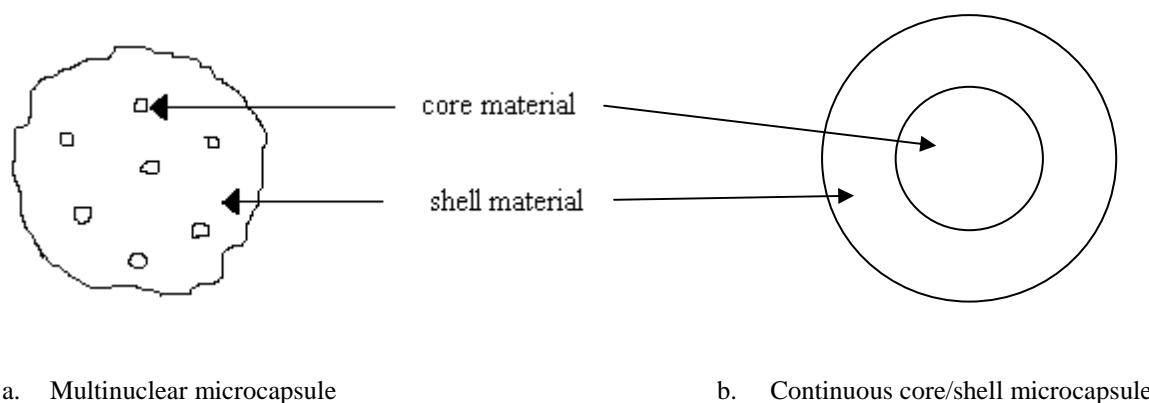


**Figure 6.1.** Schematic diagram of two types of microcapsules

When taken orally, microcapsules spread uniformly in the gastrointestinal tract, thereby avoiding exposure of the mucosal tissues to high concentrations of API and ensuring more reproducible drug absorption. The risk of dose dumping is also lower than with single-unit dosage forms (406, 407).

The application and potential for use of microencapsulation is shown by the large number of methods that have been reported (404-408). The most important methods that have been described have been classified in a variety of ways (408). An appropriate classification, based on of the method of manufacture (409) is shown in Table 6.2.



**Table 6.2.** Main methods of microencapsulation

- 
1. Phase separation
  2. Interfacial and/or *in situ* polymerization,
  3. Spray drying and spray congealing,
  4. Solvent evaporation
  5. Coating.
- 

The solvent evaporation approach was used as the preferred method of encapsulation of CPT for these studies as it requires ambient temperatures and mild emulsification techniques.

### **6.1.1. Solvent evaporation**

The solvent evaporation process entails dissolving a polymer in a suitable water-immiscible solvent, and dispersing or dissolving the API in that polymer solution. The resultant solution or dispersion is then emulsified to form an aqueous continuous phase in which discrete droplets can be observed. For the microcapsules to form, the organic solvent must diffuse into the aqueous phase and then evaporate at the water/air interface. As the solvent evaporates the microcapsules harden and free-flowing microspheres can be harvested after filtration and drying.

The solvent evaporation method has been used extensively to manufacture microspheres (410-412). Several variables can influence the properties of microcapsules. These include solubility of the API, internal morphology, solvent type, diffusion rate, temperature, polymer composition, viscosity and drug loading (413-414). The effectiveness of the solvent evaporation method producing microspheres is dependent on the successful entrapment of an API within the particles. This process has been observed to be highly successful for drugs that are either insoluble or poorly soluble in aqueous media which is usually the continuous phase in these manufacturing procedures (415-416).

Recent advances in the solvent evaporation technique have allowed successful entrapment of highly water-soluble drugs (417-419) and other thiol-containing drugs (420). Consequently the microencapsulation of CPT, a freely soluble drug, was attempted.

Various methods can be used to manufacture microcapsules by solvent evaporation (421-424). Efficient drug encapsulation is dependent on the hydrophilicity or hydrophobicity of the

API to be encapsulated (424). For insoluble or poorly water-soluble drugs the oil-in-water (o/w) method is frequently used. This method is the simplest and other methods are derived by modification of this approach. The method comprises of four major steps, summarized in Table 6.3:

**Table 6.3.** Steps used in the microencapsulation process (424)

- 
1. Dissolution of the hydrophobic drug in an organic solvent containing the polymer,
  2. Emulsification of the dispersed phase, in an aqueous continuous phase,
  3. Extraction of the solvent from the dispersed phase by the continuous phase, solvent evaporation, transformation of droplets of dispersed phase into solid particles, and,
  4. Recovery and drying of microspheres to eliminate residual solvent
- 

The conventional o/w solvent evaporation techniques cannot be used for water-soluble drugs as they result in low loading efficiency due to partitioning of the drug into the continuous phase (426). To reduce drug partitioning into the continuous phase and to enhance drug loading, o/o solvent evaporation methods have been proposed (427).

Four alternate methods are available, which make it possible to encapsulate hydrophilic drugs (428). The methods are presented in Table 6.4.

**Table 6.4.** Alternate methods to encapsulate hydrophilic drugs (428)

- 
1. A w/o/w double emulsion method in which an aqueous solution of hydrophilic drug is emulsified with an organic phase (w/o) emulsion that is dispersed in a second aqueous solution forming a second emulsion or w/o/w double emulsion,
  2. An o/w co-solvent method that is used when a drug is not soluble in the main organic solvent a co-solvent is necessary to dissolve the drug,
  3. An o/w dispersion method in which the drug is dispersed as a solid powder in a solution of polymer and organic solvent,
  4. An o/o non-aqueous solvent evaporation method in which the aqueous phase is replaced by an oil such as mineral oil for example.
- 

O' Donnell and McGinity (429) studied the main factors influencing the properties of microcapsules. These are summarized in Figure 6.2.

The dispersed phase contains the polymer and the encapsulation solvent. The polymer must be biodegradable or biocompatible and the choice of polymer is dependent on the desired drug release rate. If one polymer cannot produce the appropriate drug release profile a combination of polymers can be used.

For the successful application of solvent evaporation, a suitable solvent to dissolve /disperse the polymer must meet the criteria shown in Table 6.5:

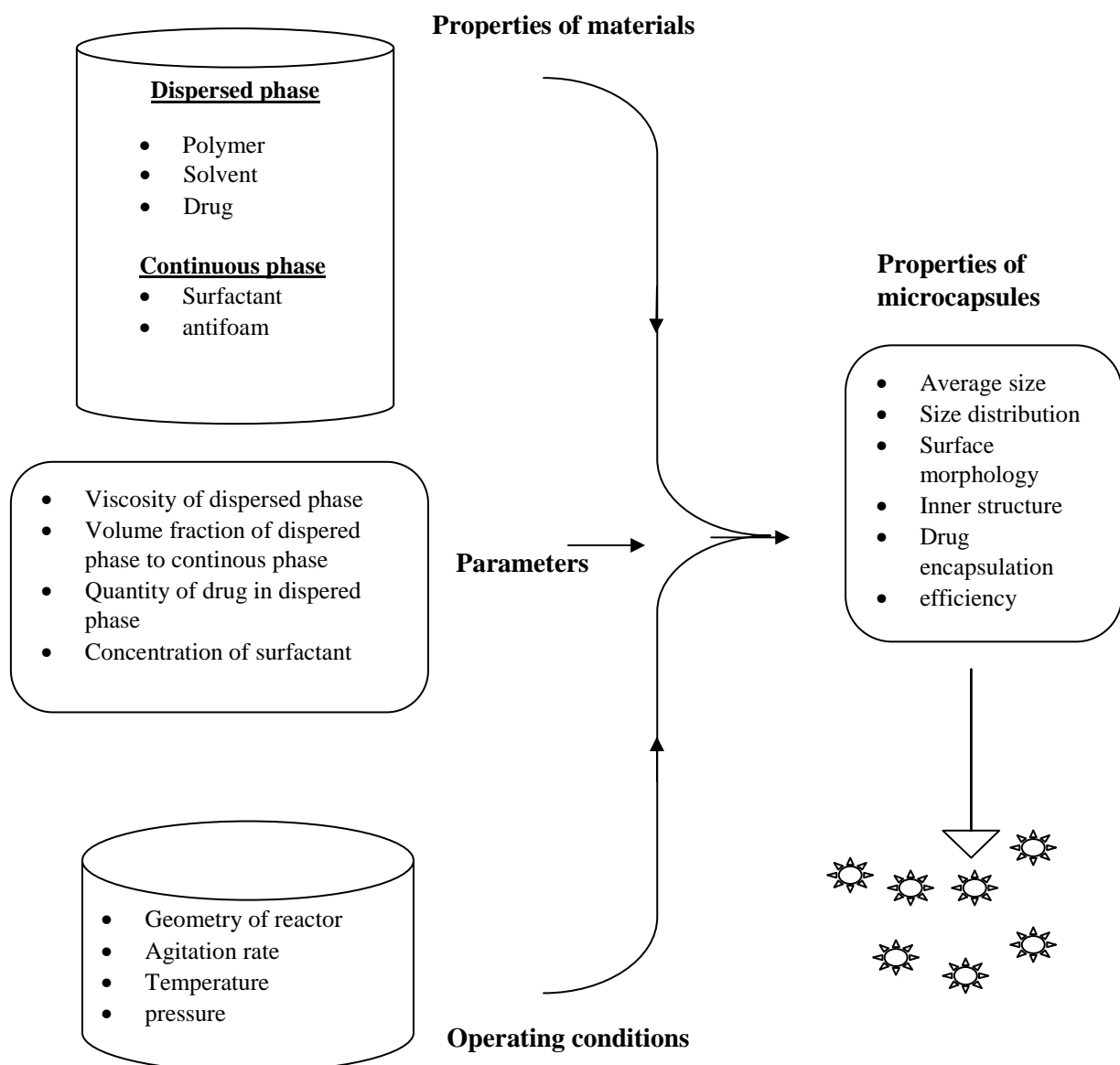


**Figure 6.2.** Schematic representation of the factors influencing the properties of microcapsules (adapted from (429))

**Table 6.5.** Criteria used to select solvents for microencapsulation (429)

- 
1. Solvent must dissolve the polymer,
  2. Solvent must be poorly soluble/miscible with the continuous phase,
  3. Solvent must have high volatility and low boiling point,
  4. Solvent must not be toxic.
- 

In certain cases, other excipients such as cosolvent and porosity generators are added to the dispersed phase (429-432). A porosity generator, (porosigen or porogen), is used to create pores within microspheres to increase the degradation rate(s) of polymers and improve or modulate drug release rates (433).

The continuous phase is the second phase in a solvent evaporation process and is larger in volume than the dispersed phase and usually also contains a surfactant. Liquid paraffin is normally used as the continuous phase in an o/o solvent evaporation procedure. The surfactant used in this work was span 80. Span 80 is a tensioactive agent that enhances the stabilization of an emulsion by reducing the surface tension of a continuous phase and avoiding coalescence and agglomeration of dispersed droplets.

In addition to the use of a surfactant an antifoaming agent may be added so that when manufacturing procedures involving aggressive agitation are used, foaming does not interfere with the formation of microspheres. After the physico-chemical properties of materials, agitation is one of the most important parameters that can be used for controlling the size of microcapsules ultimately produced. Many other factors, linked in some way to agitation, also influence the size of microspheres. These include the geometry and diameter of the reactor and the number and position of impellers (429, 434-435).

It has been observed that encapsulation efficiencies increase to a maximum, as the quantity of API used increases, and then decrease as further drug is added (429, 434)

The rate of solvent evaporation can be accelerated by increasing the temperature of the continuous phase (429, 436, 437), but there are several drawbacks to using elevated temperatures. These include a decrease in the total mass recovered and decreased encapsulation efficiencies resulting in coarse surface morphology (429, 438). Moreover, the chosen temperature should not denature the API or reach the boiling point of the solvent used in the production process.

### **6.1.2 Aim**

The aim of this work was to prepare CPT microcapsules with a controlled drug release profile suitable for oral administration of the compound.

## **6.2. EXPERIMENTAL**

### **6.2.1. Materials**

CPT powder was donated by Protea Chemicals (Midrand, South Africa). Citric acid monohydrate was purchased from Aspen Pharmacare (Port Elizabeth, South Africa). Hydroxypropyl methylcellulose (Methocel K100M and K15M) were donated by Colcocon<sup>®</sup> Ltd (Dartford, Kent, UK). Microcrystalline cellulose (Avicel 101) was purchased from FMC (Philadelphia, USA). Eudragit RS was donated by Rohm Pharma (GmbH, Darmstadt, Germany). Span 80 was purchased from Aldrich (Germany). Liquid paraffin was supplied by ADC Laboratories (Durban, South Africa). Acetone AR was purchased from Associated Chemical Enterprises (Southdale, South Africa). *n*-Hexane was acquired from Burdick and Jackson Laboratories (Michigan, USA). Dimethyl polysiloxane was purchased from Sigma-Aldrich (Kempton Park, South Africa). All chemicals were used without any further purification.

### **6.2.2. Method**

To avoid degradation of CPT all experiments were conducted under 'safe light'. All experimental work was performed on a laboratory scale. RSM in conjunction with a CCD was used to establish the number of experiments to be conducted and to interpret the resultant data.

#### **6.2.2.1. Experimental design for response surface methodology**

RSM is a rapid technique for deriving a functional relationship between a set of input variables and experimental responses. By use of RSM the number of experiments necessary for establishing a mathematical trend in the experimental design region is reduced and the determination of an optimum level of experimental factors required to produce a specific response is readily achieved (224, 225, 230, 439-441).

RSM was used to investigate the impact of four variables on microcapsule formation. These variables were Eudragit<sup>®</sup> RS ( $X_1$ ), Methocel<sup>®</sup> K15M ( $X_2$ ), Methocel<sup>®</sup> K100M ( $X_3$ ) and homogenization speed ( $X_4$ ). The variation and level and composition of the variables were

designed using a CCD approach. The variables and their concentration ranges are listed in Table 6.6.

The variables were coded to facilitate multiple regression analysis. Thirty experimental settings were generated with 4 factors at 3 levels using the principals of RSM with the aid of Design Expert 7.1 software. The quadratic polynomial regression model that was assumed for predicting  $Y_1$  (percent yield),  $Y_2$  (microcapsule size),  $Y_3$  (encapsulation efficiency),  $Y_4$  (percent drug release) and the  $Y_5$  (Hausner ratio) variables are listed as the  $Y$  fitted depicted in Equation 6.1.

$$Y = (\beta_{k_0} + \varepsilon) + \sum_{i=1}^4 \beta_{k_i} x_i + \sum_{i=1}^4 \beta_{k_{ji}} x_i^2 + \sum_{i=1}^3 \sum_{j=i+1}^4 \beta_{k_{ij}} x_i x_j \quad \text{Equation 6.1}$$

where,  $Y$  is a response viz.,  $Y_1, Y_2, Y_3, Y_4$  and  $Y_5$ .  $(\beta_{k_0} + \varepsilon)$ ,  $\beta_{k_i}$ ,  $\beta_{k_{ji}}$  and  $\beta_{k_{ij}}$  are the constant(s) of the coefficients of intercept, linear, quadratic and interaction terms, respectively.  $x_i$  and  $x_j$  are uncoded independent variables of concentration of Eudragit<sup>®</sup> RS, Methocel<sup>®</sup> K100M, Methocel<sup>®</sup> K15M and homogenizing speed.

**Table 6.6.** Coded levels for independent variables used in experimental design

Factor	Coded $X_i$	Coded level			$\Delta X^a$
		-1	0	+1	
Eudragit RS (g)	$X_1$	1.5	2.0	2.5	0.5
K100M (g)	$X_2$	0.25	0.50	0.75	0.25
K15M (g)	$X_3$	0.25	0.50	0.75	0.25
Homogenizing speed (rpm, x 1000)	$X_4$	1.0	1.5	2.0	0.5

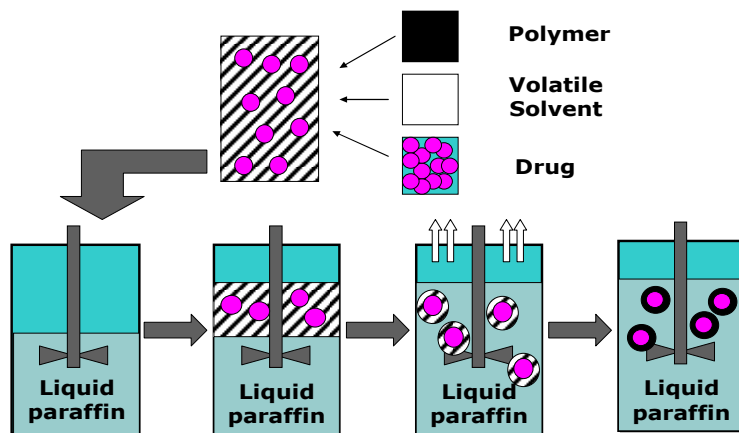
### 6.2.2.2. Manufacture of microcapsules

To produce microcapsules the emulsification and solvent evaporation technique used was based on the method reported by Khamanga *et al* (442). The representative formulations used to manufacture microspheres are listed in Table 6.7 and a schematic representation of the manufacturing procedure is shown in Figure 6.3. In all the 30 formulations, 0.75 g of CPT and 0.5 g of MCC were incorporated. MCC was used as a filler and binder in the formulations.

**Table 6.7.** Formulations used to manufacture microcapsules

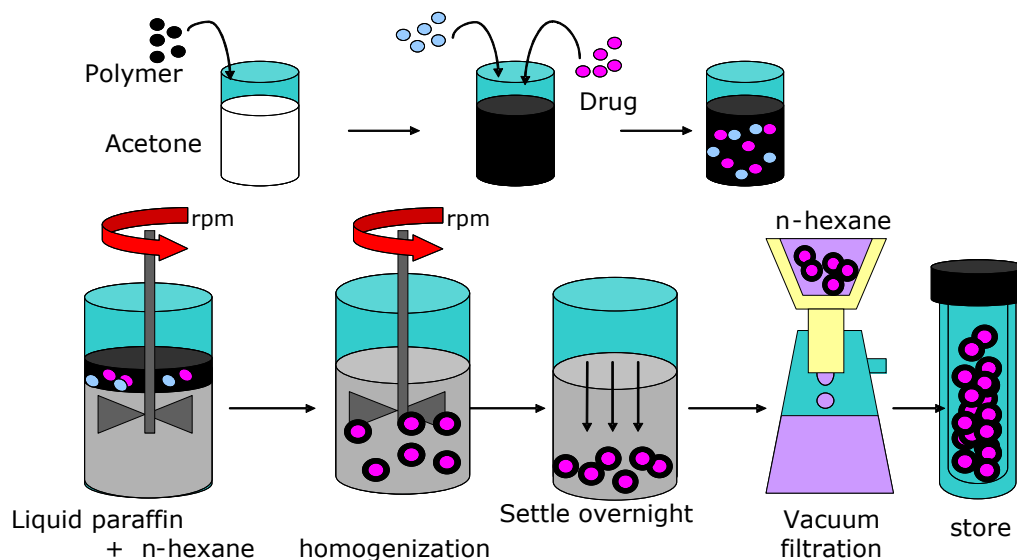
<b>RUN</b>	<b>Eudragit® RS</b>	<b> METHOCCEL® K100M</b>	<b> METHOCCEL® K15M</b>	<b> Homogenizing speed</b>
	<b>g</b>	<b>g</b>	<b>g</b>	<b>rpm (1000)</b>
1	2.0	0.50	0.50	1.5
2	2.0	0.75	0.25	1.5
3	1.5	0.50	0.50	1.0
4	2.5	0.50	0.50	2.0
5	2.0	0.50	0.25	2.0
6	2.0	0.50	0.50	1.5
7	2.0	0.75	0.75	1.5
8	1.5	0.50	0.50	1.0
9	2.0	0.25	0.75	1.5
10	2.0	0.50	0.50	1.5
11	1.5	0.75	0.50	1.5
12	2.0	0.50	0.50	1.5
13	2.0	0.25	0.50	2.0
14	2.5	0.25	0.50	1.5
15	2.0	0.50	0.50	1.5
16	2.5	0.50	0.75	1.5
17	1.5	0.50	0.75	1.5
18	2.0	0.25	0.50	1.0
19	2.5	0.75	0.50	1.5
20	2.0	0.50	0.75	1.0
21	2.0	0.50	0.75	2.0
22	2.0	0.75	0.50	1.0
23	2.5	0.50	0.25	1.5
24	2.0	0.50	0.25	1.0
25	1.5	0.25	0.50	1.5
26	2.5	0.50	0.50	1.0
27	2.0	0.25	0.25	1.5
28	1.5	0.50	0.25	1.5
29	2.0	0.75	0.50	2.0
30	2.0	0.75	0.50	2.0





(A)

**Figure 6.3.** Basic steps (A and B) of microencapsulation using a solvent evaporation process (adapted from 442)



(B)

Different amounts of polymer and MCC was dispersed in 20 ml of acetone. An accurately weighed quantity of CPT was dispersed in this solution. Light liquid paraffin (120 ml) containing 1% v/v span 80 and 0.1% v/v dimethyl polysiloxane was then placed in a 400 ml beaker and agitated with a three-blade propeller of 50 mm diameter, linked to a homogenizer

fitted with a four-blade “butterfly” propeller having a diameter of 50 mm (Virtis Company, New York, USA) to produce an homogenous oily phase. The acetone solution was then poured into the oily continuous phase. The system was maintained at 20° C to ensure evaporation of the acetone. Processing variables such as the amount of liquid paraffin and volume of acetone solution were maintained constant for all batches produced. After 2 h, 10 ml of *n*-hexane (non-solvent) was added to harden the microcapsules and stirring was continued for a further 5 h. The hardened microcapsules were collected using a Buchner funnel and were washed 2-3 times with 50 ml *n*-hexane to remove any residual liquid paraffin. The microcapsules were then dried at room temperature for 24 h. All batches were prepared in triplicate and the dried microspheres were stored in well-closed containers. All experiments in which evaluation of microcapsules was undertaken were performed the next day.

The yield (443) of microcapsules was calculated using Equation 6.2.

$$\% \text{ Yield} = \frac{\text{amount of microsphere obtained (g)}}{\text{theoretical amount (g)}} \times 100 \quad \text{Equation 6.2}$$

#### **6.2.2.3. Determination of the mean particle size**

Particle size distribution was performed using a sieve stack. The nest of sieves was vibrated at 200 rpm for at least 15 minutes, or until no change in the weight of each fraction was observed. The amount of particles retained on each sieve was weighed and the cumulative mass retained on each sieve was calculated. The particle size distribution for all formulations was determined and the mean particle size of the microcapsules calculated.

#### **6.2.2.4. Flowability**

The importance of the flowability of a powder in the production of pharmaceutical dosage forms is well-documented (50). Numerous methods for measuring powder flow have been developed and are largely based on an empirical understanding of the flow process.

##### **6.2.2.4.1. Angle of repose**

The stationary angle of repose ( $\theta$ ) for each batch was determined by placing 5 g of the microcapsules in a funnel (with orifice and base diameters of 1.0 and 5.0 cm, respectively). The tip of the orifice of the funnel was set at a fixed height (30 cm) from the horizontal

surface and the microcapsules were allowed to flow only under the force of gravity. The angle of repose (445) was calculated using Equation 6.3.

$$\tan \theta = \frac{h}{r} \quad \text{Equation 6.3}$$

where

h = height of the pile of microcapsules, and  
r = the radius of the base of the cone.

All measurements were performed in triplicate and an average for three determinations was reported.

#### 6.2.2.4.2. Bulk and tapped bulk density

The bulk and tapped bulk density of the microparticles were calculated using the initial and final volumes for a fixed mass of the microcapsules before and after tapping. Tapping was carried out by hand. The weighed microcapsules were carefully poured into a measuring cylinder and the initial volume was recorded. The cylinder was then tapped for 5 minutes, or until no measurable change in the final volume was observed. The cylinder was lightly tapped to dislodge residual powders from the wall of the measuring cylinder. Each sample was poured slowly and gently into a 10 ml measuring cylinder and tapped for 100, 200, 300, 400, 500, 600, 700, 800, 900 and 1000 times. The percent compressibility of the microcapsules was expressed using Carr's index (*CI*) (446) as shown in Equation 6.4. This equation describes the relationship between the degree of volume reduction of the powder column and the pressure applied to the powder.

$$CI = \left\{ \frac{\rho_{tap} - \rho_{bulk}}{\rho_{tap}} \right\} \times 100 \quad \text{Equation 6.4}$$

Where

*CI* = Carr's compressibility index,  
 $\rho_{tap}$  = tapped density, and  
 $\rho_{bulk}$  = bulk density.

#### 6.2.2.4.3. Hausner ratio

The Hausner ratio is the ratio of the tapped density and bulk density (447) and was calculated using Equation 6.5:

$$HR = \frac{\rho_{tapped}}{\rho_{bulk}} \quad \text{Equation 6.5}$$

where

$$\begin{aligned} \rho_{tapped} &= \text{tapped density} \\ \rho_{bulk} &= \text{bulk density} \end{aligned}$$

#### 6.2.2.4.4. Kawakita analysis

Microcapsules have also been analyzed using Athy-Heckel, Kawakita and Cooper-Eaten analysis (448). The Kawakita equation is shown in Equation 6.6.

$$\frac{n}{c} = \frac{n}{a} + \frac{1}{ab} \quad \text{Equation 6.6}$$

Where

$$\begin{aligned} n &= \text{is the tap number,} \\ C &= \text{is degree of volume reduction of the microcapsules and is a constant,} \\ \frac{1}{a} &= \text{constant, is the total degree of volume reduction at the limit of tapping and is} \\ &\quad \text{termed compactibility} \\ \frac{1}{b} &= \text{constant, related to cohesion and termed cohesiveness.} \end{aligned}$$

The plot of  $\frac{n}{c}$  versus  $n$  is linear and the compactibility,  $\frac{1}{a}$  and cohesivity,  $\frac{1}{b}$  are obtained from the slope,  $\frac{1}{a}$  and the intercept,  $\frac{1}{ab}$  of the plot of the modified Kawakita and Ludde equation (449). The data were analysed using an equation developed by Kuno (450) and that is shown in Equation 6.7:

$$\ln(\rho_f - \rho_n) = -kn + \ln(\rho_f - \rho_o) \quad \text{Equation 6.7}$$

where,  $\rho_f, \rho_n$  and  $\rho_o$  are the apparent densities at equilibrium,  $n$ th tapped and initial state, respectively and  $k$  is a constant.

It has been reported that the Kawakita constant,  $a$ , which quantifies the maximum possible volume reduction due to tapping or applied load should equal  $CI$  (449). Thus, the application of the Kawakita equation has no advantage over the use of Carr's compressibility index as an indicator of possible volume reduction.

#### 6.2.2.5. Encapsulation efficiency (EE)

The microcapsules were crushed and powdered using a mortar and pestle. Approximately 100 mg of the crushed microcapsules was accurately weighed and dissolved in 100 ml of phosphate buffer (pH 3.0) with sonication for 20 minutes. The solution was then filtered through a 0.45 µm membrane filter (Millipore). A 2 ml aliquot was withdrawn from this solution and diluted to 50 ml with buffer and analysed using a validated HPLC method to determine the CPT content of microcapsules. The % EE (451) was calculated using Equation 6.8.

$$\% EE = \frac{\text{real loaded drug}}{\text{theoretical loaded drug}} \times 100 \quad \text{Equation 6.8}$$

#### 6.2.2.6. Scanning electron microscopy (SEM)

The shape and surface morphology of the microcapsules was investigated using SEM (Tescan, VEGA LMU, Czechoslovakia Republic). The microcapsules were mounted onto a double-sized carbon stub that was placed onto a sample disc carrier (3 mm height, 10 mm diameter) and were coated with gold under vacuum (0.25 Torr) with a sputter coater (Balzers Union Ltd, Balzers, Lichtenstein). The samples were imaged using a 20 kV electron beam.

#### 6.2.2.7. Drug release studies

The percent drug released was the response selected as *in vitro* dissolution testing is the most important quality control test for drug products and has the potential to highlight possible bioavailability issues (452-453).

Several dissolution apparatus have been described (454-458). The rotating basket (USP Apparatus 1) and the paddle (USP Apparatus 2) devices are simple, robust and adequately standardized. They are used worldwide and well understood (457).

However due to the single container nature of the basket and paddle apparatus, experimental difficulties may arise when a change in pH is required or a change in sink conditions or any other test medium parameter occurs during a specific experiment (457).

The reciprocating cylinder or USP apparatus 3 (Bio-Dis<sup>®</sup>) has been described (457) and has had a relatively short history since its proposal in the 1990s for use as a dissolution test

apparatus by Borst *et al* (458) for drug release testing of extended-release products and as an alternative to USP Apparatus 1 and 2.

A VanKel<sup>®</sup> Bio-Dis<sup>®</sup> dissolution apparatus (VanKel<sup>®</sup> Industries, New Jersey, USA) was used for dissolution testing of microcapsules manufactured in these studies. A model VK 750D digitally controlled water circulation / heater (VanKel<sup>®</sup> Industries, New Jersey, USA) was used to maintain the temperature of the dissolution media at  $37\pm 0.5^{\circ}\text{C}$ . Drug loaded microcapsules were tested in 250 ml of phosphate buffers of different pH. The dissolution test was conducted at a 20 rpm rate. Drug release was determined using a validated HPLC method. Samples were collected at predetermined time intervals. A summary of the dissolution test conditions is listed in Table 6.8.

Furthermore, the dissolution behaviour of CPT microcapsules was assessed using a fully automated Hanson Research SR 8 PLUS (Chartworth, CA, USA) dissolution apparatus fitted with an Autoplus<sup>™</sup> Multifill<sup>™</sup> and Maximizer Syringe Fraction Collector, respectively. The release studies were carried out at  $37\pm 0.5^{\circ}\text{C}$  using USP Apparatus 1 fitted with 8 USP baskets (40-mesh) rotated at 100 rpm. All dosage forms were placed in the baskets that were then lowered into 900 ml of degassed phosphate buffer (Table 6.8). The percent drug released from the microcapsules after a 12 h test was determined. Samples (2 ml) were withdrawn and replaced with 2 ml of fresh medium that has automatically been filtered through a  $0.45\ \mu\text{m}$  Durapore<sup>®</sup> membrane HVLP filters (Millipore Corporation, Ireland). Samples were collected at predetermined time intervals after 1, 2, 6, 8, 10, and 12 hours. A summary of the dissolution test conditions for this study is depicted in Table 6.8. Results for USP Apparatus 1 are not shown in this report.

The response and formulation variables for all model formulations were analysed using Design-Expert<sup>®</sup> software. Statistical analysis including stepwise linear regression and response surface analysis were conducted. The significant terms ( $p < 0.05$ ) were chosen for use in establishing the final equations. The best fit mathematical model was selected based on the comparisons of several statistical parameters including the coefficient of variation (CV), multiple correlation coefficients ( $R^2$ ) and adjusted multiple correlation coefficient (adjusted  $R^2$ ).

**Table 6.8.** Summary of general dissolution conditions for basket and reciprocating cylinder dissolution test methods.

<b>Parameter</b>	<b>USP Apparatus 1</b>	<b>USP Apparatus 3</b>
Dissolution medium	Buffers (pH 1.6, 7.4)	Buffers (pH 1.6, 3.4, 4.6, 6.8)
Temperature	37.0 ± 0.5°C	37.0 ± 0.5°C
Initial volume	900 ml	250 ml
Basket / dip speed	100 rpm	20 dpm
Screen size	-	405 µm top /177 µm bottom
Filter size	0.45 µm	0.45 µm
Volume drawn	2 ml	2 ml
Dissolution time	1h in pH 1.2 and 11h in pH 7.4	1 h in pH 1.6 and 3.4 and 5 h in pH 4.6, 6.8

### 6.3. RESULTS AND DISCUSSION

All experiments were performed in a randomized fashion, resulting in thirty simplified experimental data sets being generated in order to minimize the effects of uncontrolled factors that may introduce bias on the observed response. A classical second-degree model with a cubic experimental domain was postulated for all responses. The coefficients for the second-order polynomial model were estimated and quadratic equations were generated.

The amount of Eudragit<sup>®</sup>, Methocel<sup>®</sup> K15M, Methocel<sup>®</sup> K100M and the speed of homogenization were investigated in the ranges of 1.5- 2.5g, 0.25-0.75g, 0.25-0.75g and 1000-2000 rpm, respectively. The contour and response surface plots for the percent drug release ( $Y_4$ ) are shown in Figures 6.4 to 6.15 and plots for the other responses ( $Y_1$ ,  $Y_2$ ,  $Y_3$  and  $Y_5$ ) are not reported. Percent drug released ( $Y_4$ ) was the chosen response to report. The regression coefficients calculated for percent drug release are shown in Table 6.9.

Modeling was performed using Design Expert<sup>®</sup> (Version 7.01) with a backward, stepwise linear regression technique. Significant terms ( $p < 0.05$ ) were selected in order to define the final equations. The mathematical relationships that were generated for the responses  $Y_1$ ,  $Y_2$ ,  $Y_3$ ,  $Y_4$  and  $Y_5$  are expressed as Equations 6.9 to 6.13.

In addition contour plots (Figures 6.4 to 6.9) and three dimensional graphs (Figures 6.10 to 6.15) were generated for each pair-wise combination of the four factors investigated while keeping the other two at the centre point level.



**Table 6.9.** ANOVA Table for Response Surface Quadratic Model for percent drug release

Source	Sum of Squares	Df	Mean Square	F-value	p-value	Prob > F
BLOCK	0.035	1	0.035			
Model	2699.91	14	192.85	4.44	0.033	<b>significant</b>
<b>LINEAR</b>						
X <sub>1</sub> -Eudragit RS	63.57	1	63.57	0.14	0.7100	
X <sub>2</sub> -Methocel K15M	127.69	1	127.69	3.29	0.0359	<b>significant</b>
X <sub>3</sub> -Methocel K100M	1123.46	1	1123.46	3.55	0.0132	<b>significant</b>
X <sub>4</sub> -Homogenizng speed	44.93	1	44.93	0.10	0.7544	
<b>QUADRATIC</b>						
X <sub>1</sub> X <sub>2</sub>	56.25	1	56.25	0.13	0.7264	
X <sub>1</sub> X <sub>3</sub>	576.00	1	576.00	1.31	0.2724	
X <sub>1</sub> X <sub>4</sub>	7.98	1	7.98	0.018	0.8949	
X <sub>2</sub> X <sub>3</sub>	306.25	1	306.25	0.690	0.4188	
X <sub>2</sub> X <sub>4</sub>	25.00	1	25.00	5.757	0.0102	
X <sub>3</sub> X <sub>4</sub>	342.25	1	342.25	0.78	0.3934	
<b>INTERACTION</b>						
X <sub>1</sub> <sup>2</sup>	433.72	1	433.72	6.98	0.0383	<b>significant</b>
X <sub>2</sub> <sup>2</sup>	56.85	1	56.85	0.13	0.7250	
X <sub>3</sub> <sup>2</sup>	31.94	1	31.94	0.072	0.7918	
X <sub>4</sub> <sup>2</sup>	8.75	1	8.75	0.020	0.8900	
<b>Residual</b>	6177.96	14	441.28			
<b>Lack of Fit</b>	4324.66	9	480.52	1.30	0.4065	
<b>Pure Error</b>	1853.30	5	370.66			
<b>Cor Total</b>	8877.86	28				

**Table 6.9. continued.**

---

<b>Std. Dev.</b>	6.97
<b>Mean</b>	85.10
<b>C.V. %</b>	8.19
<b>PRESS</b>	3490.94
<b>R<sup>2</sup></b>	0.8471
<b>Adj R<sup>2</sup></b>	0.7325
<b>Pred R<sup>2</sup></b>	-1.8412
<b>Adeq Precision</b>	46.680

---

---

The equation for the percent yield ( $Y_1$ ) is shown in Equation 6.9;

$$Y_1 = 96.57 - 9.92X_1 + 1.47X_2 + 49.20 X_3 - 15.72 X_4 + 12.00X_1X_2 - 16.00X_1X_3 + 18.75 X_1X_4 - 56.00 X_2X_3 + 50.00 X_2X_4 - 16.00 X_3X_4 - 3.30X_1^2 - 67.20X_2^2 + 30.80X_3^2 - 13.80 X_4^2$$

$$\begin{aligned} \text{Percent Yield} = & 96.57 - 9.92 \text{ Eudragit RS} + 1.47 \text{ X15M} + 49.20 \text{ X100M} - 15.72 \text{ homogenizing speed} + 12.00 \text{ Eudragit RS} * \text{X15M} - 16.00 \text{ Eudragit RS} * \\ & \text{X100M} + 18.75 \text{ Eudragit RS} * \text{homogenising speed} - 56.00 \text{ X15M} * \text{X100M} + 50.00 \text{ X15M} * \text{homogenisng speed} - 16.00 \text{ X100M} * \text{homogenisng speed} \\ & - 3.30 (\text{Eudragit RS})^2 - 67.20 (\text{X15M})^2 + 30.80 (\text{X100M})^2 - 13.80 (\text{homogenisng speed})^2 \end{aligned}$$

**Equation 6.9**

---

The equation for particle size distribution ( $Y_2$ ) is shown in Equation 6.10.

$$Y_2 = 425.69 - 227.08X_1 + 43.89X_2 + 173.89 X_3 - 248.75 X_4 + 0.00X_1X_2 - 100.00X_1X_3 + 147.50 X_1X_4 - 80.00 X_2X_3 - 80.00 X_2X_4 + 0.00.00 X_3X_4 + 23.61X_1^2 + 267.78X_2^2 + 47.78X_3^2 - 21.39 X_4^2$$

$$\begin{aligned} \text{Particle size distribution} = & 425.69 - 227.08 \text{ Eudragit RS} + 43.89 \text{ X15M} + 173.89 \text{ X100M} - 248.75 \text{ homogenizing speed} + 0.00 \text{ Eudragit RS} * \text{X15M} - 100.00 \\ & \text{Eudragit RS} * \text{X100M} + 147.50 \text{ Eudragit RS} * \text{homogenising speed} - 180.00 \text{ X15M} * \text{X100M} - 80.00 \text{ X15M} * \text{homogenisng speed} + 0.00.00 \text{ X100M} * \\ & \text{homogenisng speed} + 23.61(\text{Eudragit RS})^2 + 267.78(\text{X15M})^2 + 47.78(\text{X100M})^2 - 21.39 (\text{homogenisng speed})^2 \end{aligned}$$

**Equation 6.10**

---

---

The equation for encapsulation efficiency ( $Y_3$ ) factor is shown in Equation 6.11:

$$Y_3 = 89.22 + 22.60X_1 - 128.66X_2 - 23.51 X_3 - 16.57X_4 + 22.98X_1X_2 + 33.02X_1X_3 - 13.68 X_1X_4 - 26.68X_2X_3 + 47.18X_2X_4 - 26.04X_3X_4 - 7.74X_1^2 + 24.18X_2^2 + 17.8X_3^2 + 11.91 X_4^2$$

$$\text{Encapsulation efficiency} = 89.22 + 22.60 \text{ Eudragit RS} - 128.66 \text{ X15M} - 23.51 \text{ X100M} - 16.57 \text{ homogenizing speed} + 22.98 \text{ Eudragit RS} * \text{X15M} + 33.02 \text{ Eudragit RS} * \text{X100M} - 13.68 \text{ Eudragit RS} * \text{homogenising speed} - 26.68 \text{ X15M} * \text{X100M} + 47.18 \text{ X15M} * \text{homogenising speed} - 26.04 \text{ X100M} * \text{homogenising speed} - 7.74 (\text{Eudragit RS})^2 + 24.18 (\text{X15M})^2 + 17.8 (\text{X100M})^2 + 11.91 (\text{homogenising speed})^2$$

**Equation 6.11**

---

The equation for drug release ( $Y_4$ ) factor is shown in Equation 6.12:

$$Y_4 = -42.49 - 57.04X_1 + 141.90 X_2 + 420.90 X_3 + 43.74 X_4 - 30.00X_1X_2 - 96.00 X_1X_3 - 6.62 X_1X_4 - 140.00 X_2X_3 + 20.00 X_2X_4 - 74.00 X_3X_4 + 34.15 X_1^2 - 47.90 X_2^2 - 35.90 X_3^2 - 4.85 X_4^2$$

$$\text{Drug release} = -42.49 - 57.04 \text{ Eudragit RS} + 141.90 \text{ X15M} + 420.90 \text{ X100M} + 43.74 \text{ homogenizing speed} - 6.62 \text{ Eudragit RS} * \text{X15M} - 96.00 \text{ Eudragit RS} * \text{X100M} - 6.62 \text{ Eudragit RS} * \text{homogenising speed} - 140.00 \text{ X15M} * \text{X100M} + 20.00 \text{ X15M} * \text{homogenising speed} - 74.00 \text{ X100M} * \text{homogenising speed} + 34.15 (\text{Eudragit RS})^2 - 47.90 (\text{X15M})^2 - 35.90 (\text{X100M})^2 - 4.85 (\text{homogenising speed})^2$$

**Equation 6.12**

---

---

The equation for microcapsule flow ( $Y_5$ ) factor is shown in Equation 6.13:

$$Y_5 = 2.67 - 0.56X_1 + 0.09X_2 - 2.86X_3 - 0.27X_4 - 0.14X_1X_2 + 0.58X_1X_3 + 0.18X_1X_4 + 0.88X_2X_3 - 0.58X_2X_4 + 0.36X_3X_4 + 0.017X_1^2 + 0.54X_2^2 + 0.84X_3^2 - 0.028X_4^2$$

$$\begin{aligned} \text{Powder flow} = & 2.67 - 0.56 \text{ Eudragit RS} + 0.09 \text{ X15M} - 2.86 \text{ X100M} - 0.27 \text{ homogenizing speed} - 0.14 \text{ Eudragit RS} * \text{X15M} + 0.58 \text{ Eudragit RS} * \text{X100M} \\ & + 0.18 \text{ Eudragit RS} * \text{homogenising speed} + 0.88 \text{ X15M} * \text{X100M} - 0.58 \text{ X15M} * \text{homogenisng speed} + 0.36 \text{ X100M} * \text{homogenisng speed} \\ & + 0.017(\text{Eudragit RS})^2 + 0.54 (\text{X15M})^2 + 0.84(\text{X100M})^2 - 0.028 (\text{homogenisng speed})^2 \end{aligned}$$

**Equation 6.13**

---

By way of example, as can be seen in Equation 6.12, (percent drug release) the polynomial expression contains the coefficient for the intercept, first order main effects, interaction terms and higher order effects. The sign and magnitude of the main effects signify the relative influence of each factor on the response or drug release in this case. The values obtained for the main effects of each factor shown in Equation 6.12 reveal that  $X_1$ ,  $X_4$ ,  $X_1X_2$ ,  $X_1X_3$ ,  $X_1X_4$ ,  $X_2X_3$ ,  $X_3X_4$ ,  $X_2^2$ ,  $X_3^2$ , and  $X_4^2$  have a negative effect on drug release.  $X_2$ ,  $X_3$ ,  $X_2X_4$  and  $X_1^2$  individually have rather more pronounced effect on  $Y_4$ .  $X_2X_4$  showed the least synergistic effect.

ANOVA method was used to estimate the significance of the model using Design Expert Software (Table 6.9). At a 5% level of significance the model is considered significant if the significance probability or  $p$ -value is less than 0.05 (459). It is evident in Table 6.9 that for all responses, the cross-product contributions were negative except for  $X_2X_4$ . The model F-value of 0.033 implies that the model is significant and also shows that there is a 0.30% ( $p > 0.003$ ) chance that the model F-value could have been due to noise. The  $R^2$  value is close to 1 and denotes a high degree of correlation between the observed and predicted values. The coefficient of variation (CV) indicates the degree of precision with which the experiments were performed and the reliability of an experiment is indicated by a low value for the CV. A CV of 6.19 was calculated for the experiments performed in these studies thereby indicating the data are highly reliable. The  $p$ -value denotes the significance of the coefficient and is also important in understanding the pattern of mutual interactions between the variables under investigation. The  $p$ -value suggests that of the four variables studied,  $X_1$  and  $X_2$  show the maximum synergistic effect on  $Y_4$ . These effects were determined by plotting the response surface curves. The shapes of the curves reveal moderate interactions between the variables under investigation.

Design-Expert® Software

Drug release  
● Design Points  
97  
40

X1 = A: Eudragit RS  
X2 = B: Methocel K15M

Actual Factors  
C: Methocel K100M = 0.50  
D: Homogenizing speed = 1.50

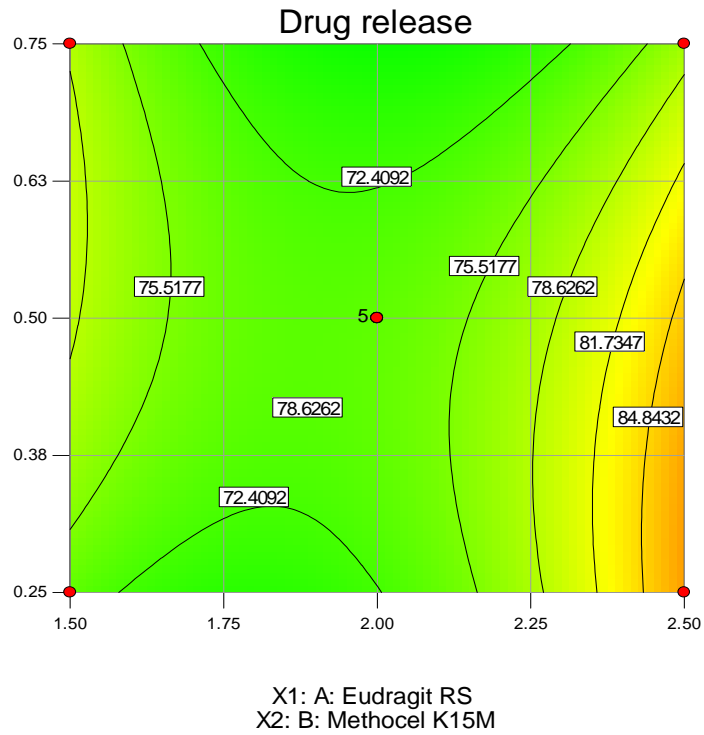


**Figure 6.4.** Contour plots showing the effect of Eudragit® RS and Methocel® K15M on drug release where A = x- axis and B = y-axis

Design-Expert® Software

Drug release  
● Design Points  
97  
40

X1 = A: Eudragit RS  
X2 = C: Methocel K100M

Actual Factors  
B: Methocel K15M = 0.50  
D: Homogenizing speed = 1.50

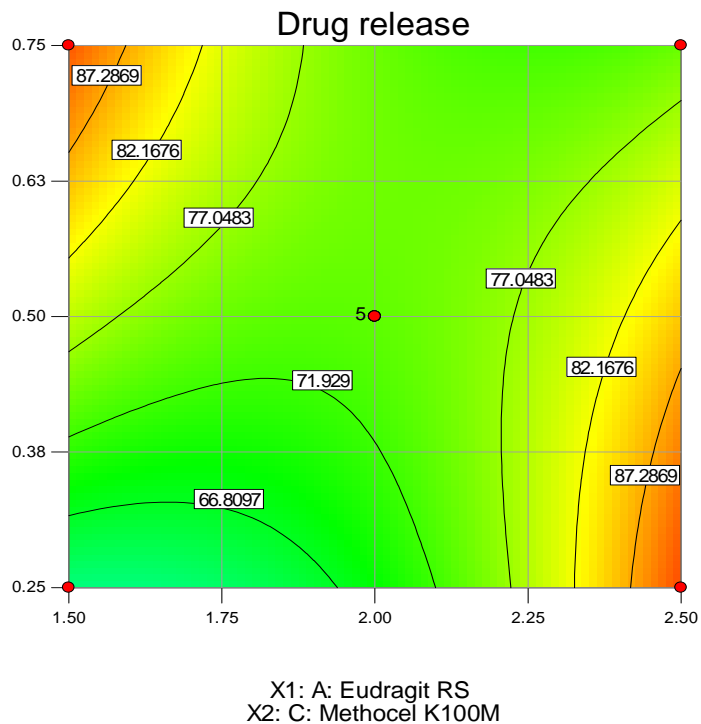


**Figure 6.5.** Contour plots showing the effects of Eudragit® RS and Methocel® K100M on drug release where A = x- axis and C = y-axis

Design-Expert® Software

Drug release  
● Design Points  
97  
40

X1 = A: Eudragit RS  
X2 = D: Homogenizing speed

Actual Factors  
B: Methocel K15M = 0.50  
C: Methocel K100M = 0.50

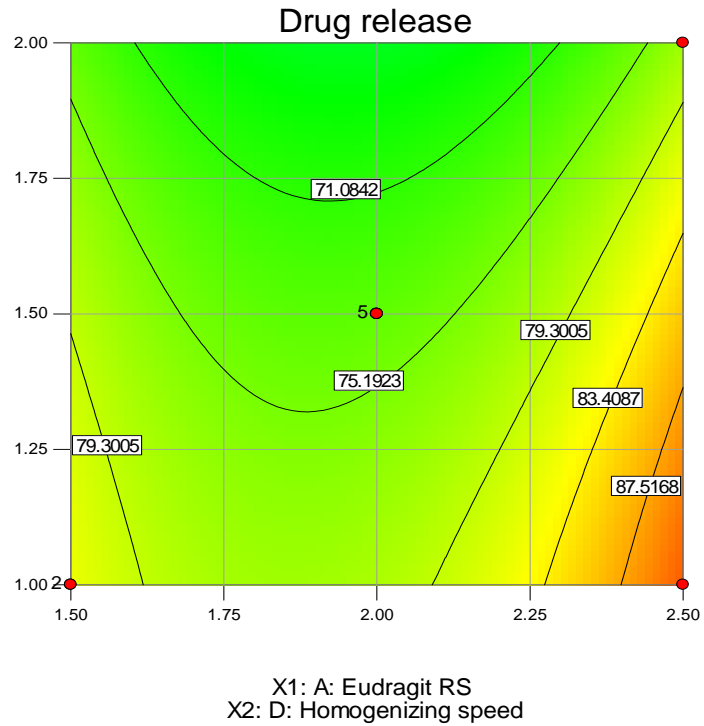


**Figure 6.6.** Contour plots showing the effects of Eudragit® RS and homogenizing speed on drug release where A = x- axis and D = y-axis

Design-Expert® Software

Drug release  
● Design Points  
97  
40

X1 = B: Methocel K15M  
X2 = C: Methocel K100M

Actual Factors  
A: Eudragit RS = 2.00  
D: Homogenizing speed = 1.50

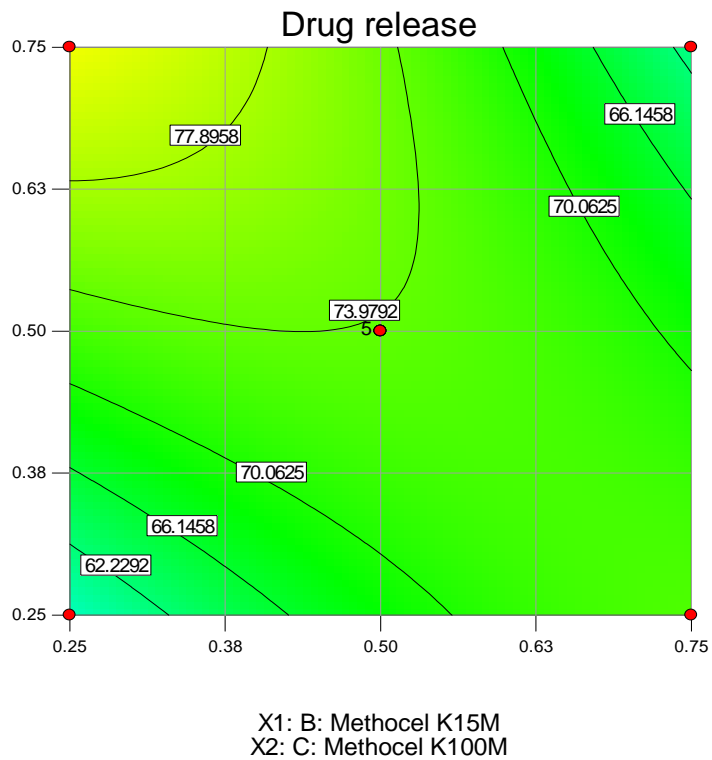


**Figure 6.7.** Contour plots showing the effects of Methocel® K15M and Methocel® K100M on drug release where B = x- axis and C = y-axis



Design-Expert® Software

Drug release  
● Design Points  
97  
40

X1 = B: Methocel K15M  
X2 = D: Homogenizing speed

Actual Factors  
A: Eudragit RS = 2.00  
C: Methocel K100M = 0.50

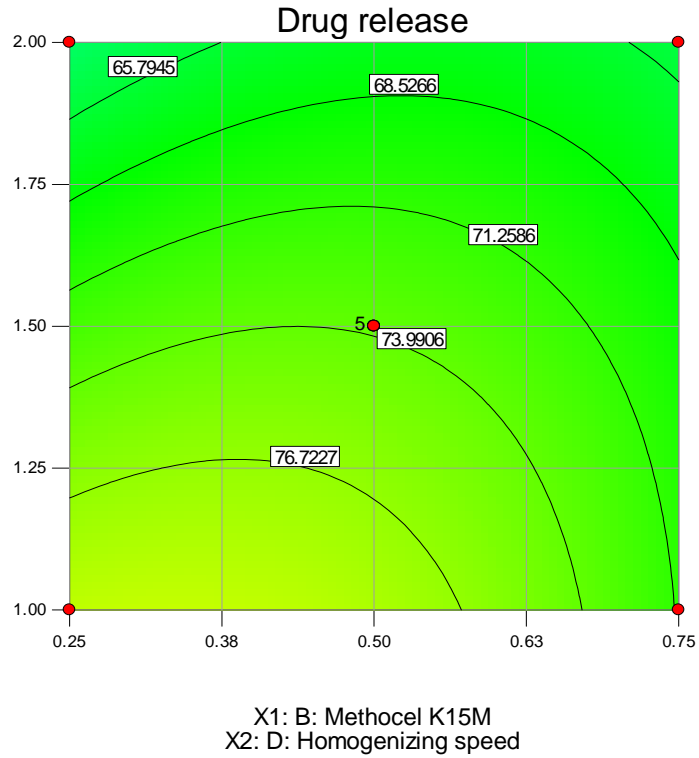


**Figure 6.8.** Contour plots showing the effects of Methocel® K15M and homogenizing speed on drug release where B = x- axis and D = y-axis

Design-Expert® Software

Drug release  
● Design Points  
97  
40

X1 = C: Methocel K100M  
X2 = D: Homogenizing speed

Actual Factors  
A: Eudragit RS = 2.00  
B: Methocel K15M = 0.50

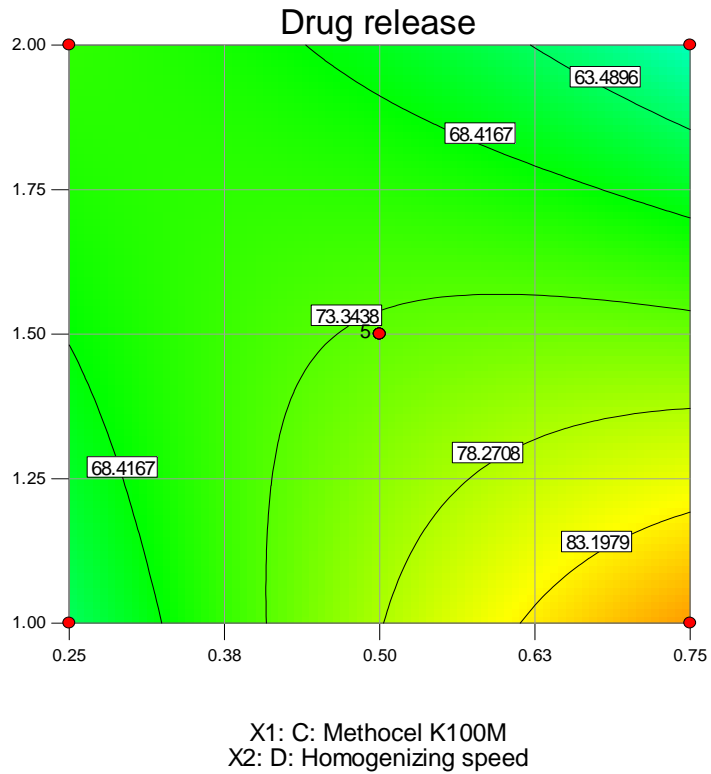


**Figure 6.9.** Contour plots showing the effects of Methocel® K100M and homogenizing speed on drug release where C = x- axis and D = y-axis

Design-Expert® Software

Drug release



X1 = A: Eudragit RS  
X2 = B: Methocel K15M

Actual Factors  
C: Methocel K100M = 0.51  
D: Homogenizing speed = 1.51

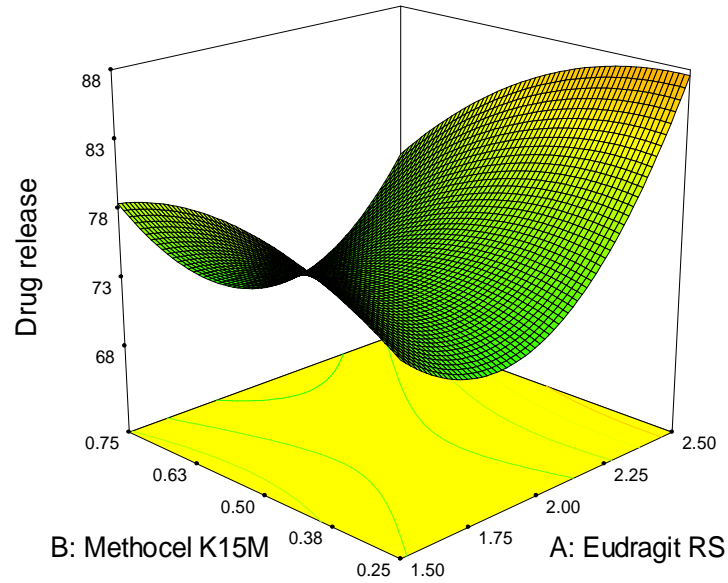


Figure 6.10. Response surface graph showing the effect of Eudragit® RS and Methocel® K15M on drug release.

Design-Expert® Software

Drug release



X1 = A: Eudragit RS  
X2 = C: Methocel K100M

Actual Factors  
B: Methocel K15M = 0.51  
D: Homogenizing speed = 1.51

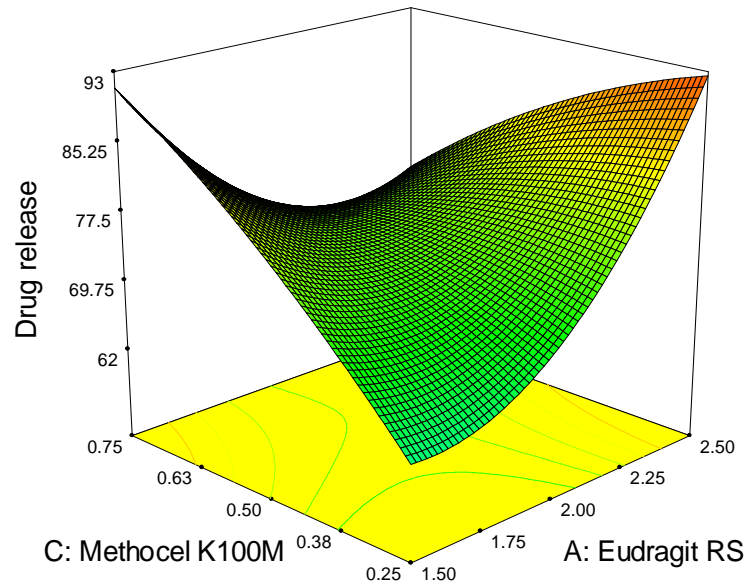
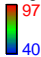


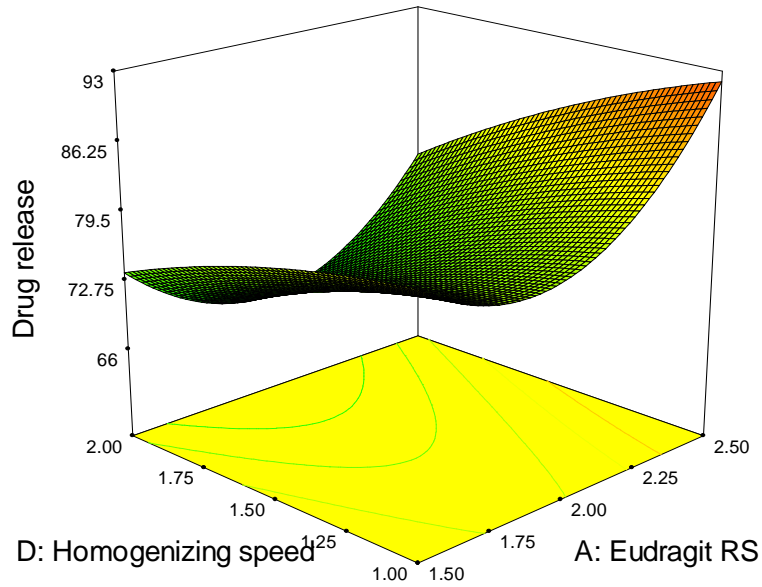
Figure 6.11. Response surface graph showing the effect of Eudragit® RS and Methocel® K100M on drug release.

Design-Expert® Software

Drug release  
  
 97  
 40

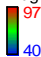
X1 = A: Eudragit RS  
 X2 = D: Homogenizing speed

Actual Factors  
 B: Methocel K15M = 0.49  
 C: Methocel K100M = 0.50



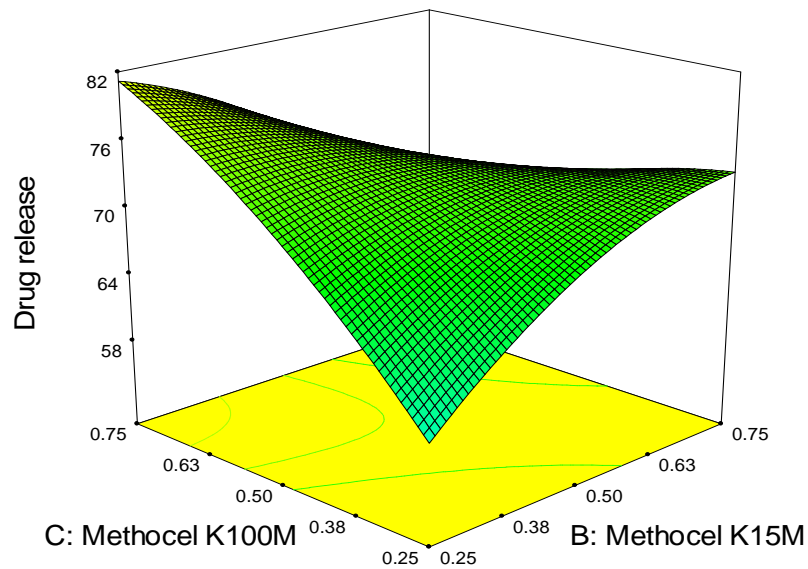
**Figure 6.12.** Response surface graph showing the effect of Eudragit® RS and homogenizing speed on drug release.

Design-Expert® Software

Drug release  
  
 97  
 40

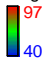
X1 = B: Methocel K15M  
 X2 = C: Methocel K100M

Actual Factors  
 A: Eudragit RS = 2.01  
 D: Homogenizing speed = 1.51



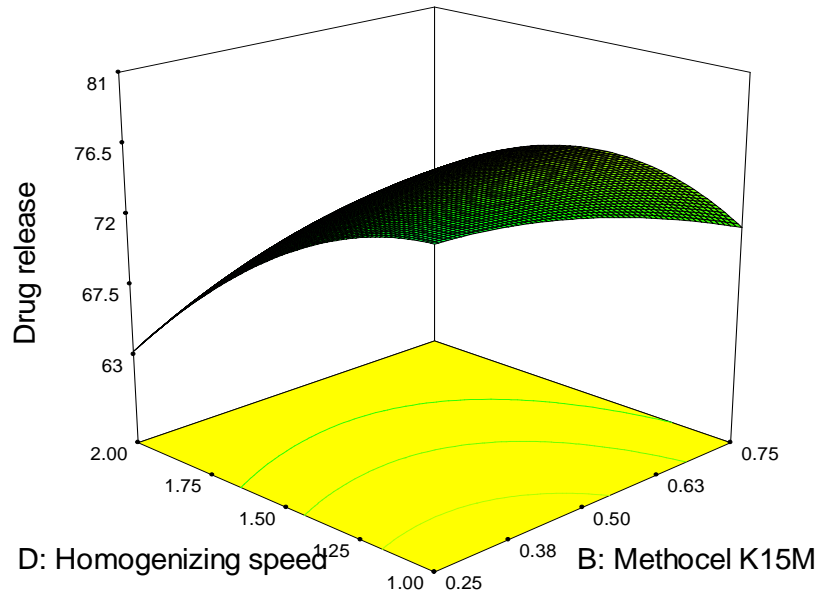
**Figure 6.13.** Response surface graph showing the effect of Methocel® K15M and Methocel® K100M on drug release.

Design-Expert® Software

Drug release  
  
 97  
 40

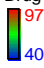
X1 = B: Methocel K15M  
 X2 = D: Homogenizing speed

Actual Factors  
 A: Eudragit RS = 2.00  
 C: Methocel K100M = 0.51



**Figure 6.14.** Response surface graph showing the effect of Methocel® K15M and homogenizing speed on drug release.

Design-Expert® Software

Drug release  
  
 97  
 40

X1 = C: Methocel K100M  
 X2 = D: Homogenizing speed

Actual Factors  
 A: Eudragit RS = 2.00  
 B: Methocel K15M = 0.49

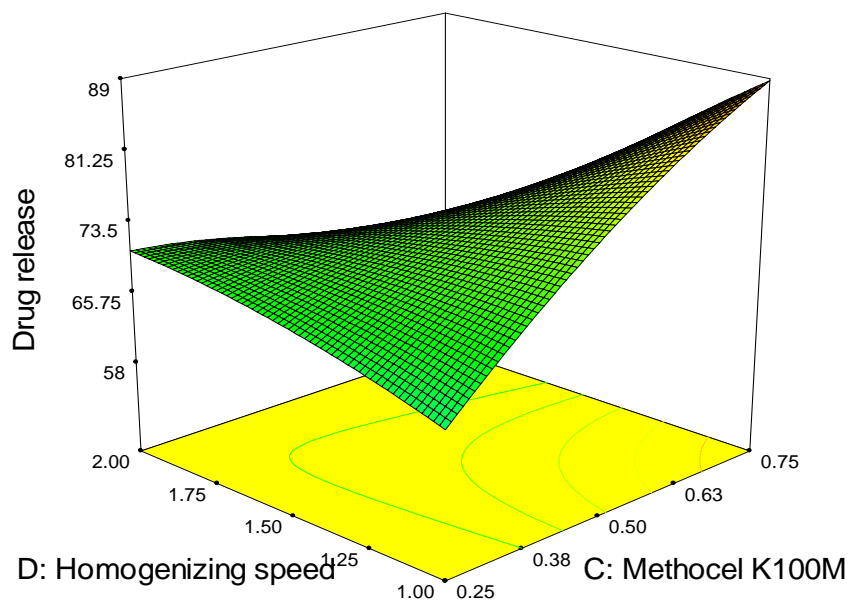


**Figure 6.15.** Response surface graph representing the interaction between Methocel® K100M and Homogenizing speed

In most cases the coefficients of the different factors reveal synergistic effects for all factors in responses  $Y_1$ ,  $Y_2$ ,  $Y_3$  and  $Y_4$ . It is obvious that Methocel<sup>®</sup> K15M ( $X_2$ ) and K100M ( $X_3$ ) had the greatest impact on drug release. This is due to the HPMC matrix that retains its viscosity and gel layer intact thereby increasing the diffusional pathlength in the particles.

As can be seen (Figures 6.4 to 6.9) drug release rates vary in a non-linear fashion between the associated variables. The pattern generated is 'horse-shoe' in shape and the resultant responses are relatively complex and difficult to interpret since there are different phases and they all show dissimilar patterns. The plot showing in Figure 6.8 reveals that drug release varies in a linear fashion as the amount of Methocel<sup>®</sup> K15M is increased. As the homogenizing speed was decreased, there is an optimum concentration where an increase in concentration results in a radial pattern. The radial pattern indicates that the homogenizing speed has a negative effect on drug release. In contrast the results observed for Methocel<sup>®</sup> K100M (Figure 6.9) indicate that there is no clear relationship between homogenizing speed and polymer type on drug release. These results are somewhat unexpected as the only difference is in the viscosity of the polymers. This may have influenced the manufacture of the microcapsules.

### **6.3.1. Particle size distribution**

On the basis of sieve-analysis data presented in Table 6.10 it can be concluded that there was a difference in the average particle size of microcapsules for all manufactured batches. On the basis of published data the formation of smaller microspheres at higher stirring rates (429, 434, 437, 438) was expected and it was presumed that, by lowering the stirring rate the average particle size would increase in comparison to the average particle size of microcapsules manufactured at high stirring speeds. The use of high stirring speeds maintained over a long period would produce uniform microcapsules. As the stirring rate decreased, the droplet size of the dispersed phase increased resulting in the production of larger microcapsules. If the stirring speed was changed at the time when solidification of the droplets has commenced, the influence on the average particle size was not likely to be great. If the microcapsules were completely formed, changes of stirring speed would have had no influence on the size of microcapsules. A change in agitation speed prior to evaporation of the acetone would probably lead to the formation of microspheres of the same size as those prepared using constant stirring speeds. However since solvent diffusion into the outer emulsion phase and its evaporation starts immediately this effect was not observed.

The microcapsules had diameters ranging between 30 and 200  $\mu\text{m}$ , and the mean diameter was directly influenced by the manufacturing parameters used (homogenizing speed and polymer concentration). Furthermore larger particles were obtained at higher polymer/drug ratios. Increasing the polymer load leads to the production of a more viscous solution and when the solution is poured into the aqueous phase, larger droplets and thus larger microcapsules are formed (460-463).

### **6.3.2. Microencapsulation**

Microcapsules were manufactured using Eudragit<sup>®</sup> and Methocel<sup>®</sup> polymers. During the evaporation process, the dispersed phase became more and more viscous and even at low agitation speeds the dispersed droplets could not fuse together.

When the solution of solvent was poured into the continuous phase whilst stirring, finely dispersed droplets formed immediately and a semi-transparent emulsion was observed. With the diffusion of acetone out of the droplets into the continuous phase, the drug and the polymer coprecipitate within the droplets and a schematic representation of droplet formation is shown in Figure 6.16. The formation of microcapsules can be described in the following manner. Initially quasiemulsion droplets are formed, after which the organic solvent diffuses out of the droplets followed by solidification of the droplets. During formation of the droplets microcapsules agglomerate to form an irregular mass and adhere to the propeller or the vessel wall. To avoid agglomeration, span 80 was added to the liquid paraffin during the manufacturing process. The use of the emulgent results in a decrease in viscosity of the continuous phase that prevents conglutination of the emulsified droplets. In addition the presence of span accelerates the solidification of droplets.

### **6.3.3. Encapsulation efficiency**

Relatively high encapsulation efficiencies of between 60 to 80% were achieved and the data are summarized in Table 6.10. The EE was expected to be relatively high as CPT is insoluble in liquid paraffin. In all cases the EE efficiency was lower than 90% perhaps due to the fact that the presence of span 80 increased the miscibility of acetone with the light liquid paraffin and which may have increased the extraction of CPT into this phase. The volume of the processing medium was kept constant as an increase in volume of the processing medium would have caused the emulsion droplets to move freely in the medium, thereby reducing collision-induced aggregation and yielding small and uniform microspheres that are

associated with higher extraction coefficients and lower encapsulation efficiencies. Although stirring rate may affect drug content significantly (464), no significant differences were observed for the batches manufactured in these studies. Consequently it was not possible to determine microsphere formation time with respect to stirring speed on the basis of encapsulation efficiency. Theoretically, the use of high homogenizing speeds would result in the production of smaller emulsion droplets, facilitating drug loss from the microcapsules before they harden and resulting in a low EE. The assumption that drug diffusion into the processing medium may occur was supported by SEM analysis which revealed the presence of drug particles on the surface(s) of the microcapsules.

The microencapsulation efficiency was found to dependent on the initial polymer loads and the high EE values summarized in Table 6.10 justify the use of an o/o emulsification technique for the manufacture of microcapsules of the water-soluble CPT. The increase in EE with increase in polymer concentrations is probably due to better encapsulation of the drug at these levels and a decrease in the amount of CPT on the surface of the capsules. The increase in CPT encapsulation observed when span 80 was used can be ascribed to the emulsifying effect of the surfactant, which ensures that CPT is finely dispersed and embedded in the polymer matrix prior to encapsulation.

Furthermore, this can also be explained by the hydrophilicity of CPT. CPT is unlikely to have an affinity for the organic solvent phase used and the decrease could most likely have been the result of CPT having partitioned into the continuous phase. The encapsulation of a drug is therefore highly dependent on the solubility of the drug in the solvent and continuous phase.

#### **6.3.4. Flowability**

The physical properties of the microcapsules that were produced are listed in Tables 6.10 (Hausner ratio) and Table 6.11. The angles of repose for almost all microcapsules were in the range of 18 to 40°, thus indicating good flowability for some batches and poor flow for others. This would result in microcapsules from other batches being poorly packed into hard capsules. The angle of repose is affected by the particle size distribution and usually increases with a decrease in particle size. Lower Hausner ratio values ( $\leq 1.25$ ) in most of the batches indicate good flow except for CPT-005, 014, 016 and CPT-022 which had Hausner ratio values of 1.93, 1.61, 1.34 and 1.42, respectively. These values indicate that the ‘particles’ that were formed from these batches were adhering to each other and that would result in poor

flow. Similar results were observed when using Carr's Index, with lower values associated with low cohesiveness and greater fluidity properties.

The denser the microcapsules and the higher their bulk density, the easier they will be to tablet. The percent compressibility calculated from density data generated in these studies showed a compressibility of less than 30%. The low compressibility further supports the fair to excellent flow properties of these microcapsules. This would be important for filling into two-piece hard capsules, or for use in directly compressible blends for tableting.

A reduction in the bulk densities of some microcapsules indicates a greater porosity in the microcapsules. The microcapsules were easily packed by tapping, and this phenomenon can be described using Kawakita and Ludde's equation (449). The apparent packing velocity produced by tapping, represented by parameter  $b$  was acceptable, since the microcapsules packed closely without tapping because of this excellent flowability and packability. Good flowability and packability may be attributed to their sphericity and particle size. These results further suggest that the microcapsules may be suitable for capsule filling and that such capsules would exhibit a high degree of mass uniformity.

In order to achieve uniformity for capsule fill mass, the fill materials must flow readily and pack smoothly. The flowability of the microcapsules was also assessed using  $CI$ . Microcapsules of similar size but non-uniform in shape can have markedly different flow properties owing to differences in the interparticle contact areas. It is also important to note that the flow properties of microcapsules will decrease as the shapes of microcapsules become more irregular.

As shown in Table 6.11, the small values for parameters  $a$  and  $b$  generated from fitting data to Kawakita and Ludde's equation indicate the high packability of the microcapsules. The values of parameter  $K$  in Kuno's equation indicate that the microcapsules from some batches will flow and pack smoothly during filling of two-piece capsules, thereby ensuring mass and dose uniformity.



**Table 6.10.** Response data generated for each experiment

<b>RUN</b>	<b>X<sub>1</sub></b>	<b>X<sub>2</sub></b>	<b>X<sub>3</sub></b>	<b>X<sub>4</sub></b>	<b>Y<sub>1</sub></b>	<b>Y<sub>2</sub></b>	<b>Y<sub>3</sub></b>	<b>Y<sub>4</sub></b>	<b>Y<sub>5</sub></b>
	<b>g</b>	<b>g</b>	<b>g</b>	<b>rpm (1000)</b>	<b>%</b>	<b>nm</b>	<b>%</b>	<b>%</b>	
1	2.0	0.5	0.50	1.5	87	100	57.66	64	1.23
2	2.0	0.75	0.25	1.5	83	200	58.64	40	1.17
3	1.5	0.50	0.50	1.0	93	200	58.25	50	1.27
4	2.5	0.50	0.50	2.0	87	100	56.87	75	1.17
5	2.0	0.50	0.25	2.0	88	50	69.92	89	1.93
6	2.0	0.50	0.50	1.5	92	50	69.07	94	0.87
7	2.0	0.75	0.75	1.5	78	100	57.76	50	1.20
8	1.5	0.50	0.50	1.0	76	50	62.55	91	1.28
9	2.0	0.25	0.75	1.5	87	20	71.52	90	1.18
10	2.0	0.50	0.50	1.5	90	50	69.98	88	1.16
11	1.5	0.75	0.50	1.5	76	100	59.79	95	1.18
12	2.0	0.50	0.50	1.5	79	100	60.95	63	1.25
13	2.0	0.25	0.50	2.0	69	50	59.57	58	1.16
14	2.5	0.25	0.50	1.5	87	100	66.83	88	1.61
15	2.0	0.50	0.50	1.5	89	50	62.2	60	1.28
16	2.5	0.50	0.75	1.5	84	50	69.92	83	1.34
17	1.5	0.50	0.75	1.5	92	50	60.85	97	1.19
18	2.0	0.25	0.5	1.0	91	80	65.53	88	1.16
19	2.5	0.75	0.50	1.5	90	150	68.45	93	1.13
20	2.0	0.50	0.75	1.0	89	100	77.98	87	1.25
21	2.0	0.50	0.75	2.0	83	50	69.47	49	1.25
22	2.0	0.75	0.50	1.0	84	100	66.65	84	1.42
23	2.5	0.50	0.25	1.5	95	100	58.29	95	1.16
24	2.0	0.50	0.25	1.0	86	100	65.41	90	1.11
25	1.5	0.25	0.50	1.5	79	50	69.66	75	1.09
26	2.5	0.50	0.50	1.0	74	100	60.45	67	1.23
27	2.0	0.25	0.25	1.5	78	75	65.73	45	1.17
28	1.5	0.50	0.25	1.5	95	50	65.73	61	1.10
29	2.0	0.75	0.50	2.0	87	30	84.28	64	1.13
30	2.0	0.75	0.50	2.0	67	30	84.28	65	1.13

**X<sub>1</sub>** = Eudragit RS  
**X<sub>2</sub>** = Methocel K100M  
**X<sub>3</sub>** = Methocel K15M  
**X<sub>4</sub>** = Homogenizing speed  
**Y<sub>1</sub>** = percent yield  
**Y<sub>2</sub>** = microcapsule size  
**Y<sub>3</sub>** = encapsulation efficiency  
**Y<sub>4</sub>** = percent released  
**Y<sub>5</sub>** = Hausner ratio

**Table 6.11.** Packability and flowability parameters for CPT microcapsules

<b>Formulation</b>	<b>a</b>	<b>b</b>	<b>K</b>	<b>Angle of repose (θ)</b>	<b>Carr's Index</b>
CPT-001	0.42 (r =0.998)	0.53	0.025 (r =0.998)	24	32
CPT-002	0.39 (r =0.989)	0.02	0.006 (r =0.987)	23	26
CPT-003	0.45 (r =0.991)	0.08	0.015 (r =0.997)	41	46
CPT-004	0.42 (r =0.999)	0.20	0.014 (r =0.963)	37	43
CPT-005	0.27 (r =0.994)	0.04	0.016 (r =0.990)	40	28
CPT-006	0.14 (r =0.998)	0.15	0.018 (r =0.971)	12	16
CPT-007	0.24 (r =0.999)	0.27	0.022 (r =0.897)	23	17
CPT-008	0.24 (r =0.996)	0.02	0.014 (r =0.996)	30	32
CPT-009	0.24 (r =0.997)	0.27	0.014 (r =0.991)	18	22
CPT-010	0.11 (r =0.993)	0.26	0.004 (r =0.939)	22	14
CPT-011	0.30 (r =0.997)	0.02	0.007 (r =0.999)	27	18
CPT-012	0.33 (r =0.998)	0.02	0.007 (r =0.967)	22	17
CPT-013	0.22 (r =0.997)	0.02	0.010 (r =0.949)	24	20
CPT-014	0.63 (r =0.999)	0.08	0.019 (r =0.958)	32	35
CPT-015	0.36 (r =0.951)	0.01	0.017 (r =0.998)	22	24
CPT-016	0.23 (r =0.999)	0.03	0.014 (r =0.999)	20	22
CPT-017	0.30 (r =0.997)	0.02	0.023 (r =0.898)	21	30
CPT-018	0.16 (r =0.995)	0.02	0.018 (r =0.912)	15	16
CPT-017	0.30 (r =0.997)	0.02	0.023 (r =0.898)	21	30
CPT-018	0.16 (r =0.995)	0.02	0.018 (r =0.912)	15	16
CPT-019	0.40 (r =0.911)	0.03	0.001 (r =0.968)	8	30
CPT-020	0.28 (r =0.977)	0.26	0.013 (r =0.957)	19	30
CPT-021	0.28 (r =0.996)	0.01	0.011 (r =0.932)	21	26
CPT-022	0.36 (r =0.981)	0.05	0.014 (r =0.978)	35	36
CPT-023	0.20 (r =0.998)	0.01	0.020 (r =0.996)	24	20
CPT-024	0.25 (r =0.999)	0.02	0.011 (r =0.960)	28	24
CPT-025	0.39 (r =0.997)	0.09	0.014 (r =0.867)	29	30
CPT-026	0.10 (r =0.867)	0.01	0.013 (r =0.999)	20	20
CPT-027	0.44 (r =0.999)	0.26	0.019 (r =0.998)	8	18
CPT-028	0.29 (r =0.998)	0.04	0.011 (r =0.976)	21	28
CPT-029	0.33 (r =0.987)	0.26	0.013 (r =0.987)	20	30
CPT-030	0.33 (r =0.999)	0.03	0.110 (r =0.993)	33	27

<sup>a,b</sup> Parameter from Equation 6.6

<sup>k</sup> Parameter from Equation 6.7

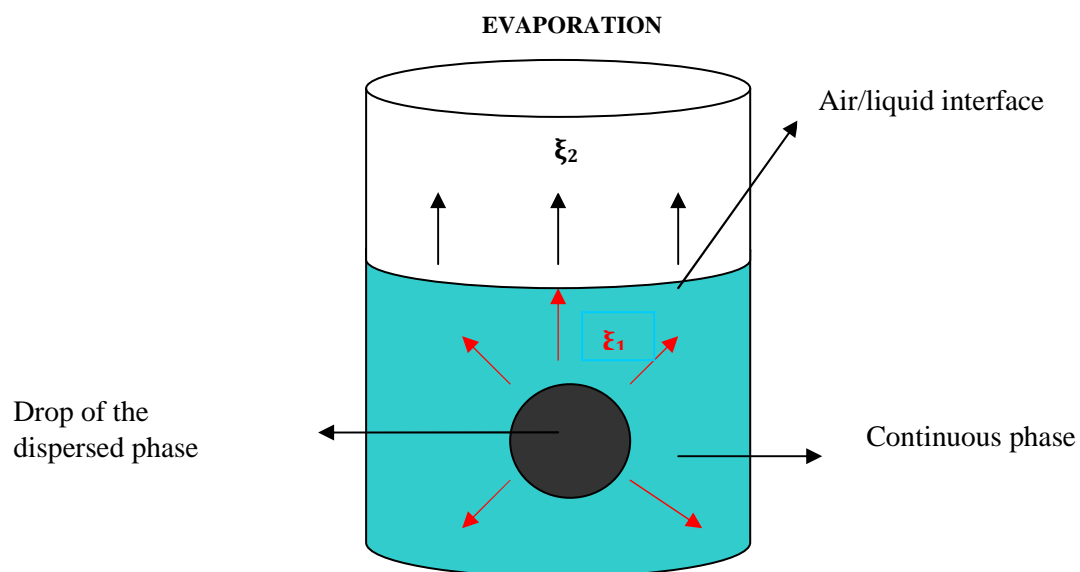


**Figure 6.16a.** Schematic representation of a solvent diffusion and evaporation

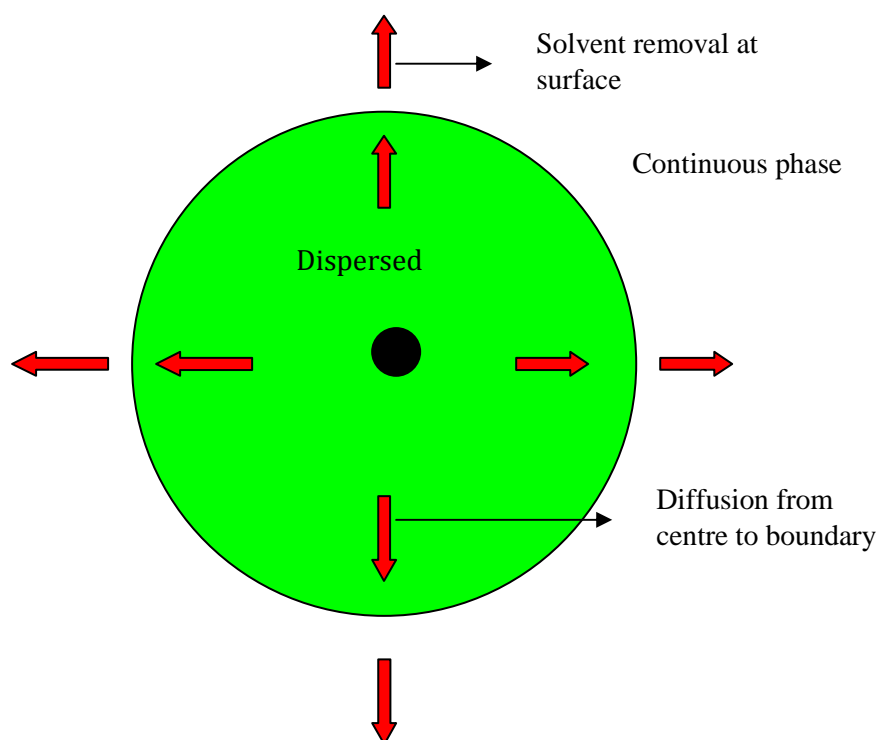


**Figure 6.16b.** Schematic representation of a mass transfer model for a single drop of polymer and solvent

The results for microcapsule yield, drug loading and encapsulation efficiency are shown in Table 6.10 for all batches. A solidification rate may have reduced the partitioning of CPT into the external phase of the emulsion resulting in high encapsulation efficiencies. Losses for the CPT may be due to drug partly going into the external phase prior to drop formation. It would be ideal for the drug not to diffuse out, but this is not always possible, some of the drug will diffuse out, resulting in reduced EE percent.

### **6.3.5. Scanning Electron Microscopy**

Typical SEM micrographs of selected microcapsules are shown in Figures 6.17-6.25. It is evident that microcapsules are not similar in shape. All micrographs taken for all batches of microcapsules manufactured in this research are presented in Appendix One with corresponding dissolution profiles.

The SEM photomicrographs indicate that most of the microcapsules were discrete, spherical and uniform in shape and that some have porous surfaces. At high magnification it is evident that the microcapsules have rough surfaces free of CPT, suggesting that the drug had been efficiently encapsulated by the polymeric matrix. This may be due in part to the fact that the drug is thoroughly wetted, finely dispersed and enveloped within the polymer matrix prior to encapsulation. In addition, the data from drug loading determinations confirm this was the case as CPT concentrations were high in these microcapsules. However, this was not so for batches CPT-006 and CPT-025 (Figures 6.18, 6.22) where CPT ‘particles’ could be seen on the surfaces of the microcapsules. The small microcapsules produced in batch CPT-022 are shown in Figure 6.25. It is clear that the small microcapsules adhere to one another and form ‘grape-like’ clusters. These microcapsules were also not visually appealing and were not free-flowing and discrete as those of other batches. These results are supported by the angle of repose and *CI* data for these batches and these are summarized in Table 6.11. Batches that failed the ‘geometry’ test could not be used any further.

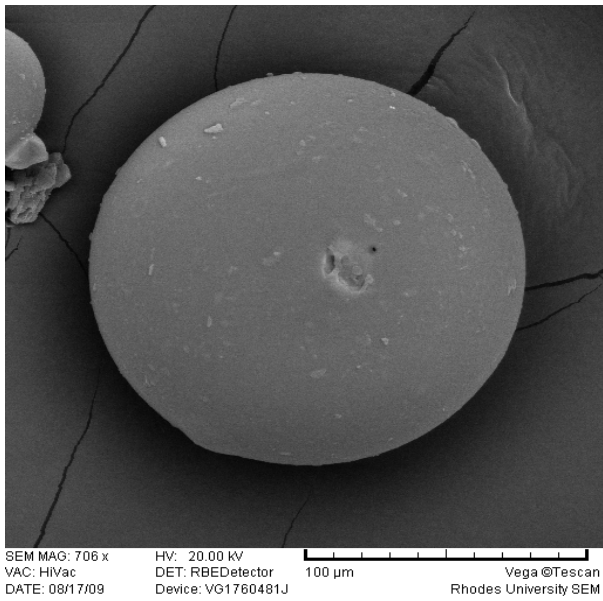


**Figure 6.17.** SEM of a microcapsule from batch CPT-002

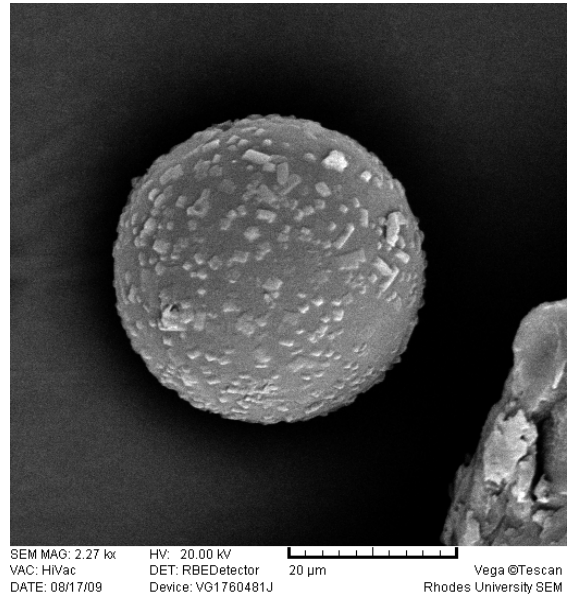


**Figure 6.18.** SEM of a microcapsule from batch CPT-006

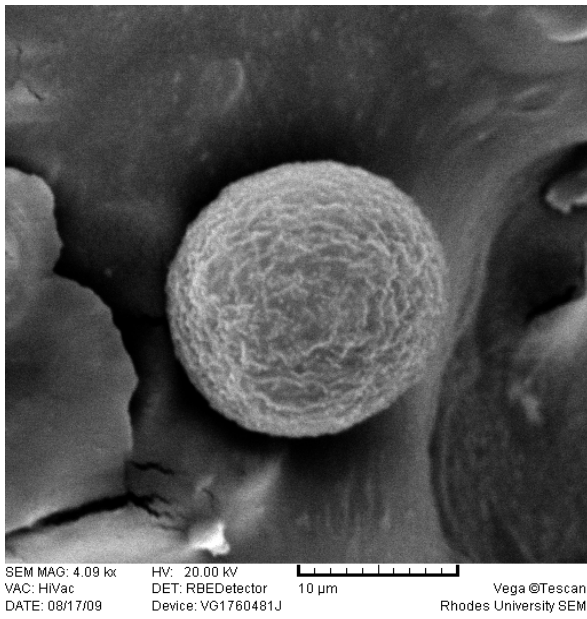


**Figure 6.19.** SEM of a microcapsule from batch CPT-009

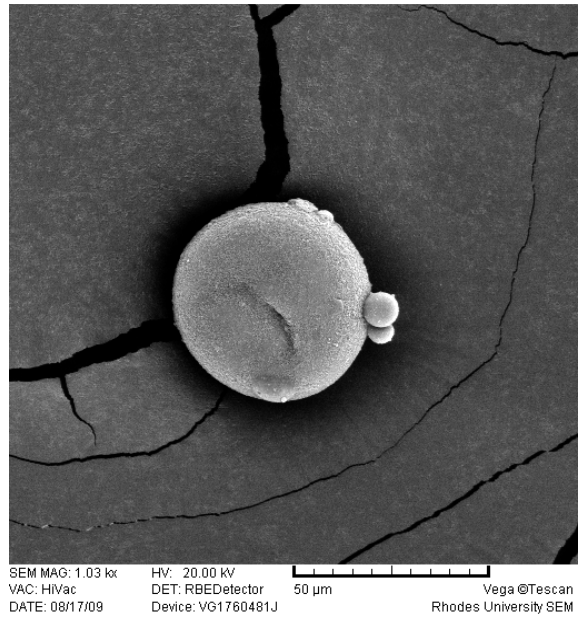


**Figure 6.20.** SEM of a microcapsule from batch CPT-015

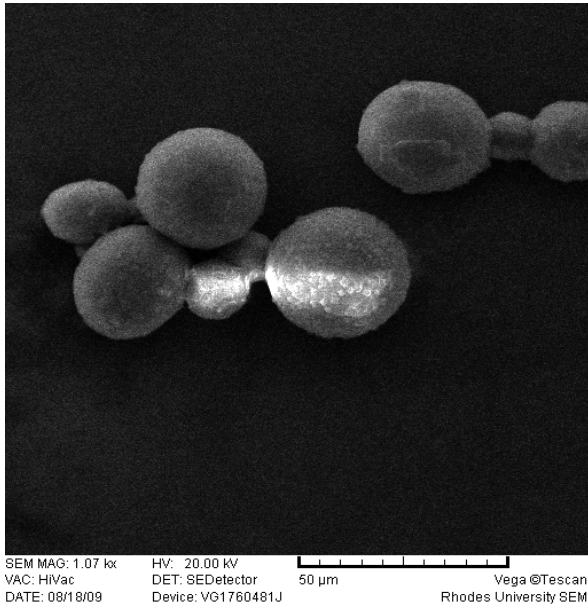


**Figure 6.21.** SEM of a microcapsule from batch CPT-020

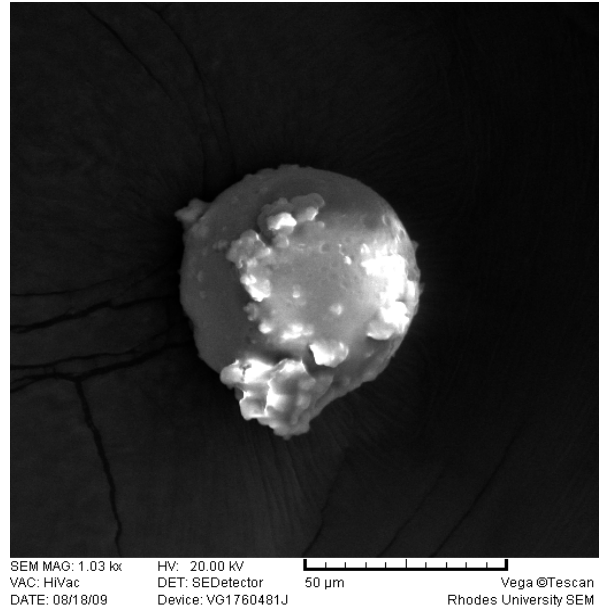


**Figure 6.22.** SEM of a microcapsule from batch CPT-025

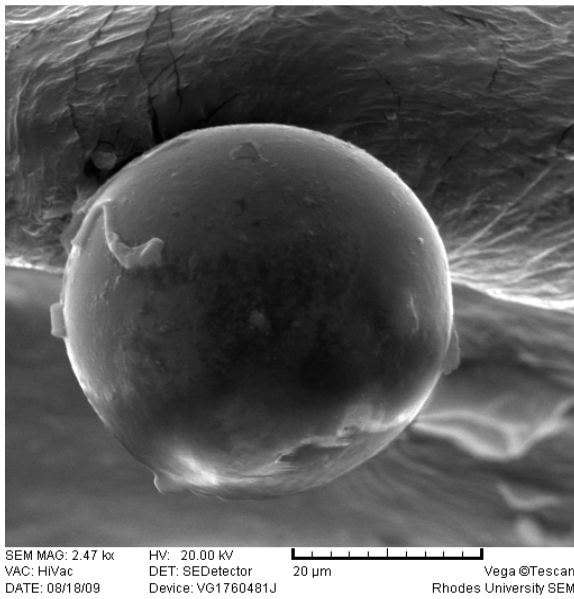


**Figure 6.23.** SEM of a microcapsule from batch CPT-030

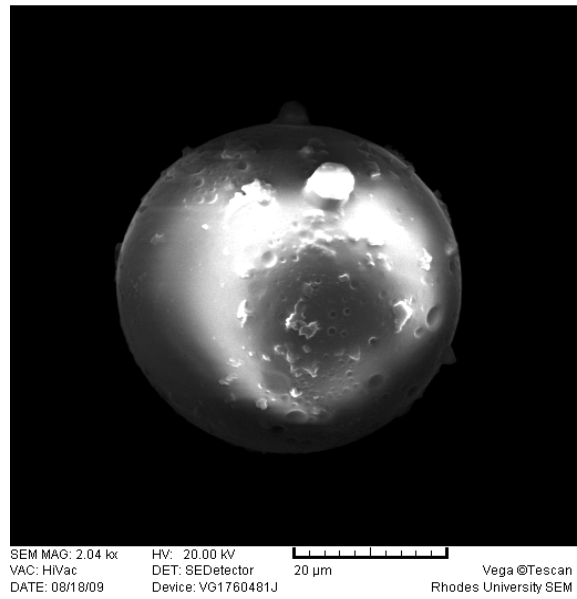


**Figure 6.24.** SEM of a microcapsule from batch CPT-029

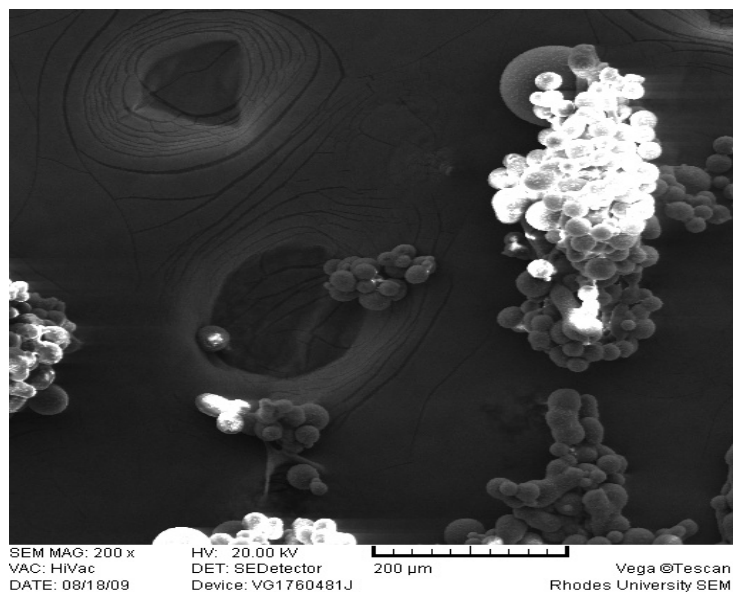


**Figure 6.25.** SEM of a microcapsule from batch CPT-022

### 6.3.6. *In vitro* drug release

Typical drug release profiles of selected microcapsules (those selected for SEM studies) are shown in Figure 6.26-6.34. All other drug release profiles are shown in Appendix One and the batch production records are shown in Appendix Two. The drug release profiles were constructed using Korsmeyer-Peppas equation as it provides a good tool for modeling of drug release. Only selected results using USP Apparatus 3 were shown in these studies as USP Apparatus 3 offers the advantages of mimicking *in vivo* conditions.

It was expected that drug release from microcapsules would be rapid when tested in USP Apparatus 3 (§ 6.2.2.7). Higher agitation rates when using USP Apparatus 3 effectively reduce the stagnant layer that forms around microcapsules during dissolution. However, rapid drug release was not observed for all batches: some microcapsules took longer to dissolve than those from other batches. The retardant effect on CPT release observed for some batches can be attributed to the formation of a diffusional barrier between the drug within the microcapsules and the dissolution medium. The results show that the release rate of CPT from the microcapsules could be modulated by adjusting the ratios of polymer/drug in the formulation and the speed of homogenizing during manufacture.

As can be seen in Figures 6.27-6.32, decreasing the concentration of polymer content resulted in a marked increase in drug release rates. In addition to the effect of polymer content this phenomenon may be attributed to the hardening sequence used to manufacture the

microcapsules. During the formation of the microcapsules, the low viscosity of the dispersed phase delayed polymer precipitation and solidification of the dispersed droplets. More water could therefore diffuse into the droplets prior to solidification, thus forming water pockets and pores in the walls of the microcapsules. The more porous the capsule wall, the easier it was for dissolution medium to penetrate the capsule and consequently the dissolution of CPT from the microcapsules was more rapid. This phenomenon has also been reported by Pygall *et al* (465). Moreover, the size of the microcapsules decreased significantly with decreasing polymer/drug ratio. This also contributed to the faster release of drug at lower polymer concentrations, which could have been a surface area effect.

In the majority of cases the microcapsules showed a burst release followed by more constant release. In this study, burst release was considered to be any profile that would show 30% release in the first hour of dissolution. This burst release phenomenon was primarily noticeable for CPT release shown in Figures 6.26, 6.27, 6.28, 6.29, 6.30, 6.31, 6.32, 6.33 and 6.34. The release profiles can be explained by the heterogeneous distribution of the drug within the matrix, as observed in some of the batches when using SEM. The profiles indicate that burst release was dominant in these microcapsules.

The drug released is shown in Table 6.10 and in most cases, the initial burst effect contributes approximately 40% of the release that was observed in the first 1h. The low polymer levels used in these formulations resulted in more drug remaining at the surface of the microcapsules producing the initial rapid release. A burst release was not evident in other formulations possibly due to the high polymer content resulting in better encapsulation of CPT within the microcapsules. The higher release rates are also associated with smaller size fractions of particles. When using SEM, drug crystals could be observed at or near the surfaces of the microcapsules. These surface crystals dissolve quickly and probably account for the observed rapid initial release. Almost all microcapsule batches produced in this study showed this behaviour to the same or similar extents for almost all microcapsule sizes produced.

During testing a point is reached when dissolution of solid drug particles results in the formation of continuous pores or channels within the matrix. Under these circumstances, drug release will follow a path of least resistance and drug will diffuse through the channels to the



bulk dissolution medium. Therefore, as the drug leaches out from the polymer, the matrix becomes more porous and faster drug release rates are observed.

The initial burst effect from HPMC matrices is a common occurrence in the release of water-soluble drugs (456, 465). Where drug release is retarded it may, in part, be due to the solid bridges that are formed between drug-drug and drug-excipient particles during processing. In addition, the internal pressure generated due to swelling and relaxation of the matrix might cause micro rupturing of the particles during dissolution.

Most of the drug profiles can be described as having two stages. Initially there occurs a burst effect, corresponding to the rapid dissolution and release of CPT from the surfaces of the microcapsules, prior to formation of a gel membrane at the surface. Secondly, the release rate decreases continuously until the end of the process. This phenomenon can be explained by an increase in diffusion pathlength for the drug, which is typical of diffusion-controlled release mechanisms. Following the formation of a gel, drug release is controlled by drug diffusion across the gel layer. The burst effect is also dependent on the amount of drug present at the surface of the microcapsules and the size and the shape of the pores generated within the microcapsule structure during dissolution testing.

A reason for the occurrence of a burst effect could be the unstable nature of the inner emulsion droplets during solvent evaporation, which leads to coalescence and may have forced drug particles to migrate to the surface of the microcapsules.

It should be noted that despite the cracks that can be clearly observed in some microcapsules, no burst could be detected later on. The hypothesis is that following crack formation and exposure of new surfaces to the dissolution medium tight and cohesive gel layers are rapidly formed and are able to maintain and control drug release. In this way the gel layer is able to 'heal' or plug the crack, thereby protecting the internal drug reservoir.

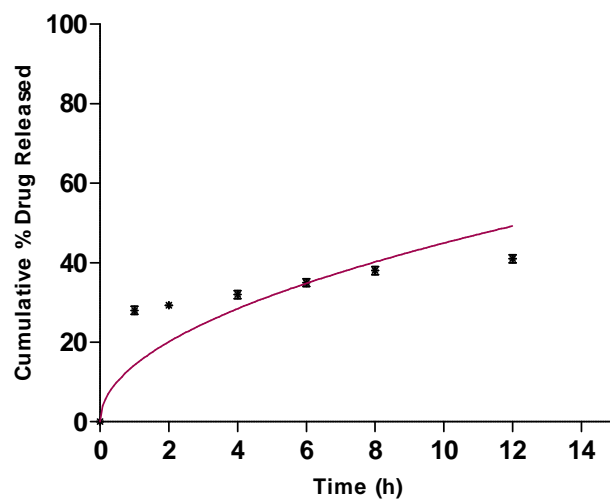


**Figure 6.26.** Cumulative percent CPT released for batch CPT-002 (mean  $\pm$  SD, n = 3)

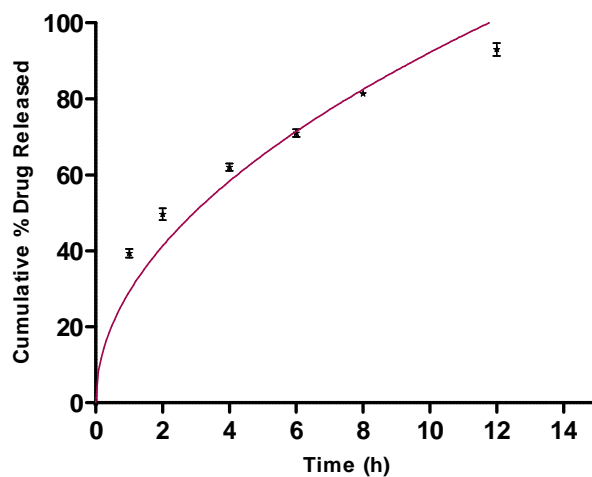


**Figure 6.27.** Cumulative percent CPT released for batch CPT-006 (mean  $\pm$  SD, n = 3)

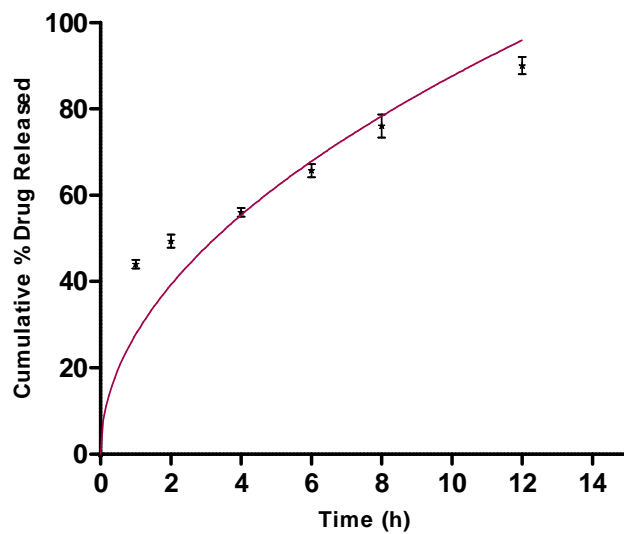


**Figure 6.28.** Cumulative percent CPT released for batch CPT-009 (mean  $\pm$  SD, n = 3)

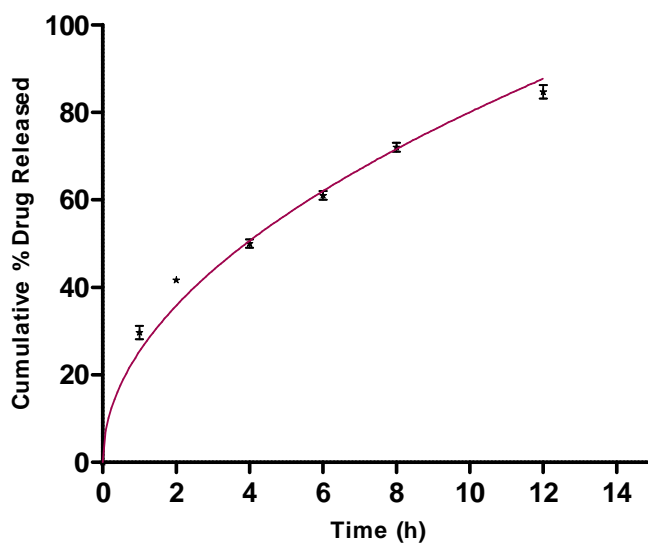


**Figure 6.29.** Cumulative % drug released for CPT-015 (mean  $\pm$  SD, n = 3)

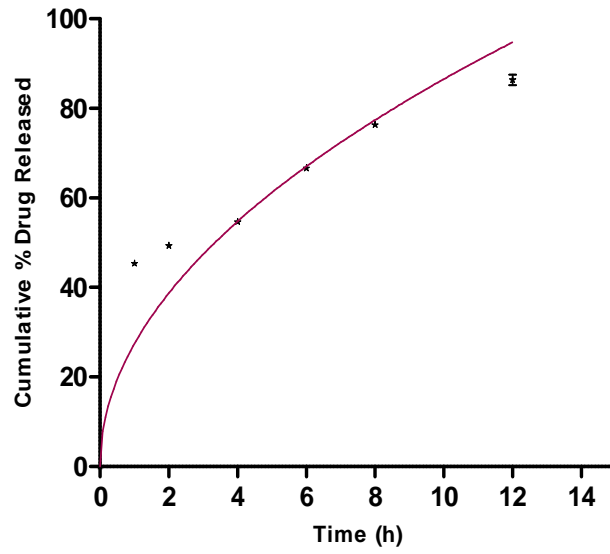


**Figure 6.30.** Cumulative % drug released for CPT-020 (mean  $\pm$  SD, n = 3)

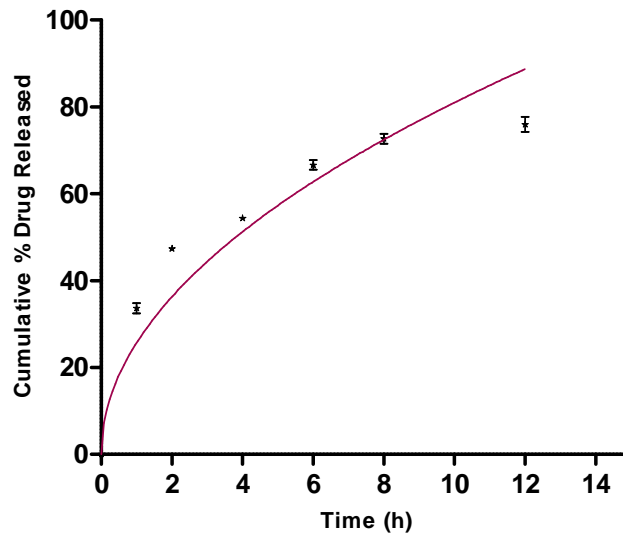


**Figure 6.31.** Cumulative % drug released for CPT-025 (mean  $\pm$  SD, n = 3)

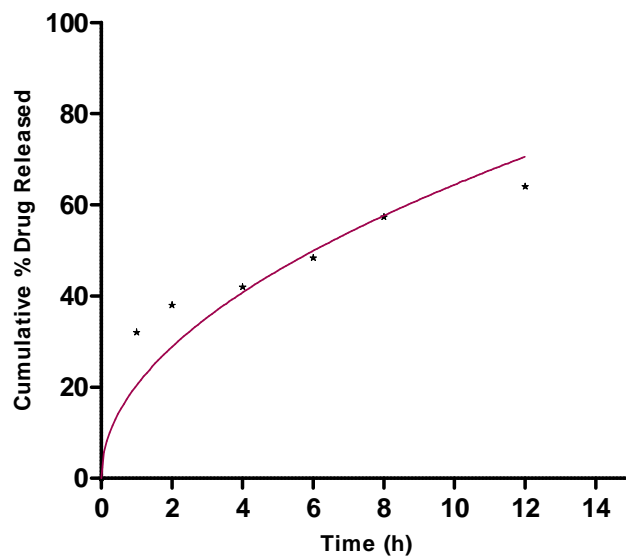


Figure 6.32. Cumulative % drug released for CPT-029 (mean  $\pm$  SD, n = 3)

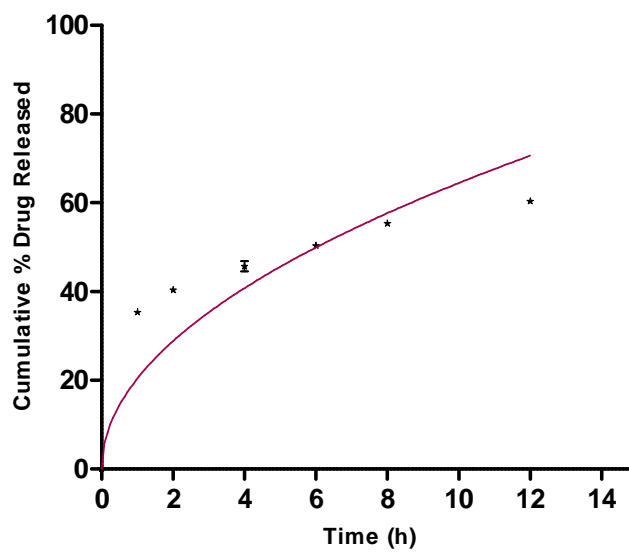
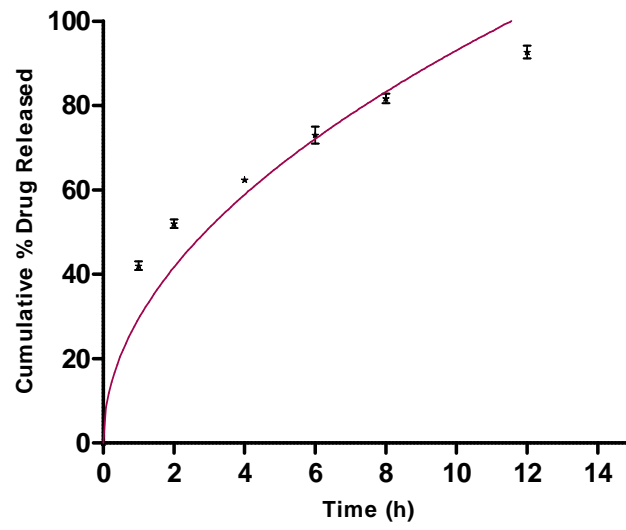


Figure 6.33. Cumulative % drug released for CPT-030 (mean  $\pm$ SD, n = 3)



**Figure 6.34.** Cumulative percent CPT released for batch CPT-008 (mean  $\pm$  SD, n = 3)

#### 6.4. CONCLUSION

The controlled release of CPT observed in this study indicates that hydrophilic matrix microcapsules of CPT manufactured using Eudragit<sup>®</sup> and Methocel<sup>®</sup>, has the potential to be used as a twice-a-day oral sustained release drug delivery system. The polymers, solvents and diluents all play a role in the formation of quality microcapsules. Moreover, optimization of microencapsulation conditions for CPT using RSM has been demonstrated. Input factors such as Eudragit<sup>®</sup> ( $X_1$ ), Methocel<sup>®</sup> K15M ( $X_2$ ) and Methocel<sup>®</sup> K100M ( $X_3$ ) content and homogenizing speed ( $X_4$ ) had an effect on the release of CPT from the microcapsules. Optimization was performed using a CCD approach to yield microcapsules releasing more than 85% CPT in 12 h. The polynomial equation generated explained the quadratic and interaction effects of the input variables on the ultimate response observed. RSM is an appropriate approach as response surface methodology permits the estimation of parameters of a quadratic model, and it can assist in detecting the poor fit of a model. The approach presented in this study provides a useful guideline for the optimization of microcapsule manufacture for other water-soluble drugs.

However, the successful development of these delivery systems requires careful consideration of a number of factors that can influence the performance of a formulation, including the physical and chemical properties of the API and excipients. Experimental design is a preferred strategy, especially with complex formulations. In particular, this multi-varied strategy of experimental design allows for the simultaneous investigation of the effects of a number of variables in addition to their actual significance on a response. Furthermore the possible interrelationship between variables can be readily established since maximum information is generated with the smallest number of experiments.

The absence of pores in other microcapsules is of major importance to this study in order to help explain the drug release mechanism, since CPT diffusion occurs through water filled cavities and is much faster than if diffusion were to take place through dense polymer networks. The poor loading efficiency and rapid drug release observed during the early stages of testing are some of the challenges encountered when microcapsules containing a freely water-soluble drug are manufactured by this method of encapsulation.

The angle of repose for the CPT microcapsules ranged between 18-40°, which indicates that some microcapsules had poor flow properties. The results were confirmed by the *CI* and Hausner ratio.

The addition of span 80 lowered the surface tension of the continuous phase and in turn decreased the sizes of microcapsules. When the homogenizing speed was increased more air was entrapped and foam was produced. An anti-foaming agent ensured that air bubbles were rapidly dissipated.



### MATHEMATICAL MODELING OF CAPTOPRIL RELEASE FROM MICROCAPSULES

#### 7.1. INTRODUCTION

*In vitro* dissolution is one of the most important elements of drug product development. Several models can be used to describe drug dissolution profiles where  $f(t)$  is a function of  $t$  (time) that is related to the amount of drug dissolved from a pharmaceutical dosage form. The quantitative interpretation of values generated in dissolution studies is facilitated by the use of generic equations that mathematically translate dissolution curves as a function of certain parameters related to the dosage forms being tested. In some cases the equations can be deduced by theoretical analysis of processes that a dosage form is subject to. A water-soluble drug incorporated into a hydrophilic matrix is released mainly by a diffusion-controlled process whereas for a poorly water-soluble compound the principal mechanism of release is a function of erosion of the matrix (466).

There have been many attempts to model the process of solvent penetration and subsequent solute release in and from polymeric matrices and there have been many valuable contributions to the understanding of the mechanisms driving these processes (467-472). However the majority of these models are either too general or require extensive knowledge of system parameters and complex differential expressions and they have not been used successfully for the development of optimized pharmaceutical formulations (467).

Swelling controlled-release technologies, based on hydrophilic polymer(s), for drug delivery have been extensively investigated (473-477). The release mechanism from these systems is primarily governed by hydration and gradual transition of a glassy core to a rubbery phase and gel layer formation as swelling progresses. Exposure of these systems to an aqueous environment, over prolonged period, results in dynamic changes in the appearance and nature of the dosage form. Initially the thickness of the gel layer increases as the swelling process dominates, after which synchronisation occurs during which time the thickness of the gel layer remains constant as swelling and erosion of the polymer occurs at the same rate. Eventually erosion predominates as the polymer dissolves and the gel layer thickness is reduced (478). The dynamics of these processes are primarily dependent on properties of the polymers used to manufacture the dosage form (479), the solubility (480) and loading dose of

the drug (481) and the characteristics of other formulation components (482). Furthermore it is known that penetration of water or biological fluids into the polymeric matrix creates boundaries or fronts and the movement(s) of the fronts influence the thermodynamic states associated with various phases of the behaviour of the polymer following hydration (483-485).

Hydrophilic matrices are widely used since they exhibit biopharmaceutical and pharmacokinetics advantages over conventional dosage forms as precise modulation of drug release as a result of hydration of the constituent polymer(s) can be achieved (486-487). Furthermore a degree of flexibility is possible in achieving a desired drug release profile and in general the polymers have FDA acceptability (486-487). Although there is a wide choice of possible matrix-forming polymeric materials, the use of HPMC predominates since it is easy to achieve a desired release profiles when using the material (486). Kim and Fassihi (488) have shown that zero-order drug release from optimized ratios of specific polymeric combinations is easily and readily achievable using HPMC (473).

Model-dependent methods were used to evaluate the dissolution or release profiles of the thirty formulations manufactured in these studies. Although mathematical models have been extensively used to characterize dissolution profiles, these methods are complicated and require caution when interpreting fitted data than when evaluating information generated using model-independent methods of analysis (489).

The *in vitro* release profiles of CPT microcapsules manufactured using solvent evaporation were generated as described in § 6.2.2.2. The applicability and reliability of several kinetic and mathematical models, and the canonical and Lagrange criterion (241), were evaluated for their ability to describe drug release from these systems.

A CCD approach (Chapter 6) was used in a multivariate experimental design to establish the number and formulae that were to be manufactured in order to optimize the formulation and manufacture of CPT microcapsules as the CCD is more efficient in mapping space. In view of the fact that CCD was used to optimize experimental variables, it was important that the coordinates of a stationary point of the response surfaces generated were estimated and interrogated. The fitted response surfaces were analyzed, in part, as described in Chapter 6. In this Chapter the modeling of percent drug release and optimization of ( $Y_4$ ) was undertaken

using canonical, mathematical and Lagrange methods. Optimization of the formulations was done by selecting the formulations (§ 6.2.2.2) based on the criteria of attaining the maximum value for percent drug released. This would be done by finding the conditions under which certain processes attain optimal results. Canonical and Lagrange methods were therefore used to determine the levels of the design parameters at which the response ( $Y_4$ , percent drug released) reaches optimum. The optimum could either be a maximum or a minimum or a function of the design parameters.

The model generated in Chapter 6 for  $Y_4$  was used in Lagrange and Canonical analysis, which allowed a compromise among various responses and helped search for a combination of factor levels that jointly optimize the selected response.

In most cases it is difficult to understand and evaluate the shape of a fitted response surface by visual inspection of the contour or surface response plots. Furthermore, when many independent variables are used in a model it is difficult to evaluate the shape of a surface by interrogating the algebraic expression of a polynomial. Canonical analysis may be necessary to facilitate interpretation of the data. Such analysis requires the original experimental variables, viz.,  $x_i$ , to be mathematically transformed into new variables viz.,  $z_i$ , in order for the response surface, to be expressed only in quadratic terms (490-492). It is therefore easier to evaluate the transformed terms.

### **7.1.1. Canonical analysis**

Canonical analysis (493) is a method of rewriting a fitted second-degree equation in a form in which it can be better understood. This is accomplished by the rotation of axes that removal of all cross-product terms. In general this simplification is termed the A canonical form. If desired this transformation may also be accompanied by a change of origin to remove first order terms, in which case a B canonical form is generated (494). The response,  $Y_4$  representing drug release was considered as a function of four variables viz, concentration of Eudragit<sup>®</sup> RS, Methocel<sup>®</sup> K15M, Methocel<sup>®</sup> K100M and homogenizing speed.

When using canonical analysis (495) mathematical expressions and analysis involve changing the origin of a plot of a response surface plot from its original coordinates to the stationary point of a response surface, after which the axes are rotated until they correspond to the principal axes of the contour plot. By use of the new coordinate system, second order

model equations are simplified and the geometrical nature of the data becomes apparent. The algebraic signs of a canonical equation coefficient(s) provide information relating to the nature of the stationary point. If all values are negative the stationary point is in fact a maximum and if all are positive the stationary point is a minimum. If the signs are mixed the point is a saddle.

In mathematics, a saddle point is a point in a domain of a function of two variables which is a stationary point but not a local extremum. In general the surface, at such a point, resembles a saddle that curves up in one direction and down in another and is in fact similar to a riding saddle or a mountain pass (496).

### 7.1.2. Lagrange's criteria

Lagrange's criteria are derived from a mathematical procedure used to determine the nature of a stationary point of a function (497). In combination with canonical analysis, Lagrange's criteria provide additional information about the nature of the response surface(s).

#### 7.1.2.1. Lagrange's criterion for four variable functions

The second order model for four variables ( $X_1, X_2, X_3$  and  $X_4$ ) is shown in Equation 7.1.

$$Y = Y_1 = W + aX_1 + bX_2 + cX_3 + dX_4 + eX_1X_2 + fX_1X_3 + gX_1X_4 + hX_2X_3 + iX_2X_4 + jX_3X_4 + kX_1^2 + lX_2^2 + mX_3^2 + nX_4^2$$

**Equation 7.1**

where

$Y$  = the experimental response to be optimised,

$W$  = a constant term,

$a, b, c$  and  $d$  = coefficients of the linear terms,

$e, f, g, h, i$  and  $j$  = coefficients of interaction between the four factors, and

$k, l, m$  and  $n$  = coefficients of the quadratic terms.

If the quadratic function in a Lagrange function shows one stationary point, ( $X_{10}, X_{20}, X_{30}, X_{40}$ ), four situations are possible. Initial information about the geometrical nature of the surface can be derived from the signs and magnitudes of the quadratic coefficients in the polynomial function. If all coefficients are negative the function can show a maximum and if positive the function can show a minimum. Should the coefficients be described with a

mixture of positive and negative signs the stationary point is a saddle point with a relative maximum for the variables with a negative term and with a relative minimum for the variables with a positive coefficient. Nevertheless it is always necessary to verify these conclusions by applying the Lagrange criteria which will give values for Hessian determinants (498).

The Hessian,  $H$ , is a real and symmetric matrix. Therefore,  $H$  can be diagonalized by an orthogonal change of basis of the configuration space. The new basis vectors are called Eigenvectors and the entries on a diagonal version of  $H$  are called Eigenvalues. This Eigenvector basis, the shape of a graph of a quadratic term becomes obvious. Directions along Eigenvectors with negative Eigenvalues have a downward curvature and those with positive Eigenvalues have an upward curvature (499). It is important to remember that eigenvectors are located in a configuration space and therefore each eigenvector represents a particular perturbation of a response surface.

### **7.1.3. Mathematical Modeling**

According to Costa and Lobo (466) drug release models with major applicability and which can best describe drug release phenomena must be used to define drug release mechanism. This helps to analyze and explain mathematically the processes that occur when a drug is released from a dosage form. In this study, several mathematical models were used to elucidate the mechanism of release from the batches of microcapsules that were manufactured 'in-house'.

## **7.2. METHODS**

### **7.2.1. Model Fitting**

#### **7.2.1.1. Canonical analysis**

The stationary point of the fitted response surfaces were computed using an Online Matrix Calculator (Blue Bit) powered by the Net matrix Library (500). The characterization of the response surfaces was performed on the  $Y_4$  polynomial equation to transform the fitted model to a new coordinate system with the origin at  $x_0$ . The polynomial equation generated using RSM in Chapter 6 (§ 6.3) is shown in Equation 7.2.

$$Y_4 = -42.49 - 57.04X_1 + 141.90 X_2 + 420.90 X_3 + 43.74 X_4 - 30.00X_1X_2 - 96.00 X_1X_3 - 6.62 X_1X_4 - 140.00 X_2X_3 + 20.00 X_2X_4 - 74.00 X_3X_4 + 34.15 X_1^2 - 47.90 X_2^2 - 35.90 X_3^2 - 4.85 X_4^2$$

**Equation 7.2**

The fitted model showing the response for  $Y_4$  written in matrix language is shown in Equation 7.3.

$$\hat{Y} = b_0 + x'b + x'Bx \tag{Equation 7.3}$$

where

$b_0$  = the constant term,

$x$  = the vector of the experimental variables,  $x'$  ( $x_1, x_2, x_3, x_4$ )

$x'$  = the vector transpose

$b$  = the vector of the linear coefficients,  $b'$  ( $b_1, b_2, b_3, b_4$ )

$B$  = the Hessian matrix

Eigenvalues derived from the symmetrical matrix,  $B$  are represented by  $\lambda_1, \lambda_2, \lambda_3$  and  $\lambda_4$ , and  $m_1, m_2, m_3$  and  $m_4$  are the corresponding Eigenvectors. All Eigenvalues and Eigenvectors satisfy the mathematical expression shown in Equation 7.3 and these are related concepts in the field of mathematics known as linear algebra (501).

$$B m_i = m_i \lambda_i, \tag{Equation 7.4}$$

where  $i = 1, 2, 3,$  and  $4$  indicate the number of factors in a model.

Since  $B$  is a symmetric and real matrix, all Eigenvalues are real. These Eigenvalues are the coefficients of the canonical model. Eigen value problems are among the most important challenges in connection with matrix analyses. An Eigen value of a square matrix is a scalar quantity that is usually represented by the Greek letter  $\lambda$ , and an Eigenvector is a non-zero vector and therefore cannot be a zero vector.

### 7.2.1.2. Lagrange's Criterion

In this study, Lagrange's criterion was used (502,503) was to determine the critical point of the second order equation based on the calculation of the Hessian determination of the

response,  $Y_4$ . The Hessian determinant of a matrix is represented by delta,  $\Delta$ . Since there are four variables in this study, the four expressions for a 4 X 4 matrix are represented by  $\Delta_1, \Delta_2, \Delta_3$  and  $\Delta_4$ , respectively (504). The mathematical representations of  $\Delta_1, \Delta_2, \Delta_3$  and  $\Delta_4$  are shown in Equations 7.5 - 7.8.

$$\Delta_1 = \frac{d^2Y}{dX_1}$$

$$\Delta_2 = \begin{bmatrix} \frac{d^2Y}{dX_1^2} & \frac{d^2Y}{dX_1dX_2} \\ \frac{d^2Y}{dX_2dX_1} & \frac{d^2Y}{dX_2^2} \end{bmatrix}$$

$$\Delta_3 = \begin{bmatrix} \frac{d^2Y}{dX_1^2} & \frac{d^2Y}{dX_1dX_2} & \frac{d^2Y}{dX_1dX_3} \\ \frac{d^2Y}{dX_2dX_1} & \frac{d^2Y}{dX_2^2} & \frac{d^2Y}{dX_2dX_3} \\ \frac{d^2Y}{dX_3dX_1} & \frac{d^2Y}{dX_3dX_2} & \frac{d^2Y}{dX_3^2} \end{bmatrix}$$

$$\Delta_4 = \begin{bmatrix} \frac{d^2Y}{dX_1^2} & \frac{d^2Y}{dX_1dX_2} & \frac{d^2Y}{dX_1dX_3} & \frac{d^2Y}{dX_1dX_4} \\ \frac{d^2Y}{dX_2dX_1} & \frac{d^2Y}{dX_2^2} & \frac{d^2Y}{dX_2dX_3} & \frac{d^2Y}{dX_2dX_4} \\ \frac{d^2Y}{dX_3dX_1} & \frac{d^2Y}{dX_3dX_2} & \frac{d^2Y}{dX_3^2} & \frac{d^2Y}{dX_3dX_4} \\ \frac{d^2Y}{dX_4dX_1} & \frac{d^2Y}{dX_4dX_2} & \frac{d^2Y}{dX_4dX_3} & \frac{d^2Y}{dX_4^2} \end{bmatrix}$$

Where,

$$\Delta_1 = \text{Equation 7.5}$$

$$\Delta_2 = \text{Equation 7.6}$$

$$\Delta_3 = \text{Equation 7.7}$$

$$\Delta_4 = \text{Equation 7.8}$$

### 7.2.1.3. Mathematical Modeling

The fitting of dissolution data of all formulations, CPT-001 - CPT-030 was performed using GraphPad Prism Software Version 4.0 (GraphPad Prism Software, San Diego, CA, USA). The software is used to estimate the parameters of a nonlinear function that provide the

closest fit between experimental observations and the non-linear function. The mathematical equations for the models used to describe the dissolution curves for CPT formulations are summarized in Table 7.1. The data that was fitted was generated in Chapter 6 using USP Apparatus 3 (§6.2.2.7). The best-fit solution was identified by evaluating the coefficient of determination ( $R^2$ ), and sum of squares of residuals (SSR) where the highest  $R^2$  value and smallest SSR values indicate the best fit (505-510).

In order to investigate the mechanism of drug release from microcapsules, the drug release data were analysed using several mathematical expressions (511). Table 7.1 shows the equations used to determine the appropriate models used to study the release.

**Table 7.1.** Mathematical representation of the models used to fit CPT release from microcapsules

<b>Model</b>	<b>Equation</b>	<b>References</b>
Zero-order	$Qt = Q_o + K_o t$	(512, 513)
First-order	$\text{Ln } Q_t = \text{Ln } Q_o - K_1 t$	(514, 515)
Higuchi	$Qt = Q_o + K_{Hi} t^{1/2}$	(516, 517)
Makoid–Banakar	$Qt = KMB t^n e^{(-ct)}$	(518)
Kopcha	$Qt = At^{1/2} + Bt$	(519)
Korsmeyer–Peppas	$Qt = K_{KP} t^n$	(520-522)



## 7.3. RESULTS AND DISCUSSION

### 7.3.1. Canonical analysis

Canonical analysis of the response surface and equations makes it possible to deduce information about the surface plots without need for graphical representation. In matrix terms an equation is represented by Equation 7.3;

$$\hat{Y} = b_0 + x'b + x'Bx$$

In matrix form the expression is then shown in Equation 7.9.

$$\hat{Y} = -42.49 + (x_1, x_2, x_3, x_4) \begin{bmatrix} -57.04 \\ 141.90 \\ 420.90 \\ 43.74 \end{bmatrix} + (x_1, x_2, x_3, x_4) \begin{bmatrix} 34.15 & -15 & -48 & -3.32 \\ -15 & -47.90 & -70 & 10 \\ -48 & -70 & -35.90 & -37 \\ -3.32 & 10 & -0.109 & -4.85 \end{bmatrix} \begin{bmatrix} x_1 \\ x_2 \\ x_3 \\ x_4 \end{bmatrix}$$

$\hat{Y} = \text{Equation 7.9}$

The Eigen values of B and the corresponding orthogonal Eigenvectors are:

$$\lambda_1 = -127.68$$

$$\lambda_2 = 70.00$$

$$\lambda_3 = 27.91$$

$$\lambda_4 = -24.74$$

Eigenvectors

$$m_1 = \begin{bmatrix} -0.27 \\ -0.64 \\ -0.70 \\ -0.16 \end{bmatrix}$$

$$m_2 = \begin{bmatrix} -0.66 \\ -0.31 \\ 0.61 \\ -0.31 \end{bmatrix}$$

$$m_3 = \begin{bmatrix} -0.69 \\ 0.45 \\ -0.26 \\ 0.51 \end{bmatrix}$$

$$m_4 = \begin{bmatrix} 0.12 \\ -0.54 \\ 0.27 \\ 0.79 \end{bmatrix}$$

$\mathbf{M}$  in matrix form will be represented by  $m_1, m_2, m_3$  and  $m_4$ .

$$\mathbf{M} = \begin{bmatrix} -0.27 & -0.66 & -0.69 & 0.12 \\ -0.64 & -0.31 & 0.45 & 0.54 \\ -0.70 & 0.61 & -0.26 & 0.27 \\ -0.16 & -0.31 & 0.51 & 0.79 \end{bmatrix}$$

$\Lambda$  is a diagonal matrix and is represented by  $\lambda_1, \lambda_2, \lambda_3$  and  $\lambda_4$ .

$$\Lambda = \begin{bmatrix} -127.68 & 0.000 & 0.000 & 0.000 \\ 0.000 & 70.00 & 0.000 & 0.000 \\ 0.000 & 0.000 & 27.91 & 0.000 \\ 0.000 & 0.000 & 0.000 & -24.74 \end{bmatrix}$$

and

$$\Theta = \mathbf{M}'\mathbf{b}$$

where  $\mathbf{M}'$ , is the inverse of  $\mathbf{M}$ .

$$\mathbf{B}\mathbf{M} = \mathbf{M} \Lambda$$

Where  $\Lambda$ , is a diagonal matrix and

$$\mathbf{M}' = \mathbf{M}^{-1}$$

which gives

$$M'BM = \Lambda$$

Now by making use of the fact that

$$MM' = I,$$

Equation 7.3 which is given by

$$\hat{Y} = b_0 + x'b + x'Bx \quad \text{Equation 7.3}$$

can be represented by Equation 7.10

$$\hat{Y} = b_0 + (x'M)(M'b) + (x'M)M'BM(M'x) \quad \text{Equation 7.10}$$

If we write

$$X = M'x$$

and

$$\Theta = M'b$$

or equivalent

$$x = MX$$

and

$$b = M\Theta$$

This can be rewritten as Equation 7.11.

$$\hat{Y} = b_0 + X'\Theta + X'\Lambda X \quad \text{Equation 7.11}$$

$$\Theta = M'b = \begin{bmatrix} -0.057 & -1.542 & -0.260 & 1.152 \\ -0.559 & -0.735 & 0.817 & 0.308 \\ -0.838 & 1.080 & -0.569 & -0.417 \\ 0.310 & -1.298 & 0.636 & 1.889 \end{bmatrix} \begin{bmatrix} -57.04 \\ 141.90 \\ 420.90 \\ 43.74 \end{bmatrix}$$

$$\Theta = \begin{bmatrix} -274.60 \\ 284.94 \\ -56.68 \\ 148.45 \end{bmatrix}$$

where the coordinates of the stationary point in relation to the rotated axes are such that

$$X_{is} = \frac{-\Theta_i}{2\lambda_i}$$

$$X_{1s} = 0.43$$

$$X_{2s} = 2.04$$

$$X_{3s} = 1.02$$

$$X_{4s} = 3.00$$

The canonical form is therefore represented by Equation 7.12

$$Y_4 = -42.49 - 274.60 X_1 + 284.94 X_2 - 56.68 X_3 + 148.45 X_4 \\ + 127.68 X_1^2 + 70.00 X_2^2 + 27.91 X_3^2 - 24.74 X_4^2$$

**Equation 7.12**

where

$$X_1 = -0.057 x_1 - 0.559 x_2 - 0.838 x_3 + 0.310 x_4$$

$$X_2 = -1.542 x_1 - 0.735 x_2 + 1.080 x_3 - 1.298 x_4$$

$$X_3 = -0.260 x_1 + 0.817 x_2 - 0.569 x_3 + 0.636 x_4$$

$$X_4 = -0.310 x_1 - 1.298 x_2 + 0.636 x_3 + 1.889 x_4$$

The important considerations in this canonical form are:

- i) The sign(s) and relative magnitude(s) of the Eigen values
- ii) The magnitude of the coordinates  $X_{is}$  of the stationary point
- iii) The nature of the transformation  $\mathbf{X} = \mathbf{M}'\mathbf{x}$

The negative and positive signs associated with the Eigenvalues indicate that the fitted response value i.e. 84% at the centre of the fitted surface is located at a saddle point. The coefficients of the Eigenvector associated with the smallest Eigenvalue are 0.12, -0.54, 0.27 and 0.79, suggesting that for the  $x_4$  direction, which is the direction of the greatest elongation of the response surface, the homogenizing speed and other factors all have the same effect. Upon 'trading of' various response variables and comprehensive evaluation of feasibility search and exhaustive grid search, the formulation composition with polymer concentration of Eudragit<sup>®</sup> RS (0.43 g), Methocel<sup>®</sup> K100M (2.04 g), Methocel<sup>®</sup> K15M (1.05 g) and Homogenizing speed of 3000 rpm was found to fulfil the maximum requirement of an optimized formulation because of optimized % released. The optimized batch was prepared accordingly and dissolution and SEM analysis were carried out using USP Apparatus 3 as shown in Table 6.8 in § 6.2.2.7.

The A canonical form can thus be represented by Equation 7.13.

$$\hat{Y} = -42.49 + 60.836 X_1 + 48.867 X_2 + 124.919 X_3 + 18.491 X_4 + 140.02 X_1^2 - 48.28 X_2^2 + 24.83 X_3^2 + 6.23 X_4^2$$

**Equation 7.13**

where,

$$\mathbf{X}_1 = 0.392x_1 + 0.330 x_2 + 0.845x_3 - 0.153x_4$$

$$\mathbf{X}_2 = 0.593x_1 + 0.438x_2 - 0.523x_3 - 0.427x_4$$

$$\mathbf{X}_3 = 0.663x_1 - 0.731x_2 + 0.007x_3 + 0.162x_4$$

$$\mathbf{X}_4 = 0.235x_1 + 0.406x_2 - 0.109x_3 + 0.876x_4$$

For the response,  $Y_4$ , the Eigen values that are the coefficients of the quadratic terms,  $X_1^2$ ,  $X_2^2$ ,  $X_3^2$  and  $X_4^2$  have different signs and therefore mean that the stationary point is also a saddle point.

### 7.3.2. Lagrange's Criterion

These matrices are used to solve large-scale optimization problems with Newton-type methods since they are the coefficient of the quadratic term of a local Taylor expansion of a function (523). The Lagrange criterion was used to solve a formulation problem. A saddle point can be recognized by a contour that appears to intersect itself.

The application of Lagrange's criteria to the models helped locate the critical point of the second order equation and was based on the Hessian determinant of  $Y_4$ .

$$\Delta_1 = 69.00$$

$$\Delta_2 = -7510.20$$

$$\Delta_3 = -736674.84$$

$$\Delta_4 = 99513387.45$$

Information about the geometric nature of the response surface was derived from the signs of the Hessian determinants. These indicate that a saddle point exists in the response surfaces showing the percent drug release versus time and formulation variable.

Both Lagrange and Canonical analysis have been used in the study. The saddle point indicates that one has to reliably analyze data because this is a dynamic system. This means that the formulation problem does not depend on a single variable performance over the design space.

### 7.3.3. Mathematical Modeling

Drug release rate is a fundamental parameter of any pharmaceutical dosage form. Quantitative analysis of the values generated in dissolution testing is easier when mathematical formulae are used to express the resultant dissolution data as a function of some of the characteristics of a dosage form. The dissolution of drugs from dosage forms has been described by kinetic models in which the amount of dissolved drug ( $M$ ) is monitored as a function of time ( $t$ ) and can be simplified as  $M = f(t)$ .

The curvilinear nature of the cumulative percentage drug released versus time plots suggest that drug release from the microcapsules does not follow zero-order kinetics. The data are summarized in Table 7.2. This observation is supported by the low correlation coefficients obtained in all cases where the dissolution data were fitted to a zero-order model. The *in vitro* dissolution studies confirmed the drug release was governed by Higuchi kinetics and data also fitted the Kopcha matrix model adequately. However, the mathematical expression that best describes drug release from these microcapsules was found to be the Makoid–Banakar model in which the resultant  $R^2$  values were greater than 0.98. The Korsmeyer–Peppas release exponent,  $n$ , is approximately 0.3, confirming that diffusion is a controlling factor for drug release. This finding was supported by evaluation of the ratios of the exponents  $A/B$  derived from the Kopcha model which were greater than 1 in all cases. The Kopcha model can also be used to quantify the relative contributions of diffusion and polymer relaxation to drug release. The data in Table 7.2 clearly show that the value of  $A$  is far greater than that for  $B$ , suggesting that drug release from the microcapsules is primarily controlled by a Fickian diffusion process.

The results of curve-fitting studies reveal as noted, that CPT release from the microcapsules could be described by the Makoid-Banakar, Korsmeyer-Peppas, Kopcha and Higuchi models. These coefficients of determination ( $R^2$ ) were higher than 0.900 for all analyses and the corresponding SSR values were lower than for the other models used. The formulations with low levels of rate-controlling polymers exhibited a higher burst release which can be ascribed to the dissolution of the CPT from the surface of the microcapsules. Furthermore the balance that exists between swelling and the gelling characteristics of the microcapsules is vital to ensure and maintain the desired release rates for CPT.

**Table7.2.** Results of model fitting of release profiles

MODEL	FORMULATION									
	CPT-001	CPT-002	CPT-003	CPT-004	CPT-005	CPT-006	CPT-007	CPT-008	CPT-009	CPT-010
<b>Zero-order</b>										
R <sup>2</sup>	0.179	0.254	0.174	0.221	0.274	0.465	0.023	0.389	0.533	0.380
k <sub>0</sub>	7.047	4.606	5.683	7.843	9.560	9.733	5.976	9.806	9.404	9.240
SSR	6844	4198	6027	8801	11422	9190	5968	10387	7640	9238
<b>First -order</b>										
R <sup>2</sup>	0.612	0.486	0.507	0.612	0.636	0.695	0.540	0.672	0.723	0.692
k <sub>1</sub>	28.10	20.63	24.99	29.94	37.03	35.18	25.40	36.53	32.92	34.10
SSR	3238	1720	2526	4389	5718	5226	2678	5562	4531	4583
<b>Higuchi</b>										
R <sup>2</sup>	0.852	0.673	0.717	0.767	0.895	<b>0.954</b>	0.785	<b>0.934</b>	<b>0.968</b>	<b>0.914</b>
k <sub>H</sub>	21.34	14.20	17.48	23.59	28.86	29.08	18.29	29.42	27.97	27.68
SSR	1232	1093	1448	2626	1638	778.7	1249	1122	515.5	1280
<b>Makoid-Banakar</b>										
R <sup>2</sup>	<b>0.983</b>	<b>0.991</b>	<b>0.996</b>	0.875	<b>0.994</b>	<b>0.998</b>	<b>0.993</b>	<b>0.997</b>	<b>0.996</b>	<b>0.982</b>
k <sub>MB</sub>	33.43	26.56	31.62	36.57	42.88	38.54	31.08	40.98	35.44	39.08
n	0.263	0.165	0.184	0.266	0.291	0.352	0.219	0.326	0.376	0.317
c	<0.001	<0.001	<0.001	<0.001	<0.001	<0.001	<0.001	<0.001	<0.001	<0.001
SSR	136.4	28.47	19.91	1410	93.39	33.48	39.88	41.28	51.90	256.7
<b>Kopcha</b>										
R <sup>2</sup>	0.852	0.673	0.717	0.767	0.895	<b>0.954</b>	0.785	<b>0.934</b>	<b>0.968</b>	<b>0.914</b>
A	21.34	14.20	17.48	23.59	28.86	29.16	18.29	29.42	27.97	27.68
B	<0.001	<0.001	<0.001	<0.001	<0.001	<0.001	<0.001	<0.001	<0.001	<0.001
SSR	1232	1093	1448	2626	1638	779.3	1249	1122	515.5	1280
<b>Korsmeyer-Peppas</b>										
R <sup>2</sup>	<b>0.980</b>	<b>0.991</b>	<b>0.996</b>	<b>0.955</b>	<b>0.991</b>	<b>0.998</b>	<b>0.993</b>	<b>0.999</b>	<b>0.998</b>	<b>0.994</b>
K <sub>KP</sub>	33.85	26.61	31.66	44.49	43.94	39.45	31.07	42.33	37.06	42.83
n	0.252	0.165	0.184	0.0173	0.263	0.327	0.219	0.281	0.325	0.222
SSR	130.6	28.45	19.90	228.7	60.25	9.489	39.88	6.021	8.193	44.95

Table7.2. Continued.

MODEL	FORMULATION									
	CPT-011	CPT-012	CPT-013	CPT-014	CPT-015	CPT-016	CPT-017	CPT-018	CPT-019	CPT-020
<b>Zero-order</b>										
R <sup>2</sup>	0.327	0.096	0.166	0.423	0.086	0.637	0.404	0.595	0.369	0.301
k <sub>0</sub>	10.26	6.801	6.429	9.338	6.803	8.570	10.88	9.072	9.909	9.092
SSR	12382	6852	5750	8934	7029	5199	13102	6423	10858	9896
<b>First -order</b>										
R <sup>2</sup>	0.647	0.595	0.610	0.693	0.571	0.754	0.632	0.733	0.667	0.660
k <sub>1</sub>	39.14	27.71	25.72	34.17	28.08	28.46	40.85	30.80	37.19	34.68
SSR	6479	3065	2685	4759	3295	3526	8086	4232	5728	4805
<b>Higuchi</b>										
R <sup>2</sup>	<b>0.915</b>	0.829	0.855	<b>0.934</b>	0.829	<b>0.985</b>	<b>0.934</b>	<b>0.977</b>	<b>0.929</b>	0.891
k <sub>H</sub>	30.89	20.68	19.49	27.93	20.72	25.30	32.69	26.87	29.76	27.35
SSR	1561	1296	996.8	1011	1309	208.2	1437	362.2	1224	1532
<b>Makoid-Banakar</b>										
R <sup>2</sup>	<b>0.995</b>	<b>0.994</b>	<b>0.992</b>	<b>0.989</b>	<b>0.992</b>	<b>0.995</b>	<b>0.995</b>	<b>0.992</b>	<b>0.998</b>	<b>0.984</b>
k <sub>MB</sub>	44.54	33.67	30.72	38.33	33.61	29.30	41.35	32.15	41.99	40.55
n	0.308	0.241	0.260	0.334	0.244	0.424	0.521	0.406	0.319	0.292
c	<0.001	<0.001	<0.001	<0.001	<0.001	<0.001	<0.001	<0.001	<0.001	<0.001
SSR	81.90	41.11	50.78	159.9	55.55	69.42	108.5	117.6	32.00	226.9
<b>Kopcha</b>										
R <sup>2</sup>	<b>0.915</b>	0.829	0.855	<b>0.934</b>	0.829	<b>0.985</b>	<b>0.931</b>	<b>0.977</b>	<b>0.929</b>	0.891
A	30.89	20.68	19.49	27.93	20.72	25.30	33.48	26.87	29.84	27.35
B	<0.001	<0.001	<0.001	<0.001	<0.001	<0.001	<0.001	<0.001	<0.001	<0.001
SSR	1561	1296	996.8	1011	1309	208.2	1498	362.2	1224	1532
<b>Korsmeyer-Peppas</b>										
R <sup>2</sup>	<b>0.996</b>	<b>0.994</b>	<b>0.992</b>	<b>0.992</b>	<b>0.992</b>	<b>0.995</b>	<b>0.998</b>	<b>0.989</b>	<b>0.998</b>	<b>0.989</b>
K <sub>KP</sub>	45.27	33.75	30.72	40.59	33.60	30.54	41.37	33.29	43.37	43.45
n	0.275	0.241	0.260	0.269	0.244	0.380	0.398	0.368	0.272	0.213
SSR	28.06	41.05	50.78	58.96	55.55	32.92	13.93	78.02	8.300	85.20



MODEL	FORMULATION									
	CPT-011	CPT-012	CPT-013	CPT-014	CPT-015	CPT-016	CPT-017	CPT-018	CPT-019	CPT-020
<b>Zero-order</b>										
R <sup>2</sup>	0.058	0.428	0.292	0.215	0.316	0.383	0.1856	0.239	0.319	0.303
k <sub>0</sub>	5.513	8.585	10.14	9.850	8.449	7.576	4.994	6.570	6.669	6.765
SSR	4722	7465	12519	12955	8744	9094	4003	5555	7234	5474
<b>First -order</b>										
R <sup>2</sup>	0.566	0.705	0.647	0.613	0.617	0.558	0.564	0.634	0.557	0.658
k <sub>1</sub>	22.91	31.15	38.97	39.03	32.64	31.68	20.83	25.69	28.09	25.83
SSR	2177	3849	6240	6393	4901	4178	1776	2669	3195	2686
<b>Higuchi</b>										
R <sup>2</sup>	0.818	<b>0.935</b>	<b>0.903</b>	0.881	0.910	0.815	0.796	0.881	0.794	0.897
k <sub>H</sub>	16.81	25.67	30.58	29.84	0.758	0.937	0.647	0.661	0.864	0.636
SSR	909.2	839.2	1703	1953	1140	1741	830.0	865.5	1479	802.2
<b>Makoid-Banakar</b>										
R <sup>2</sup>	<b>0.993</b>	<b>0.990</b>	<b>0.997</b>	<b>0.998</b>	<b>0.993</b>	<b>0.997</b>	<b>0.990</b>	<b>0.993</b>	<b>0.997</b>	<b>0.989</b>
k <sub>MB</sub>	27.62	35.03	45.10	45.39	35.04	38.05	25.58	30.15	34.45	29.96
n	0.237	0.336	0.295	0.287	0.432	0.251	0.225	0.279	0.221	0.296
c	<0.001	<0.001	<0.001	<0.001	0.024	0.004	<0.001	<0.001	<0.001	<0.001
SSR	33.65	119.1	51.63	28.21	83.42	21.41	38.63	48.70	17.58	85.54
<b>Kopcha</b>										
R <sup>2</sup>	0.818	<b>0.935</b>	<b>0.903</b>	0.881	<b>0.910</b>	0.815	0.796	0.881	0.794	0.897
A	16.81	25.67	30.70	29.98	25.61	23.13	15.24	19.85	20.38	20.36
B	<0.001	<0.001	<0.001	<0.001	<0.001	<0.001	<0.001	<0.001	<0.001	<0.001
SSR	909.2	839.2	1705	1955	1142	1741	830.0	865.5	1479	802.2
<b>Korsmeyer-Peppas</b>										
R <sup>2</sup>	<b>0.993</b>	<b>0.997</b>	<b>0.998</b>	<b>0.998</b>	<b>0.992</b>	<b>0.998</b>	<b>0.990</b>	<b>0.993</b>	<b>0.997</b>	<b>0.989</b>
K <sub>KP</sub>	27.63	37.57	45.67	45.14	34.89	38.00	25.62	30.22	34.50	30.07
n	0.237	0.270	0.291	0.294	0.353	0.240	0.225	0.278	0.221	0.295
SSR	33.65	15.36	11.51	12.01	57.16	15.06	38.62	48.62	17.57	85.39

The mean ( $n=3$ ) dissolution profiles for CPT formulations, CPT-001 – CPT-030 are shown in Appendix One. CPT release was rapid except for formulations CPT-010 to CPT-020 where complete release was observed at 12 hours.

The commonly used Makoid-Banakar, Korsmeyer-Peppas and Kopcha models are simple and robust kinetic models that adequately describe the release of CPT from the microcapsules. The Makoid-Banakar model fitted the presented data (Table 7.2) better than the other models tested when based on SSR and  $R^2$  values. When the parameter,  $c$  of the Makoid-Banakar model is equal to zero, the model is reduced to become Korsmeyer-Peppas power law ( $e^{-0t} = 1$ ). The results are in agreement with what has been observed by Costa and Lobo (511) and Khamanga *et al* (442).

The most important aspect to consider when developing new pharmaceutical products or evaluating drug release mechanisms is the suitability and predictive ability and accuracy of any model chosen to describe the release process. The presence of a highly water-soluble drug in an HPMC matrix can generate an osmotic gradient which may result in a greater rate of polymer swelling and increase in gel thickness with a corresponding initial increase followed by a drastic decrease in the rate of drug release (65).

The canonical results reveal that the sign(s) of the Eigenvalues are both negative and positive suggesting that the stationary point is a saddle point. The Lagrange criteria data confirm that the stationary point is a saddle point as the signs of the Hessian determinants were also mixed.

It should be noted that the value of  $R^2$  alone, is not an exact measure of a model's accuracy, but is a measure of the reduction in the variability of a response generated by use of additional variables in a model. However a large value for  $R^2$  does not necessarily imply that the regression model used is a good model. The addition of another variable to a model in this study, as shown in Table 7.2 increased the value for  $R^2$ , irrespective of whether the additional variable is statistically significant. The variables are  $n$  and  $c$  as shown in the Makoid-Banakar model.

#### **7.4. CONCLUSIONS**

Drug delivery systems manufactured using matrix polymers have been assessed and the release mechanisms were found to be affected by factors such as the degree of polymer swelling. The selection of an appropriate model for the analysis of drug release provided insight to the underlying mass transport mechanism of release from the delivery technologies. The value of the release exponent,  $n$ , was  $< 0.45$  indicating that CPT release was not controlled only by diffusion. Fitting of data to the Kopcha model supported the evidence that CPT release involved a combination of a diffusion-controlled and a chain relaxation/swelling mechanism for most formulations.

What has emerged from this investigation is that considerable attention must be focused on understanding mathematical models as these provide useful guidance and insight into drug release and transport mechanisms from sustained-release technologies. Canonical and Lagrange methods make it possible to determine the equations and the roles played by experimental variables in drug release studies. In this case the results have considered the shape of the stationary point of the surface plots. Information relating to the geometric nature of the response surfaces was derived from the sign and magnitudes of the quadratic coefficients in the polynomial functions.

## CHAPTER 8

---

### CONCLUSIONS

ACE inhibitors have achieved widespread usage in the treatment of cardiovascular and renal disease. They alter the balance between the vasoconstrictive, salt-retentive, and hypertrophic properties of AII and the vasodilatory and natriuretic properties of bradykinin and alter the metabolism of a number of other vasoactive substances. CPT has a relatively short elimination half-life in plasma and is a drug of choice in antihypertensive therapy due to its effectiveness and low toxicity. It is usually prescribed to patients who are chronically ill and require long-term use for its therapeutic benefits. Development of a once daily CPT oral formulation would be a significant advantage for patient compliance, accompanied by minimization of drug side effects as a result of reduction of drug blood concentration fluctuations in long term therapy.

Impurities in API are highly undesirable and in some cases can prove to be harmful to the patient. The ICH Q7 is a guidance for API manufacturers, and it is mentioned in the guidance that impurities be maintained below set limits. Thus it was pertinent to characterize the API in order to develop a suitable dosage form knowing full well that it had no impurities. A comprehensive study was undertaken using NMR spectroscopy. The  $^1\text{H}$ ,  $^{13}\text{C}$  NMR, DEPT-135, COSY, HMBC and HSQC experiments were carried out at precessional frequencies of 400 MHz and in  $\text{CDCl}_3$  at 25 °C temperature on a Varian- 400 FT NMR spectrometer to confirm the structure of CPT.

CPT is characterized by lack of a strong chromophore, and therefore is not able to absorb at the more useful UV-Vis region of the spectrum. One of the difficulties of determining CPT by UV-HPLC in dosage form is the use of a derivatizing procedure. Using ICH guidelines an HPLC-ECD method was developed and validated. The method was successfully applied for the determination of CPT in commercial and developed formulations. The method was found to be linear over the concentration range 2.0-60.0  $\mu\text{g/ml}$ . The precision of the method was measured at two levels: intra-day and inter-day precision and the % RSD values were less than 2%, which were less than the limits set in our laboratory. The method was accurate with RSD values less or equal to 2%. The content of CPT in commercial tablets was calculated as

an average from five determinations using ECD. Recoveries very close to 100% prove the suitability and accuracy of the proposed method.

To certify the quality of pharmaceutical formulation parameters such as interaction between the API and excipients to be used in formulation development studies, thermogravimetric and spectroscopic analysis were undertaken. The data generated in these studies revealed no serious incompatibility between the API and excipients. Based on the results from preliminary screening, all excipients except citric acid were selected for formulation development. Infrared spectroscopic studies confirmed the possibility of an interaction between CPT and citric acid. The DSC data generated for the different binary mixtures evaluated indicate that the characteristic endothermic peak of about 105.6 °C for CPT was present in all thermograms. This study demonstrates that DSC and FT-IR techniques can reveal potential interactions, whereas TG is not as sensitive to the presence of interactions. TG analysis revealed that the thermal degradation of CPT takes place in two major and one minor step, and that these occur in different temperature ranges. Each thermal degradation stage produced an endothermic peak on the DSC thermogram where the melting transition was observed prior to the commencement of decomposition. The theoretical basis of DSC/TGA and FT-IR experiments was examined and the overall goal providing practical guidelines for compatibility studies of CPT with several excipients was achieved.

In response to the challenges of formulating a CPT sustained-release dosage form, Eudragit<sup>®</sup>, Methocel<sup>®</sup> and Avicel<sup>®</sup> were studied, varying their quantities using RSM. The control of CPT release observed in this study indicates that hydrophilic matrix microcapsules of CPT manufactured using Eudragit<sup>®</sup> and Methocel<sup>®</sup>, can be used as a twice-a-day oral sustained release drug delivery system. The polymers, solvents and diluents all play a role in the formation of quality microcapsules. Moreover, optimization of microencapsulation conditions for CPT using RSM has been demonstrated. Input factors such as Eudragit<sup>®</sup> ( $X_1$ ), Methocel<sup>®</sup> K100M ( $X_2$ ) and Methocel<sup>®</sup> K15M ( $X_3$ ) content and homogenizing speed ( $X_4$ ) had an effect on the release of CPT from the microcapsules. Optimization was performed using a CCD approach to yield microcapsules that released more than 85% CPT in 12 h. The polynomial equation generated explained the quadratic and interaction effects of the input variables on the ultimate response observed. RSM is an appropriate approach as it allowed the estimation of parameters of a quadratic model, and it helped determine model fit. The approach presented in this study provides a useful guideline for the optimization of

microcapsule manufacture for other water-soluble drugs. The adequacy of the model was judged by ANOVA. However, the successful development of these delivery systems required careful consideration of a number of factors that influenced the performance of the formulations, including the physical and chemical properties of the API and excipients.

The microcapsules formed were spherical, with a more or less porous membrane. The absence of pores in other microcapsules was of major importance to this study in order to explain the drug release mechanism, since CPT diffusion occurs through water-filled cavities and is much faster than if diffusion were to take place through dense polymer networks. The rapid drug release observed during the early stages of testing are some of the challenges observed with microcapsules containing a freely water soluble drug such as CPT, are manufactured using this method of encapsulation.

The angle of repose for the CPT microcapsules was measured by the fixed-funnel method and ranged between 18-40°. This indicates that some microcapsules had poor flow properties, and the results were supported by Carr's Index and Hausner ratio. The addition of span 80 lowered the surface tension of the continuous phase and in turn decreased the sizes of microcapsules produced. When the stirring speed was increased, more air was entrapped and foam was produced. The use of an anti-foaming agent ensured that air bubbles were rapidly dissipated.

The technique of microencapsulation by oil-in-oil was used to prepare CPT microcapsules. The effects of polymer concentration, homogenizing speed, flow properties, morphology, surface properties and release characteristics of the prepared CPT microcapsules were examined. To decrease the complexity of the analysis and reduce cost, response surface methodology using best polynomial equations was successfully used to quantify the effect of the formulation variables and develop an optimized formulation, thereby minimizing the number of experimental trials.

There was a burst effect during the first stage of dissolution. SEM results indicated that this could be attributed to dissolution of CPT crystals present at the surface or embedded in the superficial layer of the matrix. During the preparation of microcapsules, the drug might have been trapped near the surface of the microcapsules or might have diffused quickly through the porous surface. The release data generated from the *in vitro* release studies were fitted to

various kinetic models such as Zero order, First order, Higuchi, Korsmeyer-Peppas, Kopcha and Makoid-Banakar. The release kinetics of CPT from most formulations followed classical Fickian diffusion mechanism. SEM photographs showed that diffusion took place through pores at the surface of the microcapsules. The Kopcha model diffusion and erosion terms showed predominance of diffusion relative to swelling or erosion throughout the entire test period. Drug release mechanism was also confirmed by Makoid-Banakar and Korsmeyer-Peppas models exponents. This further supports diffusion release mechanism in most formulations. The models postulate that the total of drug release is a summation of several mechanisms: burst release, relaxation induced controlled-release and diffusional release. These results suggest the potential application of Eudragit<sup>®</sup> / Methocel<sup>®</sup> microcapsules as suitable sustained-release drug delivery system for CPT.

Inspection of the 2D contour and 3D response surfaces allowed the determination of the geometrical nature of the surfaces and further provided results with regard to the interaction of the different variables used in CCD. The wide variation indicated that the factor combinations resulted in different drug release rates. Lagrange, canonical and mathematical modelling were used to determine the nature of the stationery point of the models. This represented the optimal variables or stationary points, which is the region of maximal response, by consecutively fitting the model in the experimental space. It is difficult to understand the shape of a fitted response by mere inspection of the algebraic polynomial when there are many independent variables in the model. Canonical and Lagrange analyses facilitated the interpretation of the surface plots after a mathematical transformation of the original variables into new variables.

In conclusion, the results show that pre-formulation studies, RSM including mathematical modeling, play a vital part in product development and formulation. High degree of prognosis obtained for CCD, Lagrange and Canonical analysis corroborates the finding that RSM and mathematical modelling are efficient tools in experimental design. Modeling and optimization was used to increase the efficiency of the formulation process used in this study and to determine the optimum formulation.

Beyond the present work performed with a water soluble drug, this process should be well adapted to other water soluble drugs. Future studies will focus on stability studies on the optimized formulation as per ICH guidelines.

## REFERENCES

---

1. T. A. Gaziano, K. Steyn, D.J. Cohen, M.C. Weinstein, L.H. Opie, Heart Disease in Africa, Cost Effectiveness analysis of Hypertension Guidelines in South Africa. Absolute Risk Versus Blood Pressure Level, *Circulation*, 112 (23) (2005) 3569-3576
2. R. Huang, E. Mendis, S. Kim, Improvement of ACE Inhibitory Activity of Chitooligosaccharides (COS) by Carboxyl Modification, *Bioorganic & Medicinal Chemistry*, 13 (11) (2005) 3649-3655
3. W. Cushman, M.A. Ondetti, History of the Design of Captopril and Related Inhibitors of Angiotensin Converting Enzyme, *Hypertension* 17 (1991) 589-592
4. C. G. Smith, J. R. Vane, The Discovery of Captopril, The *Federation of American Societies for Experimental Biology Journal*, 17 (2003) 788-789
5. M. J. Katovich, C. C. Barney, M. J. Fregly, R.E. McCaa. Effect of an Angiotensin Converting Enzyme Inhibitor (SQ 14,225) on  $\beta$ -adrenergic and Angiotensin-Induced Thirsts, *European Journal of Pharmacology*, 56 (1-2) (1979) 123-130
6. M. A. Ondetti, D. W. Cushman. Enzymes of the Renin-Angiotensin System and their Inhibitors, *Annual Review of Biochemistry*, 51(1982) 283-308
7. M.A. Ondetti, R.B. D.W. Cushman. Design of Specific Inhibitors of Angiotensin-Converting Enzyme: New Class of Orally Active Antihypertensive Agents, *Science*, 196 (4288) (1977) 441- 444
8. J.F. Riordan, Angiotensin-I-Converting Enzyme and its Relatives, *Genome Biology*, 4 (8) (2003) 225
9. T.A. Williams, P. Corvol, F. Soubrier, Identification of Two Active Site Residues in Human Angiotensin I-converting Enzyme, *The Journal of Biological Chemistry*, 269 (47) (1994) 29430-29434
10. T.A. Williams, A. Michaud, X. Houard, M.T. Chauvet, F. Soubrier, P. Corvol, Drosophila *Melanogaster* Angiotensin I-Converting Enzyme Expressed in *Pichia pastoris* Resembles the C Domain of the Mammalian Homologue and does not require Glycosylation for Secretion and Enzymic Activity, *Journal of Biochemistry*, 318 (1996) 125-131



11. H.M. Kim, D.R Shin, O.J. Yoo, H. Lee, J.O Lee, Crystal Structure of *Drosophila* Angiotensin I-Converting Enzyme Bound to Captopril and Lisinopril, *FEBS Letters*, 538 (1-3) (2003) 65-70
12. R. Natesh, S. L. U. Schwager, H. R. Evans, E. D. Sturrock, K. R. Acharya, Structural Details on the Binding of Antihypertensive Drugs Captopril and Enalaprilat to Human Testicular Angiotensin I-Converting Enzyme, *Biochemistry*, 43 (27) (2004) 8718-8724
13. R. Natesh, S.L. Schwager E. D.Sturrock, K. R. Acharya. Crystal Structure of the Human Angiotensin-Converting Enzyme-Lisinopril Complex, *Nature*, 421 (6922) (2003) 551-554
14. H. Ooi. W.S. Colucci, J.G. Hardman, L.E. Limbird, A.G. Gilman, Pharmacological treatment of heart failure, *The Pharmacological Basis of Therapeutics* (10th ed), (2001) 910
15. A.Gupta, S.K. Prajapati, M. Singh, M. Balamurugan, Proniosomal Powder of Captopril, Formulation and Evaluation, *Molecular Pharmaceutics*, 4 (4) (2007) 596-599
16. Katzung, B., *Basic and Clinical Pharmacology*, 7<sup>th</sup> Ed., (Appleton & Lang. Stamford, CT), (1989)
17. A.O. Nu, J.S. Zhang, Recent Progress in Sustained/Controlled Oral Delivery of Captopril: An Overview, *International Journal of Pharmaceutics*, 194 (2) (2000) 139-146
18. H.Y. Aboul-Enein, I.W. Wainer. *The Impact of Stereochemistry on Drug Development and Use*, Wiley, New York, 1997
19. M. Joshaghani, M.B. Gholivand, A.R. Mosavat, Chelation Study of Captopril with Cd<sup>2+</sup> and Pb<sup>2+</sup> Ions, *American Journal of Biochemistry and Biotechnology*, 4 (3) (2008) 245-249
20. H.Y. Aboul-Enein, A. A. Al Badr, S.E. Ibrahim, K. Florey, *Analytical Profiles of Drug Substances* Vol. 10, Academic Press, New York (1981) 665. (15<sup>th</sup> Ed.)
21. *International Pharmacopea-WHO*, 205(2006) 4<sup>th</sup> Edition Vol 1, Geneva,
22. P.J. Worland O.H. Drummer, B. Jarrott. Gastric and Intestinal Absorption of Captopril in Acutely and Chronically Treated Rats: Comparison with Salicylic Acid, *Journal of Pharmaceutical Sciences*, 73 (12) (1984)1755-1758

23. R. O. Macêdo, T. Gomes do Nascimento, C. F. Soares Aragão, A. P. Barreto Gomes, Application of Thermal Analysis in The Characterization of Anti-hypertensive Drugs, *Journal of Thermal Analysis and Calorimetry*, 59 (3), (2000) 657-661
24. R. R. Chirumamilla, R Marchant, P Nigam, Captopril and its Synthesis from Chiral Intermediates, *Journal of Chemical Technology & Biotechnology*, 76 (2) (2000) 123-127
25. D. W. Cushman, H. S. Cheung, E. F. Sabo, M. A. Ondetti, Design of Potent Competitive Inhibitors of Angiotensin-Converting Enzyme. Carboxyalkanoyl and Mercaptoalkanoyl Amino Acids, *Biochemistry*, 16 (25) (1977) 5484-5491
26. M. Shimazaki, J. Hasegawa, K. Kan, K. Nomura, Y. Nose, H. Kondo, T. Ohashi, K. Watanabe, Synthesis of Captopril Starting from an Optically Active  $\beta$ -hydroxy Acid, *Chemical and Pharmaceutical Bulletin*, 30 (9) (1982) 3139-3146
27. J. Hasegawa, M. Ogura, S. Hamaguchi, M. Shimazaki, H. Kawaharada, K. Watanabe, Stereospecific Conversion of Isobutyric acid to D- $\beta$ -Hydroxyisobutyric Acid by Microorganism. *Journal of Fermentation Technology*, 59 (1981) 203-208
28. H. M. Ogura, H. Kanema, N. Noda, H. Kawaharada, K. Watanabe, Production of D- $\beta$ -Hydroxyisobutyric Acid by *Candida rugosa* and its Mutant, *Journal of Fermentation Technology*, 60 (1982) 501-508
29. D. H. Nam, C. S. Lee, Dewey D. Y. Ryu, An Improved Synthesis of Captopril, *Journal of Pharmaceutical Sciences*, 73 (12) (1984) 1843-1844
30. S. Groszkowski, J. Sienkiewicz, L. Najman, Synthesis of Halogen-Acylated Di-substituted Derivatives of Piperazine, *Farmacia*, 15 (1967) 263
31. S.H. Pine, J.B. Hendrickson, C.J. Cram, G.S. Hammond, 'Organic Chemistry', 4<sup>th</sup> Edition., McGraw-Hill, New York, N.Y., 1980
32. C. Hongo, M. Shibazaki, S. Yamada, I. Chibata, Preparation of Optically Active Proline. Optical Resolution of N-acyl-DL-Proline by P referential Crystallization Procedure, *Journal of Agricultural and Food Chemistry*, 24 (5) (1976) 903-906

33. A.J. Nordmann, M. Krahm, A.G. Logan, C. Naglie, A.S. Detsky, The Cost Effectiveness of ACE Inhibitors as First-Line Antihypertensive Therapy, *Pharmaco Economics*, 21(8) (2003) 573-585
34. R. Janknegt, .A.M. Van Schaikb, J. Smits, W. De Leeuw, ACE inhibitors and Angiotension II Antagonists for the Treatment of Hypertension: Drug Selection by Means of the SOJA Method, *South African Medical Journal*, May (NS) (1999) 1-8
35. W. O. Foye, T.L. Lemke, D. A. Williams, (eds). Foye's Principles of Medicinal Chemistry, 5th Ed. Baltimore: Lippincott Williams and Wilkins, (2002)
36. S. Oparil, T. Koerner, G.W. Tregar, B.A. Barnes, E. Haber. Substrates Requirements for Angiotensin I Conversion In vivo and In vitro. *Circulation Research*, 32 (4) (1973) 415-423
37. A.A. Patchett, E. Harris, E.W. Tristram, M.J. Wyvratt, M.T. Wu, D. Taub, E.R. Peterson, T.J. Ikeler, J. ten Broeke, L.G. Payne, D.L. Ondeyka, E. D. Thorsett, W.J. Greenlee, N.S. Lohr, R.D. Hoffsommer, H. Joshua, W.V. Ruyle, J.W. Rothrock, S.D. Aster, A.L. Maycock, F.M. Robinson, R. Hirschmann, C.S. Sweet, E.H. Ulm, D.M. Gross, T.C. Vassil, C.A. Stone, A New Class of Angiotensin-Converting Enzyme Inhibitors, *Nature*, 288 (5788) (1980) 280-283
38. O.B. Holland, L. von Kuhnert, W.B. Campbell, R.J. Anderson, Synergistic Effect of Captopril with Hydrochlorothiazide for the Treatment of Low-Renin Hypertensive Black Patients, *Hypertension*, 5 (1983) 235-239
39. R. I. Stefan, J.F. van Staden, H.Y. Aboul-Enein, Simultaneous Detection of S and R Captopril Using Sequential Injection Analysis, *Talanta*, 51(2000) 969-975
40. W. H. Brown, C. S. Foote, B. L. Iverson, E.V. Organic Chemistry, Anslyn. Brookes Cole, 5<sup>th</sup> Ed. Belmont, CA, 94002-3098, USA., 2008
41. I. Jiménez-Martínez, A.M. Domínguez-Ramírez, L. Villafuerte-Robles, Effect of Antioxidants on Captopril Floating Matrices, *Pharmaceutical Development and Technology*, (2009) 1-11
42. A.O Nur, J.S. Zhang, Captopril Floating and/or Bioadhesive Tablets: Design and Release Kinetics, *Drug Development and Industrial Pharmacy*, 26 (9), (2000) 965-969

43. W.T Cheng, S.L. Wang, S.Y. Lin, Solid-State Interaction Study on the Captopril/ Lubricants Systems Accelerated by Grinding Process, *Journal of Physics and Chemistry of Solids*, 69 (4) (2008) 1007-1016
44. Y. B. Huang, Y. H. Tsai, J. S. Chang, J. C. Liu, M. J. Tsai, P. C. Wu, Effect of Antioxidants and Anti-irritants on the Stability, Skin Irritation and Penetration Capacity of Captopril Gel, *International Journal of Pharmaceutics*, 241 (2) (2002) 345-351
45. B. H. Migdalof, M. J. Antonaccio, D.N. McKinstry, S. M. Singhvi, S.J. Lan, P. Egli, K. J. Kripalani, Captopril: Pharmacology, Metabolism and Disposition, *Drug Metabolism Reviews*, 15 (4) (1984) 841-869
46. B. Jackson, D. Maher, P. G. Matthews, B. P. Mcgrath, C. I. Johnston, Lack of Cross Sensitivity Between Captopril and Enalapril, *Internal Medicine Journal*, 18 (1) (2008) 21-27
47. I. Jaffe, Adverse Effects Profile of Sulfhydryl Compounds in Man, *The American Journal of Medicine*, 80 (3) (1986) 471-476
48. N. Sultana, M.S. Arayne, R.U. Quraishi, In Vitro Interactions of Captopril with NSAID's, *Pakistan Journal of Pharmaceutical Sciences*, 19 (3) (2006) 202-207
49. O. Kirimli, S. Kalkan, S. Guneri, Y. Tuncok, B. Akdeniz, M. Ozdamar, H. Guven, The Effects of Captopril on Serum Digoxin Levels in Patients with Severe Congestive Heart Failure, *International Journal of Clinical Pharmacology and Therapeutics*, 39 (7) (2001) 311-314
50. C. Richer, M. Bah, M. Cadilhac, C. Thuillez, J.F. Giudicelli, Cimetidine Does Not Alter Free Unchanged Captopril Pharmacokinetics and Biological Effects in Healthy Volunteers, *Journal of Pharmacology*, 17 (3) (1986) 338-342
51. N. Sultana, M.S. Arayne, R. Quraish, In vitro Interactions of Captopril with H<sub>2</sub>-Receptor Antagonists, *Pakistan Journal of Pharmaceutical Sciences*, 20 (2) (2007) 132-139
52. R. Gugler, H. Allgayer, Effects of Antacids on the Clinical Pharmacokinetics of Drugs. An Update, *Clinical Pharmacokinetics*, 18 (3) (1990) 210-219
53. P.F. Broughton, S.R. Turner, E.M. Symonds, Possible Risk with Captopril in Pregnancy. Some

Animal Data, *Lancet*, 1 (8180) (1980) 1256

54. I.M. Keith, J.A. Will, E.K. Weir, Captopril: Association with Fetal Death and Pulmonary Vascular Changes in the Rabbit. *Proceedings of the Society for Experimental Biology and Medicine*, 170 (3) (1982) 378-383

55. A. Shrim, H. Berger, J. Kingdom, A. Hamoudi, , P.S. Shah, G. Koren, Prolonged Exposure to Angiotensin-Converting Enzyme Inhibitors During Pregnancy, Fetal Toxicity could be Reversible, *Canadian Family Physician*, 51(10) (2005) 1335-1337

56. M.J. Boutroy, P. Vert, B.H. Ligny, A. Miton, Captopril Administration in Pregnancy Impairs Fetal Angiotensin Converting Enzyme Activity and Neonatal Adaptation, *Lancet*, 2 (8408) (1984) 935-936

57. R. Fiochi, P. Lijnen, R. Fagard, J. Staessen, A. Amery, F. Van Assche, B. Spitz, M. Rademaker, Captopril During Pregnancy, *Lancet*, 2 (8412) (1984) 1153

58. N.D. Binder, J.J. Faber, Effects of Captoril on Blood Pressure, Placental Blood Flow and Uterine Oxygen Consumption in Pregnant Rabbits, *Journal of Pharmacology and Experimental Therapeutics*, 260 (1992) 294-299

59. E.R. Lumbers, N.M. Kingsford, R.I. Menzies, A.D. Stevens. Acute Effects of Captopril, an Angiotensin-Converting Enzyme Inhibitor, on the Pregnant Ewe and Fetus, *American Journal of Physiology*, 262 (1992) R754-R760

60. T.F. Ferris, E.K. Weir EK, Effect of Captopril on Uterine Blood Flow and Prostaglandin E Synthesis in the Pregnant Rabbit, *The Journal of Clinical Investigation*, 71 (1983) 809-815

61. I. R. Soares De Moura, M.A. Cerqueira Lopes, Effects of Captopril on the Human Foetal Placental Circulation: an Interaction with Bradykinin and Angiotensin, *British Journal of Clinical Pharmacology*, 39 (1995) 497-501

62. G.G. Briggs, R.K. Freeman, S.J. Yaffe. *Drugs in Pregnancy and Lactation*, Baltimore, MD, Williams and Wilkins; 1994

63. R.L. Brent, D.A. Beckman, Angiotensin-Converting Enzyme Inhibitors, an Embryopathic Class of Drugs with Unique Properties: Information for Clinical Teratology Counselors, *Teratology*, 43 (1991)

64. P.C. Duminy, P.T. Burger, Fetal Abnormality Associated with the Use of Captopril During Pregnancy, *South African Medical Journal*, 60 (1981) 805
65. S.G. Kaler, M.E. Patrinos and G.H. Lambert, Hypertrichosis and Congenital Anomalies Associated with Maternal use of Minoxidil, *Pediatrics*, 79 (1987) 434-436
66. A.D. Rothberg, R. Lorenz, Can Captopril Cause Fetal and Neonatal Renal Failure? *Pediatric Pharmacology*, 4 (1984) 189-192
67. S.L. Nightingale, Warnings on the Use of ACE Inhibitors in Second and Third Trimester of Pregnancy, *The Journal Of The American Medical Association*, 267 (1992) 2445
68. A. Tarcan, B. Gürakan, N. Özbek. Captopril-Induced Pancytopenia in a Premature Newborn, *Journal of Paediatrics and Child Health*, 40 (7) (2004) 404-405
69. M.L. Tuck, L.A. Katz, W.M. Kirkendall, P.R. Koeppe, G.E. Ruoff, D.G. Sapor, Low-dose Captopril in Mild to Moderate Geriatric Hypertension, *Journal of The American Geriatric Society*, 34(10) (1986) 693-696
70. M.M. Ottesen, R. Worck, H. Ibsen. Captopril Does Not Blunt the Sympathoadrenal Response to Cigarette Smoking in Normotensive Humans, *Blood Pressure*, 6 (1) (1997) 29-34
71. M.E. Shannon, S.E. Malecha, A. J. Cha, Angiotensin Converting Enzyme Inhibitors (ACEIs) and Angiotensin II. Receptor Blockers (ARBs) and Lactation, An Update, *Journal of Human Lactation*, 16 (2) (2000) 152-155
72. W.B. White, Management of Hypertension During Lactation, *Hypertension*, 6 (1984) 297-300
73. David B. Troy, Paul Beringer, Remington: The Science and Practice of Pharmacy, 21<sup>st</sup> Ed. Lippincott Williams & Wilkins, 2005
74. K.L. Duchin, S.M. Singhvi, D.A. Willard, B.H. Migdalof, D.N. McKinsrty, Captopril Kinetics, *Clinical Pharmacology and Therapeutics*, 31 (1982) 452-458

75. K.J. Kripalani, D.N. McKinstry, S.M. Singhvi, D.A. Willard, R.A. Vukovich, B.H. Migdalof, Disposition of Captopril in Normal Subjects, *Clinical Pharmacology and Therapeutics*, 27 (1980) 636-641
76. K. Onoyama, H. Hirakata, K. Iseki, S. Fujimi, T. Omae, M. Kobayashi, Y. Kawahara, Blood Concentration and Urinary Excretion of Captopril (SQ 14,225) in Patients with Chronic Renal Failure, *Hypertension*, 3 (1981) 456-459
77. B.C. Campbell, A.N. Shephard, H.I. Elliot, R. McClean, J.L. Reid, Prolonged Converting Enzyme Inhibition Following Captopril in Patients with renal insufficiency, *British Journal of Clinical Pharmacology*, 13 (1982) 755-757
78. L. K. Duchin, A. M. Pierides, A. Heald, S. M. Singhvi, A. J. Rommel, Elimination Kinetics of Captopril in Patients with Renal Failure, *Kidney International*, 25 (1984) 942-947
79. K.J. Kripalani, D.N. McKinstry, S.M. Singhvi, D.A. Willard, R.A. Vukovich and B.H. Migdalof. Disposition of captopril in normal subjects, *Clinical Pharmacology and Therapeutics*, 27 (5) (1980) 636-641
80. A. Jankowski, A. Skorek, K. Krzysko, P.K. Zarzycki, R.J. Ochoka, H. Lamparczyk, Captopril: Determination in Blood and Pharmacokinetics After Single Oral Dose, *Journal of Pharmaceutical and Biomedical Analysis*, 13 (4/5) (1995) 655-660
81. S.Y. Lin, Y.S. Wei, M.J. Li, S.L. Wang, Effect of Ethanol or/and Captopril on the Secondary Structure of Human Serum Albumin before and after Protein Binding, *European Journal of Pharmaceutics and Biopharmaceutics*, 57 (3) (2004) 457-464
82. K.L. Duchin, D.N. McKinstry, A.I. Cohen, B.H. Migdalof, Pharmacokinetics of Captopril in Healthy Subjects and in Patients with Cardiovascular Diseases, *Clinical Pharmacokinetics*, 14 (4) (1988) 241-259
83. O. H. Drummer, P. Miach, B. Jarrott, S-Methylation of Captopril: Demonstration of Captopril Thiol Methyltransferase Activity in Human Erythrocytes and Enzyme Distribution in Rat Tissues, *Biochemical Pharmacology*, 32 (10) (1983) 1557-1562
84. M.A. Ferroni, P.C. Giulianotti, A. Pietrabissa, F. Mosca, R. Gomeni, G.M. Pacifici. Captopril

Methylation in Human Liver and Kidney: Interindividual Variability, *Xenobiotica*, 26 (8) (1996) 877-882

85. G. M. Pacifici, S. Santerini, L. Giuliani, Methylation of Captopril in Human Liver, Kidney and Intestine, *Xenobiotica*, 21(9) (1991)1107-1112

86. G. Karimian, A. Mohammadi-Karakani, M. Sotoudeh, M. Ghazi-Khansari, G. Ghobadi, B. Shakiba. Attenuation of Hepatic Fibrosis Through Captopril and Enalapril in the Livers of Bile Duct Ligated Rats, *Biomedicine and Pharmacotherapy*, 62 (5) (2008) 312-316

87. K. Onoyama, H. Hirakata, K. Iseki, S. Fujimi, T. Omae, M. Kobayashi, Y. Kawahara, Blood Concentration and Urinary Excretion of Captopril (SQ 14,225) in Patients with Chronic Renal Failure, *Hypertension*, 3 (1981) 456-459

88. U. Holzgrabe, I. Wawer, B. Dielil, NMR Spectroscopy in Drug Development and Analysis, *Talanta*, 52 (2) (2000) 361-362

89. M. Pellecchia, D.S. Sem, K. Wüthrich, NMR in Drug Discovery, *Nature Reviews Drug Discovery*, 1 (2002) 211-219

90. V. S. Kartashov, Structure of Chemical Compounds, Methods of Analysis and Process of Control. Current State and Prospects of NMR Spectroscopy Application in Pharmaceutical Analysis (A Review), *Pharmaceutical Chemistry Journal*, 30 (5) (1996) 346-350

91. O. V. Vishnevskii, Yu. M. Volovenko, A. A. Kudryavtsev, V. M. Ovrutskii, Identification and Quality Control of the Drug Diutsifon and its Semiproduct using the <sup>1</sup>H NMR Technique, *Pharmaceutical Chemistry Journal*, 32 (8) (1998) 454-456

92. H. Metz, K. Mäder, Benchtop-NMR and MRI-A new Analytical Tool in Drug Delivery Research, *International Journal of Pharmaceutics*, 364 (2) (2008) 170-175

93. P. Soininen, K. Öörni, H. Maaheimo, R. Laatikainen, P. T. Kovanen, K. Kaski, M. Ala-Korpela, <sup>1</sup>H NMR at 800 MHz Facilitates Detailed Phospholipid follow-up during Atherogenic Modifications in Low Density Lipoproteins, *Biochemical and Biophysical Research Communications*, 360 (1) (2007) 290-294



94. B.O. Petersen, E. Vinogradov, W. Kay, P. Würtz, N. T. Nyberg, J. Ø. Duus, O. W. Sørensen, H2BC: A New Technique for NMR Analysis of Complex Carbohydrates, *Carbohydrate Research*, 341(4) (2006) 550-556
95. B. Laignel, C. Bliard, G. Massiot, J. M. Nuzillard, Proton NMR Spectroscopy Assignment of D-Glucose Residues in Highly Acetylated Starch, *Carbohydrate Research*, 298 (4) (1997) 251-260
96. C. D. Blundell, M. A. C. Reed, M. Overduin, A. Almond, NMR Spectra of Oligosaccharides at Ultra-High Field (900 MHz) have Better Resolution than Expected due to Favourable Molecular Tumbling, *Carbohydrate Research*, 341(12) (2006) 1985-1991
97. S. M. Ali, A. Maheshwari, F. Asmat, M. Koketsu, Complexation of Enalapril Maleate with  $\beta$ -Cyclodextrin: NMR Spectroscopic Study in Solution, *Química Nova*, 29 (4) (2006) 685-688
98. Y. Sakamoto, T. Ishi, Conformational Studies by  $^1\text{H}$  and  $^{13}\text{C}$  NMR of Lisinopril, *Journal of Molecular Structure*, 298 (1-2), (1993) 129-136
99. Ch. Döbler, U. Schmidt, H. W. Krause, H. -J. Kreuzfeld, M. Michalik, Enantioselective Hydrogenation Using a Rigid Bicyclic Aminophosphine Phosphinite Ligand, *Tetrahedron: Asymmetry*, 6 (2) (1995) 385-388
100. J. Li, Y. Guo, Z. George, The Solid-State Stability of Amorphous Quinapril in the Presence of  $\beta$ -Cyclodextrins, *Journal of Pharmaceutical Sciences*, 91 (1) (2002) 229-243
101. J.P. Bouchet, J.P. Volland, M. Laubie, M. Vincent, B. Marchand, N. Platzter, Stereochemistry-Activity Relationships of ACE Inhibitors. Conformational Studies by  $^1\text{H}$  and  $^{13}\text{C}$  NMR of Perindopril and Selected Stereoisomer's, *Magnetic Resonance in Chemistry*, 30 (12) (1992) 1186-1195
102. V. R. Shinde, A. Trivedi, P.R. Upadhayay, N.L. Gupta, D.G. Kanase, R. C. Chikate, Isolation and Characterization of Benazepril unknown Impurity by Chromatographic and Spectroscopic Methods, *Journal of Pharmaceutical and Biomedical Analysis*, 42 (3) (2006) 395-399
103. C. Y. Chang, T. K. Yang, Asymmetric Synthesis of ACE Inhibitor-Benazepril HCl via a Bioreductive Reaction, *Tetrahedron: Asymmetry*, 14 (15) (2003) 2239-2245
104. V.R. Shinde, A. Trivedi, P.R. Upadhayay, .L. Gupta, D.G. Kanase, C.R. Chikate, Isolation and Characterization of Benazepril unknown Impurity by Chromatographic and Spectroscopic Methods, *Journal of Pharmaceutical and Biomedical Analysis*, 42 (3) (2006) 395-399

105. L. Yu, J. Huang, C. Chang, T. Yang, Formal Synthesis of the ACE Inhibitor Benazepril·HCl via an Asymmetric Aza-Michael Reaction, *Molecules*, 11 (8) (2006) 641-648
106. F. Li, H. Zhang, L. Jiang, W. Zhang, J. Nie, Y. Feng, M. Yang, M. Liu, Dynamic NMR Study and Theoretical Calculations on the Conformational Exchange of Valsartan and Related Compounds, *Magnetic Resonance in Chemistry*, 45(11) (2007) 929-36
107. E. Theodoropoulou, D. Marsh, Effect of Angiotensin II Non-Peptide AT<sub>1</sub> Antagonist Losartan on Phosphatidylethanolamine Membranes, *Biochimica et Biophysica Acta (BBA)-Biomembranes*, 1509 (1-2) (2000) 346-360
108. M. Bauer, R. K. Harris,(the late) R. C. Rao, D. C. Apperley, C. A. Rodger, NMR Study of Desmotropy in Irbesartan, a Tetrazole-Containing Pharmaceutical Compound, *Journal of Chemical Society, Perkin Transaction 2*, 3 (1998) 475-481
109. T. Ebner, G. Heinzl, A. Prox, K. Beschke, H. Wachsmuth, Disposition and Chemical Stability of Telmisartan 1-O-Acylglucuronide, *Drug metabolism and Disposition*, 27 (10) (1999) 1143-1149
110. A. Mohan, S. Shanmugavel, A. Goyal, B. R. Venkataraman, D. Saravanan, Identification, Isolation, and Characterization of Five Potential Degradation Impurities in Candesartan Cilexetil Tablets, *Chromatographia*, 69 (11-12) (2009) 1-10
111. P. Zoumpoulakis, S. G. Grdadolnik, J. Matsoukas, T. Mavromoustakos, Structure Elucidation and Conformational Properties of Eprosartan a Non peptide Angiotensin II AT<sub>1</sub> Antagonist, *Journal of Pharmaceutical and Biomedical Analysis*, 28 (1) (2002) 125-135
112. M. M.A. Hassa, Application of Instrumental Analysis in Drug Quality Assurance, *Proceedings of the 2<sup>nd</sup> Drug Symposium SA. Pharmaceutical and Developing Countries*, (1982) 329-355
113. P. Giraudeau, N. Guignard, E. Hillion, E. Baguet, S. Akoka, Optimization of Homonuclear 2D NMR for Fast Quantitative Analysis: Application to Tropine-Nortropine Mixtures, *Journal of Pharmaceutical and Biomedical Analysis*, 43 (4) (2007) 1243-1248
114. S. Naylor, R. P. Mason, J. K. Sanders, D. H. Williams, G. Moneti, Formaldehyde Adducts of Glutathione. Structure Elucidation by Two-Dimensional NMR Spectroscopy and Fast-Atom-Bombardment Tandem Mass Spectrometry, *Biochemical Journal*, 249 (2) (1988) 573-579

115. M. Frank, J. Harald, Purity Assessment Problem in Quantitative NMR-Impurity Resonance Overlaps with Monitor Signal Multiplets from Stereoisomers, *Analytical and Bioanalytical Chemistry*, 385 (4) (2006) 760-765
116. M. Ala-Korpela, Potential Role of Body Fluid  $^1\text{H}$  NMR Metabonomics as a Prognostic and Diagnostic Tool, *Expert Review of Molecular Diagnostics*, 7 (6) (2007) 761-773
117. V.P. Mäkinen, P. Soininen, C. Forsblom, M. Parkkonen, P. Ingman, K. Kaski, P.H. Groop, M. Ala-Korpela, Diagnosing Diabetic Nephropathy by  $^1\text{H}$  NMR Metabonomics of Serum, *Magma*, 19(6) (2006) 281-296
118. G. Girjesh, Metabonomics: A new Frontier of Nuclear Magnetic Resonance (NMR), *National Academy Science Letters*, 27(9-10) (2004) 289-299
119. J. R. Smith, W. Xu, D. Raftery, Analysis of Conformational Polymorphism in Pharmaceutical Solids Using Solid-State NMR and Electronic Structure Calculations, *The Journal of Physical Chemistry B*, 110 (15) (2006) 7766-7776
120. R.K. Harris, Applications of Solid-State NMR to Pharmaceutical Polymorphism and Related Matters, *Journal of Pharmacy and Pharmacology*, 59 (2) (2007) 225-239
121. N. E. Jacobsen, Fundamentals of NMR Spectroscopy in Liquids, in: NMR spectroscopy explained. Simplified Theory, Applications and Examples for Organic Chemistry and Structural Biology, Wiley-Interscience, 2007
122. P. Bigler, R. Brenneisen, Improved Impurity Fingerprinting of Heparin by High Resolution  $^1\text{H}$  NMR Spectroscopy, *Journal of Pharmaceutical and Biomedical Analysis*, 49 (4) (2009) 1060-1064
123. U. Holzgrabe, B. W. K. Diehl, I. Wawer, NMR Spectroscopy in Pharmacy, *Journal of Pharmaceutical and Biomedical Analysis*, 17 (4-5) (1998) 557-616
124. F. Malz, H. Jancke, Quantitative NMR Spectroscopy - Principles and Applications. Validation of Quantitative NMR, *Journal of Pharmaceutical and Biomedical Analysis*, 38 (5) (2005) 813-823
125. C. D. Blundell, M. A.C. Reed, M. Overduin, A. Almond, NMR Spectra of Oligosaccharides at Ultra-High Field (900 MHz) have better Resolution than expected due to Favourable Molecular Tumbling, *Carbohydrate Research*, 341 (12) (2006) 1985-1991

126. M. Cemazar, D.K. Craik, (2006). NMR and Structural Genomics in the Pharmaceutical Sciences. In Graham A Webb (Ed.), *Modern Magnetic Resonance Part 2: Applications in Medical and Pharmaceutical Sciences* 1<sup>st</sup> ed. Netherlands: Springer
127. S. Trefi, V. Gilard, S. Balayssac, M. Malet-Martino, R. Martino, Quality Assessment of Fluoxetine and Fluvoxamine Pharmaceutical Formulations Purchased in Different Countries or via the Internet by <sup>19</sup>F and 2D DOSY <sup>1</sup>H NMR, *Journal of Pharmaceutical and Biomedical Analysis*, 46 (4) (2008) 707-722
128. I.I. Rabi, J.R. Zacharias, S. Millman, P. Kusch (1938). "A New Method of Measuring Nuclear Magnetic Moment", *Journal of Magnetic Resonance Imaging*, 2 (2) (1992)131-133
129. K. L. Ratzlaff, Development of a Fourier Transform NMR Instrument Simulator, *Journal of Chemical Information and Computer Sciences*, 33 (1993) 303-309
130. M. Bauer, A. Bertario, G. Boccardi, X. Fontaine, R. Rao, D. Verrier, Reproducibility of <sup>1</sup>H-NMR Integrals: A Collaborative Study, *Journal of Pharmaceutical and Biomedical Analysis*, 17 (3) (1998) 419-425
131. L. Yu, S. M. Reutzel, G. A. Stephenson, Physical Characterization of Polymorphic Drugs: An Integrated Characterization Strategy, *Pharmaceutical Science and Technology Today*, 1 (3) (1998) 118-127
132. D. Giron, Use of DSC Robotic Systems in Pharmaceutical Analysis, *Journal of Thermal Analysis and Calorimetry*, 35 (6) (1989) 1801-1814
133. M.A. Palacio, S. Cuffini, R. Badini, A. Karlsson, S.M. Palacios, Solid-State Characterization of Two Polymorphic Forms of *R*-Albuterol Sulphate, *Journal of Pharmaceutical and Biomedical Analysis*, 43 (4) (2007) 1531-1534
134. T. Kojima, Y. Yamauchi, S. Onoue, Y. Tsuda, Evaluation of Hydrate Formation of a Pharmaceutical Solid by Using Diffuse Reflectance Infrared Fourier-Transform Spectroscopy, *Journal of Pharmaceutical and Biomedical Analysis*, 46 (4) (2008) 788-791
135. G. Wu, K. Yamada, Residual dipolar couplings in MAS and MQMAS NMR spectra of quadrupolar nuclei, *Chemical Physics Letters*, 313 (3-4) (1999) 519-524

136. K. Castro, S. Pessanha, N. Proietti, E. Princi, D. Capitani, M. L. Carvalho, J. M. Madariaga, Noninvasive and Nondestructive NMR, Raman and XRF Analysis of a Blaeu Coloured Map from the Seventeenth Century, *Analytical and Bioanalytical Chemistry*, 391 (1) (2008) 433-441
137. R. K. Harris, P. Hodgkinson, T. Larsson, A. Muruganantham, Quantification of Bambuterol Hydrochloride in a Formulated Product Using Solid-State NMR, *Journal of Pharmaceutical and Biomedical Analysis*, 38 (5) (2005) 858-864
138. M. Kainosho, T. Torizawa, Y. Iwashita, T. Terauchi, A. M. Ono, P. Güntert, Optimal isotope labelling for NMR protein structure determinations, *Nature*, 440 (2006) 52-57
139. B. Coxon, N. Sari, G. Batta, V. Pozsgay, NMR Spectroscopy, Molecular Dynamics, and Conformation of a Synthetic Octasaccharide Fragment of the O-Specific Polysaccharide of *Shigella dysenteriae* Type 1, *Carbohydrate Research*, 324 (1) (2000) 53-65
140. R.T. Berendt, D. M. Sperger, E. J. Munson, P. K. Isbester, Solid-state NMR Spectroscopy in Pharmaceutical Research and Analysis, *Trends in Analytical Chemistry*, 25(10) (2006) 977-984
141. D. Hine, J. Kapeleris, Innovation and Entrepreneurship in Biotechnology, an International Perspective, Concepts, Theories and Cases, Edward Elgar Publishing, 2006
142. W. Jiskoot, D. J. A. Crommelin, Methods for Structural Analysis of Protein Pharmaceuticals, AAPS Press. Arlington, VA 2005
143. Y. Zou, N. Inoue, Calculation of  $^7\text{Li}$  MAS NMR Chemical Shift in  $\text{La}_{4/3-y}\text{Li}_{3y}\text{Ti}_2\text{O}_6$ , *Ionics*, 12 (2006) 185-189
144. W.E. Lamb, Internal Diamagnetic Fields, *Physical Review*, 60 (1941) 817-819
145. N.F. Ramsey, Magnetic Shielding of Nuclei in Molecules, *Physical Review*, 78 (1950) 699
146. N.F. Ramsey, Chemical Effects in Nuclear Magnetic Resonance and in Diamagnetic Susceptibility, *Physical Review*, 86 (1952) 243-246
147. U. Holzgrabe, I. Wawer, W. Jiskoot, D. J. A. Crommelin (Ed.), NMR Spectroscopy in Drug Development and Analysis: Methods for Structural Analysis of Protein Pharmaceuticals, 2005

148. P. Novak, P. Tepeš, I. Fistrić, I. Bratoš, V. Gabelica, The Application of LC–NMR and LC–MS for the Separation and Rapid Structure Elucidation of an Unknown Impurity in 5-Aminosalicylic acid, *Journal of Pharmaceutical and Biomedical Analysis*, 40 (5) (2006) 1268-1272
149. H. Kadin. In K. Florey (ed.), *Analytical Profiles of Drug Substances*, Vol. 11, Academic Press, New York, 1982
150. V. Caplar, S. Rendic, F. Kajfez, H. Hofman, J. Kuftinec, Physico-chemical and Analytical Characteristics of Captopril, *Acta Pharmaceutica Jugoslavia*, 32 (1982) 125-136
151. H. G. Brittain, H. Kadin, Ultraviolet Absorption and Circular Dichroism Spectra of Captopril, *Pharmaceutical Research*, 7(10), (1990) 1082-1085
152. B. Lin, X. C. Zhan, L. L. Li, C. R. Li, H. J. Qi, J. L. Tao, Step Nonisothermal Method in Kinetics Studies of Captopril Oxidation under Compressed Oxygen, *Akugaku Zasshi*, 128 (4) (2008) 617-624
153. J. P. Barton, J. E. Packer, and R. J. Sims, Kinetics of the reaction of hydrogen peroxide with cysteine and cysteamine, *Journal of the Chemical Society Perkin Transactions*, 2 (314) (1973) 1547-1549
154. L. Pecci, G. Montefoschi, G. Musci, D. Cavallini, Novel Findings on the Copper Catalysed Oxidation of Cysteine, *Amino Acids*, 13 (1997) 355-367
155. D. Cavallini, C. De Marko, S. Dupre, Luminol Chemiluminescence Studies of the Oxidation of Cysteine and other Thiols to Disulfides, *Archives of Biochemistry and Biophysics*, 124 (1968) 18
156. A. Bagiyan, I.K. Koroleva, N.V. Soroka, A.V. Ufimtsev, Oxidation of Thiol Compounds by Molecular Oxygen in Aqueous Solutions, *Russian Chemical Bulletin, International Edition*, 52 (5) (2003) 1135-1141
157. D. Wishart, Nuclear Magnetic Resonance Spectroscopy, in : Wim Jiskoot, D. J. A. Crommelin, *Methods for Structural Analysis of Protein Pharmaceuticals*, AAPS Press, Arlington, 2005
158. N.E. Jacobsen, Inverse Heteronuclear 2D Experiments: HSQC, HMQC, AND HMBC, in Neil E. Jacobsen (Ed.), *NMR Spectroscopy Explained. Simplified Theory, Applications and Examples for Organic Chemistry and Structural Biology*, Wiley-Interscience, 2007

159. B. A. Dawson, D. B. Black, G. A. Neville, Papers from the fifth international symposium on Pharmaceutical and Biomedical Analysis. Multinuclear NMR ( $^1\text{H}$ ,  $^{13}\text{C}$  and  $^{19}\text{F}$ ) Spectroscopic Re-examination of the Solvolytic Behaviour of Flurazepam Dihydrochloride, *Journal of Pharmaceutical and Biomedical Analysis*, 13 (4-5) (1995) 395-407
160. T. Kuwayama, S. Kato, T. Yashiro. The Behavior of 1, 4-benzodiazepine Drugs in Acidic Media. VII. Carbon-13 Nuclear Magnetic Resonance Spectra of Flurazepam in Acidic Aqueous Solution, *Journal of The Pharmaceutical Society of Japan*, 107 (1987) 318-322 E
161. T. Kuwayama, T. Yashiro, The Behaviour of 1, 4-benzodiazepine Drugs in Acidic Media. IV. Proton and Carbon-13 Nuclear Magnetic Resonance Spectra of Diazepam and Fludiazepam in Acidic Aqueous Solution, *Chemical and Pharmaceutical Bulletin of Japan*, 33 (1985) 5503-5510
162. B.A. Dawson, Chapter 7, In: T.A. Gough, Editor, The Analysis of Drugs of Abuse, Wiley & Sons Ltd, New York, 1991
163. L. A. C. Pieters, A. J. Vlietinck, Applications of Quantitative  $^1\text{H}$ - and  $^{13}\text{C}$ -NMR Spectroscopy in Drug Analysis, *Journal of Pharmaceutical and Biomedical Analysis*, 7 (12) (1989) 1405-1417
164. B.E. Padden, M.T. Zell, Z. Dong, S. A. Schroeder, D.J. W. Grant, E. J. Munson, Comparison of Solid-State  $^{13}\text{C}$  NMR Spectroscopy and Powder X-ray Diffraction for Analyzing Mixtures of Polymorphs of Neotame, *Analytical Chemistry*, 71 (1999) 3325-3331
165. P. Novak, P. Tepeš, I. Fistrić, I. Bratoš, V. Gabelica, The Application of LC–NMR and LC–MS for the Separation and Rapid Structure Elucidation of an Unknown Impurity in 5-Aminosalicylic Acid, *Journal of Pharmaceutical and Biomedical Analysis*, 40 (5) (2006) 1268-1272
166. S. G. Hiriyanna, K. Basavaiah, Isolation and Characterization of Process Related Impurities in Anastrozole Active Pharmaceutical Ingredient, *Journal of Brazilian Chemical Society*, 19 (3) (2008) 397-404
167. R. Sharma, P. K. Gupta, A. Mazumde, D. K. Dubey, K. Ganesan, R. Vijayaraghavan, A Quantitative NMR Protocol for the Simultaneous Analysis of Atropine and Obidoxime in Parenteral Injection Devices, *Journal of Pharmaceutical and Biomedical Analysis*, 49 (4) (2009) 1092-1096
168. M. Zervou, V. Katsiaras, P. Zoumpoulakis, S. Durdagi, M. G. Papadopoulos, J. M. Hayes, S. G. Grdadolnik, I. Kyrikou, D. Argyropoulos, G. Vatougia, T. Mavromoustakos, Antihypertensive Drug Valsartan in Solution and at the AT1 Receptor: Conformational Analysis, Dynamic NMR

Spectroscopy, *in Silico* Docking, and Molecular Dynamics Simulations Constantinos Potamitis  
*Journal of Chemical Information Model*, 49 (2009) 726-739 R

169. D. E. Bugay, Characterization of the Solid-State: Spectroscopic Techniques, *Advanced Drug Delivery Reviews*, 48 (1) (2001) 43-65

170. S. Byrn, R. Pfeiffer, M. Ganey, C. Hoiberg, G. Poochikian, Pharmaceuticals Solids, a Strategic Approach to Regulatory Considerations, *Pharmaceutical Research*, 12 (1995) 945-954

171. US Government, Q6A Specifications, Test Procedures and Acceptance Criteria for New Drug Substances and New Drug Products, *Chemical Substances. Federal Register*, 62 (227) (1997) 62890-62910

172. J. Haleblian, W. McCrone, Pharmaceutical Applications of Polymorphism, *Journal of Pharmaceutical Science*, 58 (8) (1969) 911-929

173. A. Burger, R. Ramberger, On the Polymorphism of Pharmaceuticals and other Molecular Crystals. I. Theory of Thermodynamic Rules, *Mikrochimica Acta (Wien)*, II (1979) 259-271

174. A. Burge, R. Ramberger, On the Polymorphism of Pharmaceuticals and other Molecular Crystals. II. Applicability of Thermodynamic Rules, *Mikrochimica Acta (Wien)*, II (1979) 273-316

175. I. Wawer, M. Pisklak, Z. Chilmonczyk,  $^1\text{H}$ ,  $^{13}\text{C}$ ,  $^{15}\text{N}$  NMR Analysis of Sildenafil Base and Citrate (Viagra) in Solution, Solid State and Pharmaceutical Dosage Forms, *Journal of Pharmaceutical and Biomedical Analysis*, 38 (5) (2005) 865- 870

176. A. M. Bond, 200 years of Practical Electroanalytical Chemistry: Past, Present and Future Directions Illustrated by Reference to the on-line, on-Stream and Off-line Determination of Trace Metals in Zinc Plant Electrolyte by Voltammetric and Potentiometric Techniques, *Analytica Chimica Acta*, 400 (1-3) (1999) 333-379

177. J. Ruzicka, E. H. Hansen. Flow Injection Analysis, 2nd ed., John Wiley, New York (1988)

178. G. Favaro, M. Fiorani, Determination of Pharmaceutical Thiols by Liquid Chromatography with Electrochemical Detection: Use of an Electrode with a Conductive Carbon Cement Matrix, Chemically Modified with Cobalt Phthalocyanine, *Analytica Chimica Acta*, 332 (2-3) (1996) 249-255



179. J. W. Bachman, J.T. Stewart, HPLC-photolysis-electrochemical detection in pharmaceutical analysis: application to the determination of clofibrac acid in human plasma, *Journal of Liquid Chromatography*, 12(15) (1989) 2947-2959
180. Wang, J. Xu, G. Zhou, O. Qu, G. Yang, X. Hu, Electrochemical Detection Coupled with High-Performance Liquid Chromatography in Pharmaceutical and Biomedical Analysis: A Mini Review, *Combination Chemistry and High Throughput Screening*, 10 (7) (2007) 547-544
181. D.P. Nikolelis, Rapid Electrochemical Detection of Propranolol and Metoprolol in Pharmaceutical Preparations Using Stabilized Lipid Films, *Electroanalysis*, 16 (9) (2004) 741-747
182. G. W. Fong, S. K. Lam, Ed. HPLC in the Pharmaceutical Industry; Published by CRC Press, 1991
183. V. Supalkova, J. Petrek, L. Havel, S. Krizkova, J. Petrlova, V. Adam, D. Potesil, P. Babula, M. Beklova, A. Horna, R. Kizek, Electrochemical Sensors for Detection of Acetylsalicylic Acid, *Sensors*, 6 (11) (2006) 1483-1497
184. K. Toth, K. Štulík, W. Kutner, Z. Feher, E. Lindner, International Union of Pure and Applied Chemistry Analytical Chemistry Division Electrochemical Detection in Liquid Flow Analytical Techniques: Characterization and Classification. (IUPAC Technical Report), *Pure and Applied Chemistry*, 76(6) (2004) 1119-1138
185. D.W. Hoffman, K. L. Jones-King, C. L. Ravaris, R.D. Edkins, Electrochemical Detection for High-Performance Liquid Chromatography of Ketoconazole in Plasma and Saliva, *Analytical Biochemistry*, 172 (2) (1988) 495-498
186. K. Suzuki, M. Katayama, K. Takamatsu, S. Kaneko, K. Miyaji, H. Ishikawa, Y. Matsuda, Improvement of Sensitivity and Selectivity of High-Performance Liquid Chromatography for Anti-retroviral Drugs (Non-Reverse Transcriptase Inhibitors) by Diamond-Electrode Electrochemical and Fluorescence Detection, *Journal of Chromatography A*, 1216 (15) (2009) 3117-3121
187. G. Hammerstein, New level of sensitivity, selectivity and flexibility in LCEC detection, *Fresenius' Journal of Analytical Chemistry*, 327 (1) (1987) 35-36

188. A. Fallon, R. F. Booth, L. D. Bell, Applications of HPLC in Biochemistry. Laboratory Techniques in Biochemistry and Molecular Biology, Vol 17, by P. H. van Knippenberg, Roy Hunter Burdon, A, Ed. 1979
189. J. Swarbrick, J. C. Boylan. Encyclopedia of Pharmaceutical Technology, Edition: 2, illustrated, Published by Informa Health Care, 2004
190. S. Polesello, S. M. Valsecchi, Electrochemical Detection in the Capillary Electrophoresis Analysis of Inorganic Compounds, *Journal of Chromatography A*, 834 (1-2) (1999) 103-116
191. G.J. Ouyang, Q. L. Li, B. H. Liu and W. R. G. Baeyens, Simultaneous Determination of Catecholamines by Ion Chromatography with Direct Conductivity Detection, *Talanta*, 50(6) (2000) 1197-1203
192. Comparative study of Coulometric and Amperometric Detection for the Determination of Macrolides in Human Urine using High-Performance Liquid Chromatography, *Analytical and Bioanalytical Chemistry*, 375(8) (2003)1031-1037
193. Methods of Analysis for Functional Foods and Nutraceuticals, By W. Jeffrey Hurst, Edition: 2, illustrated, Published by CRC Press, 2008
194. E. H. Seymour, N.S. Lawrence, M. Pandurangappa, Indirect Electrochemical Detection of Nitrite via Diazotization of Aromatic Amines, *Microchimica Acta*, 140(3-4) (2002) 211-217
195. R.G. Compton, Indirect Electrochemical Detection of Nitrite via Diazotization of Aromatic amines, Elizabeth K. Yun, April J. Prince, Johanna E. McMillin and Lawrence E. Welch, *Journal of Chromatography B, Biomedical Sciences and Applications*, 712 (1-2) (1998) 145-152
196. N. S. Lawrence, J. Davis, R. G. Compton, Electrochemical Detection of Thiols in Biological Media, *Talanta*, 53(5) (2001) 1089-1094
197. J. E. Wallace, E. L. Shimek Jr, S. Stavchansky, S. C. Harris, Determination of Promethazine and other Phenothiazine Compounds by Liquid Chromatography with Electrochemical Detection, *Analytical Chemistry*, 53 (7) (1981) 960-962

198. T. A. Ivandini, B. V. Sarada, C. Terashima, T. N. Rao, D. A. Tryk, H. Ishiguro, Y. Kubota, A. Fujishima, Electrochemical Detection of Tricyclic Antidepressant Drugs by HPLC Using Highly Boron-Doped Diamond Electrodes, *Journal of Electroanalytical Chemistry*, 521 (1-2) (2002) 117-126
199. Liquid Chromatography in Biomedical Analysis, By Toshihiko Hanai, Contributor Toshihiko Hanai, Edition: illustrated, pp. 163
200. M. Škrinjar, M. H. Kolar, N. Jelšek, A. R. Hraš, M. Bezjak, Ž. Knez, Application of HPLC with Electrochemical Detection for the Determination of Low Levels of Antioxidants, *Journal of Food Composition and Analysis*, 20 (7) (2007) 539-545
201. By Robert James Flanagan, David Perrett, Robin Whelpton, Royal. Electrochemical detection in HPLC: analysis of drugs and poisons, By Robert James Flanagan, David Perrett, Robin Whelpton, Royal Society of Chemistry (Great Britain), Published by Royal Society of Chemistry, 2005
202. M.J. G. de la Huebra, · G. Bordin, A. R. Rodríguez, Comparative Study of Coulometric and Amperometric Detection for the Determination of Macrolides in Human Urine Using High-Performance Liquid Chromatography, *Analytical and Bioanalytical Chemistry*, 375(8) (2003) 1031-1037
203. K.R. Wehmeyer, H.B. Halsall, W.R. Heineman, Heterogeneous Enzyme Immunoassay with Electrochemical Detection: Competitive and "Sandwich"-Type Immunoassays, *Clinical Chemistry*, 31 (1985) 1546-1549
204. P. C. Gunaratna, K.K. Cadle, C. B. Kissinger, An Improved Liquid Chromatographic Method with Electrochemical Detection for Direct Determination of Serotonin in Microdialysates from Caudate-Putamen and Pineal Gland Regions of Rat Brain, *Journal of Neuroscience Methods*, 155 (1) (2006) 143-148
205. A.J. M. Shiddiky, Y. B. Shim, Trace Analysis of DNA: Preconcentration, Separation, and Electrochemical Detection in Microchip Electrophoresis Using Au Nanoparticles, *Analytical Chemistry*, 79 (10) (2007) 3724-3733

206. J.J. Xu, N. Bao, X.H. Xia, Y. Peng, H.Y. Chen, Electrochemical Detection Method for Nonelectroactive and Electroactive Analytes in Microchip Electrophoresis, *Analytical Chemistry*, 76 (23) (2004) 6902-6907
207. G. Chen, Y. Lin, J. Wang, Monitoring Environmental Pollutants by Microchip Capillary Electrophoresis with Electrochemical Detection, *Talanta*, 68 (3) (2006) 497-503
208. H. Wei, J.J. Sun, Y.M. Wang, X. Li, G.N. Chen, Rapid Hydrolysis and Electrochemical Detection of Trace Carbofuran at a Disposable Heated Screen-Printed Carbon Electrode, *Analyst*, 133 (11) (2008) 1619-1624
209. A. J. Blasco, A. G. Crevillén, M. C. González, A. Escarpa, Direct Electrochemical Sensing and Detection of Natural Antioxidants and Antioxidant Capacity in Vitro Systems, *Electroanalysis*, 19 (22) (2007) 2275-2286
210. R. Munoz, P. R. M. Correia, A. N. Nascimento, C. S. Silva, P. V. Oliveira, L. Angnes, Electroanalysis of Crude Oil and Petroleum-Based Fuel for Trace Metals: Evaluation of Different Microwave-Assisted Sample Decompositions and Stripping Techniques, *Energy Fuels*, 21 (1) (2007) 295-302
211. M. Wilhelm, H. Battista, D. Obendorf, HPLC with Simultaneous UV and Reductive Electrochemical Detection at the Hanging Mercury Drop Electrode : A Highly Sensitive and Selective Tool for the Determination of Benzodiazepines in Forensic Samples, *Journal of Analytical Toxicology*, 25 (4) (2001) 250-257
212. Modern Methods and Applications in Analysis of Explosives, By Jehuda Yinon, Shmuel Zitrin, Contributor Jehuda Yinon, Shmuel Zitrin, Published by John Wiley and Sons, 1996
213. H. Chung, H. Yang, W. Kim, J. Park, Nickel Oxide-Modified Composite Electrode for Electrochemical Detection of Polyhydroxyl Compounds in Liquid Chromatographic Analysis, *Analytica Chimica Acta*, 471 (2) (2002) 195-202
214. M. T. Sulak, Ö. Gökdoğan, A. Gülce, H. Gülce, Amperometric Glucose Biosensor Based on Gold-Deposited Polyvinylferrocene Film on Pt Electrode, *Biosensors and Bioelectronics*, 21(9) (2006) 1719-1726

215. T.Y. Ou, S. Moldoveanu, J. L. Anderson, Hydrodynamic Voltammetry at an Interdigitated Electrode Array in a Flow Channel: Part II. Chemical Reaction Succeeding Electron Transfer, *Journal of Electroanalytical Chemistry*, 247 (1-2) (1988) 1-16
216. E. Fortin, J. Chane-Tune, P. Mailley, S. Szunerits, B. Marcus, J. P. Petit, M. Mermoux, E. Vieil, Proceedings of the XVIIth International Symposium on Bioelectrochemistry and Bioenergetics, Nucleosides and ODN Electrochemical Detection onto Boron Doped diamond Electrodes, *Bioelectrochemistry*, 63 (912) (2004) 303-306
217. M. H. Vela, M. B. Quinaz Garcia, M. C. B. S. M. Montenegro, Electrochemical Behaviour of Sertraline at a Hanging Mercury Drop Electrode and its Determination in Pharmaceutical Products, *Fresenius' Journal of Analytical Chemistry*, 369 (7-8) (2001) 563-566
218. Thomas J. O'Shea, Susan M. Lunte, Selective Detection of Free Thiols by Capillary Electrophoresis-Electrochemistry Using a Gold/Mercury Amalgam Microelectrode, *Analytical Chemistry*, 65 (3) (1993) 247-250
219. N. Yu. Stojko, Kh. Z. Brainina, C. Faller, G. Henze, Stripping Voltammetric Determination of Mercury at Modified Solid Electrodes: I. Development of the Modified Electrodes, *Analytica Chimica Acta*, 371(2-3) (1998) 145-153
220. A. W. Maccrehan, R. A. Durst, J.M. Bellama, Electrochemical Detection in Liquid Chromatography: Application to Organometallic Speciation, *Analytical Letters*, 10(14) (1977) 1175-1188
221. H. Zejli, N. Izaoumen, D. Bouchta, M. El Kaouttit, R.K. Tamsamani, Electrochemically Aided Solid Phase Micro-extraction of Mercury(II) at a poly(3-methylthiophene) Modified Gold Electrode, *Analytical letters*, 37 (8) (2004) 1737-1754
222. C. G. Zampronio, J. J. R. Rohwedder, R. J. Poppi, Development of a Potentiometric Flow Cell with a Stainless Steel Electrode for pH Measurements. Determination of Acid Mixtures Using Flow Injection Analysis, *Talanta*, 51(6) (2000) 1163-1169
223. G. G. Wallace, M. Meaney, M. R. Smyth, J. G. Vos, Stabilization of a Ruthenium Polymer-modified Electrode for use in Flowing Solution Analysis, *Electroanalysis*, 1(4) (2005) 357-361

224. J.S. Kwak, Application of Taguchi and Response Surface Methodologies for Geometric Error in Surface Grinding Process, *International Journal of Machine Tools and Manufacture*, 45 (3) (2005) 327-334
225. M. A. Bezerra, R. E. Santelli, E. P. Oliveira, L. S. Villar, L. A. Escaleira, Response Surface Methodology (RSM) as a Tool for Optimization in Analytical Chemistry, *Talanta*, 76 (5) (2008) 965-977
226. A. Idris, F. Kormin, M.Y. Noordin, Application of Response Surface Methodology in Describing the Performance of thin Film Composite Membrane, *Separation and Purification Technology*, 49 (3) (2006) 271-280
227. J. Z. Song, C.F. Qiao, S.L. Li, Q.B. Han, H.X. Xu, Purity Determination of Yunaconitine Reference Standard using HPLC with Experimental Design and Response Surface Optimization, *Journal of Separation Science*, 31 (22) (2008) 3809-3816
228. S. Agatonovic-Kustrin, M. Zecevic, L. J. Zivanovic, I. G. Tucker, Application of Artificial Neural Networks in HPLC Method Development, *Journal of Pharmaceutical and Biomedical Analysis*, 17(1) (1998) 69-76
229. S. E. Vignaduzzo, P.M. Castellano, T. S. Kaufman, Method Development and Validation for the Simultaneous Determination of Meloxicam and Pridinol Mesylate using RP-HPLC and its Application in Drug Formulations, *Journal of Pharmaceutical and Biomedical Analysis*, 46 (2) (2008) 219-225
230. G. Srinubabu, C.A.I. Raju, N. Sarath, P. K. Kumar, J.V.L.N. S. Rao, Development and Validation of a HPLC Method for the Determination of Voriconazole in Pharmaceutical Formulation using an Experimental Design, *Talanta*, 71(3) (2007) 1424-1429
231. A. Müller D. Flottmann, W. Schulz, W. Seitz, W.H. Weber, Assessment of Robustness for an LC-MS-MS Multi-Method by Response-Surface Methodology, and its Sensitivity, *Analytical and Bioanalytical Chemistry*, 390 (5) (2008) 1317-1326
232. Pharmaceutical experimental design, By Gareth A. Lewis, Didier Mathieu, Roger Tan Luu Phan, Edition: illustrated, Published by Informa Health Care, 1998

233. Box, G.E.P. & Wilson, K.B. 1951. On the Experimental Attainment of Optimum Conditions. *Journal of the Royal Statistical Society (Series B)* 13
234. G.E.P. Box, J.S. Hunter, Multi-Factor Experimental Designs for Exploring Response Surfaces, *The Annals of Mathematical Statistics*, 28 (1957) 195-241
235. D.P. Obeng, S. Morrell, T.J. Napier-Munn, Application of Central Composite Rotatable Design to Modeling the Effect of some Operating Variables on the Performance of the Three-Product Cyclone, *International Journal of Mineral Processing*, 76 (3) (2005) 181-192
236. J.J. Cilliers, R.C. Austin, J.P. Tucker, An Evaluation of Formal Experimental Design Procedures for Hydrocyclone Modelling. In: L. Svarovsky and M.T. Thew, Editors, Proceedings of 4th International Conference on Hydrocyclones, Kluwer Academic Publishers, Southampton, 1992
237. R.D. Crozier, Flotation Theory, Reagents and Ore Testing, Pergamon Press, New York (1992)
238. V. Wsól, A. F. Fell, E. K. Ková, I. M. Hais, The role of Chromatography and Capillary Electrophoresis in the Biosciences. Separation of the Stereoisomers of the Main Metabolite of a Non-Steroidal Anti-Inflammatory Drug, Flobufen, by Chiral High-Performance Liquid chromatography, *Journal of Chromatography B: Biomedical Sciences and Applications*, 689(1) (1997) 205-214
239. P. Barmapalexis, F. I. Kanaze, E. Georgarakis, Developing and Optimizing a Validated Isocratic Reversed-Phase High-Performance Liquid Chromatography Separation of Nimodipine and Impurities in Tablets Using Experimental Design Methodology, *Journal of Pharmaceutical and Biomedical Analysis*, 49 (5) (2009) 1192-1202
240. P. Iuliani, G. Carlucci, A. Marrone, Investigation of the HPLC Response of NSAIDs by Fractional Experimental Design and Multivariate Regression Analysis. Response Optimization and New Retention Parameters, *Journal of Pharmaceutical and Biomedical Analysis*, 51(1) (2010) 46-55
241. W. Hill, W. G. Hunter, A Review of Response Surface Methodology: A Literature Survey, *Technometrics*, 8(4) (1966) 571-590
242. R. Granot, R. Baer, A Spline for your Saddle, *Journal of Chemical Physics*, 128 (18) (2008) 184111

243. A. Kuijper, Exploring and Exploiting the Structure of Saddle Points in Gaussian Scale Space, *Computer Vision and Image Understanding*, 112 (3) (2008) 337-349
244. J. K. Kim, B. R. Oh, H. J. Shin, C.Y. Eom, S.W. Kim, Statistical Optimization of Enzymatic Saccharification and Ethanol Fermentation Using Food Waste, *Process Biochemistry*, 43(11) (2008) 1308-1312
245. R. Bonfilio, C. R. T. Tarley, G. R. Pereira, H.R. N. Salgado, M. B. de Araújo, Multivariate Optimization and Validation of an Analytical Methodology by RP-HPLC for the Determination of Losartan Potassium in Capsules, *Talanta*, 80 (1) (2009) 236-241
246. S. Jarudilokkul, L. H. Poppenborg, F. Valetti, G. Gilardi, D. C. Stuckey, Separation and Purification of Periplasmic Cytochrome c553 using Reversed Micelles, *Biotechnology Techniques*, 13(3) (1999) 159-163
247. W.J. Gong, Y. P. Zhang, S. H. Choi, Y. J. Zhang, K.P. Lee, Application of Response Surface Methodologies in Capillary Electrophoresis, *Microchimica Acta*, 156 (3-4) (2006) 327-335
248. J. J. Borkowski, Spherical Prediction-Variance Properties of Central Composite and Box-Behnken Designs, *Technometrics*, 37(4) (1995) 399-410
249. S.L. Ferreira, R.E. Bruns, H.S. Ferreira, G.D. Matos, J.M. David, G.C. Brandão, E.G. da Silva, L.A. Portugal, P.S. dos Reis, A.S. Souza, W.N. dos Santos, Box-Behnken design: an Alternative for the Optimization of Analytical Methods, *Analytica Chimica Acta*, 597 (2) (2007) 179-186
250. M. E. L.Chaves, J.M. Palacios-Santander, L.M. Cubillana-Aguilera, I. Naranjo-Rodríguez, J.L. Hidalgo-Hidalgo-de-Cisneros, Modified Carbon-Paste Electrodes as Sensors for the Determination of 1,4-benzodiazepines: Application to the Determination of Diazepam and Oxazepam in Biological Fluids, *Sensors and Actuators B: Chemical*, 115 (2) (2006) 575-583
251. Y. Hahn, H. Y. Lee, Electrochemical Behavior and Square Wave Voltammetric Determination of Doxorubicin Hydrochloride, *Archives of Pharmacal Research*, 27(1) (2004) 31-34
252. P. Fanjul-Bolado, P. J. Lamas-Ardisana, D. Hernández-Santos, A. Costa-García, Electrochemical Study and Flow Injection Analysis of Paracetamol in Pharmaceutical Formulations based on Screen-printed Electrodes and Carbon Nanotubes, *Analytica Chimica Acta*, 638 (2) (2009) 133-138



253. H. M. Carapuça, D. J. Cabral, L. S. Rocha, Adsorptive Stripping Voltammetry of Trimethoprim: Mechanistic Studies and Application to the Fast Determination in Pharmaceutical Suspensions, *Journal of Pharmaceutical and Biomedical Analysis*, 38 (2) (2005) 364-369
254. P. Norouzi, M. R. Ganjali, P. Daneshgar, T. Alizadeh, A. Mohammadi, Development of Fast Fourier Transformation Continuous Cyclic Voltammetry as a Highly Sensitive Detection System for Ultra Trace Monitoring of Penicillin V, *Analytical Biochemistry*, 360 (2) (2007) 175-181
255. Y.M. Temerk, H.S.M. Ibrahim, W. Schuhmann, Cathodic Adsorptive Stripping Voltammetric Determination of the Antitumor Drug Rutin in Pharmaceuticals, Human Urine, and Blood Serum, *Mikrochimica Acta*, 153 (1-2) (2006) 7-13
256. N. Wangfuengkanagul, O. Chailapakul, Electrochemical Analysis of Acetaminophen Using a Boron-Doped Diamond thin Film Electrode Applied to Flow Injection System, *Journal of Pharmaceutical and Biomedical Analysis*, 28 (5) (2002) 841-847
257. M. Tamba, A. Torreggiani, Free Radical Scavenging and Copper Chelation: a Potentially Beneficial action of Captopril, *Free Radical Research*, 32 (3) (2000) 199-211
258. D. Bagchi, R. Prasad, D.K. Das, Direct Scavenging of Free Radicals by Captopril, an Angiotensin Converting Enzyme Inhibitor, *Biochemical and Biophysical Research Communications*, 158(1) (1989) 52-57
259. A.O. Alnajjar, Simultaneous CE Determination of Captopril and Indapamide in Pharmaceuticals and Human Plasma, *Chromatographia*, 68 (5-6) (2008) 437-442
260. T. Huang, Z. He, B. Yang, L. Shao, X. Zheng, G. Duan, Simultaneous determination of captopril and hydrochlorothiazide in human Plasma by reverse-Phase HPLC from Linear Gradient Elution, *Journal of Pharmaceutical and Biomedical Analysis*, 41(2) (2006) 644-648
261. Amini M, Zarghi A, Vatanpour H., Sensitive High-Performance Liquid Chromatographic Method for Determination of Captopril in Plasma, *Pharmaceutica Acta Helvetiae*, 73 (6) (1999) 303-306

262. C. Arroyo, C. López-Calull, L. García-Capdevila, I. Gich, M. Barbanøj, J. Bonal, Determination of Captopril in Plasma by High-Performance Liquid Chromatography for Pharmacokinetic Studies, *Journal of Chromatography B: Biomedical Sciences and Applications*, 688 (2) (1997) 339-344
263. M. Bahmaei, A. Khosravi, C. Zamiri, A. Massoumi, M. Mahmoudian, Determination of Captopril in Human Serum by High Performance Liquid Chromatography Using Solid-Phase Extraction, *Journal of Pharmaceutics and Biomedical Analysis*, 15 (8) (1997) 1181-1186
264. M. A. Khan, S. V. Sastry, S. R. Vaithiyalingam, V. Agarwal, S. Nazzal, I. K. Reddy, Captopril Gastrointestinal Therapeutic System Coated with Cellulose Acetate Pseudolatex: Evaluation of Main Effects of Several Formulation Variables, *International Journal of Pharmaceutics*, 193 (2) (2000) 147-156
265. M. Amini, A. Zarghi, H. Vatanpour, Sensitive High-Performance Liquid Chromatographic Method for Determination of Captopril in Plasma, *Pharmaceutica Acta Helvetiae*, 73 (6) (1999) 303-306
266. Y. Matsuki, K. Fukuhara, T. Ito, H. Ono, N. Ohara, T. Yui, J. Nambara, Determination of Captopril in Biological Fluids by Gas-Liquid Chromatography, *Journal of Chromatography*, 188 (1) (1980) 177-183
267. T. Ito, Y. Matsuki, H. Kuribara, T. Nambara, Sensitive Method for Determination of Captopril in Biological Fluids by Gas Chromatography Mass Spectrometry, *Journal of Chromatograph*, 417 (1) (1987) 79-87
268. P. Siangproh, P. Ngamukot, O. Chailapakul, Electrochemical Determination of Captopril at Boron-Doped Diamond thin Film Electrode Applied to a Flow Injection System, *Sensors and Actuators, B: Chemical*, 91 (1-3) (2003) 60-66
269. R.I. Stefan, J.F. van Staden and H.Y. Aboul-Enein, Simultaneous Detection of *S*- and *R*-Captopril Using Sequential Injection Analysis, *Talanta*, 51 (5) (2000) 969-975
270. H. Wakabayashi, S. Yamato, M. Nakajima and K. Shimada, Application of an Electrochemical Detector with a Graphite Electrode to Liquid Chromatographic Determination of Penicillamine and Captopril in Biological Samples, *Journal of Pharmaceutical and Biomedical Analysis*, 12 (9) (1994) 1147-1152

271. F. Qu, G. Zhu, S. Huang, S. Li, J. Sun, D. Zhang, S. Qiu, Controlled Release of Captopril by Regulating the Pore Size and Morphology of Ordered Mesoporous Silica, *Microporous and Mesoporous Materials*, 92(1-3) (2006) 1-9
272. C.Y. Kuo, S.M. Wu, 25th International Symposium on Chromatography. Part II, High-Performance Liquid Chromatography with Electrochemical Detection for Analysis of Gliclazide in Plasma, *Journal of Chromatography A*, 1088 (1-2) (2005) 131-135
273. Practical HPLC Method Development. L. R. Snyder, J. J. Kirkland, J. L. Glajch, 2<sup>nd</sup> Ed. John Wiley and Sons, New York, USA, 1997
274. Z. Xinrong, W. R. G. Baeyens, G. Van der Weken, A. C. Calokerinos, K. Nakashima, Papers from the Fifth International Symposium on Pharmaceutical and Biomedical Analysis, Chemiluminescence Analysis of Captopril: Comparison between Luminol and Rhodamine B-sensitized Cerium (IV) Methods, *Journal of Pharmaceutical and Biomedical Analysis*, 13 (4-5) (1999) 425-429
275. A.M. el-Brashy, Titrimetric Determination of Captopril in Dosage Forms, *Acta Pharmaceutica Hungarica*, 65 (3) (1995) 91-93
276. Practical Skills in Chemistry, J.R. Dean, A.M. Jones, D. Holmes, R. Reed, J. Weyers, A. Jones, Pearson Education Ltd publishers, Essex, UK, 2002
277. Practical HPLC. C.F. Simpson., Heyden and Son Ltd, 30<sup>th</sup> Ed. Heyden and Son Ltd, The Whitefriars Press, London, UK, 1976
278. V. Das Gupta, Quantitation and Stability of Verapamil Hydrochloride using High-Performance Liquid Chromatography, *Drug Development and Industrial Pharmacy*, 11(8) (1985) 1497-1506
279. W. Sawicki, A Validated Method for the Determination of Verapamil and Norverapamil in Human Plasma, *Journal of Pharmaceutical and Biomedical Analysis*, 25 (3-4) (2001) 689-695
280. S.C. Cole, R.J. Flanagan, A. Johnston, D.W. Holt, Rapid High-Performance Liquid Chromatographic Method for the Measurement of Verapamil and Norverapamil in Blood Plasma or Serum, *Journal of Chromatography*, 218 (1981) 621-629

281. Maintaining and Troubleshooting HPLC Systems, D.J. Rusner, John Wiley and Sons, New-York, USA, 1981
282. Introduction to HPLC, R.J. Hamilton, P.A. Sewell, Chapman and Hall, London, UK, 2<sup>nd</sup> Ed. 1982
283. J. Lindholm, M. Johansson, T.Fornstedt, Guidelines for Analytical Method Development and Validation of Biotechnological Synthesis of Drugs Production of a Hydroxyprogesterone as Model, *Journal of Chromatography B*, 791 (1-2) (2003) 323-336
284. K. Hammarstrand, Internal Standard in Gas Chromatography, *Varian Instrument Applications*, 10 (1) (1976) 10-11
285. O. H. Drummer, B. Jarrott, Captopril Disulfide Conjugates may act as Prodrugs: Disposition of the Disulfide Dimer of Captopril in the Rat, *Biochemical Pharmacology*, 33 (22) (1984) 3567-3571
286. P. Timmins, Advantages of the Use of Very Short and Ultra Short HPLC Columns for Drug Analysis in Dissolution Testing, *Drug Development and Industrial Pharmacy*, 12 (11-13) (1986) 2301-2312
287. Alaa Khedr <sup>1</sup>, Hosny El-Sherief , 3-bromomethyl-propyphenazone as a new derivatization reagent for high performance liquid chromatography of captopril and hydrochlorothiazide with UV-detection, *Biomedical Chromatography*, 12 (2) (1999) 57-60
288. P. K. Owens, L. A. Svensson, J. Vessman, Direct Separation of Captopril Diastereoisomers including their Rotational Isomers by RP-LC using a Teicoplanin Column, *Journal of Pharmaceutical and Biomedical Analysis*, 25 (3-4) (2001) 453-464
289. G. A. Shabir, Validation of High-performance Liquid Chromatography Methods for Pharmaceutical Analysis: Understanding the Differences and Similarities Between Validation Requirements of the US Food and Drug Administration, the US Pharmacopeia and the International Conference on Harmonization, *Journal of Chromatography A*, 987(1-2) (2003) 57-66
290. C. M. Smith, How to find a Saddle Point, *International Journal of Quantum Chemistry*, 37 (6) (1989) 773-783

291. J. Lindholma, M. Johanssonb, T. Fornstedta, Guidelines for Analytical Method Development and Validation of Biotechnological Synthesis of Drugs Production of a Hydroxyprogesterone as Model, *Journal of Chromatography B*, 791 (1-2) (2003) 323-336
292. V.P. Shah, K.K. Midha, J.W.A. Findlay, H. M. Hill, J. D. Hulse, I. J. McGilveray, G. McKay, K. J. Miller, R. N. Patnaik, M. L. Powell, A. Tonelli, C. T. Viswanathan, A.Yacobi. *Conference Report, Pharmaceutical Research*, 17 (12) (2000) 1551-1557
293. Food and Drug Administration. Guidance for Industry: Bioanalytical Method Validation. Rockville, MD: US Department of Health and Human Services, FDA, Center for Drug Evaluation and Research; 2001
294. ICH-Topic Q2A: Validation of Analytical Procedures, International Conference on Harmonization of Technical Requirements for Registration of Pharmaceuticals for Human Use, Geneva, 1995. <http://www.ich.org/pdf/ICH/Q2A.pdf> (25 June 2004)
295. ICH-Topic Q2B: Validation of Analytical Procedures: Methodology, International Conference on Harmonization of Technical Requirements for Registration of Pharmaceuticals for Human Use, Geneva, 1997. <http://www.ich.org/pdf/ICH/Q2B.pdf> (25 June 2004)
296. ICH-Topic Q6B: Specifications Biotechnological substances, International Conference on Harmonization of Technical Requirements for Registration of Pharmaceuticals for Human Use, Geneva, 1999. <http://www.ich.org/pdf/ICH/Q6bstep4.pdf> (25 June 2004)
297. I. Taverniers, M. De Loose, E. Van Bockstaele, Trends in Quality in the Analytical Laboratory. II. Analytical Method Validation and Quality Assurance, *Trends in Analytical Chemistry*, 23 (8) (2004) 535-552
298. R. Wood. How to Validate Analytical Methods, *Trends in Analytical Chemistry*, 18 (9-10) (1999) 624-632
299. A.G. Causey, H.M. Hills, L.J. Phillips, Evaluation of Criteria for the Acceptance of Bioanalytical Data, *Journal of Pharmacy and Biomedical Analysis*, 8 (8-12) (1990) 625-628
300. I. S. Krull, M. Swartz, Analytical Method Development and Validation for the Academic Researcher, *Analytical Letters*, 32 (6) (1999) 1067- 1080

301. A. Azeem, M. Rizwan, F. J. Ahmad, Z. Iqbal, R. K. Khar, M. Aqil, S. Talegaonkar, Development and validation of a stability-indicating LC-UV method for rapid analysis of buspirone in pharmaceutical dosage forms, *Acta Chromatographica*, 21 (2) (2009) 283-297
302. A. Chmielewska, L. Konieczna, A. Plenis, H. Lamparczyk, Sensitive Quantification of Chosen Drugs by Reversed-Phase Chromatography with Electrochemical Detection at a Glassy Carbon Electrode, 4th International Symposium on Separations in the BioSciences, *Journal of Chromatography*, 839 (1-2) (2006) 102-111
303. D.B. Hibbert (2<sup>nd</sup> Ed). In: P.J. Worsfold, A. Townshend and C.F. Poole, Editors, Method Validation, Encyclopedia of Analytical Science, Vol. 7, Elsevier, Oxford, 2005
304. The Cooperation on International Traceability in Analytical Chemistry and EURACHEM (A Focus for Analytical Chemistry in Europe, Guide to Quality in Analytical Chemistry: An Aid to Accreditation, 2002.
305. Food and Drug Administration, Draft guidelines on the validation of analytical procedures: methodology, *Federal Register*, 61 (1996) 9316
306. EURACHEM, Guidenace document No. 1/WELAC, Guidenace document No. WGD 2: Guidenace on the interpretation of the EN 45000 series of standards and ISO/EIC Guide, (1997) 25, Laboratory of the Government Chemist, Teddington, UK.
307. J. M. Green, A Practical Guide to Analytical Method Validation, *Analytical Chemistry*, 68 (1996) 305A-309A
308. R.W. Lutz, W.A. Werner, Statistical Procedures to Test for Linearity and Estimate Threshold doses for Tumor Induction with Nonlinear Dose-Response Relationships in Bioassays for Carcinogenicity, *Regulatory Toxicology and Pharmacology*, 36(3) (2002) 331-337
309. V. Bewick, L. Cheek, J. Ball, Statistics review 7: Correlation and Regression, *Critical Care*, 7 (6) (2003) 451-459
310. United States Pharmacopoeia Incorporating “ The National Formulary”, United States Pharmacopoeial Convention, Maryland, 26<sup>th</sup> Ed., 2003

311. A. Marin, E. Garcia, A. Garcia, C. Barbas, Validation of an HPLC Quantitation of Acetaminophen, Phenylephrine and Chlorpheniramine in Pharmaceutical Formulations, Capsules and Satchets, *Journal of Pharmaceutical and Biomedical Analysis*, 29 (4) (2002) 701-714
312. G. C. Hokanson, A life Cycle Approach to the Validation of Analytical Methods during Pharmaceutical Product Development, Part I: The Initial Method Validation Process, *Pharmaceutical Technology*, October (1994) 118-131
313. W. Sawicki, A Validated Method for the Determination of Verapamil and Norverapamil in Human Plasma, *Journal of Pharmaceutical and Biomedical Analysis*, 25 (93-94) (2001) 689-695
314. Y. Xiong, K. P. Xiao, A. M. Rustum, Development and Validation of a Stability-Indicating RP-HPLC Method to Separate Low Levels of Dexamethasone and other Related Compounds from Betamethasone, *Journal of Pharmaceutical and Biomedical Analysis*, 49 (3-4) (2009) 646-654
315. J. S. Space, A. M. Opi, B. Nickerson, H. Jiang, M. Dumont, M. Berry, Validation of a Dissolution Method with HPLC Analysis for Lasofoxifene Tartrate Low Dose Tablets, *Journal of Pharmaceutical and Biomedical Analysis*, 44 (5) (2007) 1064-1071
316. E. Rozet, A. Ceccato, C. Hubert, E. Ziemons, R. Oprean, S. Rudaz, B. Boulanger, P. Hubert, Analysis of Recent Pharmaceutical Regulatory Documents on Analytical Method Validation, *Journal of Chromatography A*, 1158 (1-2) (2007) 111-125
317. G.S Clarke, The Validation of Analytical Methods for Drug Substances and Drug Products in UK Pharmaceutical Laboratories, *Journal of Pharmacy and Biomedical Analysis*, 12 (5) (1994) 643-652
318. Reviewer Guidance: Validation of Chromatographic Methods. United States Department of Health and Human Services, Food and Drug Administration, Center for Drug Evaluation and Research (CDER), November, 1994. <http://fda/cder/guidance/cmc3.pdf>. (Retrieved 25/06/2004)
319. M.A. Garcia, J.J. Aramayona, M.A. Bregante, L.J. Fraile, C. Solans, Simultaneous Determination of Verapamil and Norverapamil in Biological Samples by High-Performance Liquid Chromatography using Ultraviolet Detection, *Journal of Chromatography B: Biomedical Sciences and Applications*, 693 (2) (1997) 377-382

320. O. Von Richter, M. Eichelbaum, F. Schonberger, U. Hofmann, Rapid and Highly Sensitive Method for the Determination of Verapamil, [2H7] Verapamil and Metabolites in Biological Fluids by Liquid Chromatography-Mass Spectrophotometry, *Journal of Chromatography B: Biomedical Sciences and Applications*, 738 (1) (2000) 137-147
321. E. Watson, P.A. Kapur, High-Performance Liquid Chromatographic Determination of Verapamil in Plasma by Fluorescence Detection, *Journal of Pharmaceutical Sciences*, 70 (7) (1981) 800-801
322. T.C. Paino, A.D. Moore, Determination of the LOD and LOQ of an HPLC Method Using Four Different techniques, *Pharmaceutical Technology*, October (1999) 86-92
323. H.S. Shin, Y.S. Oh-Shin, H.J. Kim, Y.K. Kang, Sensitive Assay for Verapamil in Plasma using Gas-Liquid Chromatography with Nitrogen-Phosphorus Detection, *Journal of Chromatography B: Biomedical Sciences and Applications*, 677 (2) (1996) 369-373
324. H. Rosing, W.Y. Man, E. Doyle, A. Bult, J.H. Beijnen, Bioanalytical Liquid Chromatographic Method Validation. A Review of Current Practices and Procedures, *Journal of Liquid Chromatography and Related Technologies*, 23(3) (2000) 329-354
325. F. Balestrieri, A. D. Magrì, A. L. Magrì, D. Marini, A. Sacchini, Application of Differential Scanning Calorimetry to the Study of Drug-Excipient Compatibility, *Thermochimica Acta*, 285 (2) (1996) 337-345
326. M.J. Hardy. In: (3rd edn. ed.), Drug-Excipient Compatibility Prediction by DSC, *Analytical Proceedings*, 19 (12) (1982) 556-557
327. A. Smith. In: (3rd edn. ed.), Use of Thermal Analysis in Predicting Drug-Excipient Interactions, *Analytical Proceedings*, 19 (12) (1982) 559-561
328. P.V. Mroso, A.Li Wan Po, W.J. Irwin, Solid-State Stability of Aspirin in the Presence of Excipients: Kinetic Interpretation, Modeling, and Prediction, *Journal Pharmaceutical Sciences*, 71 (10) (1982) 1096-1101
329. A.P.W. Li, P.V. Mroso, Drug-Drug Incompatibility in the Solid State: Kinetic Interpretation, Modeling and Prediction, *International Journal of Pharmaceutics*, 18 (3) (1984) 287-298
330. A.Li Wan Po. In: (3rd edn. ed.), Application of Differential Scanning Calorimetry in Pharmacy: Prediction of Solid State Stability of Drugs, *Analytical Proceedings*, 23 (1986) 391



331. S.A. Botha, A.P. Lotter, Compatibility Study Between Atenolol and Tablet Excipients Using Differential Scanning Calorimetry, *Drug Development and Industrial Pharmacy*, 16 (12) (1990) 1945-1954
332. E.C. Van Tonder, A.P. Lotter, S.A. Botha, Compatibility Study Between Doxylamine Succinate With Other Drugs and Excipients Using Differential Scanning Calorimetry, *Drug Development and Industrial Pharmacy*, 16 (14) (1990) 2125-2133
333. V. Gallardo, M.A. Ruiz, A. Parera and A.V. Delgado, A DSC Study of The Chemical Stability of Nitrofurantoin in Pharmaceutical Suspensions, *Pharmazie*, 45 (8) (1990) 633-634
334. T. M. Cardoso, P. O. Rodrigues, H. K. Stulzer, M. A. S. Silva, J. Matos, Physical-Chemical Characterization and Polymorphism Determination of Two Nimodipine Samples Deriving from Distinct Laboratories, *Drug Development and Industrial Pharmacy*, 31(7) (2005) 631-637
335. D. Giron, Characterization of Salts of Drug Substances, *Journal of Thermal Analysis and Calorimetry*, 73 (2) (2003) 441-457
336. M.L.P. Leito, J. Canotilho, M.S.C. Cruz, J.C. Pereira, A.T. Sousa, J.S. Redinha, Study of Polymorphism from DSC Melting Curves-Polymorphs of Terfenadine, *Journal of Thermal Analysis and Calorimetry*, 68 (2) (2002) 397-412.
337. R. Saklatvala, P.G. Royall, D.Q.M. Craig, The Detection of Amorphous Material in a Nominally Crystalline Drug Using Modulated Temperature DSC-A Case Study, *International Journal of Pharmaceutics*, 192 (1) (1999) 55-62
338. G. Becket, S. B. Quah, J. O. Hill, A DSC Compositional Analysis of Some Binary Organic Mixtures of Pharmaceutical Significance, *Journal of Thermal Analysis and Calorimetry*, 40 (2) (1993) 537-554
339. D. Giron, Investigations of Polymorphism and Pseudo-Polymorphism in Pharmaceuticals by Combined Thermoanalytical Techniques, *Journal of Thermal Analysis and Calorimetry*, 64 (1) (2001) 37-60
340. A.C.D. Medeiros, N.A. B. Cervantes, A.P.B. Gomes, R.O. Macedo, Thermal Stability of Prednisone Drug and Tablets, *Journal of Thermal Analysis and Calorimetry*, 64 (2) (2001) 745- 750

341. R. L. O. Rezende, M. I. R. M. Santoro, J. R. Matos, Stability and Compatibility Study on Enalapril Maleate Using Thermoanalytical Techniques, *Journal of Thermal Analysis and Calorimetry*, 93 (3) (2008) 881-886
342. J. L. Ford, P. Timmins, Pharmaceutical Thermal Analysis: Techniques and Applications, Halsted Press, New York 1989
343. M. L. Cotton, D. W. Wu, E. B. Vadas, Drug-Excipient Interaction Study of Enalapril Maleate Using Thermal Analysis and Scanning Electron Microscopy, *International Journal of Pharmaceutics*, 40 (1-2) (1987) 129-142
344. R. O. Macêdo, T. G. do Nascimento, J. W. E. Veras, Compatibility and Stability Studies of Propranolol Hydrochloride Binary Mixtures and Tablets for TG and DSC-photovisual, *Journal of Thermal Analysis and Calorimetry*, 67 (2) (2002) 483-489
345. A. Marini, V. Berbenni, S. Moioli, G. Bruni, P. Cofrancesco, C. Margheritis, M. Villa, Drug-Excipient Compatibility Studies by Physico-Chemical Techniques; The Case of Indomethacin, *Journal of Thermal Analysis and Calorimetry*, 73 (2) (2003) 529-545
346. A. Marini, V. Berbenni, M. Pegoretti, G. Bruni, P. Cofrancesco, C. Sinistri, M. Villa, Drug-Excipient Compatibility Studies by Physico-Chemical Techniques; The Case of Atenolol, *Journal of Thermal Analysis and Calorimetry*, 73 (2), (2003) 547-561
347. G. G. G. Oliveira, H. G. Ferraz, J. S. R. Matos, Thermoanalytical Study of Glibenclamide and Excipients, *Journal of Thermal Analysis and Calorimetry*, 79 (2) (2005) 267-270
348. L. C. S. Cides, A. A. S. Araújo, M. Santos-Filho, J. R. Matos, Thermal Behaviour, Compatibility Study and Decomposition Kinetics of Glimepiride Under Isothermal and Non-Isothermal Conditions, *Journal of Thermal Analysis and Calorimetry*, 84 (2) (2006) 441-445
349. D. Kiss, R. Zelkó, Cs. Novák, Zs. Éhen, Application of DSC and NIRS to Study the Compatibility of Metronidazole with Different Pharmaceutical Excipients, *Journal of Thermal Analysis and Calorimetry*, 84 (2) (2006) 447-451
350. R. L. Danley, New Heat Flux DSC Measurement Technique, *Thermochimica Acta*, 395 (1-2) (2002) 201-208

351. P. Mura, A. Manderioli, G. Bramanti, S. Furlanetto, S. Pinzauti, Utilization of Differential Scanning Calorimetry as a Screening Technique to Determine the Compatibility of Ketoprofen with Excipients, *International Journal of Pharmaceutics*, 119 (1) (1995) 71-79
352. M. C. Adeyeye, H. G. Brittain, Preformulation In Solid Dosage Form Development. Drugs and the Pharmaceutical Sciences. Vol 178, Informa Healthcare USA, Inc, New York, 10017, 52 Vanderbilt Avenue, 2008
353. P. Mura, G. P. Bettinetti, M. T. Faucci, A. Manderioli, P. L. Parrini, Differential Scanning Calorimetry in Compatibility Testing of Picotamide with Pharmaceutical Excipients, *Thermochimica Acta*, 321(1-2) (1998) 59-65
354. P. Mura, M. T. Faucci, A. Manderioli, S. Furlanetto, S. Pinzauti, Thermal Analysis as a Screening Technique in Preformulation Studies of Picotamide Solid Dosage Forms, *Drug Development and Industrial Pharmacy*, 24 (8) (1998) 747-756
355. P. Mura, M.T. Faucci, A. Manderioli, G. Bramanti, L. Ceccarelli, Compatibility Study Between Ibuprofen and Pharmaceutical Excipients Using Differential Scanning Calorimetry, Hot-Stage Microscopy and Scanning Electron Microscopy, *Journal of Pharmaceutical and Biomedical Analysis*, 18 (1) (1998) 151-163
356. M. A. Phipps, L. A. Mackin, Application of Isothermal Microcalorimetry in Solid state Drug Development, *Pharmaceutical Science & Technology Today*, 3 (1) (2000) 9-17
357. Y. Huang, Y. Cheng, K. Alexander, D. Dollimore, The Thermal Analysis Study of the Drug Captopril, *Thermochimica Acta*, 367-368 (2001) 43-58
358. Satinder Ahuja, Karen Alsante, Handbook of Isolation and Characterization of Impurities in Pharmaceuticals, Volume 5, Academic Press, San Diego, California, 2003
359. R. K. Verma, S. Garg, Selection of Excipients for Extended Release Formulations of Glipizide Through Drug-Excipient Compatibility Testing, *Journal of Pharmaceutical and Biomedical Analysis*, 38 (4) (2005) 633-644
360. A.A.S. Araujo, S. Storpirtis, L.P. Mercuri, F.M.S. Carvalho, M.S. Filho, J.R. Matos, Thermal Analysis of the Antiretroviral Zidovudine (AZT) and Evaluation of the Compatibility with Excipients Used in Solid Dosage Forms, *International Journal of Pharmaceutics*, 260 (2) (2003) 303-314

361. E.C.V. Tonder, A.P. Lotter and S.A. Botha, Compatibility Study Between Doxylamine Succinate with Other Drugs and Excipients Using Differential Scanning Calorimetry, *Drug Development and Industrial Pharmacy*, 16 (1990) 2125-2133
362. S. Venkataram, M. Khohlokwane, S.H. Wallis, Differential Scanning Calorimetry as a Quick Scanning Technique for Solid State Stability Studies, *Drug Development Industrial Pharmacy*, 21(7) (1995) 847-855
363. R. Kandarapu, V. Grover, H.P.S. Chawla, S. Garg, Evaluation of the Compatibility of Ketorolac Tromethamine with Selected Polymers and Common Tablet Excipients by Thermal and Isothermal Stress Testing, *STP Pharma Sciences*, 11(6) (2001) 449-457
364. R. K. Verma, S. Garg, Compatibility Studies Between Isosorbide Mononitrate and Selected Excipients used in the Development of Extended Release Formulations, *Journal of Pharmaceutical and Biomedical Analysis*, 35 (3) (2004) 449-458
365. C. Sánchez-Lafuente, A. M. Rabasco, J. Álvarez-Fuentes, M. Fernández-Arévalo, Eudragit® RS-PM and Ethocel® 100 Premium: Influence over the Behavior of Didanosine Inert Matrix System, *II Farmaco*, 57 (8) (2002) 649-656
366. S.A. Botha, A.P. Lotter, Compatibility Study Between Naproxen and Tablet Excipients Using Differential Scanning Calorimetry, *Drug Development and Industrial Pharmacy*, 16 (4) (1990) 673-683
367. A.T.M. Serajuddin, A.B. Thakur, R.N. Ghoshal, M.G. Fakes, S.A. Ranadive, K.R. Morris, S.A. Varia, Selection of Solid Dosage form Composition through Drug-Excipient Compatibility Testing, *Journal of Pharmaceutical Sciences*, 88(7), (1999) 696-704
368. L. Gu, R.G. Strickley, L. Chi, Z.T. Chowhan, Drug-Excipient Incompatibility Studies of the Dipeptide Angiotensin-Converting Enzyme Inhibitor, Moexipril Hydrochloride: Dry Powder vs Wet Granulation, *Pharmaceutical Research*, 7 (5) (1990) 379-383
369. R. Collier, Drug development cost estimates hard to swallow, *Canadian Medical Association Journal*, 180 (3) (2009) 279-280

370. C. Gendrin, Y. Roggo, C. Collet, Pharmaceutical Applications of Vibrational Chemical Imaging and Chemometrics: A Review, *Journal of Pharmaceutical and Biomedical Analysis*, 48(3) (2008) 533-553
371. F.D. Freire, C. F. S. Aragão, T. F. A. de Lima e Moura, F. N. Raffin, Thermal Studies of Isoniazid and Mixtures with Rifampicin, *Journal of Thermal Analysis and Calorimetry*, 97 (1) (2009) 333-336
372. The Handbook of Pharmaceutical Excipients. R.C Rowe, P.J. Sheskey and P. J. Weller (eds.): American Pharmaceutical Association, Washington, USA, 4<sup>th</sup> Ed. 2003
373. J. Liu, F. Zhang, J.W. McGinity, Properties of Lipophilic Matrix Tablets Containing Phenylpropanolamine Hydrochloride Prepared by Hot-Melt Extrusion. *European Journal of Pharmaceutics and Biopharmaceutics*, 52 (2) (2001) 181-190
374. A. Streubel, J. Siepmann, A. Dashevsky, R. Bodmeier. pH-Independent Release of a Weakly Basic Drug from Water-Insoluble and Soluble Matrix Tablets, *Journal of Controlled Release*, 67 (1) (2000) 101-110
375. V. Mahaguna, R.L.Talbert, J.I. Peters, S. Adams, T.D. Reynolds, F.Y.W. Lam, R.O. Williams III. Influence of Hydroxypropylmethylcellulose Polymer on *In-Vitro* and *In-Vivo* Performance of Controlled-Release Tablets containing Alprazolam, *European Journal of Pharmaceutics and Biopharmaceutics*, 56 (3) (2003) 461-468
376. K. Tahara, K. Yamamoto, T. Nishihata, Overall Mechanism Behind Matrix Sustained-Release (SR) Tablets Prepared with Hydroxypropylmethylcellulose 2910. *Journal of Controlled Release*, 35 (1) (1995) 59-66
377. C. De Brabander, C. Vervaet, J.P. Remon, Development and Evaluation of Sustained- Release Mini-Matrices Prepared via Hot Melt Extrusion. *Journal of Controlled Release*, 89 (2) (2003) 235-247
378. K.H. Khanvilkar, Y. Huang, A.D. Moore, Influence of Hydroxymethylcellulose Mixture, Apparent Viscosity, and Tablet Hardness on Drug Release using a 2<sup>3</sup> Full Factorial Design, *Drug Development and Industrial Pharmacy*, 28 (5) (2002) 601-608

379. S. M. Samani, H. Montaseri, A. Kazemi. The Effect of Polymer Blends on Release Profiles of Diclofenac Sodium from Matrices, *European Journal of Pharmaceutics and Biopharmaceutics*, 55 (3) (2003) 351-355
380. B.J. Lee, S.G. Ryu, J.H. Cui, Controlled-Release of Dual Drug-Loaded Hydroxypropylmethylcellulose Matrix Tablet using Drug-Containing Polymeric Coatings, *International Journal of Pharmaceutics*, 188 (1) (1999)71-80
381. C.R. Soccol, L.P.S. Vandenberghe, C. Rodrigues, A. Pandey, New Perspectives for Citric Acid Production and Application, *Food Technology and Biotechnology*, 44 (2) (2006) 141-149
382. A. Loewenstein, J.D. Roberts, The Ionization of Citric Acid Studied by the Nuclear Magnetic Resonance Technique, *Journal of The American Chemical Society*, 82 (11) (1960) 2705-2710
383. F. Sadeghi, H. A. Garekani, F. Goli, Tableting of Eudragit RS and Propranolol Hydrochloride Solid Dispersion: Effect of Particle Size, Compaction Force, and Plasticizer Addition on Drug Release, *Drug Development and Industrial Pharmacy*, 30(7) (2004) 759-766
- 384 J. Fujimori, Y. Yoshihashi, E. Yonemochi, K. Terada, Application of Eudragit RS to Thermo-Sensitive Drug Delivery Systems: II. Effect of Temperature on Drug Permeability through Membrane Consisting of Eudragit RS/PEG 400 Blend Polymers, *Journal of Controlled Release*, 102 (1) (2005) 49-57
385. M.L. González-Rodríguez, F. Maestrelli, P. Mura, A.M. Rabasco, In Vitro Release of Sodium Diclofenac from a Central Core Matrix Tablet aimed for Colonic Drug Delivery, *European Journal of Pharmaceutical Sciences*, 20 (91) (2003) 125-131
386. S. Narisawa, M. Nagata, Y. Hirakawa, M. Kobayashi, H. Yoshino, An Organic Acid-Induced Sigmoidal Release System for Oral Controlled-Release Preparations: 2. Permeability Enhancement of Eudragit RS Coating led by the Physicochemical Interactions with Organic Acid, *Journal of Pharmaceutical Sciences*, 85 (2) (1996) 184-188
387. A. Kramar, S. Turk and F. Vrečer, Statistical Optimisation of Diclofenac Sustained Release Pellets Coated with Polymethacrylic Films, *International Journal of Pharmaceutics*, 256 (1-2) (2003) 43-52

388. S. Haznedar and B. Dortunç, Preparation and In Vitro Evaluation of Eudragit Microspheres Containing Acetazolamide, *International Journal of Pharmaceutics*, 269 (1) (2004) 131-140
389. Eudragit, Technical information. Rohm Pharma, Darmstadt, Germany
390. M. Donbrow, S. Benit, A. Hoffman, Microencapsulation of Dichromate and Paracetamol with Eudragit Retard Polymers Using Phase Separation by Nonsolvent Addition, *Applied Biochemistry and Biotechnology*, 10(1-3) (1984) 245-249
391. Y. Ikeda, K. Kimura, F. Hirayama, H. Arima, K. Uekama, Controlled Release of a Water-Soluble Drug, Captopril, by a Combination of Hydrophilic and Hydrophobic Cyclodextrin Derivatives, *Journal of Controlled Release*, 66 (2-3) (2000) 271-280
392. R. Kandarapu, V. Grover, H.P.S. Chawla, S. Garg, Evaluation of the Compatibility of Ketorolac Tromethamine with Selected Polymers and Common Tablet Excipients by Thermal and Isothermal Stress Testing, *S. T. P. Pharma Sciences*, 11 (6) (2001) 449-457
393. L.J. Bellamy, Infrared Spectra of Complex Molecules Chapman & Hall, New York, Vol. 1, 1975.
394. Infrared Spectra Interpretation: A Systematic Approach. By Brian C. Smith, 1999, Boca Raton, FL, CRC Press
395. Z. Tianyong, F. Xuening, S. Jian, Z. Chunlong, Properties of Copper Phthalocyanine Microencapsulated in Polystyrene by Phase Separation, *Dyes and Pigments*, 44 (1) (1999) 1-7
396. Green BK, Schleicher L. U.S.P 2730456 (1956); U.S.P 273045 (1956)
397. Ranney MW. Microencapsulation technology, Noyes Development Co., 1969
398. J.R. Nixon, Preparation of microcapsules with possible pharmaceutical use, *Endeavour*, 9 (3) (1985) 123-128
399. E.S. Robert. Kirk-Othmer Encyclo Chem Technol 3<sup>rd</sup> Ed. 1981, Vol. 15
400. C.A. Finch, Polymers for Microcapsule Walls, *Chemistry and Industry*, 22 (1985) 752-756

401. M.D. Dibiase, M. Morrel, Oral Delivery of Microencapsulated Proteins, *Pharmaceutical Biotechnology*, 10 (1997) 255-288
402. S. H. Choi, J.H. Kwon, C.W. Kim, Microencapsulation of Insulin Microcrystals, *Bioscience, Biotechnology, and Biochemistry*, 68 (3) (2004)749-752
403. J. P. Wang, X.P. Zhao, H.L. Guo, Q. Zheng, Preparation and response behavior of blue electronic ink microcapsules, *Optical Materials*, 30 (8) (2008) 1268-1272
404. H. Yoshizawa, Trends in Microencapsulation Research, *KONA*, 22 (2004) 23-30
405. Thies, C., 1987, Microencapsulation. In Encyclopedia of Polymer Science and Engineering, Vol. 9, 2<sup>nd</sup> Ed. edited by H. F. Mark, N. Bikales, C. G. Overberger, G. Menges and J. I. Kroschwitz (New York, Chichester: Wiley)
406. V. B. Junyaprasert, G. Manwiwattanakul, Release profile comparison and stability of diltiazem–resin microcapsules in sustained release suspensions. *International Journal of Pharmaceutics*, 352 (1-2) (2008) 81-91
407. B. Singh, R. Agarwal, Design, Development and Optimization of Controlled Release Microcapsules of Diltiazem Hydrochloride, *Indian Journal of Pharmaceutical Sciences*, 64 (4) (2002) 378-385
408. B. Shu, W. Yu, Y. Zhao, X. Liu, Study on Microencapsulation of Lycopene by Spray-Drying. *Journal of Food Engineering*, 76 (4) (2006) 664-669
409. S. Gouin, Microencapsulation: Industrial Appraisal of Existing Technologies and Trends, NFIF Part 2, *Trends in Food Science & Technology*,15 (7-8) (2004) 330-347
410. J.W. McGinity, P.B. O'Donnell, Preparation of Microspheres by the Solvent Evaporation Technique. *Advanced Drug Delivery Review*, 28 (1) (1997) 25-42
411. A. Amperiadou, M. Georgarakis, Controlled Release Salbutamol Sulphate Microcapsules Prepared by Emulsion Solvent-Evaporation Technique and Study on the Release affected Parameters, *International Journal of Pharmaceutics*, 115 (1) (1995) 1-8



412. M. K. Lai, R. C. C. Tsiang, Encapsulating Acetaminophen into Poly(l-lactide) Microcapsules by Solvent-Evaporation Technique in an O/W Emulsion, *Journal of Microencapsulation*, 21(3) (2004) 307-316
413. R. Bodmeier, H. Wang, J. Herrmann, Microencapsulation of Chlorpheniramine Maleate, a Drug with Intermediate Solubility Properties, by a Non-Aqueous Solvent Evaporation Technique, *STP Pharma Sciences*, 4 (1994) 275-281
414. R. Jalil, J.R. Nixon, Biodegradable Poly(lactic acid) and Poly(lactide-co-glycolide) Microcapsules: Problems Associated with Preparative Techniques and Release Properties, *Journal of Microencapsulation*, 7 (3) (1990) 297-325
415. R. Bodmeier, J.W. McGinity, The Preparation and Evaluation of Drug-Containing Poly(dl-lactide) Microspheres formed by the Solvent Evaporation Method, *Pharmaceutical Research*, 4 (6) (1987) 465-471
416. P. B. O'Donnell, J. W. McGinity, Preparation of Microspheres by the Solvent Evaporation Technique, *Advanced Drug Delivery Reviews*, 28 (1) (1997) 25-42
417. C. Aftabrouhad, E. Doelker, Preparation Methods for Biodegradable Microparticles Loaded with Water-Soluble Drugs, *STP Pharma Sciences*, 2 (1992) 365-380
418. H. Arabi, S. A. Hashemi M. Fooladi, Microencapsulation of Allopurinol by Solvent Evaporation and Controlled Release Investigation of Drugs. *Journal of Microencapsulation*, 13 (5) (1996) 527-535
419. S. Wieland-Berghausen, U. Schote, M. Frey, F. Schmidt, Comparison of Microencapsulation Techniques for the Water-Soluble Drugs Nitenpyram and Clomipramine HCl, *Journal of Controlled Release*, 85(1-3) (2002) 35-43
420. A.H. Kamel, D.H. Al-Shora, Y.M. El-Sayed, Formulation and Pharmacodynamic Evaluation of Captopril Sustained Release Microparticles, *Journal of Microencapsulation*, 23 (4) (2006) 389-404
421. Z. Mana, Y. Pellequer, A. Lamprecht, Oil-in-Oil Microencapsulation Technique with an External Perfluorohexane Phase, *International Journal of Pharmaceutics*, 338 (1-2) (2007) 231-237

422. S. Benita, *Microencapsulation—Methods and Industrial Applications, Drugs and the Pharmaceutical Sciences*, vol. 73, Marcel Dekker, New York, 1996
423. R. Alex, R. Bodmeier, Encapsulation of Water-Soluble Drugs by a Modified Solvent Evaporation Method. I. Effect of Process and Formulation Variables on Drug Entrapment, *Journal of Microencapsulation*, 7 (3) (1990) 347-355
424. J.L. Chen, C.H. Chiang, M.K. Yeh, The Mechanism of PLA Microparticle Formation by Water-in-Oil-in-Water Solvent Evaporation Method, *Journal of Microencapsulation*, 19 (3) (2002) 333-346
425. M. Li, O. Rouaud, D. Poncelet D, Microencapsulation by Solvent Evaporation: State of the Art for Process Engineering Approaches, *International Journal of Pharmaceutics*, 363 (1-2) (2008) 26-39
426. H. Fujimori, K. Makino, Factors Affecting the Loading Efficiency of Water-Soluble Drugs in PLGA Microspheres, *Colloids Surf B Biointerface*, 61 (1) (2008) 25-29
427. T. Uchida, A. Yagi, Y. Oda, S. Goto, Microencapsulation of Ovalbumin in Poly(lactide-co-glycolide) by an Oil-in-Oil (o/o) Solvent Evaporation Method, *Journal of Microencapsulation*, 13 (5) (1996) 509-518
428. H. Mahdavi, H. Mirzadeh, H. Hamishehkar, A. Jamshidi, A. Fakhari, J. Emami, A. R. Najafabadi, K. Gilani, M. Minaiyan, M. Najafi, M.Tajarod, A. Nokhodchi, The Effect of Process Parameters on the Size and Morphology of Poly(D,L-lactide-co-glycolide) Micro/Nanoparticles Prepared by an Oil in Oil Emulsion/Solvent Evaporation Technique, *Journal of Applied Polymer Science*, 116 (1) (2009) 528-534
429. P.B. O'Donnell, J.W. McGinity, Preparation of Microspheres by the Solvent Evaporation Technique, *Advanced Drug Delivery Reviews*, 28 (1) (1997) 25-42
430. P. Petruzzo, A. Cappai, G. Ruiu, E. Dessy, A. Rescigno, G. Brotzu, Development of Biocompatible Barium Alginate Microcapsules, *Transplantation Proceedings*, 29 (4) (1997) 2129-2130
431. H. Reithmeier, J. Herrmann, A. Göpferich, Lipid Microparticles as a Parenteral Controlled Release Device for Peptide, *Journal of Controlled Release*, 73 (2-3) (2001) 339-350

432. X. Luan, M. Skupin, J. Siepmann, R. Bodmeier, Key Parameters Affecting the Initial Release (burst) and Encapsulation Efficiency of Peptide-Containing Poly(lactide-co-glycolide) Microparticles, *International Journal of Pharmaceutics*, 324 (2) (2006) 168-175
433. G. Spenlehauer, M. Veillard, J.P. Benoit, Formation and Characterization of Cisplatin Loaded Poly (d,l-lactide) Microspheres for Chemo embolization, *Journal of Pharmaceutical Science*, 75 (8) (1986) 750-755
434. P.J. Watts, M.C. Davies, C.D. Melia, Microencapsulation Using Emulsification/Solvent Evaporation: An Overview of Techniques and Applications, *Critical Reviews in Therapeutic Drug Carrier Systems*, 7 (3) (1990) 235-250
435. Y.F. Maa, C. Hsu, Microencapsulation reactor scale-up by dimensional analysis, *Journal of Microencapsulation*, 13 (1) (1996) 53-66
436. W.I. Li, Mechanism and Mathematical Modeling of Microsphere Formation, University of Kentucky (1994)
437. Y. Miyazaki, Y. Onuki, S. Yakou, K. Takayama, Effect of Temperature-Increase Rate on Drug Release Characteristics of Dextran Microspheres Prepared by Emulsion Solvent Evaporation Process, *International Journal of Pharmaceutics*, 324 (2) (2006)144-151
438. S. Freitas, H.P. Merkle, B. Gander, Microencapsulation by Solvent Extraction/Evaporation: Reviewing the State of the Art of Microsphere Preparation Process Technology, *Journal of Controlled Release*, 102 (2) (2004) 313-332
439. Y. Xiong, D. Guo, L. Wang, X. Zheng, Y. Zhang, J. Chen, Development of Nobiliside, A Loaded Liposomal Formulation Using Response Surface Methodology, *International Journal of Pharmaceutics*, 371(1-2) (2009) 197-203
440. D. Attivi, P. Wehrle, N. Ubrich, C. Damge, M. Hoffman, P. Maincent, Formulation of Insulin-Loaded Polymeric Nanoparticles Using Response Surface Methodology, *Drug Development and Industrial Pharmacy*, 31 (2) (2005) 179-189
441. M. Ahuja, M. Yadav, S. Kumar, Application of Response Surface Methodology to Formulation of Ionotropically Gelled Gum Cordia/Gellan Beads, *Carbohydrate Polymers*, 80 (1) (2010) 161-167

442. S. M. Khamanga, N. Parfitt, T. Nyamuzhiwa, H. Haidula, R. B. Walker, The Evaluation of Eudragit Microcapsules Manufactured by Solvent Evaporation Using USP Apparatus 1, *Dissolution Technologies*, 16 (2) (2009) 15-22
443. G. F. Palmieri, D. Lauri, S. Martelli, P. Wehrle, Methoxybutropate Microencapsulation by Gelatin-Acacia Complex Coacervation, *Drug Development and Industrial Pharmacy*, 25 (4) (1999) 399- 407
444. Q. Li, V. Rudolph, B. Weigl, A. Earl, Interparticle Van der Waals Force in Powder Flowability and Compatibility. *International Journal of Pharmaceutics*, 280 (1-2) (2004) 77-93
445. J.S. Kaerger, S. Edge and R. Price, Influence of Particle Size and Shape on Flowability and Compactibility of Binary Mixtures of Paracetamol and MCC, *European Journal of Pharmaceutical Sciences*, 22 (2-3) (2004)173-179
446. R.L. Carr, Classifying Flow Properties of Solids, *Chemical Engineering*, 72 (1965) 69-72
447. H.H. Hausner, Friction Conditions in a Mass of Metal Powders, *International Journal of Powder Metallurgy*, 3 (1967) 7-13
448. F. Nicklasson, G. Alderborn, Analysis of the Compression Mechanics of Pharmaceutical Agglomerates of Different Porosity and Composition Using the Adams and Kawakita Equations. *Pharmaceutical Research*, 17 (8) (2000) 949-954
449. K. Kawakita, K.H. Ludde, Some Considerations on Powder Compression Equations, *Powder Technology*, 4 (1970/1971) 61-68
450. In: T. Kuno, G. Jimbo, E. Saito, H. Takahashi and S. Hayakawa, Editors, Powder (Theory and Application), Maruzen, Tokyo (1979)
451. Z. Zhang, S. Feng, The Drug encapsulation Efficiency, In Vitro Drug Release, Cellular Uptake and Cytotoxicity of Paclitaxel-Loaded Poly(lactide)–Tocopheryl Polyethylene Glycol Succinate Nanoparticles, *Biomaterials*, 27 (21) (2006) 4025-4033
452. V. P. Shah, M. Gurbarg, A. Noory, S. Dighe, J. P. Skelly, Influence of Higher Rates of Agitation on Release Patterns of Immediate-Release Drug Products, *Journal of Pharmaceutical Sciences*, 81 (6) (1992) 500-503

453. K. K. Peh and C. F. Wong, Application of Similarity Factor in Development of Controlled-Release Diltiazem Tablet, *Drug Development and Industrial Pharmacy*, 26 (7) (2000) 723-730
454. K.R. Reddy, S. Mutalik, S. Reddy. Once-Daily Sustained-Release Matrix Tablets of Nicorandil: Formulation and *In-vitro* Evaluation. *AAPS Pharmaceutical Science and Technology*, 4 (4), Article 61, 1-9, (2003). <http://www.aapspharmscitech.org>. (Retrieved 21/08/2004)
455. R.K. Verma, A.M. Kaushal, S. Garg, Development and Evaluation of Extended Release Formulations of Isosorbide Mononitrate based on Osmotic Technology, *International Journal of Pharmaceutics*, 263 (1-2) (2003) 9-24
456. S.A. Bravo, M.C. Lamas, C.J. Salomon. Swellable Matrices for the Controlled-Release of Diclofenac Sodium: Formulation and *In-Vitro* Studies, *Pharmaceutical Development and Technology*, 9 (1) (2004) 75-83
457. J.M. Aiache, N. Aoyagi, H. Blune, J. Dressman, H.D. Friedel, L.T. Grady, V. Gray. FIP Guidance for Dissolution Testing of Solid Oral Products, *Dissolution Technology*, 4 (4) (1997) 5-14
458. I. Borst, S. Ugwu, A.H. Bekett, New and Extended Application for USP Drug Release Apparatus 3. *Dissolution Technology*, 4 (1) (1997) 11-16
459. D. Qiao, B. Hu, D. Gan, Y. Sun, H. Ye, X. Zeng, Extraction Optimized by Using Response Surface Methodology, Purification and Preliminary Characterization of Polysaccharides from *Hyriopsis cumingii*, *Carbohydrate Polymers*, 76 (3) (2009) 422-429
460. Y.Y. Yang, T.S. Chung, X.L. Bai, W.K. Chan, Effect of Preparation Conditions on Morphology and Release Profiles of Biodegradable Polymeric Microspheres Containing Protein Fabricated by Double-Emulsion Method, *Chemical Engineering Science*, 55 (12) (2000) 2223-2236
461. S. V. Fulzele, P. M. Satturwar, R. H. Kasliwal A. K. Dorle, Preparation and Evaluation of Microcapsules Using Polymerized Rosin as a Novel wall Forming Material, *Journal of Microencapsulation*, 21(1) (2004) 83-89

462. C. Chemtob, J.C. Chaumeil, M. N'Dongo, Microencapsulation by Ethylcellulose Phase Separation: Microcapsule Characteristics, *International Journal of Pharmaceutics*, 29 (1) (1986) 1-7
463. S. Benita, M. Donbrow, Effect of Polyisobutylene on Ethylcellulose-Walled Microcapsules: Wall Structure and Thickness of Salicylamide and Theophylline Microcapsules, *Journal of Pharmaceutical Sciences*, 71(2) (2006) 205-210
464. T. Mateovic, B. Kriznar, M. Bogataj, A. Mrhar, The Influence of Stirring Rate on Biopharmaceutical Properties of Eudragit RS Microspheres, *Journal of Microencapsulation* 19 (1) (2002) 29-36
465. S. R. Pygall, S. Kujawinski, P. Timmins, C. D. Melia, Mechanisms of Drug Release in Citrate Buffered HPMC Matrices, *International Journal of Pharmaceutics*, 370 (1-2) (2009) 110-120
466. P. Costa, J. M. Sousa Lobo, Modeling and Comparison of Dissolution Profiles, *European Journal of Pharmaceutical Sciences*, 13 (2) (2001) 123-133
467. S. Brazel, N. A. Peppas, Modeling of Drug Release from Swellable Polymers, *European Journal of Pharmaceutics and Biopharmaceutics*, 49 (1) (2000) 47-58
468. R.W. Korsmeyer, S.R. Lustig and N.A. Peppas, Solute and Penetrant Diffusion in Swellable Polymers. I. Mathematical Modeling, *Journal of Polymer Science Part B Polymer Physics*, 24 (1986) 395-408
469. S.R. Lustig, N.A. Peppas, Solute and Penetrant Diffusion in Swellable Polymers. VII. A Free Volume-Based Model with Mechanical Relaxation, *Journal of Applied Polymwe Science*, 33 (1987) 533-549
470. J.H. Petropoulos, K.G. Papadokostaki , S.G. Amarantos, A General Model for the Release of Active Agents Incorporated in Swellable Polymeric Matrices, *Journal of Polymer Science Part B, Polymer Physics*, 30 (7) (1992) 717-7250
471. P.I. Lee, Diffusional Release of a Solute from a Polymeric Matrix – Approximate Analytical Solutions, *Journal of Membrane Science*, 7 (3) (1980) 255-275

472. S. Joshi, G. Astarita, Mathematical model of the desorption of Swelling solvents from Swollen polymer films, *Polymer*, 20 (10) (1979) 1217-1220
473. A. Viridén, B. Wittgren, A. Larsson, Investigation of Critical Polymer Properties for Polymer Release and Swelling of HPMC Matrix Tablets, *European Journal of Pharmaceutical Sciences*, 36 (2-3) (2009) 297-309
474. S. B. Gurjit, K. Hoebler, C. Sammon, P. Timmins, C.D. Melia, Microstructural Imaging of Early Gel Layer Formation in HPMC Matrices, *Journal of Pharmaceutical Sciences*, 95 (10) (2006) 2145-2157
475. K.V. Ranga Rao, D.K. Padmalatha, Swelling Controlled-Release Systems: Recent Developments and Applications, *International Journal of Pharmaceutics*, 48 (1-3) (1988) 1-13
476. K.T. Mandal, Swelling-Controlled Release System for the Vaginal Delivery of Miconazole, *European Journal of Pharmaceutics and Biopharmaceutics*, 50 (3) (2000) 337-343
477. N. S. Barakat, I. M. Elbagory, A. S. Almurshedi, Controlled-Release Carbamazepine Matrix Granules and Tablets Comprising Lipophilic and Hydrophilic Components, *Drug Delivery*, 16 (1) (2009) 57-65
478. Nicole Kavanagh and Owen I. Corrigan, Swelling and Erosion Properties of Hydroxypropylmethylcellulose (Hypromellose) Matrices-Influence of Agitation Rate and Dissolution Medium Composition, *International Journal of Pharmaceutics*, 279 (1-2) (2004) 141-152
479. C.W. Vendruscolo, I.F. Andrezza, J.L.M.S. Ganter, C. Ferrero, T.M.B. Bresolin, Xanthan and Galactomannan (from *M. scabrella*) Matrix Tablets for Oral Controlled Delivery of Theophylline, *International Journal of Pharmaceutics*, 296 (1-2) (2005) 1-11
480. S. Zuleger, B. C. Lippold, Polymer Particle Erosion Controlling Drug Release. I. Factors Influencing Drug Release and Characterization of the Release Mechanism, *International Journal of Pharmaceutics*, 217 (1-2) (2001) 139-152
481. Hyunjo Kim, Reza Fassihi, Application of Binary Polymer system in Drug Release Rate Modulation. 2. Influence of Formulation Variables and Hydrodynamic Conditions on Release Kinetics, *Journal of Pharmaceutical Sciences*, 86 (3) (1996) 323-328

482. Shahla Jamzad, Lara Tutunji and Reza Fassihi, Analysis of Macromolecular Changes and Drug Release from Hydrophilic Matrix Systems, *International Journal of Pharmaceutics*, 292 (1-2) (2005) 75-85
483. P. Colombo, R. Bettini, G. Massimo, P. L. Catellani, P. Santi, N. A. Peppas, Drug Diffusion Front Movement is Important in Drug Release Control from Swellable Matrix Tablets, *Journal of Pharmaceutical Sciences*, 84 (8) (1995) 991- 997
484. N. Wu, L.S. Wang, D. C. W. Tan, S.M. Moochhala, Y.Y. Yang, Mathematical Modeling and In Vitro Study of Controlled Drug Release via a Highly Swellable and Dissoluble Polymer Matrix: Polyethylene Oxide with High Molecular Weights, *Journal of Controlled Release*, 102 (3) (2005) 569-581
485. V. Michailova, St. Titeva, R. Kotsilkova, E. Krusteva, E. Minkov, Water Uptake and Relaxation Processes in Mixed unlimited Swelling Hydrogels, *International Journal of Pharmaceutics*, 209 (1-2) (2000) 45-56
486. P.W. Heng, L.W. Chan, M.G. Easterbrook, Investigation of the Influence of Mean HPMC Particle Size on the Release of Aspirin from Swellable Hydrophilic Matrix Tablets, *Journal of Controlled Release*, 76 (1-2) (2001) 39-49
487. S. Chopra, G. V. Patil, S. K. Motwani, Release Modulating Hydrophilic Matrix Systems of Losartan Potassium: Optimization of Formulation Using Statistical Experimental Design, *European Journal of Pharmaceutics and Biopharmaceutics*, 66 (1) (2007) 73-82
488. H. Kim, R. Fassihi, A New Ternary Polymeric Matrix System for Controlled Drug Delivery of Highly Soluble Drugs. I. Diltiazem Hydrochloride, *Pharmaceutical Research*, 14 (10) (1997) 1415-1421
489. J. E. Polli, G. S. Rekhi, L. L. Augsburger, V. P. Shah. Methods to Compare Dissolution Profiles and a Rationale for Wide Dissolution Specifications for Metoprolol Tartrate Tablets, *Journal of Pharmaceutical Sciences*, 86 (6) (1997) 691-700
490. J. H. Nogueraa, E. F. Watsonb, Response Surface Analysis of a Multi-Product Batch Processing Facility using a Simulation Metamodel, *International Journal of Production Economics*, 102 (2006) 333-343



491. N. R. Draper, F. Pukelsheim, Canonical Reduction of Second-Order Fitted Models Subject to Linear Restrictions, *Statistics & Probability Letters*, 63 (4) (2003) 401-410
492. R. Carlson, Canonical Analysis of Response Surfaces: A Valuable Tool for Process Development, *Organic Process Research & Development*, 9 (3) (2005) 321-330
493. G.E.P. Box, N.R. Draper, Empirical Model-Building and Response Surfaces, Wiley, New York, 1987
494. M. A. Alonso, S. Sanllorente, L. A. Sarabia, M. J. Arcos, Optimization of the Experimental Parameters in the Determination of Rifamycin SV by Adsorptive Stripping Voltammetry, *Analytica Chimica Acta*, 405 (1-2) (2000) 123-133
495. C. J. F. ter Braak, Interpreting Canonical Correlation Analysis through Biplots of Structure Correlations and Weights, *Psychometrika*, 55 (3) (1990) 519-531
496. C. M. Yang, J. L. Beck, Generalized Trajectory Methods for Finding Multiple Extrema and Roots of Functions, *Journal of Optimization Theory and Applications*, 97 (1) (1998) 211-227
497. A. Khalfaoui, M. Hajjaji, S. Kacim, A. Baçaoui, Evaluation of the Simultaneous Effects of Firing Cycle Parameters on Technological Properties and Ceramic Suitability of a Raw Clay Using the Response Surface Methodology, *Journal of the American Ceramic Society*, 89 (5) (2006) 1563-1567
498. S. Safak, M.özel, H. Bulut, S. A. Bulut, Some New Results on the Algebraic Characterizations of an Equality Onstrained Optimization Problem Equivalent to the Transportation Problem, *International Journal of Computer Mathematics*, 84 (7) (2007) 1021-1026
499. M. A. Solokhin, A. V. Solokhin, V. S. Timofeev, Phase-Equilibrium Stability Criterion in Terms of the Eigenvalues of the Hessian Matrix of the Gibbs Potential, *Theoretical Foundations of Chemical Engineering*, 36 (50) (2002) 444-446
500. .NET Matrix Library for VB.NET, C# C++ programming. <http://www.bluebit.gr/matrix-calculator> (Retrieved 04/01/2010)
501. R. Kalaba, M. R. Scott, An initial-Value Method for Integral Operators. II. Complex Eigenfunctions, *Journal of Optimization Theory and Applications*, 12 (4) (1973) 338-343

502. W. N. L. dos Santos, C. M. C. Santos, S. L. C. Ferreira, Application of Three-Variables Doehlert Matrix for Optimisation of an on-line Pre-Concentration System for Zinc Determination in Natural Water Samples by Flame Atomic Absorption Spectrometry *Microchemical Journal*, 75 (3) (2003) 211-221
503. C. R. T. Tarley, W. N. L. dos Santos, C. M. dos Santos, M. A. Z. Arruda, S. L. C. Ferreira, Factorial Design and Doehlert Matrix in Optimization of Flow System for Preconcentration of Copper on Polyurethane Foam Loaded with 4-(2-Pyridylazo)-resorcinol, *Analytical Letters*, 37 (7) (2004) 1437-1455
504. S. L. C. Ferreira, W. N. L. dos Santos, C. M. Quintella, B. B. Neto, J.M. Bosque-Sendra, Doehlert Matrix: A Chemometric Tool for Analytical Chemistry-Review, *Talanta*, 63 (4) (2004) 1061-1067
505. P. Kumar, S. Singh, B. Mishra, Development and Biopharmaceutical Evaluation of extended release Formulation of Tramadol Hydrochloride based on Osmotic Technology, *Acta Pharmaceutica*, 59 (1) (2009) 15-30
506. J.M. Sonnergaard, On the Misinterpretation of The correlation Coefficient in Pharmaceutical Sciences, *International Journal of Pharmaceutics*, 321 (1-2) (2006) 12-17
507. J.S. Hunter, Calibration and the straight line: current statistical practices, *Association of official Analytical Chemists Journal*, 64 (1981) 574-583
508. A. C. Badino, Jr. M. C. R. Facciotti, W. Schmidell, Volumetric Oxygen Transfer Coefficients ( $k_L a$ ) in Batch Cultivations Involving Non-Newtonian Broths, *Biochemical Engineering Journal*, 8 (2) (2001) 111-119
509. B. M. Corbett, Hypervelocity Impact Proceedings of the 2007 Symposium- HVIS 2007. Selecting a Best-Fit Temperature-Dependent Regression Model for Thin Target HVI data, *International Journal of Impact Engineering*, 35 (12) (2008) 1672-1677
510. B. Amsden, K. Grotheer, D. Angl, Influence of Polymer Ionization Degree on Solute Diffusion in Polyelectrolyte Gels, *Macromolecules*, 35 (8) (2002) 3179-3183

511. P. Costa, J.M.L Sousa, Evaluation of Mathematical Models Describing Drug Release from Estradiol Transdermal Systems, *Drug Development Industrial Pharmacy*, 29 (1) (2003) 89-97
512. M. Donbrow, Y. Samuelov, Zero Order Drug Delivery from Double-Layered Porous Films: Release Rate Profiles from Ethyl Cellulose, Hydroxypropyl Cellulose and Polyethylene Glycol Mixtures, *Journal of Pharmacy and Pharmacology*, 32 (7) (1980) 463-470
513. C.G. Varelas, D.G. Dixon, S. Carol, Zero Order Release from Biphasic Polymer Hydrogels, *Journal of Controlled Release*, 34 (2) (1995) 185-192
514. M. Gibaldi, S. Feldman, Establishment of Sink Conditions in Dissolution Rate Determinations-Theoretical Considerations and Application to Nondisintegrating Dosage Forms, *Journal of Pharmaceutical Sciences*, 56 (10) (1967)1238-1242
515. J.G. Wagner, Interpretation of Percent Dissolved Time Plots Derived from In Vitro Testing of Conventional Tablets and Capsules, *Journal of Pharmaceutical Sciences*, 58 (10) (1969) 1253-1257
516. T. Higuchi, Rate of Release of Medicaments from Ointment Bases Containing Drugs in Suspension, *Journal of Pharmaceutical Sciences*, 50 (10) (1961) 874-875
517. T. Higuchi, Mechanism of Sustained-Action Medication. Theoretical Analysis of Rate of Release of Solid Drugs Dispersed in Solid Matrices, *Journal of Pharmaceutical Sciences*, 52 (12) (1963) 1145-1149
518. Pais, J. Intuiting mathematical objects using diagrams and kinetigrams, *Journal of online mathematics and its applications*, 1 (2) (2001)  
<http://www.bham.ac.uk/ctimath/talum/newsletter/pais.htm>. (Retrieved 01 /05/ 2004).
519. M. Kopcha, N. Lordi, K.J. Tojo, Evaluation of Release from Selected Thermosoftening Vehicles. *Journal of Pharmacy and Pharmacology*, 43 (1991) 382-387
520. R.W. Korsmeyer, N.A. Peppas, Macromolecular and Modeling Aspects of Swelling-Controlled Systems. In *Controlled Release Delivery Systems*; Roseman, T.J., Mansdorf, S.Z., Eds.; Marcel Dekker, Inc: New York and Basel, 1981
521. R.W. Korsmeyer, R. Gurny,E.M. Doelker, P. Buri, N.A. Peppas, Mechanism of Solute Release from Porous Hydrophilic Polymers, *International Journal of Pharmaceutics*, 15 (1) (1983) 25-35

522. N.A. Peppas, Analysis of Fickian and Non-Fickian Drug Release from Polymers, *Pharmaceutica Acta Helvetiae*, 60 (4) (1985) 110-111

523. J. M. Bofill, I. de P. R. Moreira, J. M. Anglada, F. Illas, Large-Scale Matrix Diagonalization Methods by Direct Optimization of Taylor Expansion of Rayleigh-Ritz Quotient up to Third Order, *Chemical Physics Letters*, 329 (1-2) (2000) 160-167

**APPENDIX ONE**

---

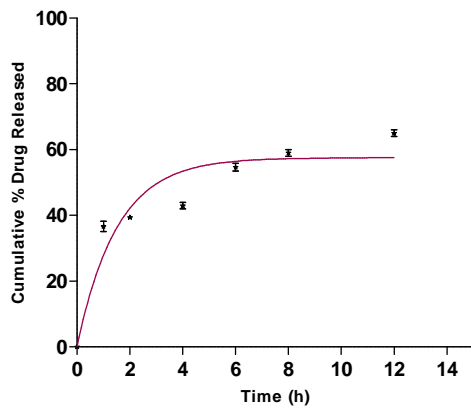
**BATCH SUMMARY**

**RHODES UNIVERSITY**  
**FACULTY OF PHARMACY, GRAHAMSTOWN, SOUTH AFRICA**  
**BATCH SUMMARY**

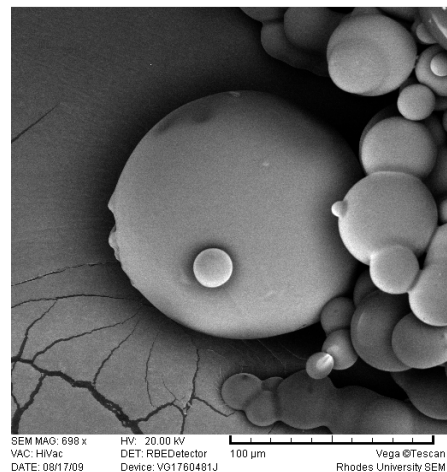
<b>Formulator</b>	Sandile Khamanga	<b>Batch Size</b>	5 g
<b>Product</b>	Captopril	<b>Microencapsulation Time (start)</b>	07:00
<b>Batch ID</b>	CPT-001	<b>(end)</b>	15:00
<b>Microencapsulation Date</b>	16-August-2009		

Material	Amount added	Production	Model
CPT	0.75g	Top load balance	Mettler® Toledo
Eudragit® RS	2.00 g	Homogenizer	Virtis®
Methocel® K100M	0.50 g	<b>Analysis</b>	<b>Model</b>
Methocel® K15M	0.50 g	SEM	Tescan, VEGA LMU
Avicel® 102	0.50 g	Dissolution	VanKel® Bio-Dis® dissolution tester
Liquid paraffin	120 ml	<b>Temperature</b>	22.3 °C
Acetone	20 ml	<b>Humidity</b>	66.0 % RH

**Dissolution**



**SEM**



- Smooth, free-flowing spherical microcapsules of different sizes.

**RHODES UNIVERSITY**  
**FACULTY OF PHARMACY, GRAHAMSTOWN, SOUTH AFRICA**  

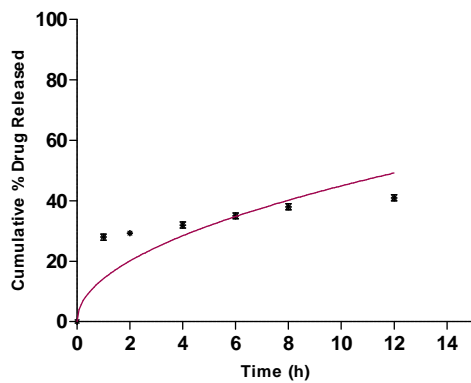

---

**BATCH SUMMARY**

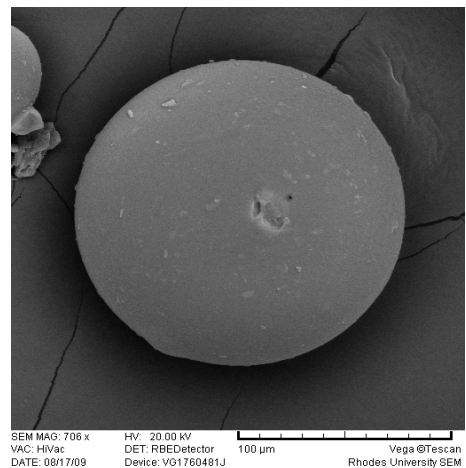
<b>Formulator</b>	Sandile Khamanga	<b>Batch Size</b>	5 g
<b>Product</b>	Captopril	<b>Microencapsulation Time (start)</b>	07:00
<b>Batch ID</b>	CPT-002	<b>(end)</b>	15:00
<b>Microencapsulation Date</b>	16-August-2009		

Material	Amount added	Production	Model
CPT	0.75g	Top load balance	Mettler® Toledo
Eudragit® RS	2.00 g	Homogenizer	Virtis®
Methocel® K100M	0.25 g	<b>Analysis</b>	<b>Model</b>
Methocel® K15M	0.75 g	SEM	Tescan, VEGA LMU
Avicel® 102	0.50 g	Dissolution	VanKel® Bio-Dis® dissolution tester
Liquid paraffin	120 ml	<b>Temperature</b>	22.6 °C
Acetone	20 ml	<b>Humidity</b>	68.0 % RH

**Dissolution**



**SEM**



- Smooth, spherical, free-flowing microcapsules

**RHODES UNIVERSITY**  
**FACULTY OF PHARMACY, GRAHAMSTOWN, SOUTH AFRICA**  

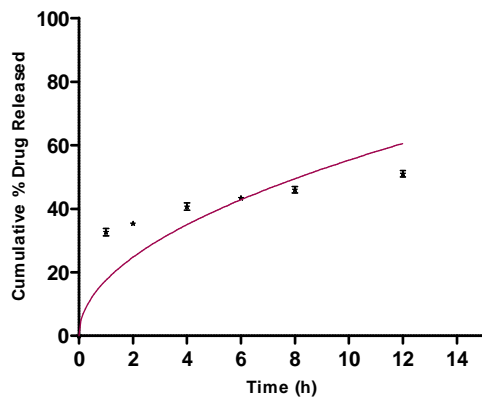

---

**BATCH SUMMARY**

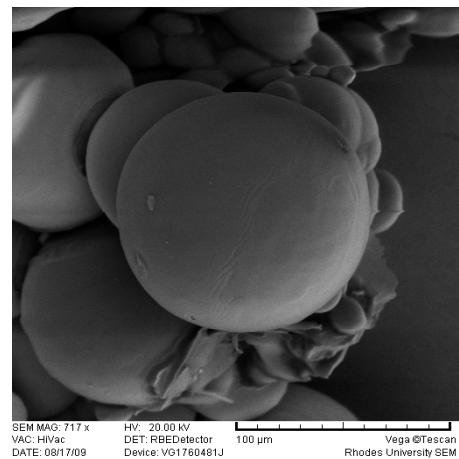
<b>Formulator</b>	Sandile Khamanga	<b>Batch Size</b>	5g
<b>Product</b>	Captopril	<b>Microencapsulation Time (start)</b>	07:00
<b>Batch ID</b>	CPT-003	<b>(end)</b>	15:00
<b>Microencapsulation Date</b>	11-August-2009		

Material	Amount added	Production	Model
CPT	0.75 g	Top load balance	Mettler® Toledo
Eudragit® RS	1.50 g	Homogenizer	Virtis®
Methocel® K100M	0.50 g	<b>Analysis</b>	<b>Model</b>
Methocel® K15M	0.50 g	SEM	Tescan, VEGA LMU
Avicel® 102	0.50 g	Dissolution	VanKel® Bio-Dis® dissolution tester
Liquid paraffin	120 ml	<b>Temperature</b>	24.8 °C
Acetone	20 ml	<b>Humidity</b>	67.0 % RH

**Dissolution**



**SEM**



- Spherical, smooth microcapsules which adhere to one another



**RHODES UNIVERSITY**  
**FACULTY OF PHARMACY, GRAHAMSTOWN, SOUTH AFRICA**  

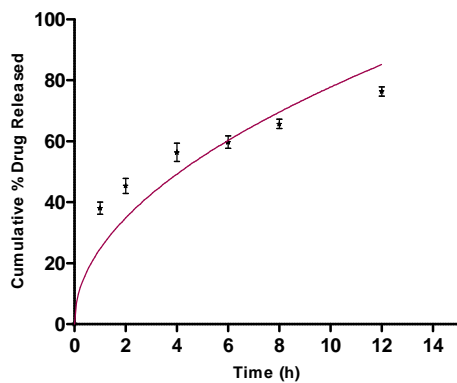

---

**BATCH SUMMARY**

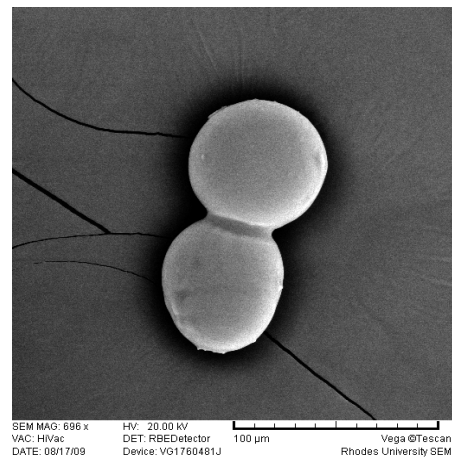
<b>Formulator</b>	Sandile Khamanga	<b>Batch Size</b>	5g
<b>Product</b>	Captopril	<b>Microencapsulation Time (start)</b>	07:00
<b>Batch ID</b>	CPT-004	<b>(end)</b>	15:00
<b>Microencapsulation Date</b>	11-August-2009		

Material	Amount added	Production	Model
CPT	0.75 g	Top load balance	Mettler® Toledo
Eudragit® RS	2.50 g	Homogenizer	Virtis®
Methocel® K100M	0.50 g	<b>Analysis</b>	<b>Model</b>
Methocel® K15M	0.50 g	SEM	Tescan, VEGA LMU
Avicel® 102	0.50 g	Dissolution	VanKel® Bio-Dis® dissolution tester
Liquid paraffin	120 ml	<b>Temperature</b>	23.5 °C
Acetone	20 ml	<b>Humidity</b>	68.0 % RH

**Dissolution**



**SEM**



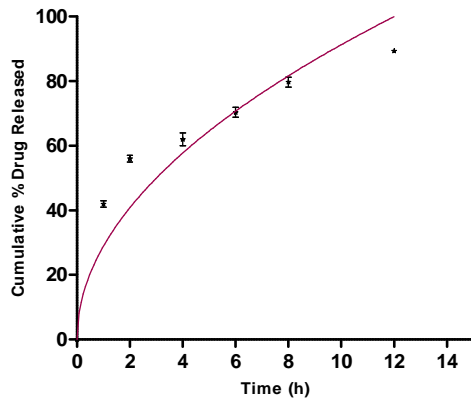
- Surface of microcapsule is smooth but they adhere to one another forming a ‘diploid’

**RHODES UNIVERSITY**  
**FACULTY OF PHARMACY, GRAHAMSTOWN, SOUTH AFRICA**  
**BATCH SUMMARY**

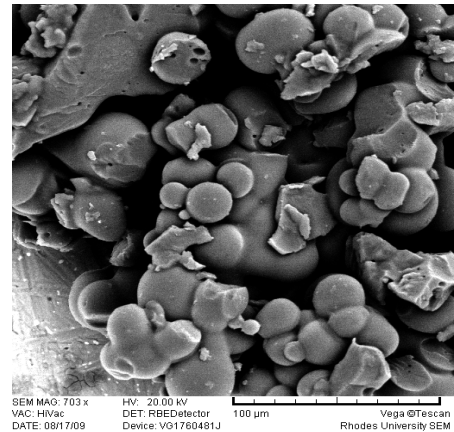
<b>Formulator</b>	Sandile Khamanga	<b>Batch Size</b>	5 g
<b>Product</b>	Captopril	<b>Microencapsulation Time (start)</b>	06:00
<b>Batch ID</b>	CPT-005	<b>(end)</b>	15:00
<b>Microencapsulation Date</b>	10-August-2009		

Material	Amount added	Production	Model
CPT	0.75 g	Top load balance	Mettler® Toledo
Eudragit® RS	2.00 g	Homogenizer	Virtis®
Methocel® K100M	0.25 g	<b>Analysis</b>	<b>Model</b>
Methocel® K15M	0.50 g	SEM	Tescan, VEGA LMU
Avicel® 102	0.50 g	Dissolution	VanKel® Bio-Dis® dissolution tester
Liquid paraffin	120 ml	<b>Temperature</b>	21.8 °C
Acetone	20 ml	<b>Humidity</b>	547 % RH

**Dissolution**



**SEM**



- Small, spherical particles about to form microcapsules

**RHODES UNIVERSITY**  
**FACULTY OF PHARMACY, GRAHAMSTOWN, SOUTH AFRICA**  

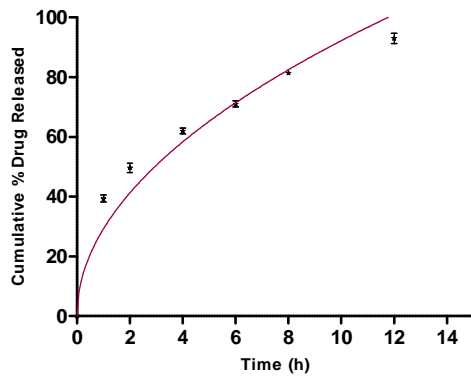

---

**BATCH SUMMARY**

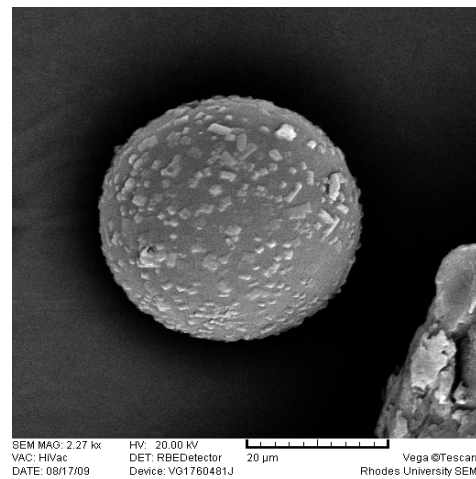
<b>Formulator</b>	Sandile Khamanga	<b>Batch Size</b>	5 g
<b>Product</b>	Captopril	<b>Microencapsulation Time (start)</b>	08:00
<b>Batch ID</b>	CPT-006	<b>(end)</b>	16:00
<b>Microencapsulation Date</b>	10-August-2009		

Material	Amount added	Production	Model
CPT	0.75 g	Top load balance	Mettler® Toledo
Eudragit® RS	2.00 g	Homogenizer	Virtis®
Methocel® K100M	0.50 g	<b>Analysis</b>	<b>Model</b>
Methocel® K15M	0.50 g	SEM	Tescan, VEGA LMU
Avicel® 102	0.50 g	Dissolution	VanKel® Bio-Dis® dissolution tester
Liquid paraffin	120 ml	<b>Temperature</b>	25.6 °C
Acetone	20 ml	<b>Humidity</b>	59.0 % RH

**Dissolution**



**SEM**



- Rough, spherical microcapsule with indentation and deformities

**RHODES UNIVERSITY**  
**FACULTY OF PHARMACY, GRAHAMSTOWN, SOUTH AFRICA**  

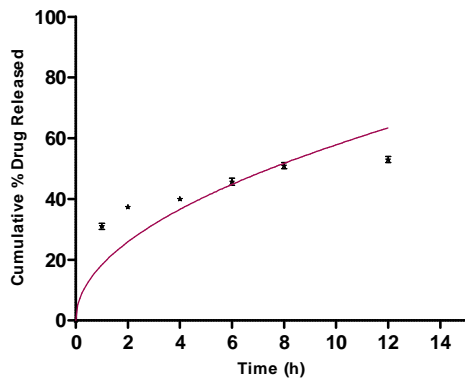

---

**BATCH SUMMARY**

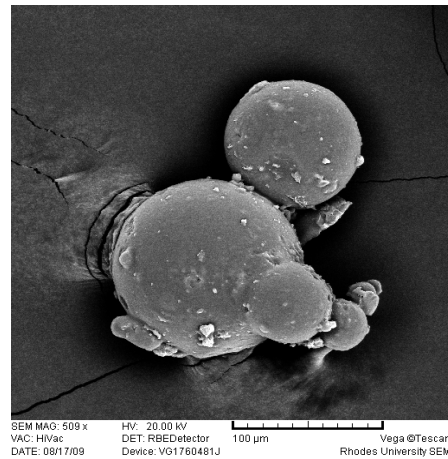
<b>Formulator</b>	Sandile Khamanga	<b>Batch Size</b>	5 g
<b>Product</b>	Captopril	<b>Microencapsulation Time (start)</b>	07:00
<b>Batch ID</b>	CPT-007	<b>(end)</b>	15:00
<b>Microencapsulation Date</b>	9-August-2009		

Material	Amount added	Production	Model
CPT	0.75 g	Top load balance	Mettler® Toledo
Eudragit® RS	2.00 g	Homogenizer	Virtis®
Methocel® K100M	0.75 g	<b>Analysis</b>	<b>Model</b>
Methocel® K15M	0.75 g	SEM	Tescan, VEGA LMU
Avicel® 102	0.50 g	Dissolution	VanKel® Bio-Dis® dissolution tester
Liquid paraffin	120 ml	<b>Temperature</b>	25.4 °C
Acetone	20 ml	<b>Humidity</b>	65.0 % RH

**Dissolution**



**SEM**



- Spherical microcapsules which adhere to one another and there are white, small particles at the surface

**RHODES UNIVERSITY**  
**FACULTY OF PHARMACY, GRAHAMSTOWN, SOUTH AFRICA**  

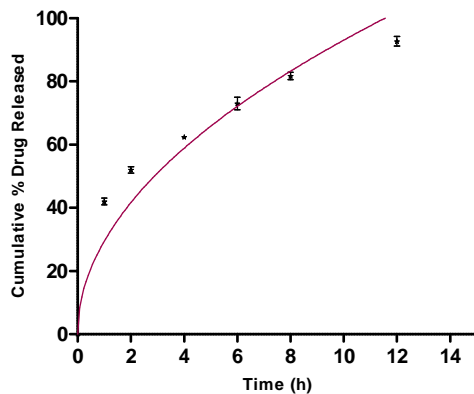

---

**BATCH SUMMARY**

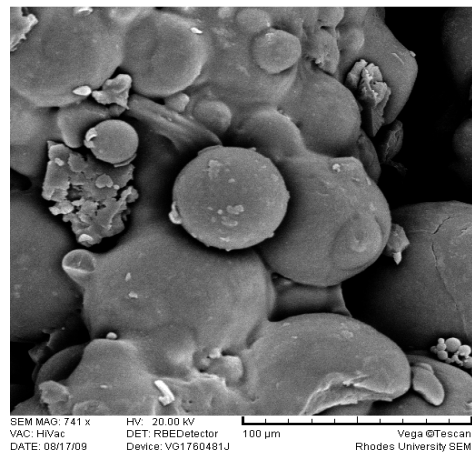
<b>Formulator</b>	Sandile Khamanga	<b>Batch Size</b>	5 g
<b>Product</b>	Captopril	<b>Microencapsulation Time (start)</b>	09:00
<b>Batch ID</b>	CPT-008	<b>(end)</b>	17:00
<b>Microencapsulation Date</b>	9-August-2009		

Material	Amount added	Production	Model
CPT	0.75 g	Top load balance	Mettler® Toledo
Eudragit® RS	1.5 g	Homogenizer	Virtis®
Methocel® K100M	0.50 g	<b>Analysis</b>	<b>Model</b>
Methocel® K15M	0.50 g	SEM	Tescan, VEGA LMU
Avicel® 102	0.50 g	Dissolution	VanKel® Bio-Dis® dissolution tester
Liquid paraffin	120 ml	<b>Temperature</b>	26.6 °C
Acetone	20 ml	<b>Humidity</b>	66.0 % RH

**Dissolution**



**SEM**



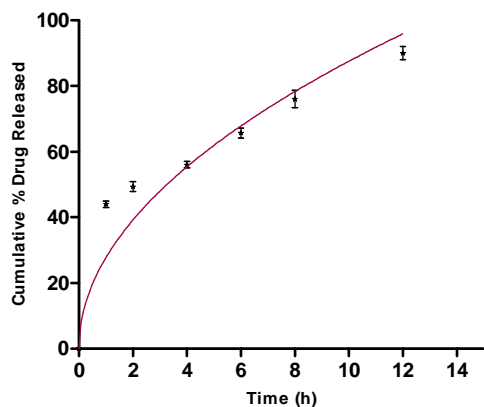
- Irregular- shaped particles which looks damp and ‘dough-like’

**RHODES UNIVERSITY**  
**FACULTY OF PHARMACY, GRAHAMSTOWN, SOUTH AFRICA**  
**BATCH SUMMARY**

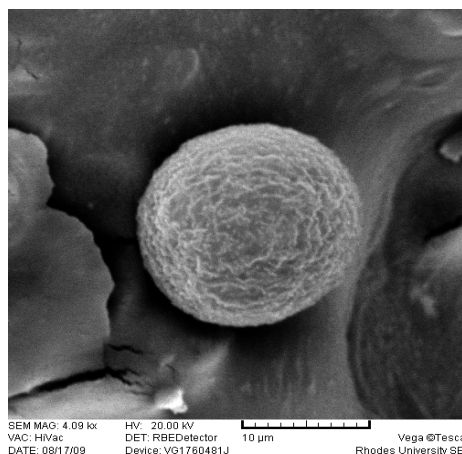
<b>Formulator</b>	Sandile Khamanga	<b>Batch Size</b>	5 g
<b>Product</b>	Captopril	<b>Microencapsulation Time (start)</b>	06:00
<b>Batch ID</b>	CPT-009	<b>(end)</b>	14:00
<b>Microencapsulation Date</b>	11-August-2009		

Material	Amount added	Production	Model
CPT	0.75 g	Top load balance	Mettler® Toledo
Eudragit® RS	1.5 g	Homogenizer	Virtis®
Methocel® K100M	0.50 g	<b>Analysis</b>	<b>Model</b>
Methocel® K15M	0.50 g	SEM	Tescan, VEGA LMU
Avicel® 102	0.50 g	Dissolution	VanKel® Bio-Dis® dissolution tester
Liquid paraffin	120 ml	<b>Temperature</b>	18.2 °C
Acetone	20 ml	<b>Humidity</b>	56.0 % RH

**Dissolution**



**SEM**



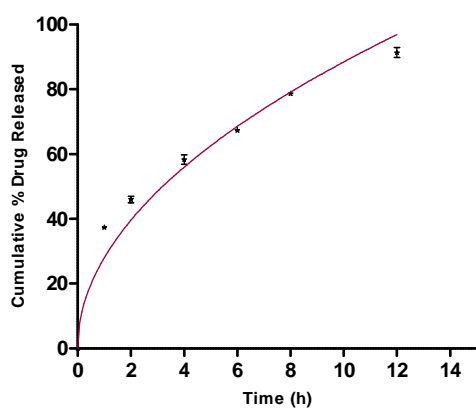
- Rough, spherical, free-flowing microcapsule and free from coalescence

**RHODES UNIVERSITY**  
**FACULTY OF PHARMACY, GRAHAMSTOWN, SOUTH AFRICA**  
**BATCH SUMMARY**

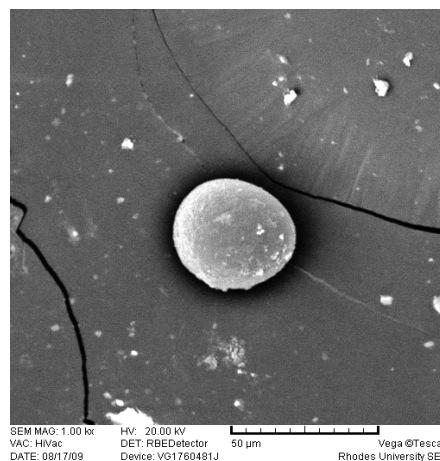
<b>Formulator</b>	Sandile Khamanga	<b>Batch Size</b>	5 g
<b>Product</b>	Captopril	<b>Microencapsulation Time (start)</b>	07:00
<b>Batch ID</b>	CPT-010	<b>(end)</b>	15:00
<b>Microencapsulation Date</b>	11-August-2009		

Material	Amount added	Production	Model
CPT	0.75 g	Top load balance	Mettler® Toledo
Eudragit® RS	2.00 g	Homogenizer	Virtis®
Methocel® K100M	0.50 g	<b>Analysis</b>	<b>Model</b>
Methocel® K15M	0.50 g	SEM	Tescan, VEGA LMU
Avicel® 102	0.50 g	Dissolution	VanKel® Bio-Dis® dissolution tester
Liquid paraffin	120 ml	<b>Temperature</b>	20.6 °C
Acetone	20 ml	<b>Humidity</b>	57.7 % RH

**Dissolution**



**SEM**



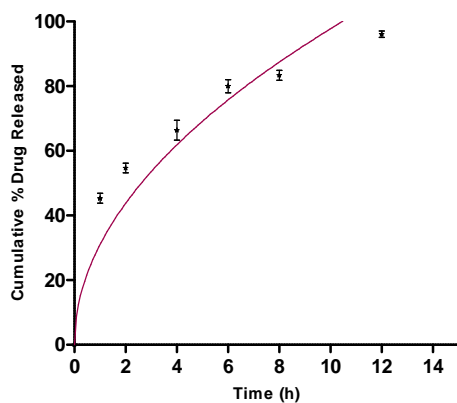
- Spherical, free-flowing, smooth microcapsule and free from coalescence

**RHODES UNIVERSITY**  
**FACULTY OF PHARMACY, GRAHAMSTOWN, SOUTH AFRICA**  
**BATCH SUMMARY**

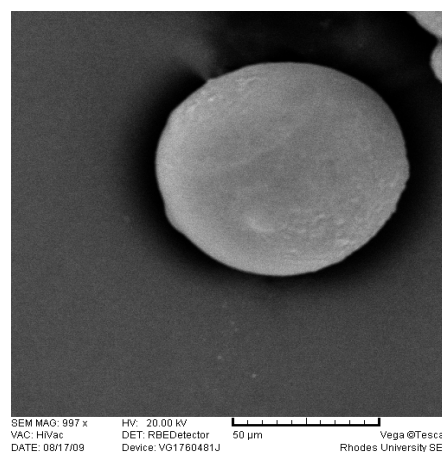
<b>Formulator</b>	Sandile Khamanga	<b>Batch Size</b>	5 g
<b>Product</b>	Captopril	<b>Microencapsulation Time (start)</b>	08:00
<b>Batch ID</b>	CPT-011	<b>(end)</b>	16:00
<b>Microencapsulation Date</b>	08-August-2009		

Material	Amount added	Production	Model
CPT	0.75 g	Top load balance	Mettler® Toledo
Eudragit® RS	1.50 g	Homogenizer	Virtis®
Methocel® K100M	0.50 g	<b>Analysis</b>	<b>Model</b>
Methocel® K15M	0.75 g	SEM	Tescan, VEGA LMU
Avicel® 102	0.50 g	Dissolution	VanKel® Bio-Dis® dissolution tester
Liquid paraffin	120 ml	<b>Temperature</b>	21.5 °C
Acetone	20 ml	<b>Humidity</b>	57.7 % RH

**Dissolution**



**SEM**



- Spherical, free-flowing, smooth microcapsule and free from coalescence



**RHODES UNIVERSITY**  
**FACULTY OF PHARMACY, GRAHAMSTOWN, SOUTH AFRICA**  

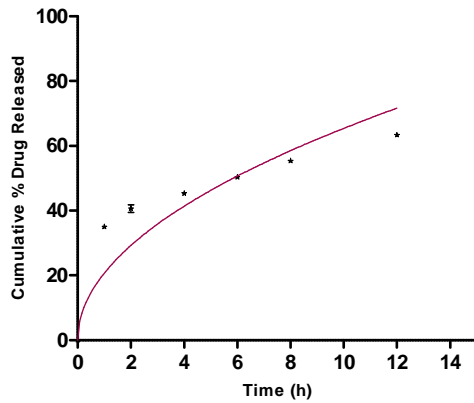

---

**BATCH SUMMARY**

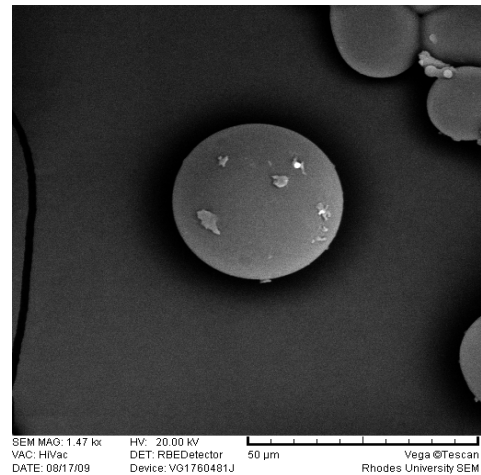
<b>Formulator</b>	Sandile Khamanga	<b>Batch Size</b>	5 g
<b>Product</b>	Captopril	<b>Microencapsulation Time (start)</b>	09:00
<b>Batch ID</b>	CPT-012	<b>(end)</b>	17:00
<b>Microencapsulation Date</b>	08-August-2009		

Material	Amount added	Production	Model
CPT	0.75 g	Top load balance	Mettler® Toledo
Eudragit® RS	2.00 g	Homogenizer	Virtis®
Methocel® K100M	0.50 g	<b>Analysis</b>	<b>Model</b>
Methocel® K15M	0.50 g	SEM	Tescan, VEGA LMU
Avicel® 102	0.50 g	Dissolution	VanKel® Bio-Dis® dissolution tester
Liquid paraffin	120 ml	<b>Temperature</b>	22.0 °C
Acetone	20 ml	<b>Humidity</b>	59.0 % RH

**Dissolution**



**SEM**



- Spherical, free-flowing, smooth microcapsule and free from coalescence

**RHODES UNIVERSITY**  
**FACULTY OF PHARMACY, GRAHAMSTOWN, SOUTH AFRICA**  

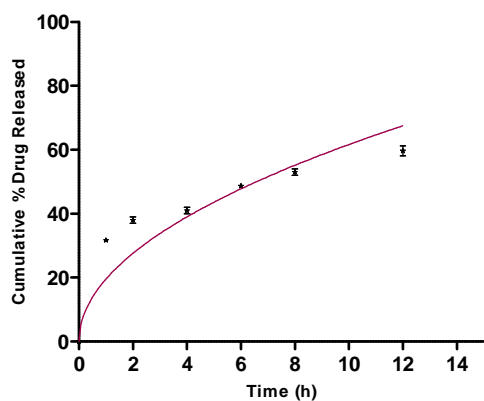

---

**BATCH SUMMARY**

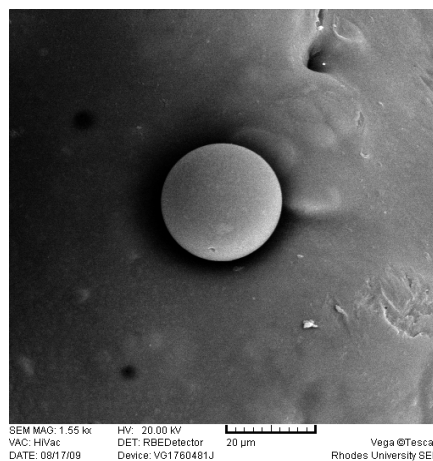
<b>Formulator</b>	Sandile Khamanga	<b>Batch Size</b>	5 g
<b>Product</b>	Captopril	<b>Microencapsulation Time (start)</b>	06:00
<b>Batch ID</b>	CPT-013	<b>(end)</b>	14:00
<b>Microencapsulation Date</b>	07-August-2009		

Material	Amount added	Production	Model
CPT	0.75 g	Top load balance	Mettler® Toledo
Eudragit® RS	2.00 g	Homogenizer	Virtis®
Methocel® K100M	0.50 g	<b>Analysis</b>	<b>Model</b>
Methocel® K15M	0.25 g	SEM	Tescan, VEGA LMU
Avicel® 102	0.50 g	Dissolution	VanKel® Bio-Dis® dissolution tester
Liquid paraffin	120 ml	<b>Temperature</b>	21.5 °C
Acetone	20 ml	<b>Humidity</b>	58.0 % RH

**Dissolution**



**SEM**



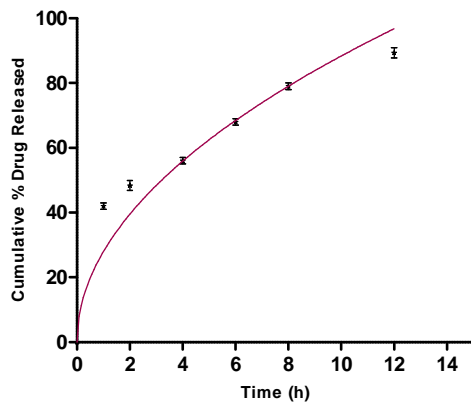
- Spherical, free-flowing, smooth microcapsule and free from coalescence

**RHODES UNIVERSITY**  
**FACULTY OF PHARMACY, GRAHAMSTOWN, SOUTH AFRICA**  
**BATCH SUMMARY**

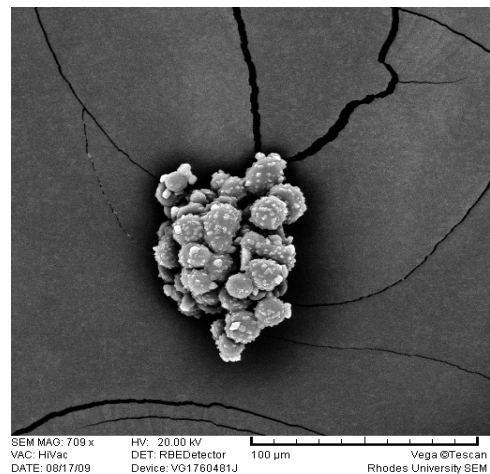
<b>Formulator</b>	Sandile Khamanga	<b>Batch Size</b>	5 g
<b>Product</b>	Captopril	<b>Microencapsulation Time (start)</b>	07:00
<b>Batch ID</b>	CPT-014	<b>(end)</b>	15:00
<b>Microencapsulation Date</b>	07-August-2009		

Material	Amount added	Production	Model
CPT	0.75 g	Top load balance	Mettler® Toledo
Eudragit® RS	2.50 g	Homogenizer	Virtis®
Methocel® K100M	0.50 g	<b>Analysis</b>	<b>Model</b>
Methocel® K15M	0.25 g	SEM	Tescan, VEGA LMU
Avicel® 102	0.50 g	Dissolution	VanKel® Bio-Dis® dissolution tester
Liquid paraffin	120 ml	<b>Temperature</b>	22.5 °C
Acetone	20 ml	<b>Humidity</b>	56.8 % RH

**Dissolution**



**SEM**



- Irregular-shaped particles which formed aggregates and drug particles seen at the surface

**RHODES UNIVERSITY**  
**FACULTY OF PHARMACY, GRAHAMSTOWN, SOUTH AFRICA**  

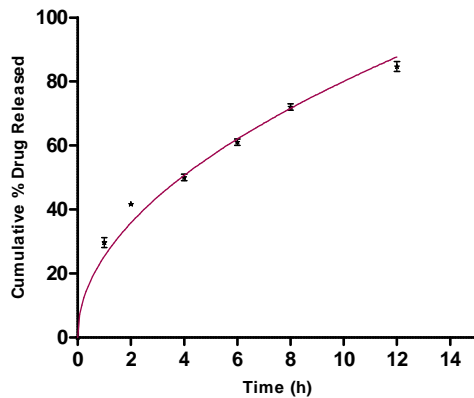

---

**BATCH SUMMARY**

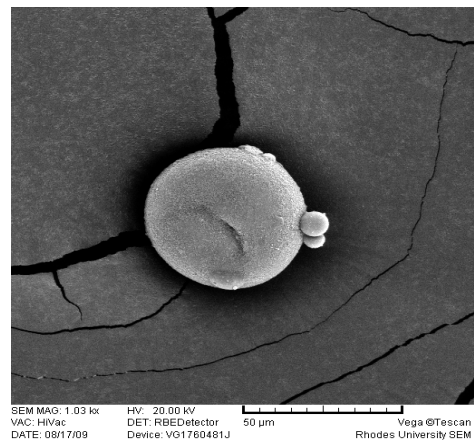
<b>Formulator</b>	Sandile Khamanga	<b>Batch Size</b>	5 g
<b>Product</b>	Captopril	<b>Microencapsulation Time (start)</b>	08:00
<b>Batch ID</b>	CPT-015	<b>(end)</b>	16:00
<b>Microencapsulation Date</b>	05-August-2009		

Material	Amount added	Production	Model
CPT	0.75 g	Top load balance	Mettler® Toledo
Eudragit® RS	2.00 g	Homogenizer	Virtis®
Methocel® K100M	0.50 g	<b>Analysis</b>	<b>Model</b>
Methocel® K15M	0.50 g	SEM	Tescan, VEGA LMU
Avicel® 102	0.50 g	Dissolution	VanKel® Bio-Dis® dissolution tester
Liquid paraffin	120 ml	<b>Temperature</b>	26.3 °C
Acetone	20 ml	<b>Humidity</b>	68.0 % RH

**Dissolution**



**SEM**



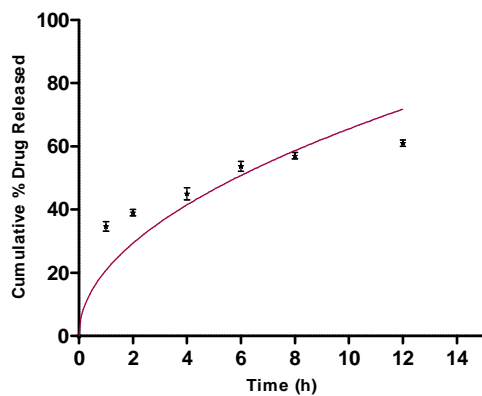
- Spherical microcapsule, free-flowing and free from coalescence except for tiny spherical particles attaching to the surface

**RHODES UNIVERSITY**  
**FACULTY OF PHARMACY, GRAHAMSTOWN, SOUTH AFRICA**  
**BATCH SUMMARY**

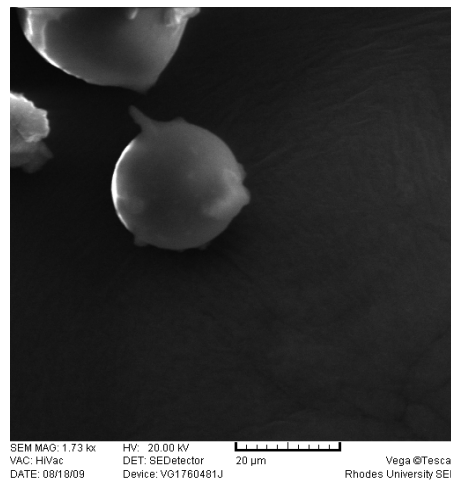
<b>Formulator</b>	Sandile Khamanga	<b>Batch Size</b>	5 g
<b>Product</b>	Captopril	<b>Microencapsulation Time (start)</b>	08:00
<b>Batch ID</b>	CPT-016	<b>(end)</b>	17:00
<b>Microencapsulation Date</b>	05-August-2009		

Material	Amount added	Production	Model
CPT	0.75 g	Top load balance	Mettler® Toledo
Eudragit® RS	2.50 g	Homogenizer	Virtis®
Methocel® K100M	0.75 g	<b>Analysis</b>	<b>Model</b>
Methocel® K15M	0.50 g	SEM	Tescan, VEGA LMU
Avicel® 102	0.50 g	Dissolution	VanKel® Bio-Dis® dissolution tester
Liquid paraffin	120 ml	<b>Temperature</b>	25.4 °C
Acetone	20 ml	<b>Humidity</b>	67.5 % RH

**Dissolution**



**SEM**



- Irregular-shaped microcapsule, not free-flowing

**RHODES UNIVERSITY**  
**FACULTY OF PHARMACY, GRAHAMSTOWN, SOUTH AFRICA**  

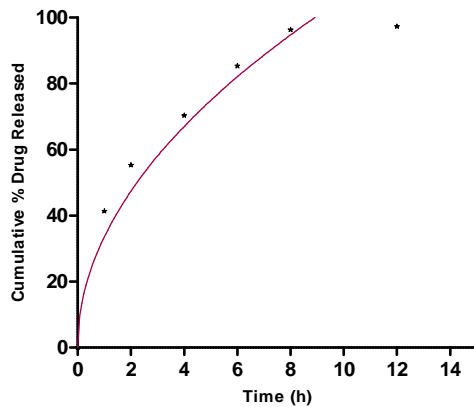

---

**BATCH SUMMARY**

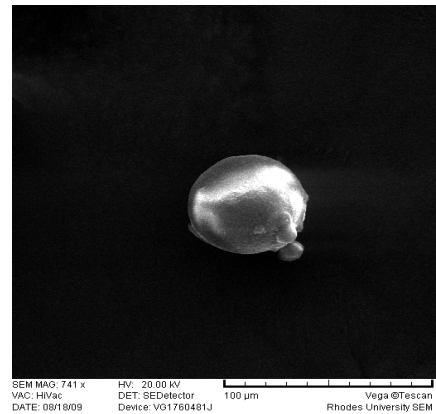
<b>Formulator</b>	Sandile Khamanga	<b>Batch Size</b>	5 g
<b>Product</b>	Captopril	<b>Microencapsulation Time (start)</b>	07:00
<b>Batch ID</b>	CPT-017	<b>(end)</b>	15:00
<b>Microencapsulation Date</b>	04-August-2009		

Material	Amount added	Production	Model
CPT	0.75 g	Top load balance	Mettler® Toledo
Eudragit® RS	1.50 g	Homogenizer	Virtis®
Methocel® K100M	0.75 g	<b>Analysis</b>	<b>Model</b>
Methocel® K15M	0.50 g	SEM	Tescan, VEGA LMU
Avicel® 102	0.50 g	Dissolution	VanKel® Bio-Dis® dissolution tester
Liquid paraffin	120 ml	<b>Temperature</b>	18.4 °C
Acetone	20 ml	<b>Humidity</b>	52.6 % RH

**Dissolution**



**SEM**



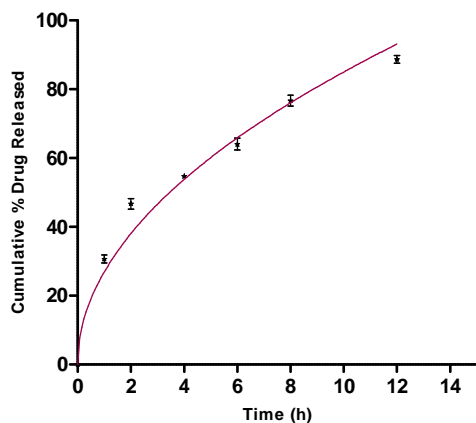
- Spherical, free-flowing microcapsule with small attachments at the surface

**RHODES UNIVERSITY**  
**FACULTY OF PHARMACY, GRAHAMSTOWN, SOUTH AFRICA**  
**BATCH SUMMARY**

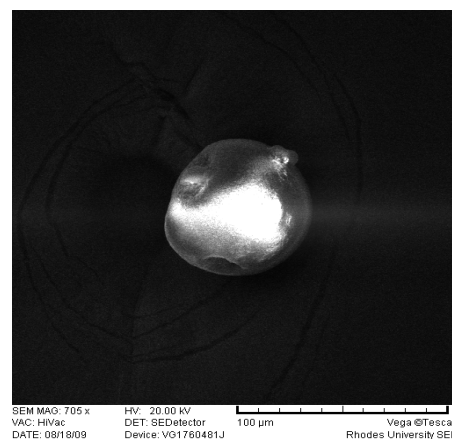
<b>Formulator</b>	Sandile Khamanga	<b>Batch Size</b>	5 g
<b>Product</b>	Captopril	<b>Microencapsulation Time (start)</b>	08:00
<b>Batch ID</b>	CPT-018	<b>(end)</b>	17:00
<b>Microencapsulation Date</b>	04-August-2009		

Material	Amount added	Production	Model
CPT	0.75 g	Top load balance	Mettler® Toledo
Eudragit® RS	2.00 g	Homogenizer	Virtis®
Methocel® K100M	0.50 g	<b>Analysis</b>	<b>Model</b>
Methocel® K15M	0.25 g	SEM	Tescan, VEGA LMU
Avicel® 102	0.50 g	Dissolution	VanKel® Bio-Dis® dissolution tester
Liquid paraffin	120 ml	<b>Temperature</b>	18.5 °C
Acetone	20 ml	<b>Humidity</b>	54.6 % RH

**Dissolution**



**SEM**



- Surface of microcapsule irregular but smooth

**RHODES UNIVERSITY**  
**FACULTY OF PHARMACY, GRAHAMSTOWN, SOUTH AFRICA**  

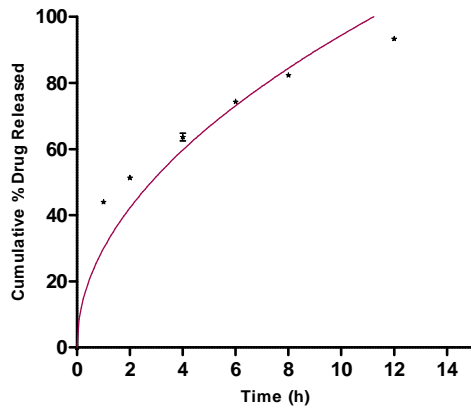

---

**BATCH SUMMARY**

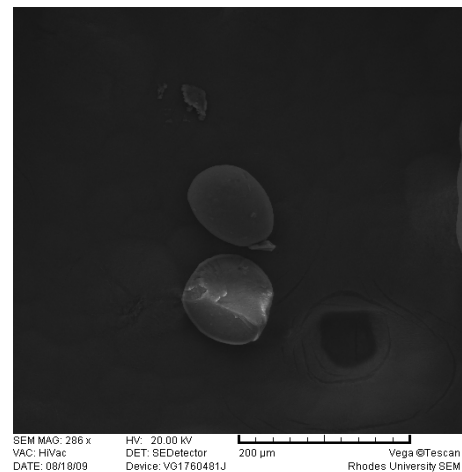
<b>Formulator</b>	Sandile Khamanga	<b>Batch Size</b>	5 g
<b>Product</b>	Captopril	<b>Microencapsulation Time (start)</b>	07:00
<b>Batch ID</b>	CPT-019	<b>(end)</b>	15:00
<b>Microencapsulation Date</b>	01-August-2009		

Material	Amount added	Production	Model
CPT	0.75 g	Top load balance	Mettler® Toledo
Eudragit® RS	2.50 g	Homogenizer	Virtis®
Methocel® K100M	0.50 g	<b>Analysis</b>	<b>Model</b>
Methocel® K15M	0.75 g	SEM	Tescan, VEGA LMU
Avicel® 102	0.50 g	Dissolution	VanKel® Bio-Dis® dissolution tester
Liquid paraffin	120 ml	<b>Temperature</b>	18.5 °C
Acetone	20 ml	<b>Humidity</b>	53.5 % RH

**Dissolution**



**SEM**



- Particles have collapsed surface and are irregular in shape



**RHODES UNIVERSITY**  
**FACULTY OF PHARMACY, GRAHAMSTOWN, SOUTH AFRICA**  

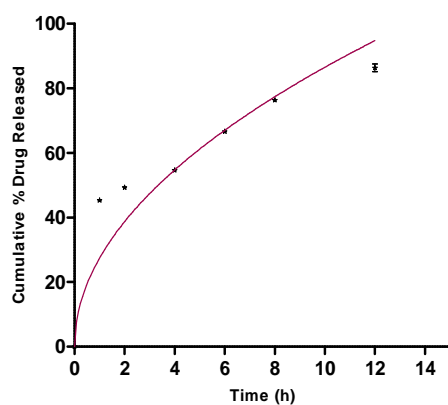

---

**BATCH SUMMARY**

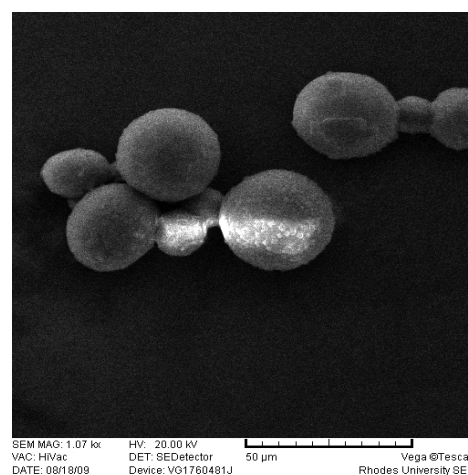
<b>Formulator</b>	Sandile Khamanga	<b>Batch Size</b>	5 g
<b>Product</b>	Captopril	<b>Microencapsulation Time (start)</b>	07:00
<b>Batch ID</b>	CPT-020	<b>(end)</b>	15:00
<b>Microencapsulation Date</b>	01-August-2009		

Material	Amount added	Production	Model
CPT	0.75 g	Top load balance	Mettler® Toledo
Eudragit® RS	2.50 g	Homogenizer	Virtis®
Methocel® K100M	0.50 g	<b>Analysis</b>	<b>Model</b>
Methocel® K15M	0.75 g	SEM	Tescan, VEGA LMU
Avicel® 102	0.50 g	Dissolution	VanKel® Bio-Dis® dissolution tester
Liquid paraffin	120 ml	<b>Temperature</b>	18.3 °C
Acetone	20 ml	<b>Humidity</b>	54.9 % RH

**Dissolution**



**SEM**



- Spherical, free-flowing microcapsules that were coarse on the surface

**RHODES UNIVERSITY**  
**FACULTY OF PHARMACY, GRAHAMSTOWN, SOUTH AFRICA**  

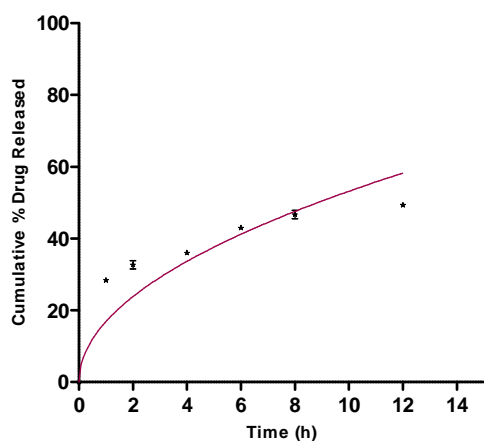

---

**BATCH SUMMARY**

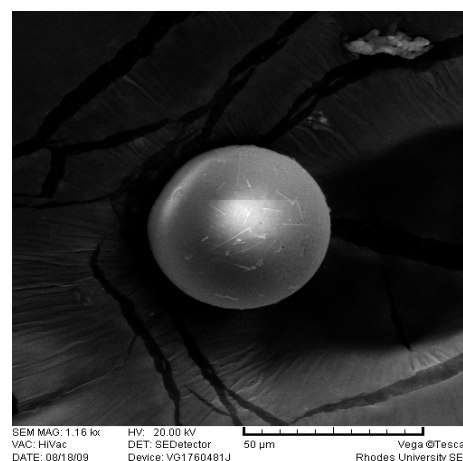
<b>Formulator</b>	Sandile Khamanga	<b>Batch Size</b>	5 g
<b>Product</b>	Captopril	<b>Microencapsulation Time (start)</b>	07:00
<b>Batch ID</b>	CPT-021	<b>(end)</b>	15:00
<b>Microencapsulation Date</b>	02-August-2009		

Material	Amount added	Production	Model
CPT	0.75 g	Top load balance	Mettler® Toledo
Eudragit® RS	2.00 g	Homogenizer	Virtis®
Methocel® K100M	0.75 g	<b>Analysis</b>	<b>Model</b>
Methocel® K15M	0.50 g	SEM	Tescan, VEGA LMU
Avicel® 102	0.50 g	Dissolution	VanKel® Bio-Dis® dissolution tester
Liquid paraffin	120 ml	<b>Temperature</b>	19.4 °C
Acetone	20 ml	<b>Humidity</b>	48.0 % RH

**Dissolution**



**SEM**



- Spherical, free-flowing microcapsules

**RHODES UNIVERSITY**  
**FACULTY OF PHARMACY, GRAHAMSTOWN, SOUTH AFRICA**  

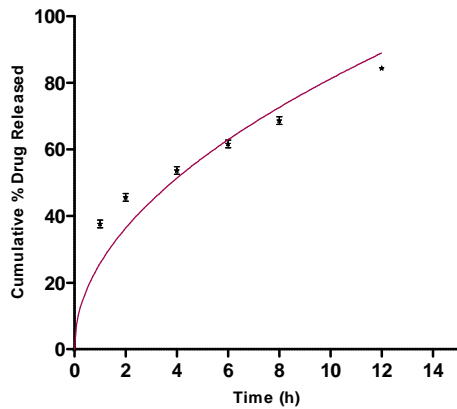

---

**BATCH SUMMARY**

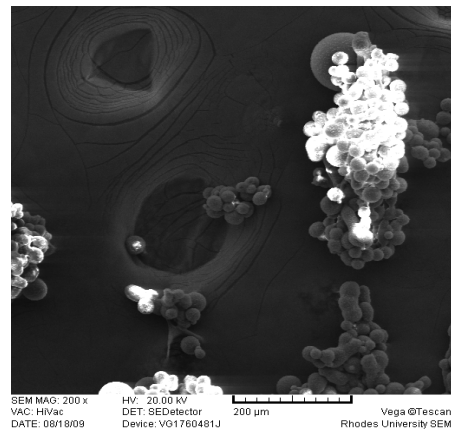
<b>Formulator</b>	Sandile Khamanga	<b>Batch Size</b>	5 g
<b>Product</b>	Captopril	<b>Microencapsulation Time (start)</b>	10:00
<b>Batch ID</b>	CPT-022	<b>(end)</b>	20:00
<b>Microencapsulation Date</b>	02-August-2009		

Material	Amount added	Production	Model
CPT	0.75 g	Top load balance	Mettler® Toledo
Eudragit® RS	2.00 g	Homogenizer	Virtis®
Methocel® K100M	0.50 g	<b>Analysis</b>	<b>Model</b>
Methocel® K15M	0.75 g	SEM	Tescan, VEGA LMU
Avicel® 102	0.50 g	Dissolution	VanKel® Bio-Dis® dissolution tester
Liquid paraffin	120 ml	<b>Temperature</b>	19.3 °C
Acetone	20 ml	<b>Humidity</b>	46.0 % RH

**Dissolution**



**SEM**



- ‘Grape-like’ structures, which appear as tiny particles that have formed aggregates

**RHODES UNIVERSITY**  
**FACULTY OF PHARMACY, GRAHAMSTOWN, SOUTH AFRICA**  

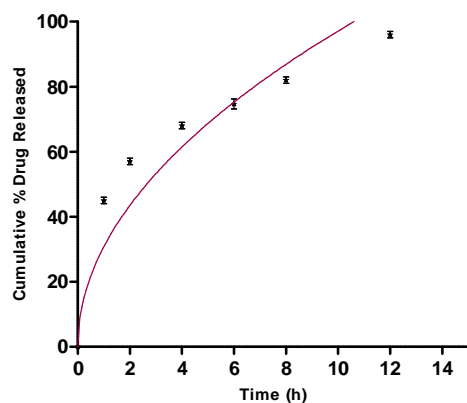

---

**BATCH SUMMARY**

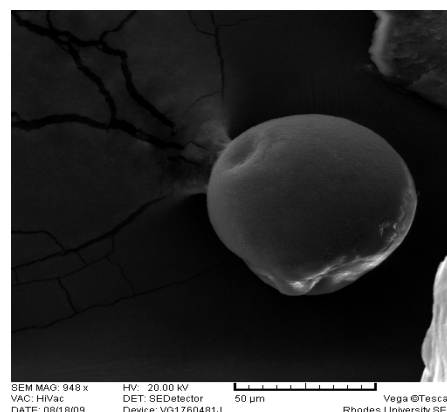
<b>Formulator</b>	Sandile Khamanga	<b>Batch Size</b>	5 g
<b>Product</b>	Captopril	<b>Microencapsulation Time (start)</b>	08:00
<b>Batch ID</b>	CPT-023	<b>(end)</b>	16:00
<b>Microencapsulation Date</b>	04-August-2009		

Material	Amount added	Production	Model
CPT	0.75 g	Top load balance	Mettler® Toledo
Eudragit® RS	2.50 g	Homogenizer	Virtis®
Methocel® K100M	0.25 g	<b>Analysis</b>	<b>Model</b>
Methocel® K15M	0.50 g	SEM	Tescan, VEGA LMU
Avicel® 102	0.50 g	Dissolution	VanKel® Bio-Dis® dissolution tester
Liquid paraffin	120 ml	<b>Temperature</b>	26.7 °C
Acetone	20 ml	<b>Humidity</b>	66.0 % RH

**Dissolution**



**SEM**



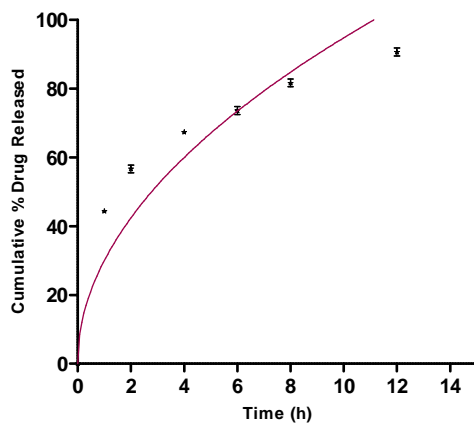
- Spherical, free-flowing microcapsule

**RHODES UNIVERSITY**  
**FACULTY OF PHARMACY, GRAHAMSTOWN, SOUTH AFRICA**  
**BATCH SUMMARY**

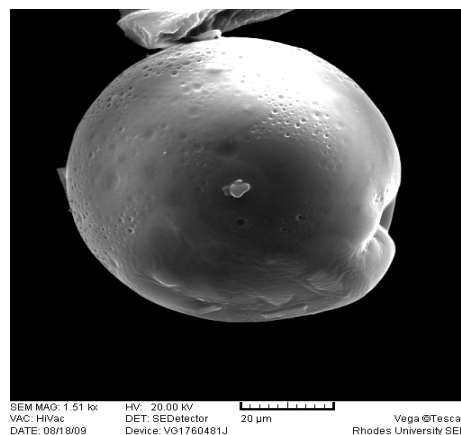
<b>Formulator</b>	Sandile Khamanga	<b>Batch Size</b>	5 g
<b>Product</b>	Captopril	<b>Microencapsulation Time (start)</b>	07:00
<b>Batch ID</b>	CPT-024	<b>(end)</b>	15:00
<b>Microencapsulation Date</b>	04-August-2009		

Material	Amount added	Production	Model
CPT	0.75 g	Top load balance	Mettler® Toledo
Eudragit® RS	2.00 g	Homogenizer	Virtis®
Methocel® K100M	0.25 g	<b>Analysis</b>	<b>Model</b>
Methocel® K15M	0.50 g	SEM	Tescan, VEGA LMU
Avicel® 102	0.50 g	Dissolution	VanKel® Bio-Dis® dissolution tester
Liquid paraffin	120 ml	<b>Temperature</b>	26.3 °C
Acetone	20 ml	<b>Humidity</b>	68.0 % RH

**Dissolution**



**SEM**



- Spherical microcapsule, with depression on the surface

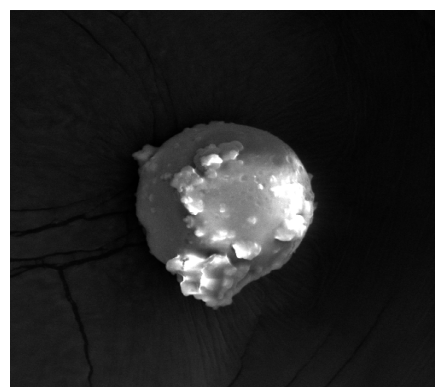
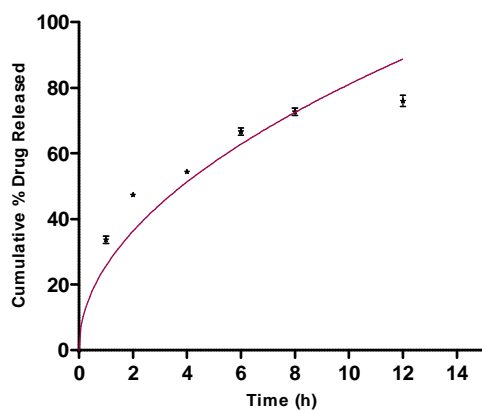
**RHODES UNIVERSITY**  
**FACULTY OF PHARMACY, GRAHAMSTOWN, SOUTH AFRICA**  
**BATCH SUMMARY**

<b>Formulator</b>	Sandile Khamanga	<b>Batch Size</b>	5 g
<b>Product</b>	Captopril	<b>Microencapsulation Time (start)</b>	08:00
<b>Batch ID</b>	CPT-025	<b>(end)</b>	17:00
<b>Microencapsulation Date</b>	15-August-2009		

Material	Amount added	Production	Model
CPT	0.75 g	Top load balance	Mettler® Toledo
Eudragit® RS	1.50 g	Homogenizer	Virtis®
Methocel® K100M	0.50 g	<b>Analysis</b>	<b>Model</b>
Methocel® K15M	0.25 g	SEM	Tescan, VEGA LMU
Avicel® 102	0.50 g	Dissolution	VanKel® Bio-Dis® dissolution tester
Liquid paraffin	120 ml	<b>Temperature</b>	18.8 °C
Acetone	20 ml	<b>Humidity</b>	56.0 % RH

**Dissolution**

**SEM**



SEM MAG: 1.03 kx HV: 20.00 kV  
VAC: HVac DET: SEDetector Vega®/Tescan  
DATE: 08/18/09 Device: V91750481J 50 µm Rhodes University SEM

- Microcapsules appear as roughly spherical with particles protruding from the surface

**RHODES UNIVERSITY**  
**FACULTY OF PHARMACY, GRAHAMSTOWN, SOUTH AFRICA**  

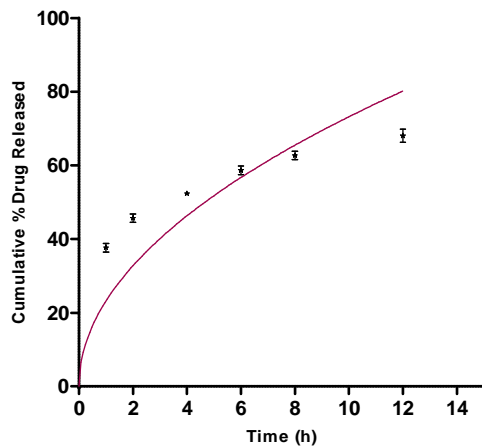

---

**BATCH SUMMARY**

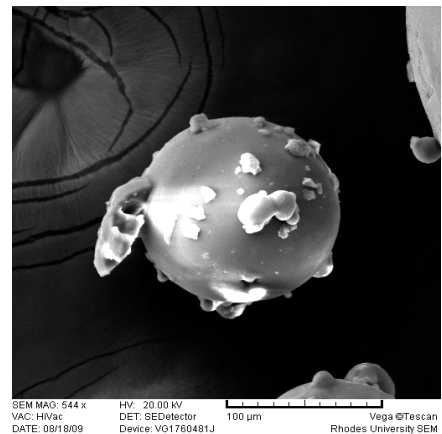
<b>Formulator</b>	Sandile Khamanga	<b>Batch Size</b>	5 g
<b>Product</b>	Captopril	<b>Microencapsulation Time (start)</b>	10:00
<b>Batch ID</b>	CPT-026	<b>(end)</b>	18:00
<b>Microencapsulation Date</b>	15-August-2009		

Material	Amount added	Production	Model
CPT	0.75 g	Top load balance	Mettler® Toledo
Eudragit® RS	2.50 g	Homogenizer	Virtis®
Methocel® K100M	0.50 g	<b>Analysis</b>	<b>Model</b>
Methocel® K15M	0.50 g	SEM	Tescan, VEGA LMU
Avicel® 102	0.50 g	Dissolution	VanKel® Bio-Dis® dissolution tester
Liquid paraffin	120 ml	<b>Temperature</b>	19.5 °C
Acetone	20 ml	<b>Humidity</b>	58.0 % RH

**Dissolution**



**SEM**



- Spherical microcapsule which still has some particles adhering strongly to the surface

**RHODES UNIVERSITY**  
**FACULTY OF PHARMACY, GRAHAMSTOWN, SOUTH AFRICA**  

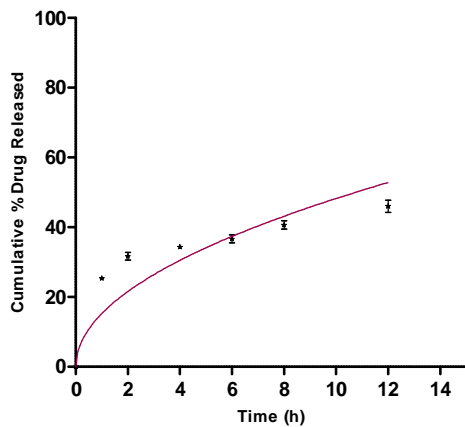

---

**BATCH SUMMARY**

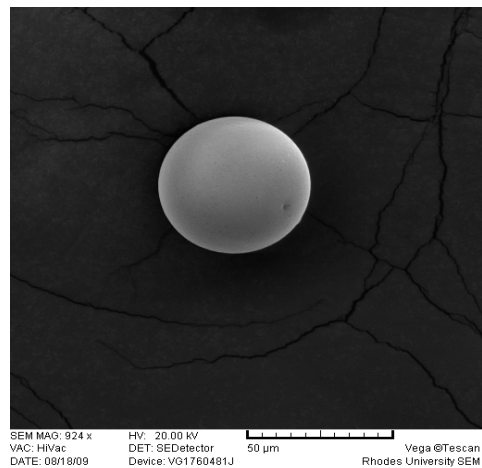
<b>Formulator</b>	Sandile Khamanga	<b>Batch Size</b>	5 g
<b>Product</b>	Captopril	<b>Microencapsulation Time (start)</b>	11:00
<b>Batch ID</b>	CPT-027	<b>(end)</b>	20:00
<b>Microencapsulation Date</b>	17-August-2009		

Material	Amount added	Production	Model
CPT	0.75 g	Top load balance	Mettler® Toledo
Eudragit® RS	2.00 g	Homogenizer	Virtis®
Methocel® K100M	0.25 g	<b>Analysis</b>	<b>Model</b>
Methocel® K15M	0.25 g	SEM	Tescan, VEGA LMU
Avicel® 102	0.50 g	Dissolution	VanKel® Bio-Dis® dissolution tester
Liquid paraffin	120 ml	<b>Temperature</b>	24.7 °C
Acetone	20 ml	<b>Humidity</b>	64.0 % RH

**Dissolution**



**SEM**



- Smooth, free-flowing spherical microcapsules



**RHODES UNIVERSITY**  
**FACULTY OF PHARMACY, GRAHAMSTOWN, SOUTH AFRICA**  

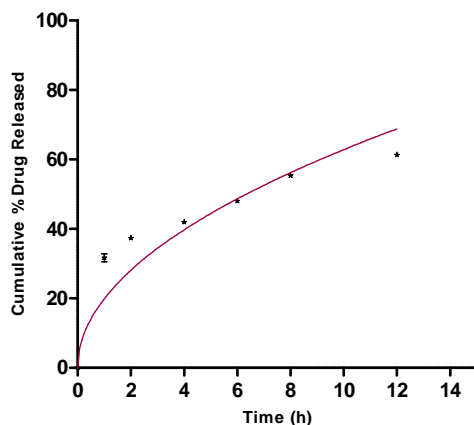

---

**BATCH SUMMARY**

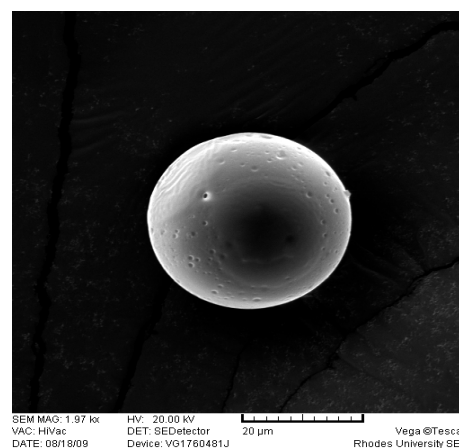
<b>Formulator</b>	Sandile Khamanga	<b>Batch Size</b>	5 g
<b>Product</b>	Captopril	<b>Microencapsulation Time (start)</b>	12:00
<b>Batch ID</b>	CPT-028	<b>(end)</b>	22:00
<b>Microencapsulation Date</b>	16-August-2009		

Material	Amount added	Production	Model
CPT	0.75 g	Top load balance	Mettler® Toledo
Eudragit® RS	1.50 g	Homogenizer	Virtis®
Methocel® K100M	0.25 g	<b>Analysis</b>	<b>Model</b>
Methocel® K15M	0.50 g	SEM	Tescan, VEGA LMU
Avicel® 102	0.50 g	Dissolution	VanKel® Bio-Dis® dissolution tester
Liquid paraffin	120 ml	<b>Temperature</b>	23.3 °C
Acetone	20 ml	<b>Humidity</b>	64.0 % RH

**Dissolution**



**SEM**



- Smooth free-flowing spherical microcapsules

**RHODES UNIVERSITY**  
**FACULTY OF PHARMACY, GRAHAMSTOWN, SOUTH AFRICA**  

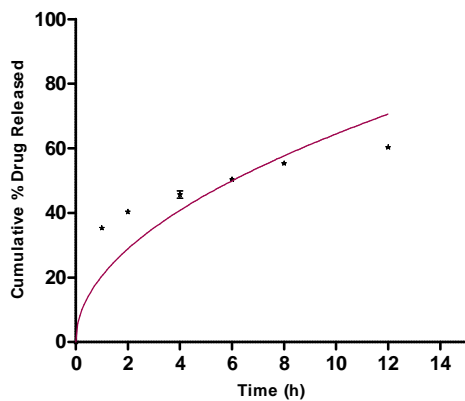

---

**BATCH SUMMARY**

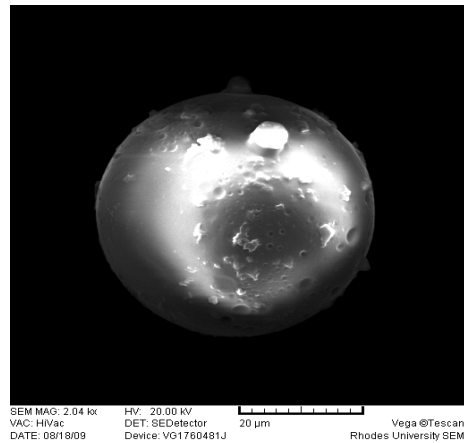
<b>Formulator</b>	Sandile Khamanga	<b>Batch Size</b>	5 g
<b>Product</b>	Captopril	<b>Microencapsulation Time (start)</b>	07:00
<b>Batch ID</b>	CPT-029	<b>(end)</b>	15:00
<b>Microencapsulation Date</b>	16-August-2009		

CPT	0.75 g	Top load balance	Mettler® Toledo
Eudragit® RS	2.00 g	Homogenizer	Virtis®
Methocel® K100M	0.50 g	<b>Analysis</b>	<b>Model</b>
Methocel® K15M	0.75 g	SEM	Tescan, VEGA LMU
Avicel® 102	0.50 g	Dissolution	VanKel® Bio-Dis® dissolution tester
Liquid paraffin	120 ml	<b>Temperature</b>	22.7 °C
Acetone	20 ml	<b>Humidity</b>	61.0 % RH

**Dissolution**



**SEM**



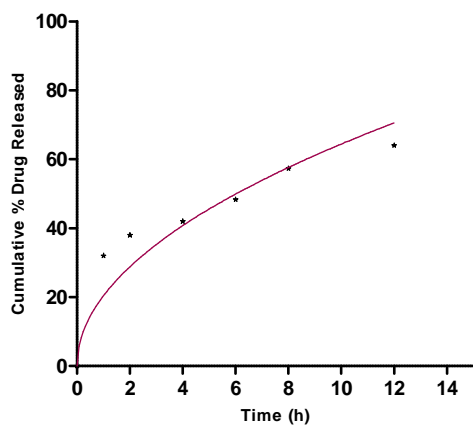
- Smooth, free-flowing spherical microcapsules

**RHODES UNIVERSITY**  
**FACULTY OF PHARMACY, GRAHAMSTOWN, SOUTH AFRICA**  
**BATCH SUMMARY**

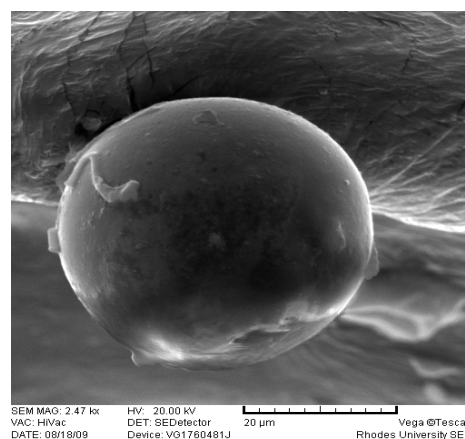
<b>Formulator</b>	Sandile Khamanga	<b>Batch Size</b>	5 g
<b>Product</b>	Captopril	<b>Microencapsulation Time (start)</b>	10:00
<b>Batch ID</b>	CPT-030	<b>(end)</b>	19:00
<b>Microencapsulation Date</b>	16-August-2009		

CPT	0.75 g	Top load balance	Mettler® Toledo
Eudragit® RS	2.00 g	Homogenizer	Virtis®
Methocel® K100M	0.50 g	<b>Analysis</b>	<b>Model</b>
Methocel® K15M	0.75 g	SEM	Tescan, VEGA LMU
Avicel® 102	0.50 g	Dissolution	VanKel® Bio-Dis® dissolution tester
Liquid paraffin	120 ml	<b>Temperature</b>	26.3 °C
Acetone	20 ml	<b>Humidity</b>	60.0 % RH

**Dissolution**



**SEM**



- Smooth, spherical microcapsules with tiny particles adhering to the surface

## **APPENDIX TWO**

---

### **BATCH PRODUCTION RECORDS FOR CPT-001**

Only one solvent evaporation record is included for this study. The records for the other batches, CPT-002 – CPT-030 are available on request.

**RHODES UNIVERSITY, FACULTY OF PHARMACY,  
GRAHAMSTOWN, SOUTH AFRICA**

---

**BATCH PRODUCTION RECORD**

---

<b>Product name</b>	Captopril
<b>Batch</b>	CPT-001
<b>Batch Size</b>	5 g

---

**MANUFACTURING APPROVALS**

---

<b>Batch record issued by</b>	_____	<b>Date :</b>	_____
<b>Master record issued by</b>	_____	<b>Date :</b>	_____

---

**RHODES UNIVERSITY, FACULTY OF PHARMACY,  
GRAHAMSTOWN, SOUTH AFRICA**

---

**BATCH PRODUCTION RECORD**

---

<b>Product name</b>	Captopril
<b>Batch</b>	CPT-001
<b>Batch Size</b>	5 g

---

**MASTER FORMULA AND BATCH FORMULA**

<b>Component</b>	<b>% m/m (v/m)</b>	<b>Amount dispensed</b>	<b>Dispensed by</b>	<b>Checked</b>
CPT	0.75g			
Eudragit® RS	2.00 g			
Methocel® K100M	0.50 g			
Methocel® K15M	0.50 g			
Avicel® 102	0.50 g			
Liquid paraffin	120 ml			
Acetone	20 ml			

**RHODES UNIVERSITY, FACULTY OF PHARMACY,  
GRAHAMSTOWN, SOUTH AFRICA**

---

**BATCH PRODUCTION RECORD**

<b>Product name</b>	Captopril
<b>Batch</b>	CPT-001
<b>Batch Size</b>	5 g

**EQUIPMENT VERIFICATION**

<b>Description</b>	<b>Type</b>	<b>Verified By</b>	<b>Confirmed By</b>
Scale	Mettler Model PM 6000		
Homogenizer	Virtis		

**RHODES UNIVERSITY, FACULTY OF PHARMACY,  
GRAHAMSTOWN, SOUTH AFRICA**

**BATCH PRODUCTION RECORD**

<b>Product name</b>	Captopril
<b>Batch</b>	CPT-001
<b>Batch Size</b>	5 g

**MANUFACTURING DIRECTIONS**

<b>Step</b>	<b>Procedure</b>	<b>Time</b>	<b>Done By</b>	<b>Checked By</b>
1	Screen separately the following materials through a 20# mesh screen CPT, Eudragit <sup>®</sup> RS, Methocel <sup>®</sup> K100M, Methocel <sup>®</sup> K15M, Avicel <sup>®</sup> 102			
2	Place acetone in a 100 ml beaker and liquid paraffin in a 400 ml beaker. Add a drop of span 80 and dimethyl polysiloxane			
3	Place the material in (1) in the beaker containing acetone and homogenize at 1500 rpm for 5 minutes			
4	Mix the acetone dispersion with the content in the 400 ml beaker			
5	Agitate with a three blade stirrer to prepare a homogenous oily phase			
6	After 2 h n-hexane was added in drops to harden the formed microcapsules and stirring continued for a further 5 h			
7	Collect microcapsules in a Buchner funnel, washed 2 -3 times with n-hexane and dried at room temperature overnight. Microcapsules transferred to airtight container until ready for analysis			
8	Mean particle size was determined using a series of laboratory sieves, microcapsule flowability was determined, encapsulation efficiency and dissolution studies were conducted			

**RHODES UNIVERSITY, FACULTY OF PHARMACY,  
GRAHAMSTOWN, SOUTH AFRICA**

---

**BATCH PRODUCTION RECORD**

---

<b>Product name</b>	Sandile Khamanga
<b>Batch</b>	Captopril
<b>Batch ID</b>	CPT-001
<b>Batch Size</b>	5 g

---

**SIGNATURE AND INITIAL REFERENCE**

<b>Full Name (Print)</b>	<b>Signature</b>	<b>Initials</b>	<b>Date</b>